NEURODEGENERATION AND NEUROPROTECTION IN RETINAL DISEASE, VOLUME II

EDITED BY: Giovanni Casini, Mohammad Shamsul Ola and Peter Koulen
PUBLISHED IN: Frontiers in Neuroscience

frontiers Research Topics

frontiers

ISSN 1664-8714
ISBN 978-2-83250-140-5
DOI 10.3389/978-2-83250-140-5

About Frontiers

Frontiers is more than just an open-access publisher of scholarly articles: it is a pioneering approach to the world of academia, radically improving the way scholarly research is managed. The grand vision of Frontiers is a world where all people have an equal opportunity to seek, share and generate knowledge. Frontiers provides immediate and permanent online open access to all its publications, but this alone is not enough to realize our grand goals.

Frontiers Journal Series

The Frontiers Journal Series is a multi-tier and interdisciplinary set of open-access, online journals, promising a paradigm shift from the current review, selection and dissemination processes in academic publishing. All Frontiers journals are driven by researchers for researchers; therefore, they constitute a service to the scholarly community. At the same time, the Frontiers Journal Series operates on a revolutionary invention, the tiered publishing system, initially addressing specific communities of scholars, and gradually climbing up to broader public understanding, thus serving the interests of the lay society, too.

Dedication to Quality

Each Frontiers article is a landmark of the highest quality, thanks to genuinely collaborative interactions between authors and review editors, who include some of the world's best academicians. Research must be certified by peers before entering a stream of knowledge that may eventually reach the public - and shape society; therefore, Frontiers only applies the most rigorous and unbiased reviews.
Frontiers revolutionizes research publishing by freely delivering the most outstanding research, evaluated with no bias from both the academic and social point of view. By applying the most advanced information technologies, Frontiers is catapulting scholarly publishing into a new generation.

What are Frontiers Research Topics?

Frontiers Research Topics are very popular trademarks of the Frontiers Journals Series: they are collections of at least ten articles, all centered on a particular subject. With their unique mix of varied contributions from Original Research to Review Articles, Frontiers Research Topics unify the most influential researchers, the latest key findings and historical advances in a hot research area! Find out more on how to host your own Frontiers Research Topic or contribute to one as an author by contacting the Frontiers Editorial Office: frontiersin.org/about/contact

NEURODEGENERATION AND NEUROPROTECTION IN RETINAL DISEASE, VOLUME II

Topic Editors:
Giovanni Casini, University of Pisa, Italy
Mohammad Shamsul Ola, King Saud University, Saudi Arabia
Peter Koulen, University of Missouri–Kansas City, United States

Citation: Casini, G., Ola, M. S., Koulen, P., eds. (2022). Neurodegeneration and Neuroprotection in Retinal Disease, Volume II. Lausanne: Frontiers Media SA. doi: 10.3389/978-2-83250-140-5

Table of Contents

frontiers | Frontiers in Neuroscience

TYPE Editorial
PUBLISHED 23 August 2022
DOI 10.3389/fnins.2022.1009228

OPEN ACCESS

APPROVED BY
Wonkyu Ju,
University of California, San Diego, United States

*CORRESPONDENCE
Peter Koulen
koulenp@umkc.edu

SPECIALTY SECTION
This article was submitted to Neurodegeneration, a section of the journal Frontiers in Neuroscience

RECEIVED 01 August 2022
ACCEPTED 03 August 2022
PUBLISHED 23 August 2022

CITATION
Casini G, Ola MS and Koulen P (2022) Editorial: Neurodegeneration and Neuroprotection in Retinal Disease, Volume II.
Front. Neurosci. 16:1009228.
doi: 10.3389/fnins.2022.1009228

Editorial: Neurodegeneration and Neuroprotection in Retinal Disease, Volume II

Giovanni Casini[1], Mohammad Shamsul Ola[2] and Peter Koulen[3,4]*

[1]Department of Biology, University of Pisa, Pisa, Italy, [2]Department of Biochemistry, College of Science, King Saud University, Riyadh, Saudi Arabia, [3]Department of Ophthalmology, Vision Research Center, School of Medicine, University of Missouri–Kansas City, Kansas City, MO, United States, [4]Department of Biomedical Sciences, School of Medicine, University of Missouri–Kansas City, Kansas City, MO, United States

KEYWORDS

oxidative stress, inflammation, apoptosis, nutraceuticals, drug delivery

Editorial on the Research Topic
Neurodegeneration and Neuroprotection in Retinal Disease, Volume II

The goal of the Frontiers Research Topic, *Neurodegeneration and Neuroprotection in Retinal Disease, Volume II*, was to expand on Volume I of this Research Topic. Specifically, the Research Topic aimed to *elucidate (i) pathophysiological mechanisms of neurodegeneration in retinal diseases; (ii) new neuroprotective substances, with a particular attention to nutraceuticals, that may be used to treat retinal pathologies; (iii) new methods of neuroprotective drug delivery to the retina.*

Diseases impairing retina function continue to generate an increasing healthcare burden across the globe affecting both patients and their families. As a majority of these diseases produces vision loss and blindness by impairing the viability and ultimately inducing cell death of retinal neurons, mechanisms underlying retinal neurodegeneration remain only partially identified. While the pathophysiology of glaucoma, diabetic retinopathy (DR), age-related macular degeneration (AMD), and retinitis pigmentosa differ widely, all have degeneration of the neural retina in common. Therefore, common features of neurodegeneration leading ultimately to the loss of neurons and visual function, can be not only determined, but can also lead to insights into its molecular, cellular and systemic mechanisms. The growing field of neuroprotection utilizes these novel insights into the causes of neurodegeneration to devise both preventative and therapeutic strategies covering areas ranging from traditional nutraceutical and pharmaceutical approaches to groundbreaking new

cell-based and personalized medicine therapies. Due to the complex, chronic and multifactorial nature of neurodegeneration in retinal pathologies research efforts continue and increase to innovate and improve impactful *in vitro* and *in vivo* models. Innovation of such preclinical research tools remains a critical component of research benefiting both the neurodegeneration and neuroprotection fields and accelerating and strengthening the critical interaction between both of these fields.

The Frontiers Research Topic, *"Neurodegeneration and Neuroprotection in Retinal Disease, Volume II,"* contributes to this broad range of complementary research efforts with two reviews and seven research articles:

Aldosari et al. provide a systematic review in the field of DR, specifically focusing on a synthesis of recent advances in preclinical and clinical studies on the role of metabolites in neurovascular damage contributing to neurodegeneration in DR. Reviewing key signaling pathways affecting or affected by sugar, lipid, and amino acid metabolites of carbohydrate, lipid, and amino acids the authors integrate key aspects of endocrinology, immunology and ophthalmology research including underlying seminal basic science research. At the same time, the authors also identify challenges and opportunities, where clinical phenotypes obtained through metabolic profiling have not been linked with mechanisms underlying pathophysiology and where new research tools to identify mechanisms underlying metabolic defects have become available, respectively (Aldosari et al.).

Bridging the fields of nutraceuticals, dietary supplements and small molecule therapeutics as they relate to neuroprotection, Edwards et al. provide a review of molecular mechanisms underlying the therapeutic actions of vitamin E in AMD. Starting with successes and shortcomings in the clinical use of vitamin E to control retinal neurodegeneration and other medical conditions, the authors integrate recent mechanistic findings from the preclinical and clinical scientific literature to come full circle and provide conclusions and directions for research to improve future clinical intervention approaches for AMD and potentially other retinal diseases (Edwards et al.).

Three of the research articles advance research tools and novel approaches to identify mechanisms of neurodegeneration geared toward improved neuroprotective strategies:

Rohowetz et al. explore the impact of abnormalities of the anterior segment on ocular hypertension in a widely used mouse model of glaucoma, the DBA/2J mouse, and in DBA/2J-Gpnmb+/SjJ control mice. They found that while common in both the glaucomatous and the control mouse strains, corneal calcification does not contribute to the development of an elevated intraocular pressure in DBA/2J mice, while iris pigment dispersion does. These findings provide important insights in the use of and for the interpretation of data obtained from this key preclinical glaucoma model (Rohowetz et al.).

Gajendran et al. present a novel strategy to identify and analyze changes in electroretinography signals resulting from glaucoma. Using a machine-learning algorithm, they were able to identify functional changes and deficits in a mouse model of glaucoma and conclude that the novel tool can potentially facilitate the quantitative and non-invasive assessment of both early-stage glaucoma and the success of therapeutic intervention (Gajendran et al.).

Asatryan et al. describe a new human retinal pigment epithelial cell line as an innovative tool to conduct research on a cell type critical for retina and particularly photoreceptor cell function and health. Gene expression profiling, and developmental, structural, functional and pharmacological characterization of these cells lead the authors to conclude that the new cell line will be able to contribute significantly to the field of neuroprotection research (Asatryan et al..

Four of the research articles report new mechanisms of action representing clinically relevant targets for neuroprotective strategies:

Nath and Fort identify distinct molecular signaling pathways underlying αA-crystallin-mediated neuroprotection. The authors describe neuroprotective activity of αA-crystallin independent of well characterized neuroprotective kinase signaling pathways and leading to the identification of new potential neuroprotective approaches (Nath and Fort).

Piano et al. measure the neuroprotective potential of the nutraceuticals naringenin and quercetin in a mouse model of retinal degeneration. The authors find robust protection from photoreceptor cell degeneration mediated by antioxidant and anti-apoptotic properties of the nutraceutical molecules suggesting potential efficacy as nutraceutical therapy for retinitis pigmentosa patients (Piano et al.).

Wei et al. identify sirtuin 4 (SIRT4) in Müller glia of the retina and describe how activation of SIRT4 can be used to increase glutamine synthetase expression and thereby neuroprotection. The authors conclude that SIRT4 can potentially become a target for long-term pharmacotherapy of retinal pathologies (Wei et al.).

Fedotkina et al. determine genetic risk factors for proliferative diabetic retinopathy resulting from exposure to starvation and observe changes in retina development resulting from glucose starvation. The authors suggest opportunities for neuroprotective intervention with respect to both developmental stage and potential molecular targets (Fedotkina et al.).

In summary, together with Volume I, this Volume II of the Frontiers Research Topic on Neurodegeneration and Neuroprotection in Retinal Disease constitutes a valid contribution to the understanding of the neurodegeneration phenomena in retinal diseases and to the possible design of

new therapeutic approaches that could limit the socio-economic burden of sight-threatening pathologies.

Author contributions

PK conceived and wrote the editorial. All authors edited and reviewed the manuscript. All authors contributed to the article and approved the submitted version.

Funding

This publication was supported by the Felix and Carmen Sabates Missouri Endowed Chair in Vision Research.

Conflict of interest

The authors declare that the editorial was written in the absence of any commercial or financial relationships that could be construed as a potential conflict of interest.

Publisher's note

frontiers in Neuroscience

ORIGINAL RESEARCH
published: 03 February 2022
doi: 10.3389/fnins.2021.801184

The Contribution of Anterior Segment Abnormalities to Changes in Intraocular Pressure in the DBA/2J Mouse Model of Glaucoma: DBA/2J-*Gpnmb*$^{+}$/SjJ Mice as Critical Controls

Landon J. Rohowetz[1], *Marc E. Mardelli*[1], *R. Scott Duncan*[1], *Sean M. Riordan*[1] *and Peter Koulen*[1,2]*

[1] *Department of Ophthalmology, Vision Research Center, School of Medicine, University of Missouri – Kansas City, Kansas City, MO, United States,* [2] *Department of Biomedical Sciences, School of Medicine, University of Missouri—Kansas City, Kansas City, MO, United States*

OPEN ACCESS

Edited by:
Rafael Linden, Federal University of Rio de Janeiro, Brazil

Reviewed by:
Sabrina Reinehr, Ruhr-University Bochum, Germany
Denise M. Inman, University of North Texas Health Science Center, United States

***Correspondence:**
Peter Koulen
koulenp@umkc.edu

Specialty section:
This article was submitted to Neurodegeneration, a section of the journal Frontiers in Neuroscience

Received: *25 October 2021*
Accepted: *29 December 2021*
Published: *03 February 2022*

Citation:
Rohowetz LJ, Mardelli ME, Duncan RS, Riordan SM and Koulen P (2022) The Contribution of Anterior Segment Abnormalities to Changes in Intraocular Pressure in the DBA/2J Mouse Model of Glaucoma: DBA/2J-Gpnmb^{+}/SjJ Mice as Critical Controls. Front. Neurosci. 15:801184. doi: 10.3389/fnins.2021.801184

The contributions of anterior segment abnormalities to the development of ocular hypertension was determined in the DBA/2J mouse model of glaucoma. Intraocular pressure (IOP) was measured non-invasively. Iris pigment dispersion (IPD) and corneal calcification were measured weekly starting at 20 weeks of age in DBA/2J and DBA/2J-*Gpnmb*$^{+}$/SjJ mice. Thickness, surface area, auto-fluorescence intensity, and perimeter length of calcified regions were measured in postmortem corneas using confocal microscopy. DBA/2J mice developed elevated IOP between 9 and 12 months of age, but DBA/2J-*Gpnmb*$^{+}$/SjJ mice did not. Corneal calcification was found at all ages observed and at similar frequencies in both strains with 83.3% of DBA/2J eyes and 60.0% of DBA/2J-*Gpnmb*$^{+}$/SjJ eyes affected at 12 months (P = 0.11). Calcification increased with age in both DBA/2J (P = 0.049) and DBA/2J-*Gpnmb*$^{+}$/SjJ mice (P = 0.04) when assessed qualitatively and based on mixed-effects analysis. No differences in the four objective measures of calcification were observed between strains or ages. At 12 months of age, DBA/2J mice with corneal calcification had greater mean IOP than DBA/2J mice without corneal calcification. IOP was not correlated with the qualitatively assessed measures of calcification. For the subset of eyes with ocular hypertension, which were only found in DBA/2J mice, IOP was negatively correlated with the qualitative degree of calcification, but was not correlated with the four quantitative measures of calcification. Differences in IOP were not observed between DBA/2J-*Gpnmb*$^{+}$/SjJ mice with and without calcification at any age. IPD increased with age and demonstrated a moderate correlation with IOP in DBA/2J mice, but was not observed in DBA/2J-*Gpnmb*$^{+}$/SjJ mice. In the DBA/2J mouse model of glaucoma, increased IPD is positively correlated with an increase in IOP and corneal calcification is present in the majority of eyes at and after age 9 months. However, while IPD causes ocular hypertension, corneal calcification does not appear to contribute to the elevation of

IOP, as the control strain DBA/2J-*Gpnmb*$^{+}$/SjJ exhibits corneal calcification similar to DBA/2J mice, but does not develop ocular hypertension. Corneal calcification, therefore, does not appear to be a contributing factor to the development of elevated IOP in DBA/2J mice.

Keywords: glaucoma, retina, iris pigment dispersion, intraocular pressure, iris stromal atrophy, cornea, corneal calcification, anterior chamber

INTRODUCTION

Glaucoma is characterized by progressive dysfunction and degeneration of the optic nerve and is the leading cause of irreversible blindness worldwide, affecting 64.3 million individuals in 2013 (Tham et al., 2014). Experimental models of glaucoma are important to understanding the disease and identifying potential therapeutic strategies. The DBA/2J inbred mouse is one of the most widely used models of ocular hypertension-induced glaucoma and was first described as a model for glaucoma in 1995 (Sheldon et al., 1995; Inman et al., 2006; Schlamp et al., 2006; Burroughs et al., 2011; Bosco et al., 2018; Mathieu et al., 2018; Buchanan et al., 2019; Jassim et al., 2019). DBA/2J mice develop severe iris pigment dispersion (IPD), which causes elevated intraocular pressure (IOP) as a result of occluded aqueous humor drainage pathways (John et al., 1998; Libby et al., 2005; Scholz et al., 2008). IPD occurs in DBA/2J mice due to a mutation in the glycoprotein (transmembrane) nmb gene (*Gpnmb*^{R150X}). A separate iris abnormality, iris stromal atrophy (ISA), occurs as a result of a mutation in the tyrosinase related protein 1 gene (*Tyrp1*^{b}) (Chang et al., 1999; Anderson et al., 2002; Libby et al., 2005; Howell et al., 2007). Homozygosity for both of these genes accounts for the severe iris abnormalities including ISA and IPD seen in DBA/2J mice (Anderson et al., 2002).

In addition to these factors rendering DBA/2J mice a model of ocular hypertension-induced glaucoma, DBA/2J mice are also predisposed to a variety of systemic disorders including seizures, high-frequency hearing loss, thoracic cavity malformation and dystrophic calcification (van den Broek and Beynen, 1998; Shin et al., 2010; Jackson et al., 2015; Turner et al., 2017). Evidence of calcification has been reported in several tissues and organs throughout the body, including the heart, skeletal muscle, tongue, kidney, testes and diaphragm (van den Broek and Beynen, 1998). The cornea is also a common site for calcification in DBA/2J mice that increases in incidence and severity with age (John et al., 1998; Inman et al., 2006; Chou et al., 2011; Rutsch et al., 2011; Bricker-Anthony and Rex, 2015). This is particularly important for the use of DBA/2J mice as a glaucoma model, as calcification may impact non-invasive IOP measurement due to its effects on corneal thickness and elasticity (Brandt, 2001; Turner et al., 2017). Indeed, when compared with invasive IOP measurement, non-invasive measurement of IOP has been shown to be unreliable and often falsely elevated in DBA/2J mice (Turner et al., 2017). Furthermore, in DBA/2J mice, increased corneal thickness has been associated with elevated IOP measured non-invasively (Inman et al., 2006; Chou et al., 2011). However, despite these shortcomings non-invasive rebound tonometry continues to be used in mouse studies. Non-invasive measurement is a more humane method of measurement, it does not require anesthesia, and it is essential to longitudinal and histological studies where damage to the eye due to measurement is unacceptable.

IOP- and age-dependent decreases in visual acuity are characteristic components of glaucoma disease progression in DBA/2J mice (Wong and Brown, 2007; Burroughs et al., 2011; Grillo et al., 2013; Kaja et al., 2014; Grillo and Koulen, 2015; Montgomery et al., 2016; Yang et al., 2018). At the same time, adequate fundus and retinal imaging can be difficult to obtain due to anterior chamber abnormalities, including corneal calcification, in DBA/2J mice (Turner et al., 2017). In addition, other forms of corneal pathology have been identified in DBA/2J mice, including ulcers, erosions, neovascularization and basement membrane mineralization (John et al., 1998; Inman et al., 2006). Given the extent and severity of corneal and anterior chamber abnormalities in DBA/2J mice, the goal of the present study was to determine the relative contributions of such abnormalities to the development of ocular hypertension in the DBA/2J mouse model of glaucoma. A recently described control strain for DBA/2J mice, DBA/2J-*Gpnmb*$^{+}$/SjJ, is characterized by a functional *Gpnmb* allele. Although these mice develop very mild ISA due to the homozygous mutation in *Tyrp1*^{b}, they do not develop IPD, elevated IOP, or glaucoma and therefore have been suggested

TABLE 1 | Qualitative corneal calcification grading system.

Severity of corneal calcification	Observation
0.5	Calcification visible. Multiple observations needed to confirm presence of calcification.
1.0	Calcification approaches edge of constricted pupil but did not overlap
1.5	Calcification bordered constricted pupil
2.0	Calcification ended within constricted pupil
2.5	Calcification crossed half of constricted pupil
3.0	Calcification crossed at least three–fourths of constricted pupil

Measurements were obtained weekly in all mice beginning at 20 weeks of age. Large calcifications across the top or bottom of pupil were down-graded by 0.5 points and severely opaque or vascularized small calcifications were upgraded by 0.5 points.

Abbreviations: ANOVA, analysis of variance; IOP, intraocular pressure; IPD, iris pigment dispersion; ISA, iris stromal atrophy.

as a more closely matched control for DBA/2J mice (Howell et al., 2007). Therefore, we employed a comparison of the DBA/2J and DBA/2J-*Gpnmb*$^{+}$/SjJ mouse strains to determine the relative roles of age-related changes in IOP and corneal pathology, specifically corneal calcification in the DBA/2J mouse model of glaucoma.

MATERIALS AND METHODS

Animals

DBA/2J (n = 30) and DBA/2J-*Gpnmb*$^{+}$/SjJ (n = 30) mice were purchased from Jackson Laboratories (Bar Harbor, ME). Mice were socially housed with *ad libitum* access to food and water and were kept under a 12-h dark/light cycle. 10 mice from each strain were euthanized at 6, 9, or 12 months of age. One DBA/2J animal from the 12-month group was lost to sampling and follow-up. All animal husbandry and experimental procedures had been approved by the Institutional Animal Care and Use Committee and were conducted in compliance with the Public Health Service Policy on Humane Care and Use of Laboratory Animals and in accordance with the ARVO Animal Statement and institutional guidelines.

Measurement of Intraocular Pressure

As validated previously (Pease et al., 2011), IOP was measured weekly starting at 9 weeks of age until the end of the study with rebound tonometry (Icare TONOLAB, Colonial Medical Supply Co., Inc., Franconia, NH) not requiring anesthesia. Three measurements, each consisting of the average of six repeated measurements performed by the tonometry system, were obtained in each eye and the average was used for analysis.

Qualitative Assessment of Structural Changes of the Cornea and Iris

A qualitative assessment of corneal calcification and IPD was conducted weekly beginning at 20 weeks of age by the same investigator, who was blinded to the strain identity or age of mice. Imaging of the anterior segment and for evaluation of corneal calcification and IPD was performed non-invasively and without the need for anesthesia. The investigator used the grading system illustrated in **Table 1** and **Figure 1** for corneal calcification and as described previously for IPD (Swaminathan et al., 2013). As the pupillary light reflex in some animals becomes diminished over time, such qualitative assessment, while both biologically and clinically relevant due to their non-invasiveness and ease-of-use in longitudinal studies, were complemented with quantitative measures as follows.

Quantitative Assessment of Structural Changes of Cornea Calcification

Confocal microscopy was carried out using a Nikon FN/C2 upright confocal microscope with a Coherent OBIS and Sapphire

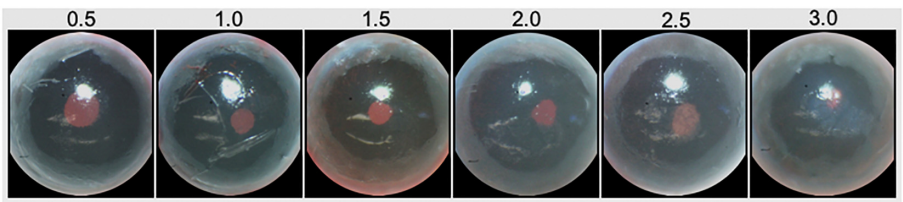

FIGURE 1 | Qualitative measures of corneal calcification in DBA/2J and DBA/2J-*Gpnmb*$^{+}$/SjJ mice. Brightness and contrast have been adjusted to increase visibility of calcifications.

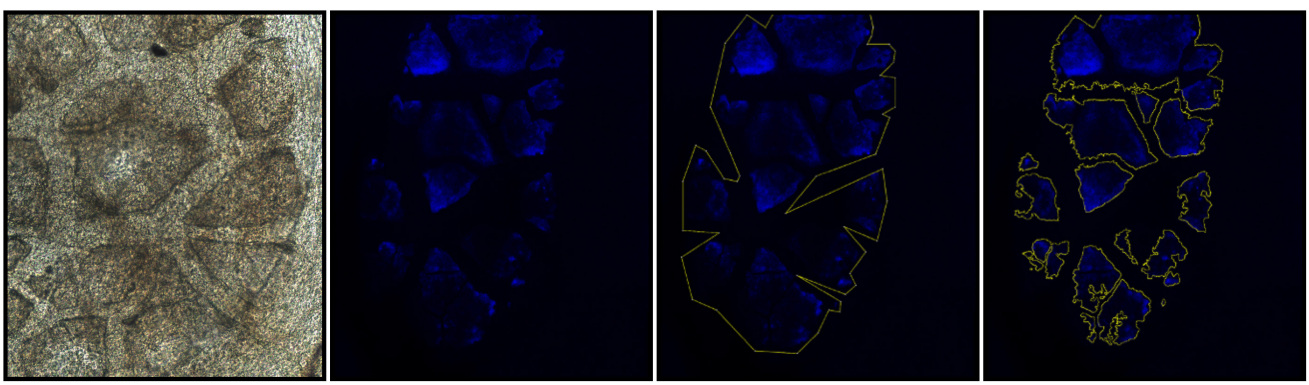

FIGURE 2 | Quantitative measures of corneal calcification in DBA/2J and DBA/2J-*Gpnmb*$^{+}$/SjJ mice. Image-J/FIJI was used to generate maximum intensity projections of corneal autofluorescence. Calcified regions of interest (ROIs) were isolated using Image-J/FIJI thresholding, binary, and outline tools. ROIs were subsequently used to measure thickness, signal intensity, surface area, and perimeter length.

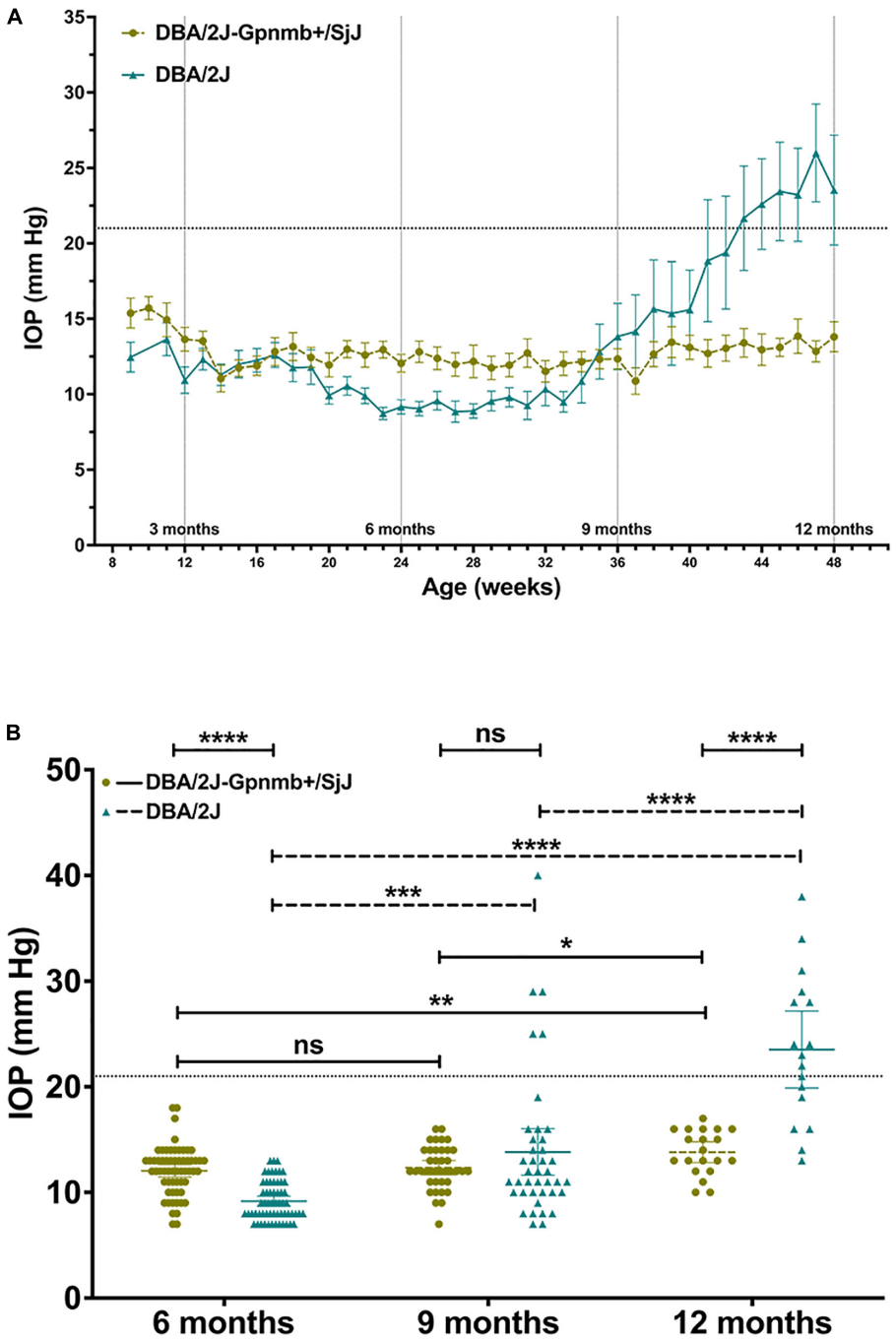

FIGURE 3 | (A) Line graph illustrating mean intraocular pressure of DBA/2J and DBA/2J-*Gpnmb*$^{+}$/SjJ mice by age. Mean intraocular pressure became consistently greater in DBA/2J mice than DBA/2J-*Gpnmb*$^{+}$/SjJ at 41 weeks. **(B)** Column graph demonstrating intraocular pressure between groups and age. Line at 21 mm Hg indicates demarcation between normal tension and ocular hypertension. Mean intraocular pressure of DBA/2J and DBA/2J-*Gpnmb*$^{+}$/SjJ mice increased at 12 months from 6 months. Mean intraocular pressure also increased at 9 months from 6 months in the DBA/2J group. *$P < 0.05$, **$P < 0.01$, ***$P < 0.001$, ****$P < 0.0001$. Error bars represent 95% confidence intervals. Sample sizes for A varied at each time point due to the availability of mice to be measured and ranged from 17 to 60 eyes for each point. Sample sizes for B were, from left to right (60, 60, 38, 40, 20, 17).

lasers (Nikon Instruments Inc., Melville, NY, United States; Coherent, Inc., Santa Clara, CA, United States). Corneal calcification was measured quantitatively after euthanasia using confocal microscopy imaging of corneal autofluorescence (Nikon, Melville NY). A total of 62 images (left and right eyes from 31 mice: 17 DBA/2J, 2 at 6 months, 5 at 9 months and 7 at 12 months of age, and 14 DBA/2J-*Gpnmb*$^{+}$/SjJ control mice, 4 at 6 months, 5 at 9 months and 8 at 12 months of

age) were obtained under identical conditions and were analyzed with Image-J/FIJI (National Institute of Health, United States). Each image was acquired as a Z-stack from each eye of each animal used for calcification measurement. Optical sectioning along the Z-axis was used to determine the thickness of calcified areas and maximum intensity projection images were generated to measure average signal intensity (a correlate of calcium crystal density), surface area, and perimeter length of calcified segments (**Figure 2**).

Statistical Methods

All analyses were performed with GraphPad Prism Versions 8 and 9 (GraphPad Software, San Diego, CA), Microsoft Excel (Microsoft Corporation, Redmond, WA) and IBM SPSS Statistics Version 25 (IBM Corp., Armonk, NY). Pearson correlation coefficients were measured using bivariate correlations and strength of association was determined as follows: no correlation for $0.0 \leq r < 0.2$, weak correlation for $0.2 \leq r < 0.4$, moderate correlation for $0.4 \leq r < 0.6$, and strong correlation for $0.6 \leq r \leq 1.0$. Sample means, mean differences, and 95% confidence intervals were obtained using independent *t*-tests, dependent *t*-tests, mixed-effects analyses and analyses of variance (ANOVAs). Tukey's tests and Bonferroni corrections were used to account for multiple comparisons.

RESULTS

Iris Pigment Dispersion—Comparisons Among Strains and Age Groups

At 6 months of age, 6.7% (4/60) of DBA/2J eyes demonstrated evidence of IPD. At 9 months of age, 77.5% (31/40) of DBA/2J

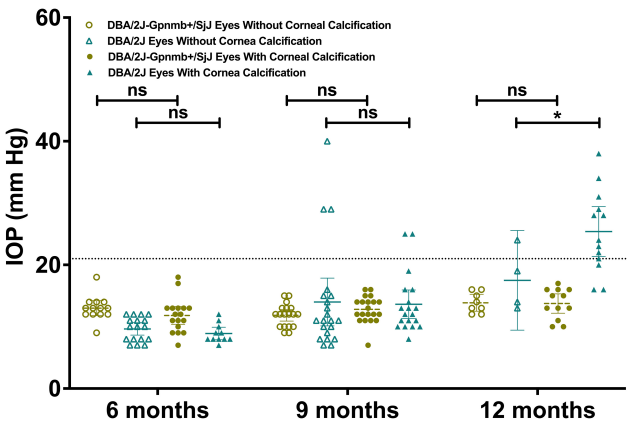

FIGURE 4 | Column graph illustrating IOP in DBA/2J mice and DBA/2J-*Gpnmb*$^{+}$/SjJ mice stratified by age and presence of corneal calcification. Line at 21 mm Hg indicates demarcation between normal tension and ocular hypertension. Mean intraocular pressure at 12 months was greater in calcified DBA/2J eyes when compared to non-calcified DBA/2J eyes. No difference in mean IOP was observed between DBA/2J-*Gpnmb*$^{+}$/SjJ mice with or without corneal calcification. *$P < 0.05$. Error bars represent 95% confidence intervals. Sample sizes were, from left to right [(13, 17, 17, 11) (18, 21, 20, 19) (8, 4, 12, 13)].

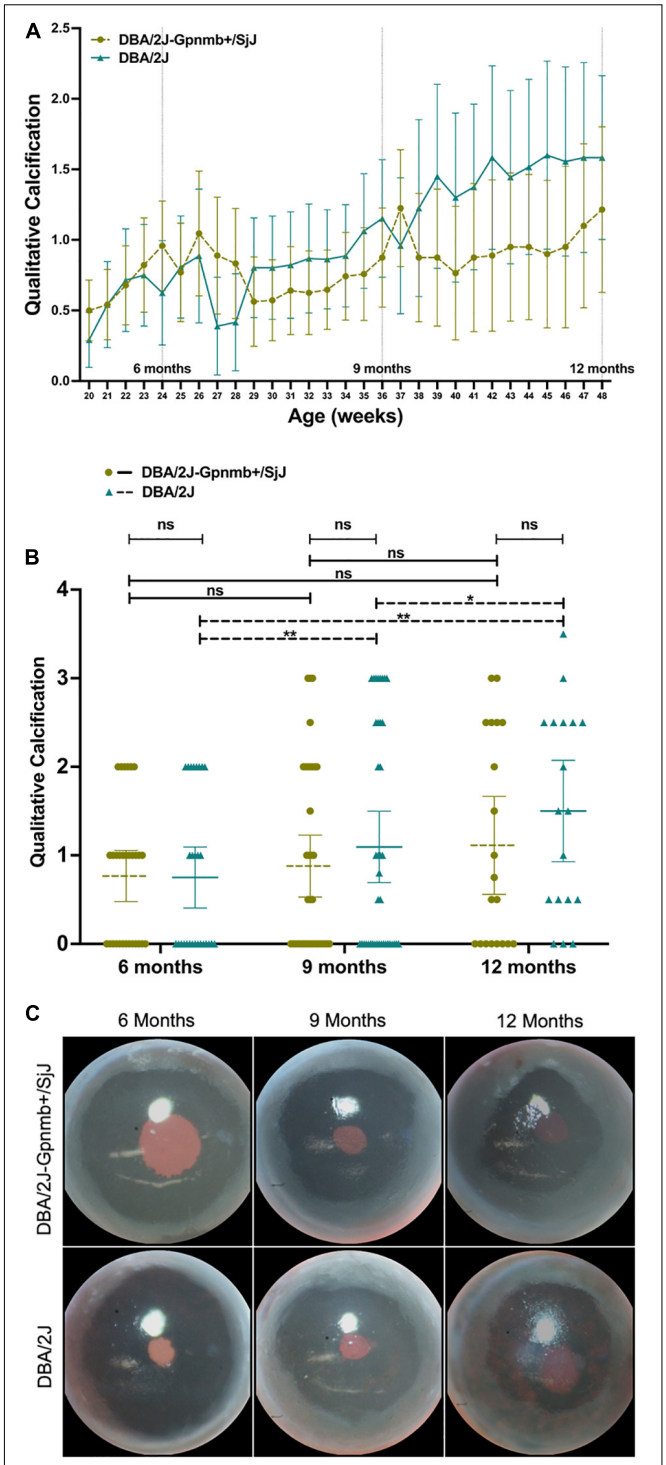

FIGURE 5 | (A) Line graph, **(B)** column graph and **(C)** photographs illustrating the degree of qualitative corneal calcification in both DBA/2J and DBA/2J-*Gpnmb*$^{+}$/SjJ mice euthanized at 12 months. The degree of qualitative calcification increased with age in both DBA/2J and DBA/2J-*Gpnmb*$^{+}$/SjJ mice. No differences in qualitative calcification were observed between groups. *$P < 0.05$, **$P < 0.01$. Error bars represent 95% confidence intervals. Sample sizes for A varied at each time point due to the availability of mice to be measured and ranged from 18 to 40 eyes for each point. Sample sizes for B were, from left to right [(30, 28),(37, 40),(20, 18)].

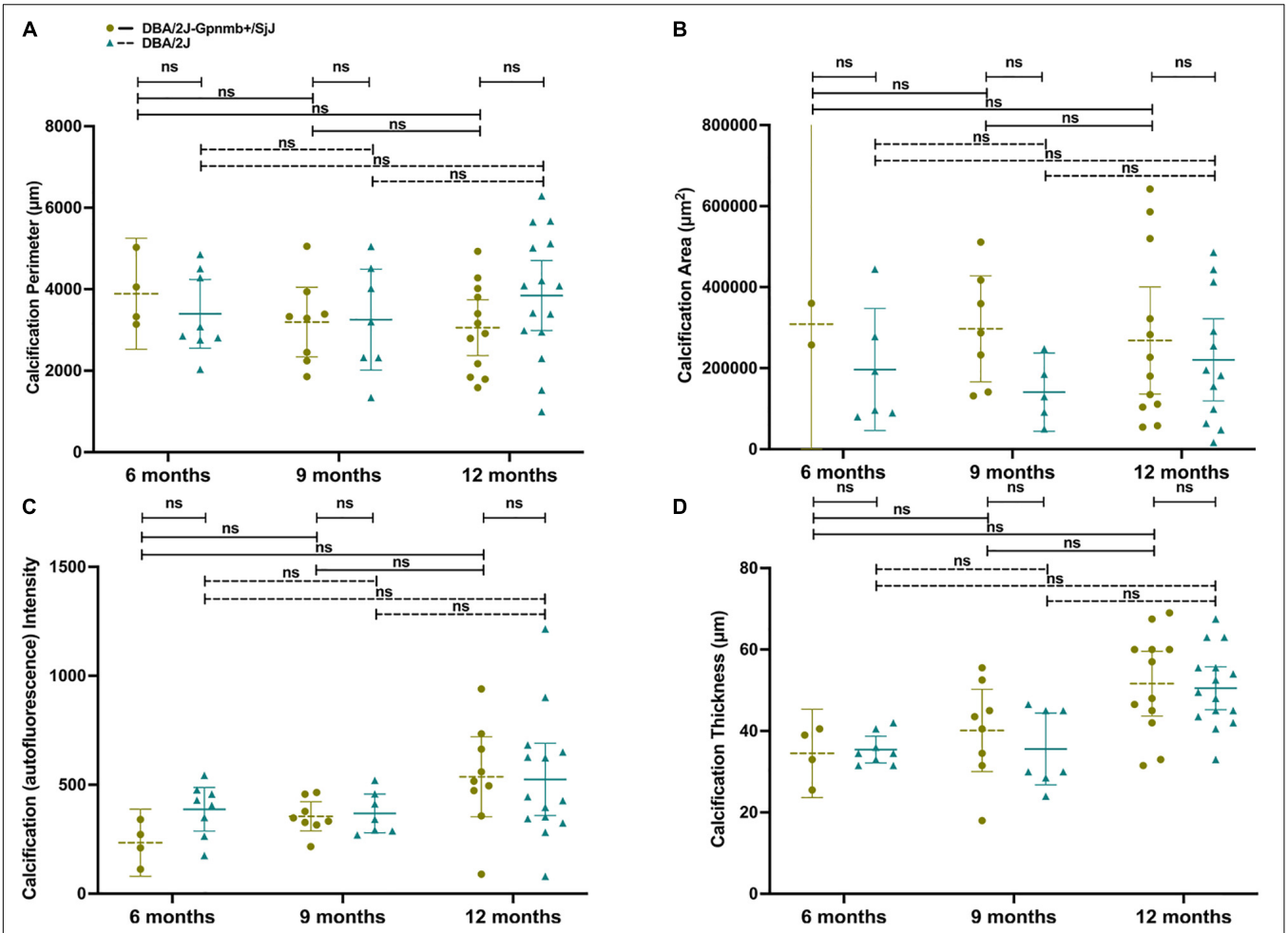

FIGURE 6 | No differences in calcification **(A)** perimeter length, **(B)** area, **(C)** autofluorescence intensity, or **(D)** thickness were observed between groups or ages in eyes with cornea calcification. Error bars represent 95% confidence intervals. Sample sizes varied at each time point due to the number of mice with calcification. Sample sizes were from left to right A[(4, 8),(8, 7),(12, 15)], B[(2, 6),(7, 5),(12, 12)], C[(4, 8),(8,7),(9, 14)], D[(4, 8),(8, 7),(12, 15)].

eyes demonstrated evidence of IPD and at 12 months of age, 100% (18/18) of DBA/2J eyes showed evidence of IPD. No DBA/2J-*Gpnmb*$^{+}$/SjJ mice developed IPD.

Intraocular Pressure—Comparisons Among Strains and Age Groups

Mean IOP of DBA/2J-*Gpnmb*$^{+}$/SjJ mice increased (P = 0.005; 95% CI, 0.480–3.02 mm Hg) at 12 months (13.8 ± 0.47 mm Hg) from 6 months (12.05 ± 0.30 mm Hg). Mean IOP increased at both 9 months (13.53 ± 0.88 mm Hg) and 12 months (23.53 ± 1.72 mm Hg) when compared with IOP measured at 6 months (9.3 ± 0.24 mm Hg; P < 0.001; 95% CI 2.22–6.23 and 11.57–16.89 mm Hg, respectively) in the DBA/2J group. At 41 weeks, IOP became consistently higher in DBA/2J mice (mean difference 6.15 ± 1.98 mm Hg; P = 0.003; **Figure 3A**) and at 12 months, mean IOP was significantly greater (P < 0.001; 95% CI, 5.99–13.47 mm Hg; **Figure 3B**) in DBA/2J mice (23.53 ± 1.72 mm Hg) when compared with DBA/2J-*Gpnmb*$^{+}$/SjJ mice (13.8 ± 0.47 mm Hg; **Figure 3B**). While no DBA/2J-*Gpnmb*$^{+}$/SjJ mice developed ocular hypertension, IOPs over 21 mm Hg were seen in DBA/2J mice for 5 out of 40 eyes (from 3 animals) at 9 months and in 11 out of 20 eyes (from 8 animals) at 12 months (**Figure 3B**).

Mean IOP at 12 months was greater (P = 0.048; 95% CI, 0.010–16.67 mm Hg) in DBA/2J eyes with corneal calcification (25.38 ± 1.85 mm Hg) when compared to DBA/2J eyes without corneal calcification (17.5 ± 2.53 mm Hg; **Figure 4**). No difference in mean IOP was observed between DBA/2J-*Gpnmb*$^{+}$/SjJ mice with or without corneal calcification (**Figure 4**).

Qualitative Assessment of Corneal Calcification—Comparisons Among Strains and Age Groups

Corneal calcification was found in 46.4% of DBA/2J eyes and 56.7% of DBA/2J-*Gpnmb*$^{+}$/SjJ eyes at 6 months (P = 0.32), 52.5 and 52.6% at 9 months (P = 0.99) and 83.3 and 60.0% at 12 months (P = 0.11). Mixed-effects analysis demonstrated

an increase in qualitative calcification with age in both DBA/2J (P = 0.049) and DBA/2J-*Gpnmb*$^{+}$/SjJ mice (P = 0.04). While two-way ANOVA examining the effects of group and age on qualitative calcification revealed an interaction between groups (P = 0.03), multiple comparisons analyses revealed no individual differences between groups (**Figures 5A–C**).

Objective Measures of Calcification—Comparisons Among Strains and Age Groups

Using objective measures of corneal calcification, we determined an increase in the number of eyes affected with age (**Figure 6**): calcification was found in 40% of DBA/2J eyes and 20% of DBA/2J-*Gpnmb*$^{+}$/SjJ eyes at 6 months (P = 0.17), 35 and 47% at 9 months (P = 0.46), and 83 and 60% at 12 months (P = 0.11).

When comparing 9 and 12 month-old mice with corneal calcification, DBA/2J mice did not demonstrate an increase in calcification perimeter length (**Figure 6A**; P = 0.61), area (**Figure 6B**; P = 0.67), autofluorescence intensity (**Figure 6C**; P = 0.66) or thickness (**Figure 6D**; P = 0.07). Furthermore, DBA/2J-*Gpnmb*$^{+}$/SjJ mice did not demonstrate changes in any of the aforementioned parameters between 9 and 12 months of age (P = 0.98, 0.98, 0.23, and 0.20, respectively; **Figures 6A–D**). Moreover, DBA/2J mice did not exhibit significantly greater mean calcification perimeter length at 12 months (**Figure 6A**; P = 0.35) or calcification intensity at 6 months (**Figure 6C**; P = 0.65) when compared to DBA/2J-*Gpnmb*$^{+}$/SjJ mice of the same age. In sum, no differences in objective measures of calcification were observed between groups or ages (**Figures 6A–D**).

Intraocular Pressure and Calcification—Comparisons Among Strains and Age Groups

IOP demonstrated no correlation with qualitative calcification (r = 0.19, P = 0.08; **Figure 7A**) when all eyes of DBA/2J mice were included. These parameters were also not correlated in DBA/2J-*Gpnmb*$^{+}$/SjJ mice (r = 0.07, P = 0.54; **Figure 7B**) and for the three ages investigated in either strain (DBA/2J mice at 6, 9 and 12 months, r = –0.18, P = 0.37, r = 0.06, P = 0.73, r = 0.02, P = 0.94, respectively; DBA/2J-*Gpnmb*$^{+}$/SjJ mice at 6, 9 and 12 months, r = 0.24, P = 0.20, r = 0.15, P = 0.38, r = 0.18, P = 0.44, respectively; **Figure 7**). For eyes with ocular hypertension (red symbols in **Figure 7**), which were only found in DBA/2J mice, IOP was negatively correlated with qualitatively assessed calcification (r = –0.55, P = 0.03; **Figure 7A**).

For quantitative measures of corneal calcification, DBA/2J mice demonstrated weak to moderate correlations between IOP and calcification thickness (r = 0.42, P = 0.004; **Figure 8A**), IOP and calcification perimeter length (r = 0.36, P = 0.01; **Figure 8B**) and IOP and calcification intensity (r = 0.39, P = 0.007; **Figure 8C**) but not calcification area (r = 0.25, P = 0.09; **Figure 8D**). These parameters were not significantly positively correlated in DBA/2J-*Gpnmb*$^{+}$/SjJ mice (r = 0.16, P = 0.29, r = 0.01, P = 0.95, r = 0.26, P = 0.08, r = –0.01, P = 0.93, respectively; **Figures 8E–H**) and for the three ages investigated in either strain (**Figures 8A–H** and **Table 2**).

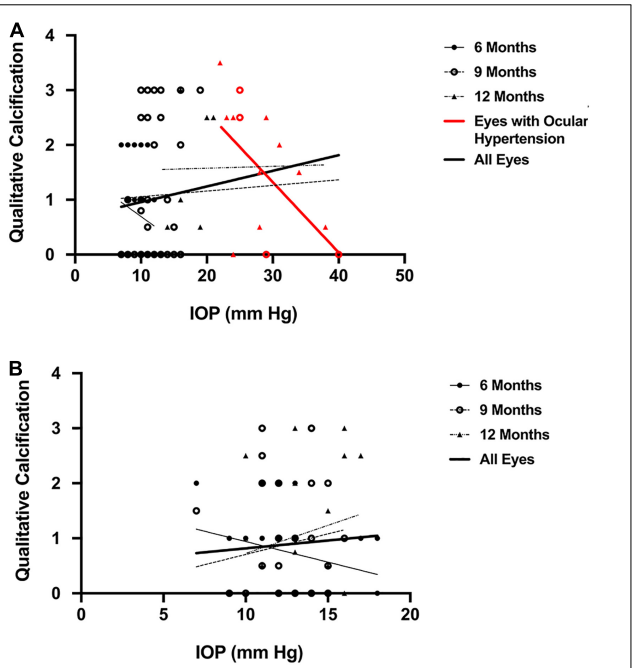

FIGURE 7 | Scatterplot demonstrating **(A)** no correlation between qualitative calcification and intraocular pressure (r = 0.19) in all eyes of DBA/2J mice and **(B)** of DBA/2J-*Gpnmb*$^{+}$/SjJ mice (r = 0.07). Qualitative calcification and intraocular pressure (r = –0.55, P = 0.03) were negatively correlated in eyes with ocular hypertension (highlighted in red). Sample sizes for each group in A were (6 mo = 28; 9 mo = 66, 12 mo = 18, Hypertensive = 15, All eyes = 86). Sample sizes for each group in B were (6 mo = 30; 9 mo = 38, 12 mo = 20, All eyes = 87).

For eyes with ocular hypertension (red symbols in **Figure 8**), which were only found in DBA/2J mice, IOP was not correlated with quantitative measures of calcification (calcification thickness, r = –0.29, P = 0.32; **Figure 8A**; calcification perimeter length, r = –0.19, P = 0.51; **Figure 8B**; calcification intensity, r = 0.33, P = 0.26; **Figure 8C**; calcification area, r = 0.52, P = 0.057; **Figure 8D**).

Intraocular Pressure and Iris Pigment Dispersion—Comparisons Among Strains and Age Groups

IOP and the degree of IPD development were moderately correlated in DBA/2J mice (r = 0.57, P < 0.001; **Figure 9A**). This correlation was even stronger when only mice with corneal calcification were analyzed (r = 0.60, P < 0.001; **Figure 9B**) and was absent in the subset of mice that did not exhibit corneal calcification (r = 0.22, P = 0.33; **Figure 9C**). For the three ages investigated in DBA/2J mice, the correlation between IOP and the degree of IPD development did not increase with age (9 months: r = 0.09, P = 0.60; 12 months: r = 0.08, P = 0.76, respectively; **Figure 9**). For eyes with ocular hypertension (red symbols in **Figure 9**), which were only found in DBA/2J mice, IOP was not correlated with qualitatively assessed IPD development (r = –0.05, P = 0.91; **Figure 9**). IPD was not observed in DBA/2J-*Gpnmb*$^{+}$/SjJ mice.

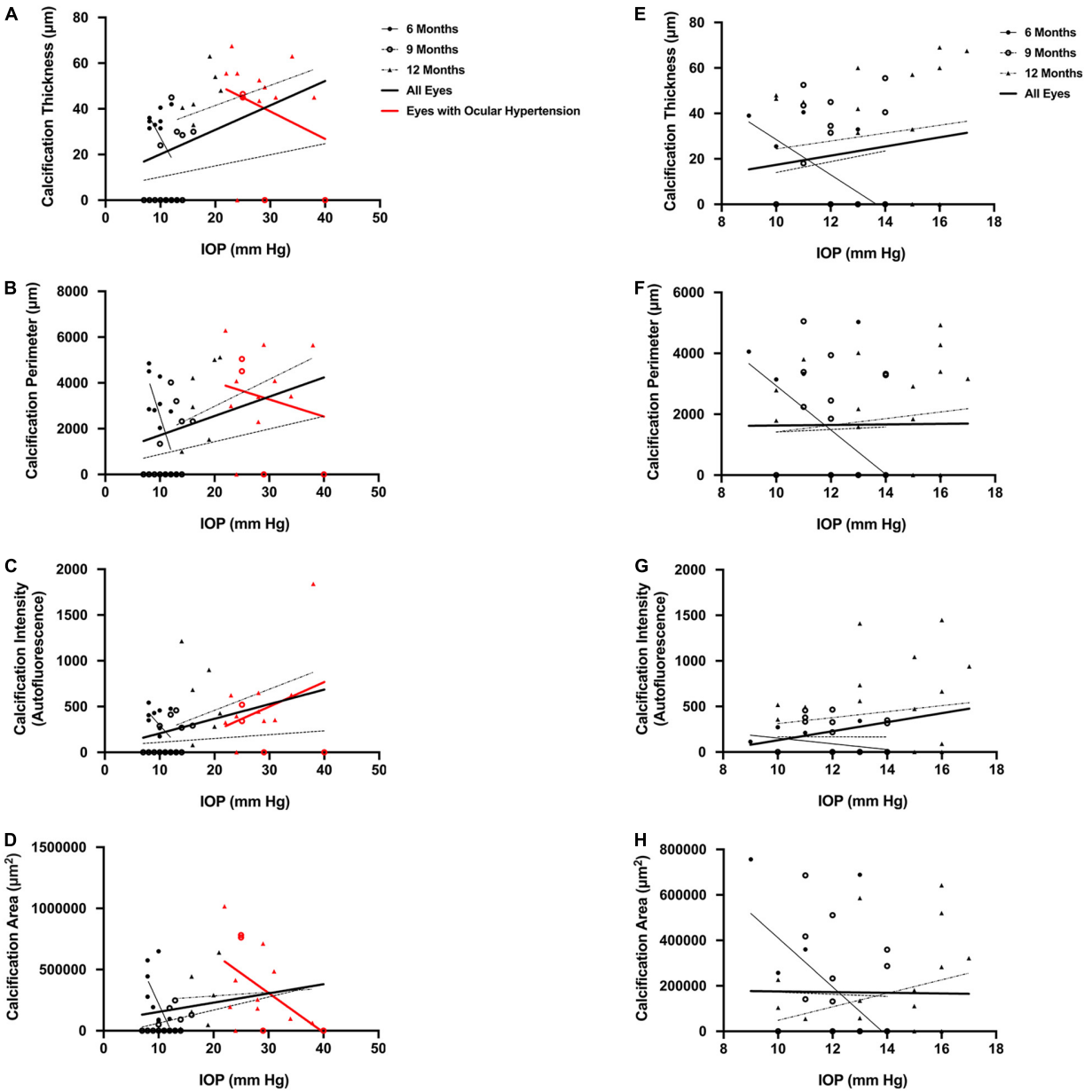

FIGURE 8 | Scatterplots for DBA/2J mice demonstrating weak to moderate correlations between **(A)** intraocular pressure (IOP) and calcification thickness among all eyes ($r = 0.42$, $P = 0.004$), **(B)** IOP and calcification perimeter length among all eyes ($r = 0.36$, $P = 0.01$), and **(C)** IOP and calcification intensity among all eyes ($r = 0.39$, $P = 0.007$), but not **(D)** IOP and calcification area among all eyes ($r = 0.25$, $P = 0.09$). Scatterplots for *Gpnmb*$^{+}$/SjJ mice demonstrate no relationship between **(E)** IOP and calcification thickness among all eyes ($r = 0.16$, $P = 0.29$), **(F)** IOP and calcification perimeter length among all eyes ($r = 0.01$, $P = 0.95$), **(G)** IOP and calcification intensity among all eyes ($r = 0.26$, $P = 0.08$), and **(H)** IOP and calcification area among all eyes ($r = –0.01$, $P = 0.93$). There were no significant positive correlations when mice in either strain were examined at 6, 9, and 12 months of age and there were no relationships between IOP and quantitative measures of calcification in mice with ocular hypertension. Error bars represent 95% confidence intervals. Sample sizes varied at each time point due to the number of mice with calcification. Sample sizes as in **Figure 6**.

Iris Pigment Dispersion and Corneal Calcification—Comparisons Among Age Groups

At time of euthanasia, DBA/2J mice demonstrated weak to moderate correlations between IPD and calcification thickness ($r = 0.48$, $P = 0.004$; **Figure 10A**), calcification perimeter ($r = 0.47$, $P = 0.008$; **Figure 10B**), calcification intensity ($r = 0.34$, $P = 0.048$; **Figure 10C**), calcification area ($r = 0.38$, $P = 0.03$; **Figure 10D**), and qualitative calcification ($r = 0.35$, $P = 0.04$). No correlations were observed in DBA2/J mice when IPD and corneal calcification were examined by individual age cohorts (6, 9, and 12 months).

TABLE 2 | Correlations between intraocular pressure and quantitative measures of corneal calcification in DBA/2J and DBA/2J-*Gpnmb*$^+$/SjJ mice.

Measure of corneal calcification	Pearson correlation coefficient (correlation with IOP)	*P*-value
All DBA2J eyes (*n* = 48)		
Thickness	0.42	0.004
Perimeter length	0.36	0.01
Intensity	0.39	0.007
Area	0.25	0.09
DBA/2J eyes at 6 months (*n* = 10)		
Thickness	−0.45	0.19
Perimeter length	−0.69	0.03
Intensity	−0.54	0.11
Area	−0.64	0.048
DBA/2J eyes at 9 months (*n* = 20)		
Thickness	0.23	0.33
Perimeter length	0.27	0.25
Intensity	0.19	0.42
Area	0.39	0.09
DBA/2J eyes at 12 months (*n* = 18)		
Thickness	0.33	0.20
Perimeter length	0.02	0.94
Intensity	0.36	0.16
Area	0.07	0.78
Eyes with ocular hypertension (*n* = 14)		
Thickness	−0.29	0.32
Perimeter length	−0.19	0.51
Intensity	0.33	0.26
Area	0.52	0.057
All DBA/2J-*Gpnmb*$^+$/SjJ eyes (*n* = 47)		
Thickness	0.16	0.29
Perimeter length	0.01	0.95
Intensity	0.26	0.08
Area	−0.01	0.93
DBA/2J-*Gpnmb*$^+$/SjJ eyes at 6 months (*n* = 10)		
Thickness	−0.65	0.04
Perimeter length	−0.54	0.11
Intensity	−0.36	0.31
Area	−0.54	0.10
DBA/2J-*Gpnmb*$^+$/SjJ eyes at 9 months (*n* = 17)		
Thickness	0.13	0.61
Perimeter length	0.03	0.91
Intensity	−0.002	0.99
Area	−0.03	0.92
DBA/2J-*Gpnmb*$^+$/SjJ eyes at 12 months (*n* = 20)		
Thickness	0.13	0.58
Perimeter length	0.13	0.58
Intensity	0.14	0.54
Area	0.30	0.20

IOP, intraocular pressure.

DISCUSSION

In the present study, we used DBA/2J-*Gpnmb*$^+$/SjJ mice as a control for DBA/2J mice to characterize anterior segment abnormalities in the context of the development of elevated IOP and ocular hypertension. The genotype of DBA/2J-*Gpnmb*$^+$/SjJ mice is identical to the DBA/2J genotype with the exception of a functional allele that prevents the development of IPD and thus of an elevated IOP (Howell et al., 2007). Therefore, it is assumed that DBA/2J-*Gpnmb*$^+$/SjJ mice serve as an appropriate control strain to evaluate the role of elevated IOP in the development of visual dysfunction characteristic of the DBA/2J mouse. However, the use of a rebound tonometer in the presence of corneal calcification on the DBA/2J mouse prompted the question of whether the increase in IOP was a result of an artificial elevation. To evaluate whether increased IOP in DBA/2J was due to IPD or corneal calcification the DBA/2J-*Gpnmb*$^+$/SjJ strain would need to have reduced or absent IPD, reduced or absent elevation in IOP, and similar levels of corneal calcification.

Only DBA/2J Mice, but Not DBA/2J-*Gpnmb*$^+$/SjJ Mice, Exhibit IPD and Clinically Significant Increases in Intraocular Pressure

We confirmed that DBA/2J-*Gpnmb*$^+$/SjJ mice do not develop IPD (Howell et al., 2007) by age 12 months, a time point when all DBA/2J mice in the present study showed evidence of IPD in both eyes. IPD is considered a principal contributor to the development of elevated IOP through the obstruction of aqueous outflow in DBA/2J mice (John et al., 1998; Libby et al., 2005; Scholz et al., 2008). We identified ocular hypertension in DBA/2J mice, where IOP increased on average by approximately 2.5 fold from age 6 to 12 months (**Figure 3**). IOP increased in a statistically significant manner from 6 to 9 months of age and then again more pronounced from 9 to 12 months in DBA/2J mice, with ocular hypertension developing and continuing after 43 weeks of age (**Figure 3**), a time-course pattern of IOP increase that is consistent with previous reports (Libby et al., 2005; Williams et al., 2013; Wang and Dong, 2016) and that is absent in DBA/2J-*Gpnmb*$^+$/SjJ mice.

Previous studies have demonstrated the absence of an age-related IOP elevation in DBA/2J-*Gpnmb*$^+$/SjJ mice (Howell et al., 2007). The present study confirmed this for the first 9 months of life, while we observed a statistically significant increase in IOP in the last quarter of the 12-month observation period. We observed a modest average increase in IOP of approximately 1 mm Hg in DBA/2J-*Gpnmb*$^+$/SjJ mice by age 12 months. While this finding itself was statistically significant it appears biologically and clinically not significant as it does not lead to ocular hypertension (**Figures 3**, **4**). The lack of significantly elevated IOP, and the lack of IPD supports the use of the DBA/2J-*Gpnmb*$^+$/SjJ strain as a suitable control animal for the DBA/2J strain up to 12 months of age.

The Degree of Corneal Calcification Does Not Differ Between DBA/2J and DBA/2J-*Gpnmb*$^+$/SjJ Mice

At the same time, we measured a moderate but clinically relevant generalized increase in qualitative corneal calcification with age in both DBA/2J and DBA/2J-*Gpnmb*$^+$/SjJ mice (**Figure 5**),

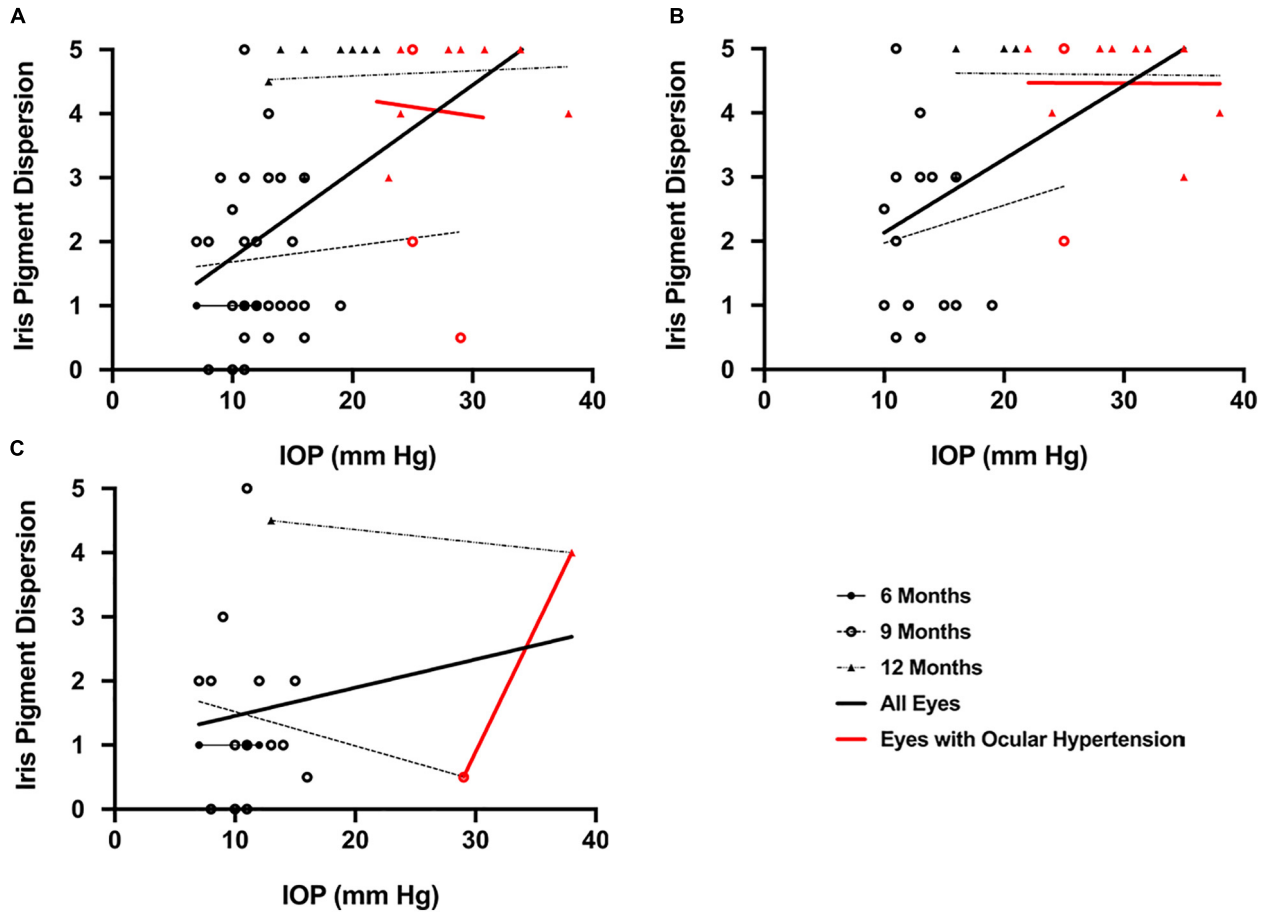

FIGURE 9 | Scatterplots demonstrating a moderate correlation between **(A)** intraocular pressure (IOP) and qualitative iris pigment dispersion (IPD) in DBA/2J mice ($r = 0.57$, $P < 0.001$) which **(B)** increased when only mice with calcification were included in the analysis ($r = 0.60$, $P < 0.001$) and **(C)** was not detected when mice without calcification were excluded from analysis ($r = 0.22$). There were no significant correlations between IOP and qualitative IPD in mice with ocular hypertension. Error bars represent 95% confidence intervals. Sample sizes varied at each time point due to the number of mice with calcification. Sample sizes as in **Figure 6**.

where at age 12 months the degree of corneal calcification was not statistically significantly different between the two strains when assessed qualitatively (**Figure 5B**) or quantitatively (**Figures 6A–D**).

Elevated IOP characteristic of the DBA/2J mouse strain has previously been attributed to blockage of the aqueous humor pathway due to IPD, peripheral synechiae, and iris atrophy (John et al., 1998; Chang et al., 1999; Anderson et al., 2002; Libby et al., 2005; Howell et al., 2007; Scholz et al., 2008). While corneal thickness has been associated with elevated IOP in DBA/2J mice (Inman et al., 2006; Chou et al., 2011), corneal calcification, although previously described (John et al., 1998; Bricker-Anthony and Rex, 2015; Turner et al., 2017), has not been studied in the context of elevated IOP. Furthermore, the presence and extent of corneal calcification has not been evaluated in DBA/2J-*Gpnmb*$^{+}$/SjJ mice.

Not surprisingly, nearly identical incidences of corneal calcification were seen in both DBA/2J and DBA/2J-*Gpnmb*$^{+}$/SjJ mice (**Figure 5**). These data indicate that the genetic alterations introduced into the DBA/2J-*Gpnmb*$^{+}$/SjJ strain do not affect corneal calcification as expected. The lack of significant differences in corneal calcification supports the use of the DBA/2J-*Gpnmb*$^{+}$/SjJ strain as a suitable control animal for the DBA/2J strain up to 12 months of age. DBA/2J mice demonstrated a statistically significant increase in the qualitative (**Figure 5B**) but not quantitative measures of corneal calcification (**Figure 6**) from 9 to 12 months while differences among the three ages of DBA/2J-*Gpnmb*$^{+}$/SjJ mice were not statistically significant (**Figures 5B**, **6**). However, we observed no statistically significant differences in qualitative and quantitative measures of corneal calcification when comparing DBA/2J to DBA/2J-*Gpnmb*$^{+}$/SjJ mice (**Figures 5B**, **6**). In sum, while not statistically significantly increasing over time, DBA/2J-*Gpnmb*$^{+}$/SjJ mice nevertheless display corneal calcification at age 12 months that is not different from that in DBA/2J mice.

When the dependence of IOP on the degree of corneal calcification was analyzed in DBA/2J mice, a trend toward a correlation with increased IOP using qualitative measures was found, though it was not statistically significant (**Figure 7**). Quantitative measures of calcification were significantly

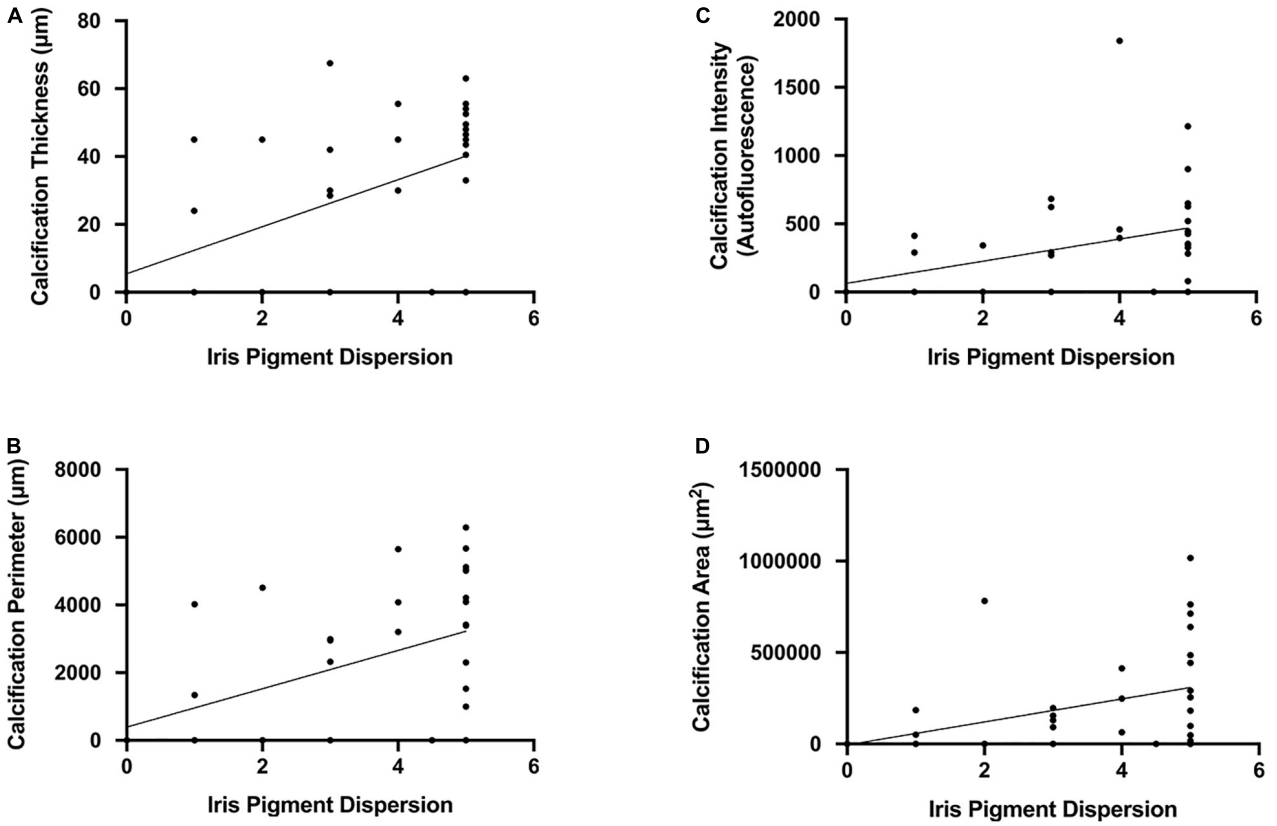

FIGURE 10 | Scatterplots demonstrating weak to moderate correlations between iris pigment dispersion and **(A)** calcification thickness (r = 0.48, P = 0.004), **(B)** calcification perimeter (r = 0.47, P = 0.008), **(C)** calcification intensity (r = 0.34, P = 0.048), and **(D)** calcification area (r = 0.38, P = 0.03). Error bars represent 95% confidence intervals. Sample sizes varied at each time point due to the number of mice with calcification. Sample sizes as in **Figure 6**.

correlated with IOP in DBA/2J mice (**Figure 8**). However, for the subset of eyes in DBA/2J mice that developed ocular hypertension, IOP was not positively correlated with measures of calcification (**Figures 7**, **8**). DBA/2J-*Gpnmb*$^{+}$/SjJ mice did not demonstrate significant increases in IOP with increases in qualitative (**Figure 7**) or quantitative measures of calcification (**Figure 8**) and at 12 months of age the degree of corneal calcification in DBA/2J-*Gpnmb*$^{+}$/SjJ mice was statistically not different from that in DBA/2J mice (**Figures 5**, **6**).

Taken together these findings indicate that while increasing levels of IPD as an anterior chamber abnormality are highly correlated with the development of increased IOP and ultimately ocular hypertension, the development of corneal calcification as an anterior chamber abnormality in both DBA/2J-*Gpnmb*$^{+}$/SjJ and DBA/2J mice was independent of changes in IOP over time.

Limitations and Future Studies

A limitation of the present study is the lack of an invasive cannulation IOP measurement to confirm the results of the rebound tonometer measurements. While it would have been insightful to identify whether the increase in IOP in the DBA/2J was influenced by the method of IOP determination, rebound tonometry is a widely accepted and validated method and ocular hypertension in the DBA/2J strain is well documented. Furthermore, the method of measurement does not affect our primary observation that corneal calcification does not cause elevated IOP readings. This is evident by the consistent, longitudinal, IOP measurements in both strains, consistently elevated IOP in the DBA/2J, a lack of ocular hypertension in the DBA/2J-*Gpnmb*$^{+}$/SjJ strain combined with similar corneal calcification in both strains. As we only evaluated mice up to 12 months of age, further investigation should seek to evaluate the role of corneal calcification on IOP beyond this age.

In addition, given the small sample size of the present study and the variability in disease progression seen for the DBA/2J strain, statistically significant results from the present study suggest that future, larger sized studies consider the potential impact of corneal calcification in both the DBA/2J and the DBA/2J-*Gpnmb*$^{+}$/SjJ strain on relevant preclinical outcome measures other than IOP.

SUMMARY

Previous reports indicated that DBA/2J mice exhibit falsely elevated IOP when measured non-invasively (Turner et al., 2017). One possible explanation for this artifact was the presence of calcium deposits on the cornea disrupting rebound tonometry

readings. In the present study we have shown in the DBA/2J-*Gpnmb*$^{+}$/SjJ strain, a strain derived from the DBA/2J strain to lack IPD, that even in the presence of significant corneal calcification IOP measurement stays consistent and is not artificially elevated. While there was a positive correlation between calcification and IOP in the 12-month-old DBA/2J animals, similar levels of calcification in the 12-month-old sub-groups combined with a lack of elevated IOP in the DBA/2J-*Gpnmb*$^{+}$/SjJ control strain does not support a causative relationship between these factors. These data strongly support the argument that corneal calcification does not cause false readings of IOP measured non-invasively and support the use of the DBA/2J-*Gpnmb*$^{+}$/SjJ animal as an ideal control animal to be paired with the DBA/2J mouse to investigate diseases of the eye related to elevated intraocular pressure.

The DBA/2J mouse strain has been widely used as a model for ocular hypertension and glaucoma due to the presence of progressively worsening anterior chamber abnormalities and IOP increasing with age (Sheldon et al., 1995; Inman et al., 2006; Schlamp et al., 2006; Burroughs et al., 2011; Bosco et al., 2018; Mathieu et al., 2018; Buchanan et al., 2019; Jassim et al., 2019). In this study, we used strain-matched DBA/2J-*Gpnmb*$^{+}$/SjJ mice to determine the relative contributions of corneal calcification and IPD to the apparent elevation of IOP characteristic of the DBA/2J mouse strain.

DATA AVAILABILITY STATEMENT

The original contributions presented in the study are included in the article. Further inquiries can be directed to the corresponding author.

ETHICS STATEMENT

The animal study was reviewed and approved by the University of Missouri—Kansas City, Institutional Animal Care and Use Committee.

AUTHOR CONTRIBUTIONS

PK conceived and designed the experiments. LR, RD, and MM performed the experiments. LR and PK wrote the manuscript. All authors analyzed the data, edited, and reviewed the manuscript.

FUNDING

Research reported in this publication was supported in part by grants from the National Eye Institute (EY022774 and EY031248), the National Center for Research Resources and National Institute of General Medical Sciences (RR027093) of the National Institutes of Health (PK). The content was solely the responsibility of the authors and does not necessarily represent the official views of the National Institutes of Health. This research project was also partially funded in memory of Dr. Larry Piebenga by the Dawe Family Foundation. Additional support by the Felix and Carmen Sabates Missouri Endowed Chair in Vision Research, a Challenge Grant from Research to Prevent Blindness and the Vision Research Foundation of Kansas City was gratefully acknowledged.

ACKNOWLEDGMENTS

Support by Heather Johnson and Christa Montgomery is gratefully acknowledged.

REFERENCES

Anderson, M. G., Smith, R. S., Hawes, N. L., Zabaleta, A., Chang, B., Wiggs, J. L., et al. (2002). Mutations in genes encoding melanosomal proteins cause pigmentary glaucoma in DBA/2J mice. *Nat. Genet.* 30, 81–85. doi: 10.1038/ng794

Bosco, A., Anderson, S. R., Breen, K. T., Romero, C. O., Steele, M. R., Chiodo, V. A., et al. (2018). Complement C3-Targeted gene therapy restricts onset and progression of neurodegeneration in chronic mouse glaucoma. *Mol. Ther.* 26, 2379–2396. doi: 10.1016/j.ymthe.2018.08.017

Brandt, J. D. (2001). The influence of corneal thickness on the diagnosis and management of glaucoma. *J. Glaucoma* 10(5 Suppl. 1), S65–S67. doi: 10.1097/00061198-200110001-200110023

Bricker-Anthony, C., and Rex, T. S. (2015). Neurodegeneration and vision loss after mild blunt trauma in the C57Bl/6 and DBA/2J mouse. *PLoS One* 10:e0131921. doi: 10.1371/journal.pone.0131921

Buchanan, R. A., Foley, K. E., Pepper, K. W., Reagan, A. M., Keezer, K. J., Hewes, A. A., et al. (2019). Meox2 haploinsufficiency accelerates axonal degeneration in DBA/2J glaucoma. *Invest. Ophthalmol. Vis. Sci.* 60, 3283–3296. doi: 10.1167/iovs.18-26126

Burroughs, S. L., Kaja, S., and Koulen, P. (2011). Quantification of deficits in spatial visual function of mouse models for glaucoma. *Invest. Ophthalmol. Vis. Sci.* 52, 3654–3659. doi: 10.1167/iovs.10-7106

Chang, B., Smith, R. S., Hawes, N. L., Anderson, M. G., Zabaleta, A., Savinova, O., et al. (1999). Interacting loci cause severe iris atrophy and glaucoma in DBA/2J mice. *Nat. Genet.* 21, 405–409. doi: 10.1038/7741

Chou, T. H., Kocaoglu, O. P., Borja, D., Ruggeri, M., Uhlhorn, S. R., Manns, F., et al. (2011). Postnatal elongation of eye size in DBA/2J mice compared with C57BL/6J mice: in vivo analysis with whole-eye OCT. *Invest. Ophthalmol. Vis. Sci.* 52, 3604–3612. doi: 10.1167/iovs.10-6340

Grillo, S. L., and Koulen, P. (2015). Psychophysical testing in rodent models of glaucomatous optic neuropathy. *Exp. Eye Res.* 141, 154–163. doi: 10.1016/j.exer.2015.06.025

Grillo, S. L., Keereetaweep, J., Grillo, M. A., Chapman, K. D., and Koulen, P. (2013). N-Palmitoylethanolamine depot injection increased its tissue levels and those of other acylethanolamide lipids. *Drug Des. Dev. Ther.* 7, 747–752. doi: 10.2147/DDDT.S48324

Howell, G. R., Libby, R. T., Marchant, J. K., Wilson, L. A., Cosma, I. M., Smith, R. S., et al. (2007). Absence of glaucoma in DBA/2J mice homozygous for wild-type versions of Gpnmb and Tyrp1. *BMC Genet.* 8:45. doi: 10.1186/1471-2156-8-45

Inman, D. M., Sappington, R. M., Horner, P. J., and Calkins, D. J. (2006). Quantitative correlation of optic nerve pathology with ocular pressure and corneal thickness in the DBA/2 mouse model of glaucoma. *Invest. Ophthalmol. Vis. Sci.* 47, 986–996. doi: 10.1167/iovs.05-0925

Jackson, H. M., Onos, K. D., Pepper, K. W., Graham, L. C., Akeson, E. C., Byers, C., et al. (2015). DBA/2J genetic background exacerbates spontaneous lethal

seizures but lessens amyloid deposition in a mouse model of Alzheimer's disease. *PLoS One* 10:e0125897. doi: 10.1371/journal.pone.0125897

Jassim, A. H., Coughlin, L., Harun-Or-Rashid, M., Kang, P. T., Chen, Y. R., and Inman, D. M. (2019). Higher reliance on glycolysis limits glycolytic responsiveness in degenerating glaucomatous optic nerve. *Mol. Neurobiol.* 56, 7097–7112. doi: 10.1007/s12035-019-1576-1574

John, S. W., Smith, R. S., Savinova, O. V., Hawes, N. L., Chang, B., Turnbull, D., et al. (1998). Essential iris atrophy, pigment dispersion, and glaucoma in DBA/2J mice. *Invest. Ophthalmol. Vis. Sci.* 39, 951–962.

Kaja, S., Naumchuk, Y., Grillo, S. L., Borden, P. K., and Koulen, P. (2014). Differential up-regulation of Vesl-1/Homer 1 protein isoforms associated with decline in visual performance in a preclinical glaucoma model. *Vision Res.* 94, 16–23. doi: 10.1016/j.visres.2013.10.018

Libby, R. T., Anderson, M. G., Pang, I. H., Robinson, Z. H., Savinova, O. V., Cosma, I. M., et al. (2005). Inherited glaucoma in DBA/2J mice: pertinent disease features for studying the neurodegeneration. *Vis. Neurosci.* 22, 637–648. doi: 10.1017/S0952523805225130

Mathieu, E., Gupta, N., Paczka-Giorgi, L. A., Zhou, X., Ahari, A., Lani, R., et al. (2018). Reduced cerebrospinal fluid inflow to the optic nerve in glaucoma. *Invest. Ophthalmol. Vis. Sci.* 59, 5876–5884. doi: 10.1167/iovs.18-24521

Montgomery, C. L., Keereetaweep, J., Johnson, H. M., Grillo, S. L., Chapman, K. D., and Koulen, P. (2016). Changes in retinal N-Acylethanolamines and their oxylipin derivatives during the development of visual impairment in a mouse model for glaucoma. *Lipids* 51, 857–866. doi: 10.1007/s11745-016-4161-x

Pease, M. E., Cone, F. E., Gelman, S., Son, J. L., and Quigley, H. A. (2011). Calibration of the TonoLab tonometer in mice with spontaneous or experimental glaucoma. *Invest. Ophthalmol. Vis. Sci.* 52, 858–864. doi: 10.1167/iovs.10-5556

Rutsch, F., Nitschke, Y., and Terkeltaub, R. (2011). Genetics in arterial calcification: pieces of a puzzle and cogs in a wheel. *Circ. Res.* 109, 578–592. doi: 10.1161/CIRCRESAHA.111.247965

Schlamp, C. L., Li, Y., Dietz, J. A., Janssen, K. T., and Nickells, R. W. (2006). Progressive ganglion cell loss and optic nerve degeneration in DBA/2J mice is variable and asymmetric. *BMC Neurosci.* 7:66. doi: 10.1186/1471-2202-7-66

Scholz, M., Buder, T., Seeber, S., Adamek, E., Becker, C. M., and Lutjen-Drecoll, E. (2008). Dependency of intraocular pressure elevation and glaucomatous changes in DBA/2J and DBA/2J-Rj mice. *Invest. Ophthalmol. Vis. Sci.* 49, 613–621. doi: 10.1167/iovs.07-0745

Sheldon, W. G., Warbritton, A. R., Bucci, T. J., and Turturro, A. (1995). Glaucoma in food-restricted and ad libitum-fed DBA/2NNia mice. *Lab Anim. Sci.* 45, 508–518.

Shin, J. B., Longo-Guess, C. M., Gagnon, L. H., Saylor, K. W., Dumont, R. A., Spinelli, K. J., et al. (2010). The R109H variant of fascin-2, a developmentally regulated actin crosslinker in hair-cell stereocilia, underlies early-onset hearing loss of DBA/2J mice. *J. Neurosci.* 30, 9683–9694. doi: 10.1523/JNEUROSCI.1541-10.2010

Swaminathan, S., Lu, H., Williams, R. W., Lu, L., and Jablonski, M. M. (2013). Genetic modulation of the iris transillumination defect: a systems genetics analysis using the expanded family of BXD glaucoma strains. *Pigment Cell Melanoma Res.* 26, 487–498. doi: 10.1111/pcmr.12106

Tham, Y. C., Li, X., Wong, T. Y., Quigley, H. A., Aung, T., and Cheng, C. Y. (2014). Global prevalence of glaucoma and projections of glaucoma burden through 2040: a systematic review and meta-analysis. *Ophthalmology* 121, 2081–2090. doi: 10.1016/j.ophtha.2014.05.013

Turner, A. J., Vander Wall, R., Gupta, V., Klistorner, A., and Graham, S. L. (2017). DBA/2J mouse model for experimental glaucoma: pitfalls and problems. *Clin. Exp. Ophthalmol.* 45, 911–922. doi: 10.1111/ceo.12992

van den Broek, F. A., and Beynen, A. C. (1998). The influence of dietary phosphorus and magnesium concentrations on the calcium content of heart and kidneys of DBA/2 and NMRI mice. *Lab. Anim.* 32, 483–491. doi: 10.1258/002367798780599758

Wang, J., and Dong, Y. (2016). Characterization of intraocular pressure pattern and changes of retinal ganglion cells in DBA2J glaucoma mice. *Int. J. Ophthalmol.* 9, 211–217. doi: 10.18240/ijo.2016.02.05

Williams, P. A., Howell, G. R., Barbay, J. M., Braine, C. E., Sousa, G. L., John, S. W., et al. (2013). Retinal ganglion cell dendritic atrophy in DBA/2J glaucoma. *PLoS One* 8:e72282. doi: 10.1371/journal.pone.0072282

Wong, A. A., and Brown, R. E. (2007). Age-related changes in visual acuity, learning and memory in C57BL/6J and DBA/2J mice. *Neurobiol. Aging* 28, 1577–1593. doi: 10.1016/j.neurobiolaging.2006.07.023

Yang, X. L., van der Merwe, Y., Sims, J., Parra, C., Ho, L. C., Schuman, J. S., et al. (2018). Age-related changes in eye, brain and visuomotor behavior in the DBA/2J mouse model of chronic glaucoma. *Sci. Rep.* 8:4643. doi: 10.1038/s41598-018-22850-22854

Conflict of Interest: The authors declare that the research was conducted in the absence of any commercial or financial relationships that could be construed as a potential conflict of interest.

Publisher's Note: All claims expressed in this article are solely those of the authors and do not necessarily represent those of their affiliated organizations, or those of the publisher, the editors and the reviewers. Any product that may be evaluated in this article, or claim that may be made by its manufacturer, is not guaranteed or endorsed by the publisher.

frontiers in Neuroscience

ORIGINAL RESEARCH
published: 04 February 2022
doi: 10.3389/fnins.2022.840443

SIRT4 Is Highly Expressed in Retinal Müller Glial Cells

*Wei Wei†, Piaopiao Hu†, Mengqi Qin, Guiping Chen, Feifei Wang, Shengrui Yao, Ming Jin, Zhi Xie and Xu Zhang**

Jiangxi Provincial Key Laboratory for Ophthalmology, Jiangxi Clinical Research Center of Ophthalmic Disease, Affiliated Eye Hospital of Nanchang University, Nanchang, China

Sirtuin 4 (SIRT4) is one of seven mammalian sirtuins that possesses ADP-ribosyltransferase, lipoamidase and deacylase activities and plays indispensable role in metabolic regulation. However, the role of SIRT4 in the retina is not clearly understood. The purpose of this study was to explore the location and function of SIRT4 in the retina. Therefore, immunofluorescence was used to analyze the localization of SIRT4 in rat, mouse and human retinas. Western blotting was used to assess SIRT4 and glutamine synthetase (GS) protein expression at different developmental stages in C57BL/6 mice retinas. We further analyzed the retinal structure, electrophysiological function and the expression of GS protein in SIRT4-deficient mice. Excitotoxicity was caused by intravitreal injection of glutamate (50 nmol) in mice with long-term intraperitoneal injection of resveratrol (20 mg/Kg), and then retinas were subjected to Western blotting and paraffin section staining to analyze the effect of SIRT4 on excitotoxicity. We show that SIRT4 co-locates with Müller glial cell markers (GS and vimentin). The protein expression pattern of SIRT4 was similar to that of GS, and both increased with development. There were no significant retinal structure or electrophysiological function changes in 2-month SIRT4-deficient mice, while the expression of GS protein was decreased. Moreover, long-term administration of resveratrol can upregulate the expression of SIRT4 and GS while reducing the retinal injury caused by excessive glutamate. These results suggest that SIRT4 is highly expressed in retinal Müller glial cells and is relevant to the expression of GS. SIRT4 does not appear to be essential in retinal development, but resveratrol, as an activator of SIRT4, can upregulate GS protein expression and protect the retina from excitotoxicity.

Keywords: SIRT4, Müller glia cell, glutamine synthetase, resveratrol, retina, excitotoxicity

OPEN ACCESS

Edited by:
Peter Koulen,
University of Missouri–Kansas City, United States

Reviewed by:
Monica Lamas,
Centro de Investigaciones y Estudios Avanzados, Instituto Politécnico Nacional de México (CINVESTAV), Mexico
Heberto Quintero,
University of Montreal Hospital Centre (CRCHUM), Canada
Mairaj Mohammad Siddiquei,
King Saud University, Saudi Arabia

***Correspondence:**
Xu Zhang
xuzhang19@163.com

†These authors have contributed equally to this work

Specialty section:
This article was submitted to Neurodegeneration, a section of the journal Frontiers in Neuroscience

Received: *21 December 2021*
Accepted: *13 January 2022*
Published: *04 February 2022*

Citation:
Wei W, Hu P, Qin M, Chen G, Wang F, Yao S, Jin M, Xie Z and Zhang X (2022) SIRT4 Is Highly Expressed in Retinal Müller Glial Cells. Front. Neurosci. 16:840443. doi: 10.3389/fnins.2022.840443

INTRODUCTION

Sirtuins are a class of histone deacetylases that regulate a range of pathophysiological processes, including cell senescence, inflammation, metabolism, and cell proliferation (Luo et al., 2017; Yang et al., 2020). Mammals have seven kinds of sirtuins (SIRT1-7), among them, SIRT3-5 is expressed in cell mitochondria. Previous studies have explored the role of SIRT3 and SIRT5 in the retina (Lin et al., 2016), while few studies have investigated the role of SIRT4 in the retina. SIRT4 is one of seven mammalian sirtuins that use NAD to ADP-ribosylate and

downregulate glutamate dehydrogenase (GDH) activity. SIRT4 inhibits the enzymatic activity of GDH and limits the metabolism of glutamate and glutamine in order to produce ATP (Haigis et al., 2006). The physiological effects of SIRT4 include the role of the insulin response (Haigis et al., 2006), fatty acid metabolism (Laurent et al., 2013), tumor inhibition (Jeong et al., 2013), and regulation of ATP levels in muscles and liver (Ho et al., 2013). In the brain, SIRT4 is localized to mitochondria, expressed at high levels in astrocytes in the postnatal brain and radial glia in embryonic tissues, and shows a lower expression during development (Komlos et al., 2013). However, little is known about the function of SIRT4 in the retina, especially its role in the development of Müller glial cells (MGCs). Recently, there have been new insights into the activity of SIRT4 that SIRT4 is a lysine deacylase (Anderson et al., 2017). Our understanding of SIRT4 enzyme activity is still incomplete and whether there are other enzyme activities of SIRT4 in MGCs remains to be explored.

MGCs have a unique localization, in that they span the entire retina and are present between vessels and neurons (Bringmann et al., 2006; Goldman, 2014; Toft-Kehler et al., 2017). Loss of mature MGCs in a range of species leads to disruptions in retinal structure, which causes impaired neuronal function and visual deficits (Wohl et al., 2017). MGC dysfunction is implicated in many retinal diseases, such as glaucoma, proliferative retinopathies and age-related macular degeneration (AMD) (Devoldere et al., 2019; Simón et al., 2019). MGCs participate in the uptake glutamate released by synapses and amidate glutamate to the nontoxic amino acid glutamine by glutamine synthetase (GS) (Fletcher et al., 2005). Numerous studies have demonstrated that MGC dysfunction always results in an increase in retinal glutamate level that leads to excitatory neural toxicity (Bringmann et al., 2009; Mysona et al., 2009; Bringmann and Wiedemann, 2011). Our previous studies suggest that SIRT4 protein is the only filamentous expression of the sirtuins family in the retina of adult rats (Luo et al., 2017). The expression pattern of SIRT4 is similar to that of MGCs, suggesting that SIRT4 is associated with the function of MGCs.

Resveratrol (RES) is a kind of SIRT4 activator that increases SIRT4 gene and protein expression (Sheng et al., 2018). In this study, we upregulated SIRT4 by intraperitoneal injection of RES to explore the influence of SIRT4 on the retina. Given that SIRT4 is a therapeutic target for neurodegenerative disorders (Dai et al., 2018), and plays a role in the metabolism of glutamate and glutamine (Haigis et al., 2006), we wanted to determine whether SIRT4 works in excitatory toxicity caused by glutamate and the role of GS. Although SIRT4 protein and MGCs have similar localization in the retina, and both participate in the regulation of glutamate-glutamine, there are still many questions. Whether SIRT4 affects the morphology and function of MGCs and even the retina remains unknown.

Thus, we studied the location of SIRT4 in the retina and explore whether SIRT4 affects retinal structure and function by regulating MGC maturation to clarify the role of SIRT4 in the retina. Furthermore, SIRT4 expression was downregulated by gene knockout and upregulated by intraperitoneal injection of RES to study the effects of SIRT4 on GS protein expression and retinal structure.

MATERIALS AND METHODS

Tissue Preparation

C57BL/6 mice and Sprague-Dawley (SD) rats aged 6-8 weeks were originally obtained from Hunan Slac Jinda Laboratory Animal Co., Ltd. (license number: SCXK1201-0004) and the Center of Jiangxi University of Traditional Chinese Medicine (license number: SCXX12018-0003), respectively. SIRT4 knockout (KO) mice from a pure C57BL/6 background were produced by Cyagen Biosciences, Suzhou, China. Mice were interbred to yield SIRT4^{KO} mice and the corresponding wide-type control. Genotypes were determined by PCR analysis from genomic DNA obtained from tail biopsy specimens before the experiments. The animals were housed under standard conditions with free access to food and water and were maintained in temperature-controlled rooms on a normal 12-h light/12-h dark cycle. All experiments were conducted in accordance with the Animal Care and Use Committees of Nanchang University Medical School.

Three pairs of donor eyes of different ages (age range 18-59 years old) were obtained from the Red Cross Society of China Jiangxi Branch, and all volunteers signed informed consent documents in written form in accordance with the principles of the Declaration of Helsinki. All experiments involving human samples were approved by the Ethics Committee of Affiliated Eye Hospital of Nanchang University. To obtain fresh eye tissues for protein extraction and staining, we restricted the samples in the present study to those received less than 48 h postmortem. The previous medical and ocular histories of all donors were assessed to exclude donors with any eye disease. The retinas were processed as described below.

Drug Treatment

Resveratrol (RES) (3,4′,5-trihydroxy-trans-stilbene, Sigma-Aldrich) was dissolved in 6.67% dimethylsulfoxide (DMSO) to a concentration of 5 mg/ml. Two-month-old C57BL/6 mice were intraperitoneally injected with RES (20 mg/kg) for five consecutive days before glutamate intravitreal injection. The control group was intraperitoneally injected with an equal volume of 6.67% DMSO.

Intravitreal Injection

The mice were anesthetized by i.p., injection of 3.6% chloral hydrate (10 ml/kg). Before injection, pupillary dilatation was maintained by administering tropicamide phenylephrine eye drops 3 times (Santen Pharmaceutical Co., Ltd., Japan), and topical anesthesia was achieved by administering proparacaine hydrochloride eye drops 3 times (Alcon Co., Ltd., Belgium). Levofloxacin eye drops (Santen Pharmaceutical Co., Ltd., Japan) were administered three times to clean conjunctival sacs.

One microliter 50 nmol glutamate (Solarbio) soluble in 37°C normal saline (NS) was injected into the right eye with a 30-gauge (30 G) needle (Hamilton). The needle punctured the center of the vitreous chamber approximately 1.5 mm from the limbus in the superior temporal quadrant. The tip of the needle was pointed in the direction of the optic nerve to avoid injuring the lens. The

tip was visible through the dilated pupil, and the drug was slowly injected. The needle was left in the eye for an additional 20 s to allow the eye to adjust to the increase in volume and then pulled out. The left eye received the same volume of NS as this was used as the solvent for glutamate. After injection, the eyes were treated three times with levofloxacin eye drops (Santen Pharmaceutical Co., Ltd., Japan). While recovering from anesthesia, the animals were placed in their cages. At least three animals were used for each experimental condition.

Histopathology

The eyes were enucleated and fixed in FAS for 24 h at 4°C. After washing in PBS, the tissues were transferred to 70% ethanol overnight, then dehydrated and embedded in paraffin. Fixed eyeballs were cut into 5-μm-thick pieces parallel to the maximal circumference of the eyeball through the optic disk. The tissues were stained with hematoxylin and eosin (H&E) and observed under light microscope (Leica, Heidelberg, Germany). Light microscope images were obtained at 20 × and 40 × magnification. To evaluate the differences in retinal structure, the thickness of the total retina, the ganglion cell layer (GCL), the inner plexiform layer (IPL), the inner nuclear layer (INL), the outer plexiform layer (OPL), the outer nuclear layers (ONL) and the layer of photoreceptor outer segment (POSL). All measurements were measured at 1 mm away from the center of the optic disk, and three sections per eye were averaged.

TUNEL Assay

For the detection of apoptotic cells, terminal deoxynucleotidyl transferase dUTP nick end labeling (TUNEL) staining was performed using the TransDetect *In situ* Fluorescein TUNEL Cell Apoptosis Detection Kit (TransGen Biotech, Beijing, China). Before staining, the paraffin sections were dewaxed and rehydrated. The nuclei were costained with 4-6-diamidino-2-phenylindole (DAPI, Boster, Wuhan, China).

Immunofluorescence Staining

The animals were anesthetized with an intraperitoneal injection of 3.6% chloral hydrate (10 ml/kg). Retinas were harvested at postnatal days 5 (P5), 10 (P10), 15 (P15), 25 (P25), and 60 (P60). The eye were fixed in 4% PFA in phosphate-buffered saline (PBS) overnight and sequentially immersed in 10%, 20%, and 30% sucrose in PBS, mounted in optimal cutting temperature (OCT) compound (Tissue-Tek; Sakura Finetek, Torrance, CA, United States) and frozen at −80°C. Frozen sections of eyes were dried at room temperature after cutting to 7 μm thickness with a Leica cryostat (CM1950, Heidelberger, Germany). The sections were washed with PBS and blocked in PBS containing 0.1% Triton X-100 and donkey serum (Solarbio, Beijing, China) for 1 h at room temperature. The slides were incubated with antibody overnight at 4°C. The working dilutions and sources of antibodies are listed in **Table 1**. The secondary antibodies included donkey-anti-rabbit-AlexaFlour® 488/594, donkey-anti-mouse- AlexaFlour® 488/594, and donkey-anti-goat-AlexaFlour® 488(Abcam, Cambridge, MA, United States) diluted to 1:200 in PBS plus 0.2% Triton X-100 at room temperature for 1 h. Subsequently, the sections were counterstained with DAPI.

TABLE 1 | Primary antibodies used in the study.

Antibody	Source	RRID	Type of Antibody	Dilution	MW
SIRT4	Abcam	ab10140	Goat polyclonal	1:100 (IHC) 1:1000 (WB)	36kDa
SIRT4	Abcam	ab124521	Rabbit polyclonal	1:1000 (WB)	32kDa
GS	Abcam	ab64613	Mouse mAb	1:100 (IHC)	37kDa
GS	Abcam	ab49873	Rabbit polyclonal	1:1000 (WB)	42kDa
Vimentin	CST	#5741	Rabbit mAb	1:100 (IHC) 1:1000 (WB)	57kDa
GFAP	Sigma	G3893	Mouse mAb	1:100 (IHC)	50kDa
CRALBP	Abcam	Ab243664	Rabbit mAb	1:1000 (WB)	36kDa
β-tubulin	TRANKS	J10715	Donkey anti-mouse	1:1000 (WB)	55kDa
β-actin	SCB	#L0117	Mouse mAb	1:1000 (WB)	42kDa

RRID = Research Resource Identification number; W = Molecular weight; IHC = immunohistochemical; WB = Western blot; kDa = kilo Dalton.

Coverslips were affixed to glass slides using anti-fading buffer (Bioworld Technology Inc., St. Louis Park, MN, United States) and visually examined under a Zeiss microscope (ZEISS, LSM800, GÖttingen, Germany) equipped with epifluorescence. Digitized images were obtained by using a Zeiss camera and the images were processed and compiled using Photoshop Software. The staining was repeated three or more times for each antibody.

Western Blotting

Retinas were lysed in the radioimmune precipitation assay buffer (RIPA) containing PMSF (Solarbio, Beijing, China). The lysates were processed with ultrasound and centrifuged. The protein concentration was determined using the BCA assay (Solarbio, Beijing, China) according to the manufacturers' instructions. For the Western blot analysis, aliquots containing an equal amount of protein (10 μg) were analyzed by SDS-polyacrylamide gel electrophoresis on 10% gels and were transferred to polyvinylidene fluoride membranes (PVDF, Millipore, United Kingdom), Membranes were blocked with 5% nonfat milk powder dissolved in Tris-buffered saline (TBS) containing 0.1% Tween 20 (TBST) for 1 h and incubated with the appropriate primary antibody (**Table 1**) overnight at 4°C. Membranes were then washed in TBST and incubated with HRP-conjugated secondary antibodies (Cell Signaling) for 1 h at room temperature. After further washing in TBST, target proteins on the membranes were detected with the EasySee Western Blot Kit (TRANS, Beijing, China) to collect digital images. The bands were quantified by integration of pixel intensity using ImageJ software and normalized to β-tubulin, which served as an internal control.

Electroretinogram

The mice were subjected to dim red light following overnight dark adaptation (> 12 h), and anesthetized with isoflurane to induce and chloral hydrate at 3.6% (10 ml/kg) to maintain anesthesia. Then, 1% tropicamide was used to dilate the pupils. The mouse temperature was maintained at 37°C with a heating pad. Stainless steel wire loops (0.1 mm diameter) were placed on the center of the cornea in 1% methylcellulose to prevent corneal dehydration. A reference electrode was placed at the midpoint of the line between the eye and ear and a grounding

electrode was placed near the tail. Two-month mice (n = 3) were subjected to the guidelines of the International Society for Clinical Electrophysiology of Vision (ISCEV), including the scotopic 0.01 ERG test (rod response) elicited by white light flashes at an intensity of 0.003 phot cd s/m^2, the scotopic 3.0 ERG test (cone and rod response) elicited by white light flashes at an intensity of 3.0 phot cd s/m^2, the scotopic 3.0 OPS test (oscillatory potentials) simultaneously elicited by white light flashes at an intensity of 20.0 phot cd s/m^2, the photopic 3.0 ERG test (cone response) under a white background elicited by white light flashes at an intensity of 2.8 phot cd s/m^2 and under a white background light at 29.0 phot cd/m^2 after 10 min of light adaptation. The amplitude of the a-wave was measured from the baseline to the trough, while that of the b-wave was measured from the maximum of the a-wave trough to the peak of the b-wave.

DNA Extraction and Quantitative PCR Assay

Quantitative PCR was used to measure SIRT4 gene expression in SIRT4^{KO} mice. Total DNA was extracted from mouse tails with the Ezup column animal genomic DNA extraction kit (B518251; Sangon Biotech, Shanghai, China). Mice were PCR-genotyped using the following primers: Primer 1 (for wide-type allele): 5′- ACGCTACCAACCTAATGGCATC -3′ (forward) and 5′- TCCAGACACCTTGAGTCGCCTAG -3′ (reverse). Primer 2 (for knockout allele): 5′- ACGCTACCAACCTAATGGCATC -3′ (forward) and 5′- GAAGGCGACACAGCTACTCCATC -3′ (reverse). The primers were chosen to amplify DNA using 2xSpecificTMTaq Master Mix (E010; Novoprotein Scientific Inc.). The procedure was initial denaturation (94°C for 3 min), then 35 cycles (94°C for 30 s, 60°C for 35 s and 72°C for 35 s), and then an extension step (72°C for 5 min). All data were chosen from the linear phase of amplification. Amplified DNA was analyzed on a 0.8% agarose gel (with ethidium bromide) and observed by Image Lab under UV light. The DNA Ladder (DM033; Novoprotein Scientific Inc.) were used to benchmark the DNA band sizes.

Data Analysis

All quantified data represent an average of at least three samples. SPSS 22.0, ImageJ and GraphPad Prism 8.0 software were used for statistical analysis. All data were presented as the mean ± standard error of the mean (SEM). Unpaired Student's t-test was used for two groups of samples to determine the significance of the response, while one-way ANOVA and Post Hoc Turkey Test were used for three or more groups of samples. $P < 0.05$ was considered to be statistically significant.

RESULTS

Sirtuin 4 Co-located With GS and Vimentin

MGCs span all cellular and plexiform layers of the retina, forming microvilli at the apical surface. We found that in rat, mouse and human retinas SIRT4-positive cells continuously penetrated the inner nuclear layer (INL) and the outer nuclear layer (ONL) in a longitudinal filamentous pattern, consistent with radial glial-like cell localization. To prove that SIRT4 is expressed in MGCs, we used two MGC markers (GS and vimentin) and glial fibrillary acidic protein (GFAP) to costain SIRT4 (**Figure 1**). Immunostaining showed that SIRT4 co-localized with GS, vimentin and GFAP which means that SIRT4 was highly

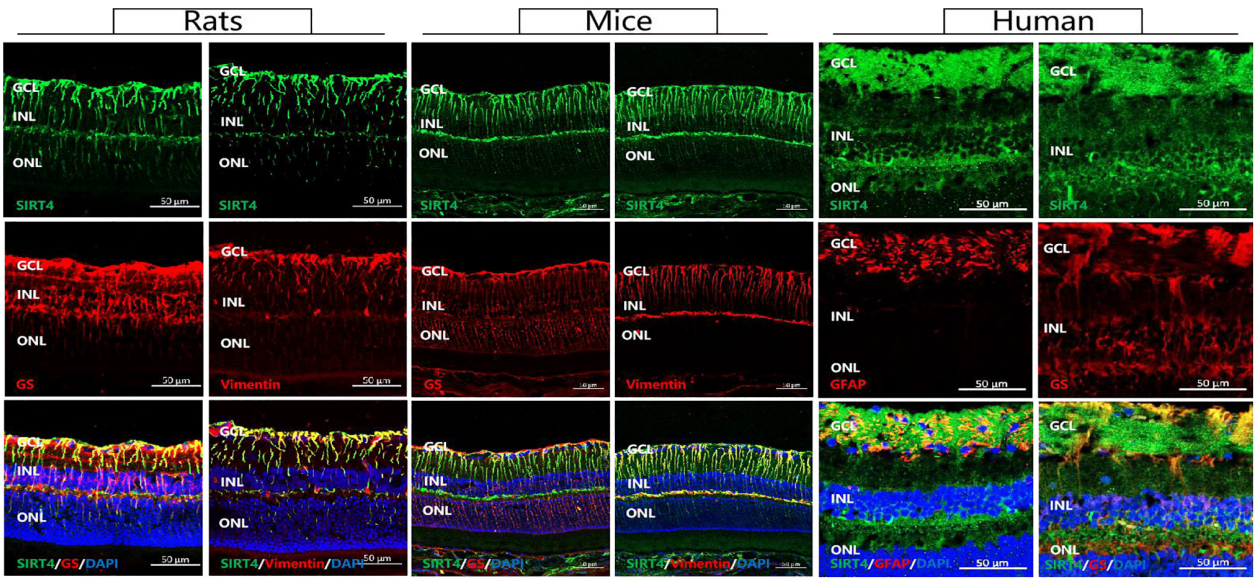

FIGURE 1 | Sirtuin 4 co-localized with MGC markers GS and vimentin. In rats and mice, SIRT4 was mainly expressed in the GCL and the INL in the form of longitudinal filamentous. GCL, ganglion cell layer; INL, inner nuclear layer; ONL, outer nuclear layer. GS, glutamine synthetase; GFAP, glial fibrillary acidic portein; DAPI was used to stain the nuclei (blue). Scale bar = 50 μm.

expressed in MGCs. Notably, SIRT4 was also expressed in the inner plexiform layer (IPL).

Expression of Sirtuin 4 in the Mice Retinas at Different Developmental Stages

To investigate the postnatal expression of SIRT4, we performed immunofluorescence labeling for SIRT4 from postnatal day 5 (P5), 10 (P10), 15 (P15), 25 (P25), and 60 (P60) in the mouse retina (**Figure 2A**). From P5 to P25, we found that SIRT4 had high expression in the nerve fiber layer (NFL), and SIRT4-positive cell processes ran perpendicular through the layers from the NFL to the ONL. For the P60 groups, the filamentous expression of SIRT4 was intermittently expressed in the inner plexiform layer (IPL), while little expression was noted in the outer plexiform layer (OPL). The protein expression of SIRT4 was detected, and it was found that the expression of SIRT4 increased during retinal development and reached its peak at 2 months (**Figure 2B**). The growth trend of GS protein expression was similar to that of SIRT4, and also reached its peak at P60, although the protein expression contents of the two were not completely consistent (**Figure 2C**). Cellular retinaldehyde-binding protein (CRALBP) and vimentin protein expression peaked at P25 (**Figures 2D,E**).

Retinal progenitor cells (RPCs) give rise to all six types of retinal neurons in a distinct spatiotemporal order spanning embryonic day 12 to postnatal day 10 in the murine retina (Turner and Cepko, 1987). MGCs, which mature later than most retinal cells, were observed to have the lowest GS and SIRT4 protein expression at P5 and the highest at P60. These results indicate that SIRT4 may be a relevant protein in the development of MGCs.

Retinal Structure of 2-Month Sirtuin 4-Deficient Mice

The $SIRT4^{KO}$ mice generated from Cyagen US inc., by removing exons 3-4 of the SIRT4 gene (**Figure 3A**). PCR was used to identify $SIRT4^{KO}$ mice, SIRT4 knockdown ($SIRT4^{KD}$) mice and wild-type ($SIRT4^{WT}$) mice (**Figure 3B**). The Western blotting results showed that SIRT4 and GS expression were lower in $SIRT4^{KD}$ mice than that in $SIRT4^{WT}$ mice, and SIRT4 was barely expressed in $SIRT4^{KO}$ mice (**Figures 3C,D**). There was no significant difference in retinal structure between $SIRT4^{KO}$ mice and $SIRT4^{WT}$ mice according to the paraffin section H&E staining analysis (**Figure 3E**). However, compared with $SIRT4^{WT}$, SIRT4 immunofluorescence, especially filamentous staining in the GCL and the INL, was significantly reduced in $SIRT4^{KO}$. Although the brightness of SIRT4 in the IPL did not change significantly, it became fractured and discontinuous. We observed that GS was downregulated in $SIRT4^{KO}$ mouse retinas and that MGCs exhibited a disrupted radial morphology of MGCs (**Figure 3F**). The results indicated that SIRT4 deletion

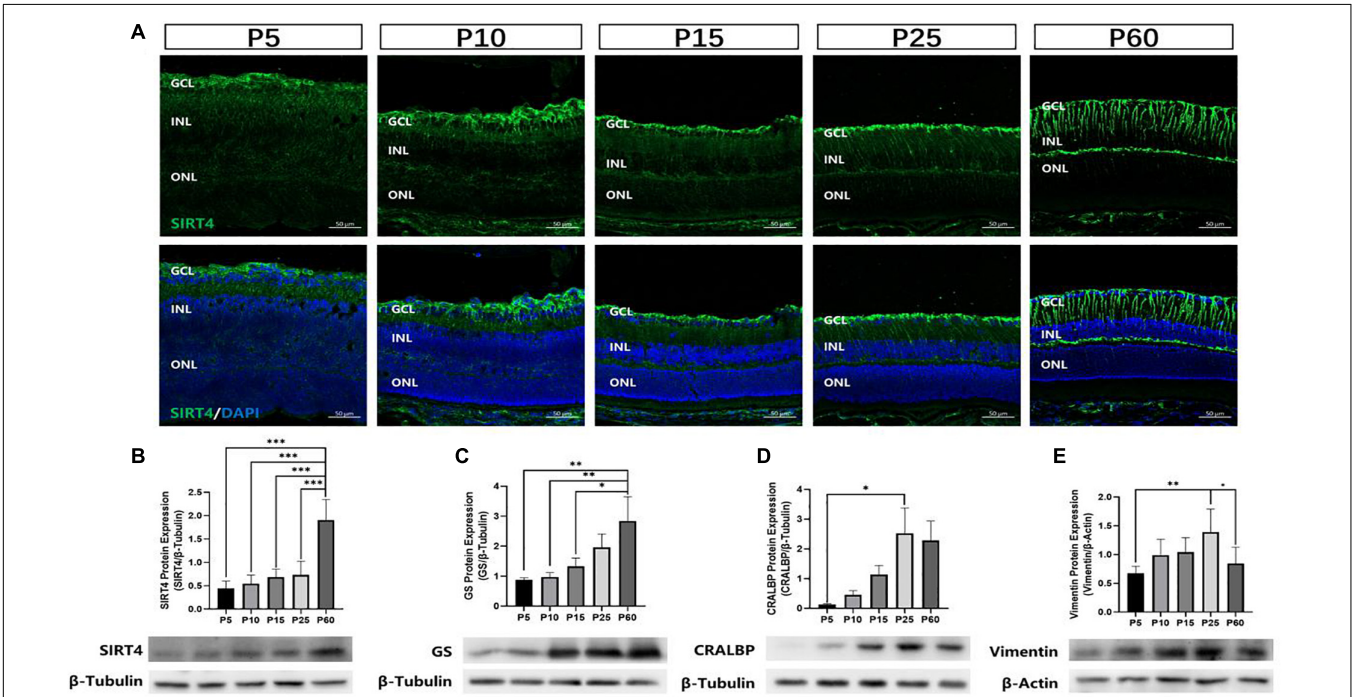

FIGURE 2 | Expression of SIRT4 in mice retinas at different developmental stages. **(A)** Expression pattern of SIRT4 during retinal development in mice retinas by immunohistochemistry at postnatal day 5 (P5), P10, P15, P25, and P60. **(B–E)** Western blot analysis of SIRT4, GS, CRALBP and vimentin protein levels in the retina of C57BL/6 mice at different developmental stages. GCL: ganglion cell layer; INL: inner nuclear layer; ONL: outer nuclear layer. GS: glutamine synthetase; CRALBP: cellular retinaldehyde binding protein; DAPI was used to stain the nuclei (blue). Data are shown as mean ± SEM. (n = 6 per group, $^{*}P < 0.05$, $^{**}P < 0.01$, $^{***}P < 0.001$). Scale bar = 50 μm.

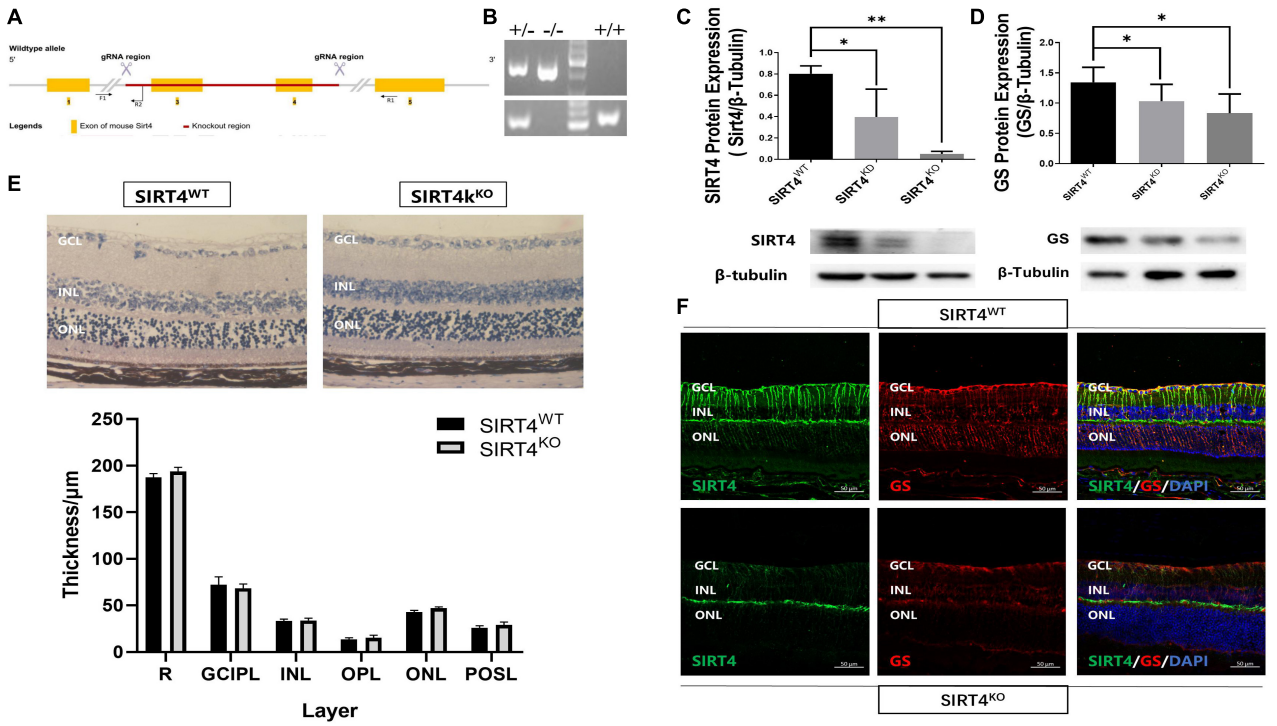

FIGURE 3 | Retinal structure of 2-month SIRT4-deficient mice. **(A)** Schematic diagram of SIRT4 gene knockout. **(B)** Genotyping identification. **(C,D)** SIRT4 and GS protein expression in SIRT4^{WT}, SIRT4^{KD} and SIRT4^{KO} mice were analyzed using western blotting. **(E)** Retinal thickness analysis after H&E staining of paraffin sections of SIRT4^{WT} and SIRT4^{KO} mice. **(F)** Immunofluorescence analysis of SIRT4 and GS in the retina of SIRT4^{WT} and SIRT4^{KO} mice. WT, wild type; KD, knock down; KO, knock out; NFL, nerve fiber layer; GCL, ganglion cell layer; GCIPL, ganglion cell-inner plexiform layer; INL, inner nuclear layer; OPL, out plexiform layer; ONL, outer nuclear layer; POSL, photoreceptor outer segment layer; GS, glutamine synthetase; DAPI was used to stain the nuclei (blue). Data are shown as mean ± SEM. (n = 3 per group, $^*P < 0.05$, $^{**}P < 0.01$). Scale bar = 50 μm.

scarcely affected the retinal structure of mice, but downregulated the expression of GS protein.

Retinal Electrophysiological Function of 2-Month Sirtuin 4-Deficient Mice

To explore the effect of SIRT4 deletion on retinal electrophysiology in mice, we conducted electroretinogram (ERG) in SIRT4^{KO} mice and SIRT4^{WT} mice. The ERG showed no significant difference in implicit time and amplitude between SIRT4^{KO} mice and SIRT4^{WT} mice in the scotopic 0.01, 3.0, and 10.0 categories (**Figures 4A–C**). In the scotopic 3.0 oscillatory potential, the implicit time was similar and the amplitude difference was not significant (**Figure 4D**). Although the ERG waveform in the photopic 3.0 was not completely consistent, there was no significant difference between the SIRT4^{KO} and SIRT4^{WT} groups (**Figure 4E**). The ERG results revealed that SIRT gene knockout had no significant effect on retinal electrophysiological function in mice.

Resveratrol Upregulated SIRT4 and GS Protein Expression in Mice

We previously found that resveratrol significantly increased SIRT4 protein expression in zebrafish retina (Sheng et al., 2018). With this result in mind, we intraperitoneally injected 2-month mice with RES (20 mg/kg) for five consecutive days. SIRT4 (**Figure 5A**) and GS (**Figure 5B**) protein expression significantly increased following administration of RES. Filamentous staining of SIRT4 in the retina of RES intraperitoneal injection group was denser and longer than that of normal control group, so as the GS (**Figure 5C**).

Resveratrol Protected Mice Retines From Excitatory Neurotoxic Damage

Previous studies have shown that GS can regulate retinal glutamate metabolism, and reduce apoptosis (Bui et al., 2010). As RES upregulates the expression of SIRT4 and GS, we hypothesized that RES could protect mice retines from excitatory neurotoxic damage. Thus, we injected large doses of glutamate (50 nmol) intravitreally into mice and analyzed the effects of long-term administration of RES on glutamate injury. The eyeball was removed 3 days after the injury. The results showed that RES upregulated SIRT4 and GS protein expression in the glutamate injury group (**Figures 6A,B**). TUNEL staining showed that intravitreal injection of glutamate caused retinal GCL, INL and ONL cell apoptosis similar to kainate (a kind of glutamate receptor agonist) (Fleming et al., 2019), while there was no significant cell apoptosis in the group with RES (**Figure 6C**). After glutamate injury, the retinal structure of all layers was obviously

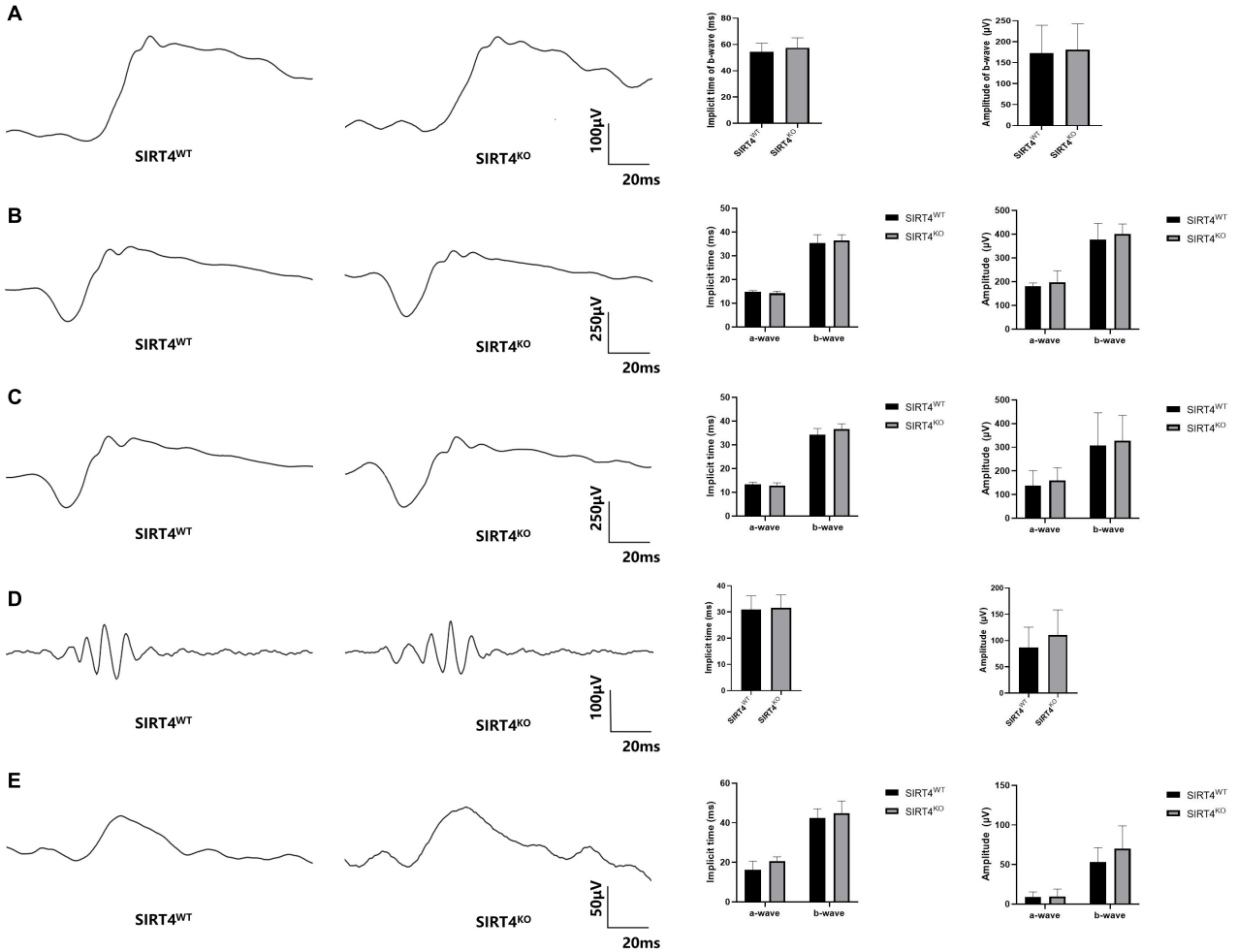

FIGURE 4 | Electroretinogram of 2-month SIRT4-deficient mice. **(A)** Scotopic 0.01 ERG waveforms analysis of SIRT4^{KO} mice and SIRT4^{WT} mice. **(B)** Scotopic 3.0 ERG waveforms analysis of SIRT4^{KO} mice and SIRT4^{WT} mice. **(C)** Scotopic 10.0 ERG waveforms analysis of SIRT4^{KO} mice and SIRT4^{WT} mice. **(D)** Scotopic 3.0 oscillatory potential ERG waveforms analysis of SIRT4^{KO} mice and SIRT4^{WT} mice. **(E)** Photopic 3.0 ERG waveforms analysis of SIRT4^{KO} mice and SIRT4^{WT} mice. WT: wild type; KO: knock out. Data are shown as mean ± SEM. (n = 3 per group).

disordered, the GCL became edematous, the nuclei of the GCL layer and ONL layer were scattered, and the photoreceptor outer segment layer (POSL) was broken (**Figure 6D**). In addition, scattered cells are seen in the vitreous cavity. The retinal thickness analysis showed a significant reduction in the thickness of the retina, the OPL and the ONL, and incrassation of the GCL thickness after glutamate injury while they were similar to the control with the help of RES (**Figure 6E**).

DISCUSSION

Our study revealed for the first time that the role of SIRT4 in the retina is highly correlated with MGCs. We found that SIRT4 was co-expressed with MGCs markers (GS and Vimentin). The expression of SIRT4 protein in the retina increased with postnatal time and reached its peak at 2 months with diffuse changes in its expression pattern. The distribution of SIRT4 protein was similar to that of MGC markers (GS and CRALBP) during the development of MGCs (Bachleda et al., 2016). SIRT4 gene knockout did not affect the structure and electrophysiological function of mouse retina under basal conditions but resulted in the downregulation of GS protein expression. In addition, our experiments suggested that RES, as a SIRT4 activator, can mitigate excitatory neurotoxic damage caused by glutamate excess.

Previous studies have shown that SIRT4 is highly expressed in glial cells, specifically astrocytes, in the brain and radial glia (Komlos et al., 2013). SIRT4 was filamentously localized in cells that were likely radial glia and co-expressed with vimentin and nestin. Similar expression patterns of SIRT4 were observed in our experiments. GS and vimentin, as specific markers of MGCs (Hayashi et al., 2021), have similar protein expression and fluorescence localization to SIRT4, suggesting that SIRT4 may play a role in MGCs. Given that MGCs play a crucial role in retinal function and structure, we were curious about the role of

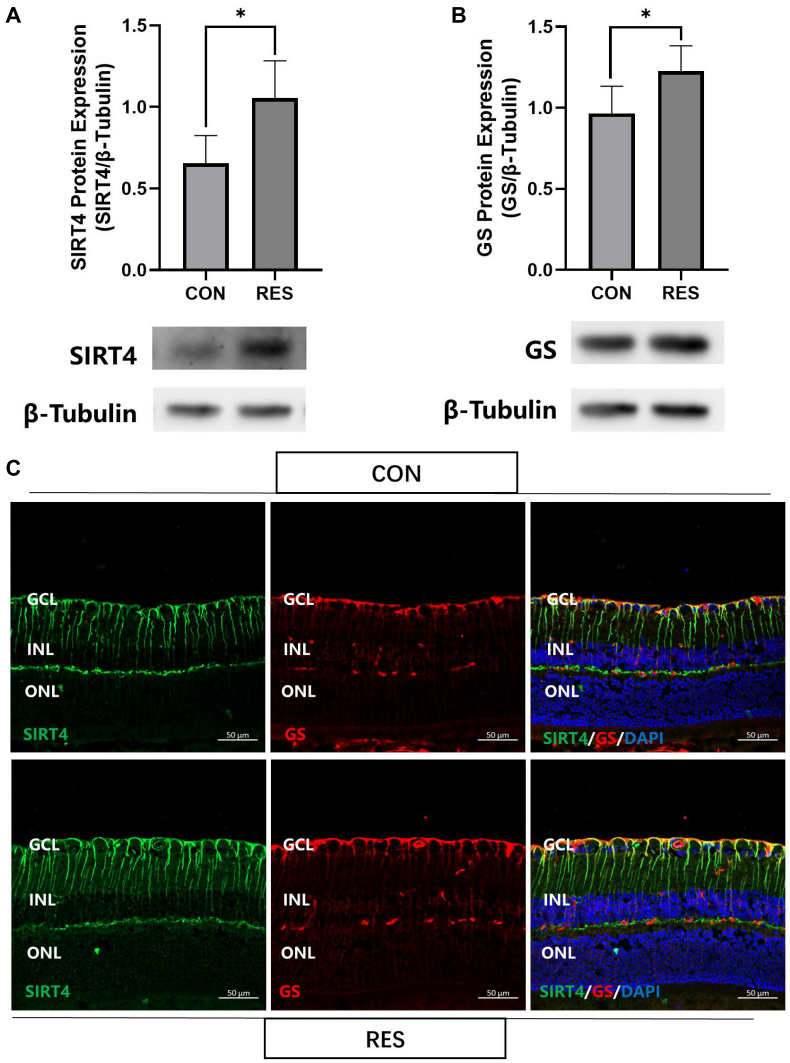

FIGURE 5 | Resveratrol up-regulate SIRT4 and GS protein expression in 2 month mice retinas. Western blot analysis of SIRT4 **(A)** and GS **(B)** expression. **(C)** Immunofluorescence analysis of SIRT4 and GS in the retina of normal control group and RES intraperitoneal injection group mice. CON: normal control; RES: resveratrol intraperitoneal injection; GS: glutamine synthetase. Data are shown as mean ± SEM. (n = 5 per group, $^*P < 0.05$).

SIRT4 in the retina. Therefore, we further analyzed the effects of SIRT4 gene deletion on the structure and function of MGCs and the retina. The loss of SIRT4 had no significant effect on retinal structure or electrophysiological function under basal conditions, which was consistent with the results of Lin et al. (2018). Three reasons may explained this situation. First, SIRT4 had a low expression level in the early stage of the retina and had little influence on retinal development. Then, the phenotype of SIRT family knockout mice was insidious. The structure and function of mouse retina may not change under basic conditions, but it tends to change under specific stimuli like SIRT3 and SIRT5 (Lin et al., 2016). Finally, the function of SIRT4 may compensate for other sirtuins, such as SIRT1 and SIRT3, which have been confirmed to be increased in $SIRT4^{KO}$ mice (Nasrin et al., 2010; Balaiya et al., 2017). We speculate that the increase of other sirtuins in SIRT4 KO mice may partially compensate for the function of SIRT4, and the increase in SIRT1 protein was found in our preliminary. We found that the expression of GS was downregulated and discontinuous in SIRT4-deficient mice. After upregulating SIRT4 expression by RES, GS showed enhanced radial filamentous expression and increased protein expression consistent with SIRT4. These results convinced us that SIRT4 may be involved in the regulation of GS expression in MGCs.

Sirtuin 4 inhibits the enzymatic activity of glutamate dehydrogenase (GDH) and limits the metabolism of glutamate and glutamine to produce ATP (Haigis et al., 2006; Fernandez-Marcos and Serrano, 2013). GDH and SIRT4 play opposing roles in the development of astroglia from radial glia in the central nervous system (Komlos et al., 2013). Interestingly, we observed that SIRT4 and GS may play similar roles in the development of MGCs. Glutamine immunoreactivity was highest in horizontal cells and MGC endfeet (Bui et al., 2010), which

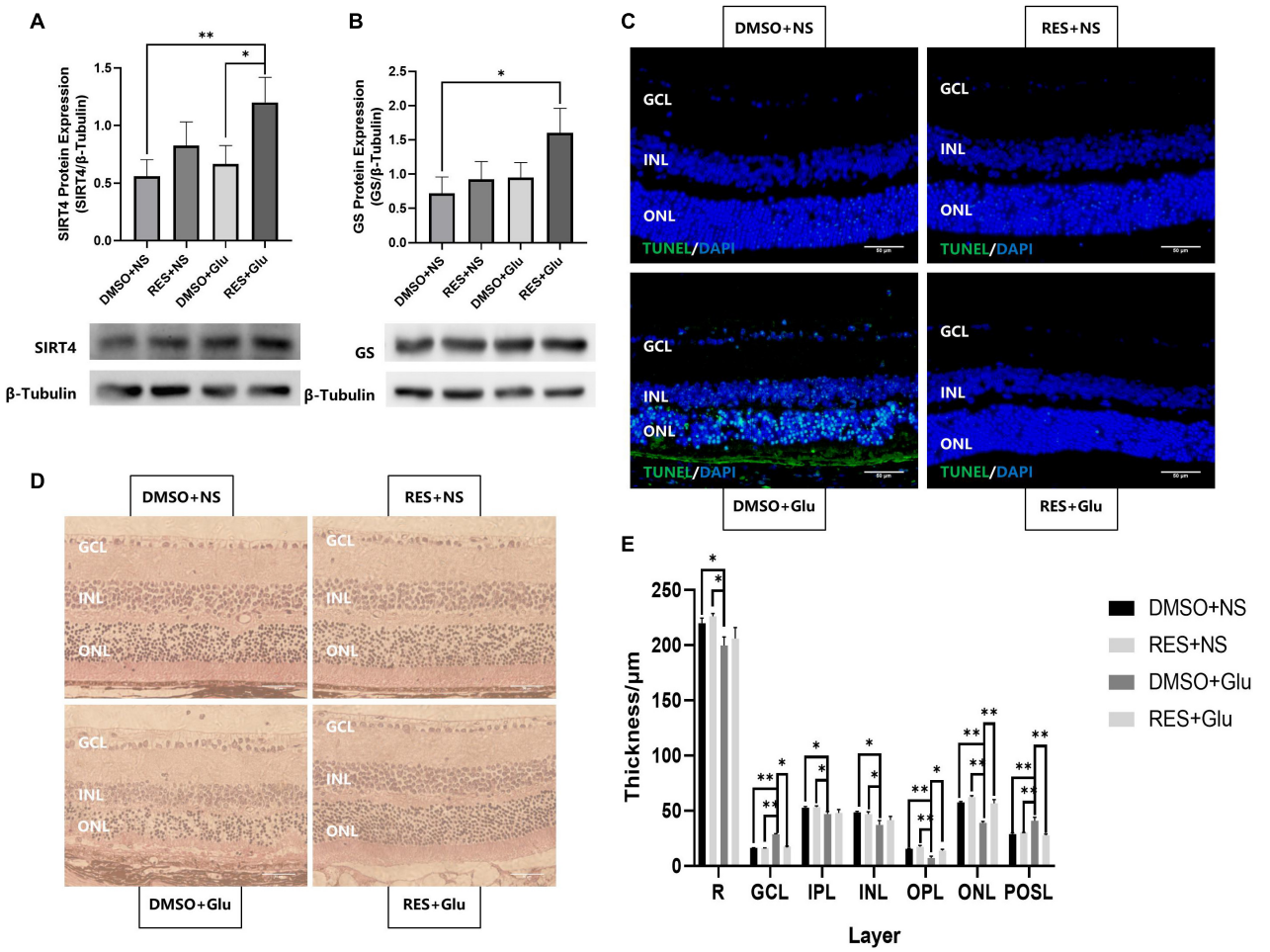

FIGURE 6 | Resveratrol protected mice retines from excitatory neurotoxic damage. Western blot analysis of SIRT4 **(A)** and GS **(B)** protein expression of DMSO+NS, RES+NS, DMSO+Glu and RES+Glu. **(C)** TUNEL labeling of retinal section 3 day after glutamate injury showed that apoptosis was attenuated in RES+Glu compared to DMSO+Glu. **(D)** H&E staining of mice retina Paraffin section. **(E)** Retinal thickness analysis showed a significant reduction in retinal thickness of DMSO+Glu and there was no signifucant changes in that of RES+Glu. GCL, ganglion cell layer; IPL, inner plexiform layer; INL, inner nuclear layer; OPL, outer plexiform layer; ONL, outer nuclear layer; POSL, photoreceptor outer segment layer. GS, glutamine synthetase; DMSO, dimethylsulfoxide; RES, resveratrol; NS, normal saline; Glu, glutamate; DMSO+NS: DMSO (6.67%) was intraperitoneal injection every 2 days from postnatal 20 days to 2 months of age and Glu (50 nmol) was injected intravitreal 3 days before sampling; RES+NS: RES (20 mg/L) soluble in DMSO (6.67%) was intraperitoneal injection every 2 days from postnatal 20 days to 2 months of age and NS was injected intravitreal 3 days before sampling; DMSO+Glu: DMSO (6.67%) was intraperitoneal injection every 2 days from postnatal 20 days to 2 months of age and Glu (50 nmol) soluble in NS was injected intravitreal 3 days before sampling; RES+Glu: RES (20 mg/L) soluble in DMSO (6.67%) was intraperitoneal injection every 2 days from postnatal 20 days to 2 months of age and Glu (50 nmol) soluble in NS was injected intravitreal 3 days before sampling. TUNEL was used to stain apoptotic cell (green) and DAPI was used to stain the nuclei (blue). Data are shown as mean ± SEM. (n = 3 per group, $^{*}P < 0.05$, $^{**}P < 0.01$). Scale bar = 50 μm.

corresponded to the localization of SIRT4 in the retina, indicated that SIRT4 plays a role in regulating glutamate-glutamine metabolism in the retina. By excess glutamate intravitreal injection, we found that intraperitoneal injection of RES in mice upregulated the expression of SIRT4 and GS and reduced the apoptosis of retinal cells induced by glutamate, indicating the regulatory effect of SIRT4 on glutamate through GS and its protective effect on the retina. Inhibition of Müller glial cell glutamine synthetase blocked glutamatergic neurotransmission, which could contribute to neuronal degeneration and the animals became functionally blind (Barnett et al., 2000; Bringmann et al., 2013). Brain studies in SIRT4 knockout mice have also shown that SIRT4 has a neuroprotective effect against excitatory toxic injury by promoting GLT-1-dependent glutamate uptake (Shih et al., 2014). Combined with this study, we hypothesized that SIRT4 may regulate the retinal glutamate-glutamine cycle through multiple pathways. Considering that excitotoxicity caused by glutamate is an important part of glaucoma injury, investigating the role of SIRT4 in glutamate-glutamine metabolism is of great significance.

Resveratrol, a natural polyphenol compound found chiefly in grapes and wine, is regarded as an antioxidant, anti-inflammatory agent, anti-apoptotic agent and antineoplastic agent (Malhotra et al., 2015). It has been reported to inhibit oxidative stress in

diabetic cells, mitigate the effects of retinal ischemic injury in rats, and inhibit pathologic retinal neovascularization in very low-density lipoprotein receptor mutant mice (Hua et al., 2011; Luo et al., 2018; Popescu et al., 2018). Human sirtuin isoforms are considered attractive therapeutic targets for neurodegenerative disorders (Dai et al., 2018). Activation of SIRT4 expression by RES may have a protective effect on neurodegenerative diseases, which was preliminarily validated in mice in our study. In addition, we found that resveratrol inhibits the Akt/mTOR pathway in the retina (not shown). Previous studies have demonstrated that resveratrol can inhibit mTOR signaling induced autophagy, which can mediate many beneficial effects, including protection against oxidative stress damage (Park et al., 2016). Experiments on zebrafish and retinal pigment epithelial cells also showed that resveratrol could downregulate the Akt/mTOR pathway, promote autophagy and improve mitochondrial function (Wang et al., 2019; Josifovska et al., 2020). The role of SIRT4 in the mechanisms above needs to be further studied.

In summary, we found co-localization of SIRT4 and MGCs, and SIRT4 was involved in the role of MGCs and MGC maker GS. The results above provide a direction for the follow-up study of retinal SIRT4. However, this study did not further study SIRT4 gene knockout mice under stress state, nor did it discuss the role of other SIRT family proteins. In addition, we also observed that SIRT4 was highly expressed in choroid and ciliary body epithelium in mice, and its significance remains to be further studied.

CONCLUSION

We show for the first time that SIRT4 co-localized with Müller glial cell markers (including vimentin and glutamine synthetase) in human, mouse and rat retinas. Resveratrol, as a SIRT4 activator, increased the expression of glutamine synthetase protein and protected the mice retina against excitotoxicity caused by excessive glutamate. Upregulation of SIRT4 expression may be a new direction for the treatment of retinal neuronal degeneration caused by glaucoma and age-related macular degeneration.

DATA AVAILABILITY STATEMENT

The original contributions presented in the study are included in the article/supplementary material, further inquiries can be directed to the corresponding author/s.

ETHICS STATEMENT

The studies involving human participants were reviewed and approved by Affiliated Eye Hospital of Nanchang University. Written informed consent to participate in this study was provided by the participants' legal guardian/next of kin. The animal study was reviewed and approved by Affiliated Eye Hospital of Nanchang University. Written informed consent was obtained from the owners for the participation of their animals in this study.

AUTHOR CONTRIBUTIONS

WW, PH, and XZ conceived the study. WW, PH, MQ, SY, and ZX performed the experiments. WW, FW, GC, MJ, and XZ analyzed the data. WW, PH, and XZ drafted the manuscript. All authors read and approved the final version of manuscript.

FUNDING

This research was funded by the National Natural Science Foundation of China (81271425 and 81860170) and Natural Science Foundation of Jiangxi (20181ACG70010).

REFERENCES

Anderson, K. A., Huynh, F. K., Fisher-Wellman, K., Stuart, J. D., Peterson, B. S., Douros, J. D., et al. (2017). SIRT4 Is a Lysine Deacylase that Controls Leucine Metabolism and Insulin Secretion. *Cell. Metab*. 25, 838–855.e15. doi: 10.1016/j.cmet.2017.03.003

Bachleda, A. R., Pevny, L. H., and Weiss, E. R. (2016). Sox2-deficient muller glia disrupt the structural and functional maturation of the mammalian retina. *Invest. Ophthalmol. Vis. Sci*. 57, 1488–1499. doi: 10.1167/iovs.15-17994

Balaiya, S., Abu-Amero, K. K., Kondkar, A. A., and Chalam, K. V. (2017). Sirtuins expression and their role in retinal diseases. *Oxid. Med. Cell. Longev*. 2017:3187594. doi: 10.1155/2017/3187594

Barnett, N. L., Pow, D. V., and Robinson, S. R. (2000). Inhibition of Müller cell glutamine synthetase rapidly impairs the retinal response to light. *Glia* 30, 64–73. doi: 10.1002/(sici)1098-1136(200003)30:1

Bringmann, A., Grosche, A., Pannicke, T., and Reichenbach, A. (2013). GABA and glutamate uptake and metabolism in retinal glial (Müller) cells. *Front. Endocrinol*. 4:48. doi: 10.3389/fendo.2013.00048

Bringmann, A., Pannicke, T., Biedermann, B., Francke, M., Iandiev, I., Grosche, J., et al. (2009). Role of retinal glial cells in neurotransmitter uptake and metabolism. *Neurochem. Int*. 54, 143–160. doi: 10.1016/j.neuint.2008.10.014

Bringmann, A., Pannicke, T., Grosche, J., Francke, M., Wiedemann, P., Skatchkov, S. N., et al. (2006). Müller cells in the healthy and diseased retina. *Prog. Retin. Eye. Res*. 25, 397–424. doi: 10.1016/j.preteyeres.2006.05.003

Bringmann, A., and Wiedemann, P. (2011). Müller glial cells in retinal disease. *Ophthalmologica* 227, 1–19. doi: 10.1159/000328979

Bui, B. V., Hu, R. G., Acosta, M. L., Donaldson, P., Vingrys, A. J., and Kalloniatis, M. (2010). Glutamate metabolic pathways and retinal function. *J. Neurochem*. 111, 589–599. doi: 10.1111/j.1471-4159.2009.06354.x

Dai, H., Sinclair, D. A., Ellis, J. L., and Steegborn, C. (2018). Sirtuin activators and inhibitors: Promises, achievements, and challenges. *Pharmacol. Ther*. 188, 140–154. doi: 10.1016/j.pharmthera.2018.03.004

Devoldere, J., Peynshaert, K., De Smedt, S. C., and Remaut, K. (2019). Müller cells as a target for retinal therapy. *Drug. Discov*. 24, 1483–1498. doi: 10.1016/j.drudis.2019.01.023

Fernandez-Marcos, P., and Serrano, M. (2013). Sirt4: the glutamine gatekeeper. *Cancer. Cell*. 23, 427–428. doi: 10.1016/j.ccr.2013.04.003

Fleming, T., Balderas-Márquez, J. E., Epardo, D., Epardo, D., Ávila-Mendoza, J., Carranza, M., et al. (2019). Growth hormone neuroprotection against kainate excitotoxicity in the retina is mediated by Notch/PTEN/Akt signaling. *Invest. Ophthalmol. Vis. Sci*. 60, 4532–4547. doi: 10.1167/iovs.19-27473

Fletcher, E. L., Phipps, J. A., and Wilkinson-Berka, J. L. (2005). Dysfunction of retinal neurons and glia during diabetes. *Clin. Exp. Optom.* 88, 132–145. doi: 10.1111/j.1444-0938.2005.tb06686.x

Goldman, D. (2014). Müller glial cell reprogramming and retina regeneration. *Nat. Rev. Neurosci.* 15, 431–442. doi: 10.1038/nrn3723

Haigis, M. C., Mostoslavsky, R., Haigis, K. M., Fahie, K., Christodoulou, D. C., Murphy, A., et al. (2006). SIRT4 inhibits glutamate dehydrogenase and opposes the effects of calorie restriction in pancreatic beta cells. *Cell* 126, 941–954. doi: 10.1016/j.cell.2006.06.057

Hayashi, H., Mori, M., Harashima, M., Hashizume, T., Furiya, M., Mukaigaito, C., et al. (2021). Apolipoprotein E-containing lipoproteins and LRP1 protect from NMDA-induced excitotoxicity associated with reducing α2-macroglobulin in Müller glia. *Invest. Ophthalmol. Vis. Sci.* 62:23. doi: 10.1167/iovs.62.13.23

Ho, L., Titus, A. S., Banerjee, K. K., George, S., and Kolthur-Seetharam, U. (2013). SIRT4 regulates ATP homeostasis and mediates a retrograde signaling via AMPK. *Aging* 5, 835–849. doi: 10.18632/aging.100616

Hua, J., Guerin, K. I., Chen, J., Michán, S., Stahl, A., Krah, N. M., et al. (2011). Resveratrol inhibits pathologic retinal neovascularization in Vldlr(-/-) mice. *Invest. Ophthalmol. Vis. Sci.* 52, 2809–2816. doi: 10.1167/iovs.10-6496

Jeong, S. M., Xiao, C., Finley, L. S., Lahusen, T., Souza, A., Pierce, K., et al. (2013). SIRT4 has tumor-suppressive activity and regulates the cellular metabolic response to DNA damage by inhibiting mitochondrial glutamine metabolism. *Cancer. Cell* 23, 450–463. doi: 10.1016/j.ccr.2013.02.024

Josifovska, N., Albert, R., Nagymihály, R., Lytvynchuk, L., Moe, M. C., Kaarniranta, K., et al. (2020). Resveratrol as inducer of autophagy, pro-survival, and anti-inflammatory stimuli in cultured human RPE cells. *Int. J. Mol. Sci.* 21:813. doi: 10.3390/ijms21030813

Komlos, D., Mann, K. D., Zhuo, Y., Ricupero, C. L., Hart, R. P., Liu, Y. C., et al. (2013). Glutamate dehydrogenase 1 and SIRT4 regulate glial development. *Glia* 61, 394–408. doi: 10.1002/glia.22442

Laurent, G., German, N., Saha, A., De Boer, V. J., Davies, M., Koves, T., et al. (2013). SIRT4 coordinates the balance between lipid synthesis and catabolism by repressing malonyl CoA decarboxylase. *Mol. Cell.* 50, 686–698. doi: 10.1016/j.molcel.2013.05.012

Lin, J. B., Kubota, S., Ban, N., Yoshida, M., Santeford, A., Sene, A., et al. (2016). Nampt-mediated NAD+ biosynthesis is essential for vision in mice. *Cell. Rep.* 17, 69–85. doi: 10.1016/j.celrep.2016.08.073

Lin, J. B., Kubota, S., Mostoslavsky, R., and Apte, R. S. (2018). Role of Sirtuins in retinal function under basal conditions. *Adv. Exp. Med. Biol.* 1074, 561–567. doi: 10.1007/978-3-319-75402-4_68

Luo, H., Min, Z., Ji, K., Zhuang, J., Dang, W., Fu, S., et al. (2017). Expression of sirtuins in the retinal neurons of mice, rats, and humans. *Front. Aging. Neurosci.* 9:366. doi: 10.3389/fnagi.2017.00366

Luo, H., Zhuang, J., Hu, P., Ye, W., Chen, S., Pang, Y., et al. (2018). Resveratrol delays retinal ganglion cell loss and attenuates gliosis-related inflammation from ischemia-reperfusion injury. *Invest. Ophthalmol. Vis. Sci.* 59, 3879–3888. doi: 10.1167/iovs.18-23806

Malhotra, A., Bath, S., and Elbarbry, F. (2015). An organ system approach to explore the antioxidative, anti-inflammatory, and cytoprotective actions of resveratrol. *Oxid. Med. Cell. Longev.* 2015, 1–15. doi: 10.1155/2015/803971

Mysona, B., Dun, Y., Duplantier, J., Ganapathy, V., and Smith, S. B. (2009). Effects of hyperglycemia and oxidative stress on the glutamate transporters GLAST and system xc- in mouse retinal Müller glial cells. *Cell. Tissue Res.* 335, 477–488. doi: 10.1007/s00441-008-0742-1

Nasrin, N., Wu, X., Fortier, E., Feng, Y., Bare', O. C., Chen, S., et al. (2010). SIRT4 regulates fatty acid oxidation and mitochondrial gene expression in liver and muscle cells. *J. Biol. Chem.* 285, 31995–32002. doi: 10.1074/jbc.M110.124164

Park, D., Jeong, H., Lee, M. N., Koh, A., Kwon, O., Yang, Y. R., et al. (2016). Resveratrol induces autophagy by directly inhibiting mTOR through ATP competition. *Sci. Rep.* 6:21772. doi: 10.1038/srep21772

Popescu, M., Bogdan, C., Pintea, A., Ruginã, D., and Ionescu, C. (2018). Antiangiogenic cytokines as potential new therapeutic targets for resveratrol in diabetic retinopathy. *Drug. Des. Devel. Ther.* 12, 1985–1996. doi: 10.2147/DDDT.S156941

Sheng, W., Lu, Y., Mei, F., Wang, N., Liu, Z., Han, Y., et al. (2018). Effect of resveratrol on sirtuins, OPA1, and Fis1 expression in adult zebrafish retina. *Invest. Ophthalmol. Vis. Sci.* 59, 4542–4551. doi: 10.1167/iovs.18-24539

Shih, J., Liu, L., Mason, A., Higashimori, H., and Donmez, G. (2014). Loss of SIRT4 decreases GLT-1-dependent glutamate uptake and increases sensitivity to kainic acid. *J. Neurochem.* 131, 573–581. doi: 10.1111/jnc.12942

Simón, M. V., Prado Spalm, F. H., Vera, M. S., and Rotstein, N. P. (2019). Sphingolipids as emerging mediators in retina degeneration. *Front. Cell. Neurosci.* 13:246. doi: 10.3389/fncel.2019.00246

Toft-Kehler, A. K., Skytt, D. M., and Kolko, M. (2017). A perspective on the Müller cell-neuron metabolic partnership in the inner retina. *Mol. Neurobiol.* 55, 5353–5361. doi: 10.1007/s12035-017-0760-7

Turner, D. L., and Cepko, C. L. (1987). A common progenitor for neurons and glia persists in rat retina late in development. *Nature* 328, 131–136. doi: 10.1038/328131a0

Wang, N., Luo, Z., Jin, M., Sheng, W., Wang, H., Long, X., et al. (2019). Exploration of age-related mitochondrial dysfunction and the anti-aging effects of resveratrol in zebrafish retina. *Aging* 11, 3117–3137. doi: 10.18632/aging.101966

Wohl, S. G., Jorstad, N. L., Levine, E. M., and Reh, T. A. (2017). Müller glial microRNAs are required for the maintenance of glial homeostasis and retinal architecture. *Nat. Commun.* 8:1603. doi: 10.1038/s41467-017-01624-y

Yang, Q., Zhou, Y., Sun, Y., Luo, Y., Shen, Y., and Shao, A. (2020). Will Sirtuins be promising therapeutic targets for TBI and associated neurodegenerative diseases? *Front. Neurosci.* 14:791. doi: 10.3389/fnins.2020.00791

Conflict of Interest: The authors declare that the research was conducted in the absence of any commercial or financial relationships that could be construed as a potential conflict of interest.

Publisher's Note: All claims expressed in this article are solely those of the authors and do not necessarily represent those of their affiliated organizations, or those of the publisher, the editors and the reviewers. Any product that may be evaluated in this article, or claim that may be made by its manufacturer, is not guaranteed or endorsed by the publisher.

frontiers | Frontiers in Neuroscience

ORIGINAL RESEARCH
published: 19 April 2022
doi: 10.3389/fnins.2022.868750

Nutraceutical Molecules Slow Down Retinal Degeneration, in Tvrm4 Mice a Model of Retinitis Pigmentosa, by Genetic Modulation of Anti-oxidant Pathway

Ilaria Piano[1]†, Francesca Corsi[1†], Beatrice Polini[2] and Claudia Gargini[1,3]*

[1] Department of Pharmacy, University of Pisa, Pisa, Italy, [2] Department of Surgical, Medical and Molecular Pathology and Critical Care Medicine, University of Pisa, Pisa, Italy, [3] Interdepartmental Center for Nutraceutical Research and Nutrition or Health, University of Pisa, Pisa, Italy

OPEN ACCESS

Edited by:
Mohammad Shamsul Ola, King Saud University, Saudi Arabia

Reviewed by:
Yoshiki Koriyama, Suzuka University of Medical Science, Japan
Enzo Maria Vingolo, Sapienza University of Rome, Italy

***Correspondence:**
Ilaria Piano
ilaria.piano@unipi.it

† These authors have contributed equally to this work

Specialty section:
This article was submitted to Neurodegeneration, a section of the journal Frontiers in Neuroscience

Received: *03 February 2022*
Accepted: *21 March 2022*
Published: *19 April 2022*

Citation:
Piano I, Corsi F, Polini B and Gargini C (2022) Nutraceutical Molecules Slow Down Retinal Degeneration, in Tvrm4 Mice a Model of Retinitis Pigmentosa, by Genetic Modulation of Anti-oxidant Pathway. Front. Neurosci. 16:868750. doi: 10.3389/fnins.2022.868750

Rhodopsin (RHO) mutations are responsible for 25–40% of the dominant cases of retinitis pigmentosa (RP) with different severity and progression rates. The Tvrm4 mice, heterozygous for an I307N dominant mutation of RHO, display a normal retinal phenotype when raised in ambient light conditions, but undergo photoreceptor degeneration when briefly exposed to strong white light. Here, The Tvrm4 mice is pre-treated with naringenin 100 mg/kg/die, quercetin 100 mg/kg/die, naringenin 50 + quercercetin 100 mg/kg/die or vehicle dimethyl sulfoxide (DMSO 0.025%) in the drinking water for 35 days. On the 30th day, retinal degeneration was induced by exposure for 1 min to the white light of 12,000 lux intensity, and the treatment was repeated for another 5 days. At the end of the protocol retinal functionality was tested by recording an electroretinogram (ERG). The retinal tissue was collected and was used for further analyses, including immunohistochemically, biochemical, and molecular biology assays. The data obtained show that treatment with nutraceutical molecules is effective in counteracting retinal degeneration by preserving the functionality of photoreceptors and increasing the antioxidant and anti-apoptotic pathways of retinal cells. The present data confirm that nutraceutical molecules are effective in slowing photoreceptor degeneration in a mutation-independent way by modulating the antioxidant response of the retina at the gene expression level.

Keywords: nutraceutical treatment, photoreceptors degeneration, genetic modulation, oxidative stress, retinitis pigmentosa

INTRODUCTION

In recent years, the role of oxidative stress in the progression of neurodegenerative diseases, also due to specific genetic mutations, has become increasingly important (Bacci et al., 2021). The oxidative stress is due to the disruption of a delicate balance between free radicals of oxygen or nitrogen and the presence of antioxidant molecules and involves the accumulation of radical species that are intrinsically unstable thus leading to the oxidation of molecules in the cellular environment

(Castelli et al., 2021). The small amounts of reactive oxygen species (ROS), generated by nicotinamide adenine dinucleotide phosphate (NADPH) oxidases within the cytoplasm, or by oxygen–electron mismatch donors present in the mitochondria, are neutralized by glutathione and by enzymes of the superoxide dismutase (Sod) family. However, under pathological conditions, such as high oxygen levels or other sources of free radical generators, the antioxidant system may be insufficient to cleanse the environment from ROS, leading to the production of radicals even more harmful to the cell, such as hydroxyl radicals. When the free radicals encounter macromolecules, they produce the characteristic modifications that compromise lipids, proteins, and DNA constituting oxidative damage (Campochiaro and Mir, 2018). In the mouse retina, rods make up 97.2% of cells in the outer nuclear layer and present a high number of mitochondria that make them highly metabolically active (Jeon et al., 1998).

In diseases characterized by primary rod death as in retinitis pigmentosa (RP), there is a progressive reduction in oxygen consumption as a result of rod death, leading to an increase in oxidative stress that, in a second phase of the disease, contributes to the death of cones. The hypothesis that oxidative stress is the initial cause of cone degeneration, independently of the type of genetic mutation that underlies the primary degeneration and death of the rods, is supported by studies showing that the use of antioxidant molecules is effective in slowing the death of cones in several models of RP, including rd1, Q344ter, and rd10 mice (Komeima et al., 2007, 2008; Oveson et al., 2011; Piano et al., 2019) and P23H rats (Fernández-Sánchez et al., 2012).

Here, we demonstrate how two nutraceutical molecules, naringenin a bioflavonoid compound present in high concentrations in the citrus species (Viswanatha et al., 2017) and quercetin a flavonoid present in various vegetables; tea and red wine (D'Andrea, 2015; Ortega and Jastrzebska, 2021), administered individually or in combination, can modulate genes encoding for key proteins involved in the antioxidant response in an animal model of autosomal dominant RP, Tvrm4 (Budzynski et al., 2010; Gargini et al., 2017). This study adds to those already in the literature demonstrating that natural molecules can slow retinal degeneration in genetic models of RP (Liu et al., 2021) and induced models (Kim et al., 2015).

MATERIALS AND METHODS

Animals

Animals were treated according to the guidelines of the Declaration of Helsinki and according to Italian and European institutional guidelines, following experimental protocols approved by the Animal Welfare Organization (OPBA – Ethics Committee) of the University of Pisa and the Italian Ministry of Health (Protocol #653/2017-PR-DB173.3.EXT.0, Department of Pharmacy, University of Pisa). Heterozygous Tvrm4 (RhoTvrm4/Rho+) mice on a C57Bl/6J background, were selected by genotyping (Budzynski et al., 2010) and males and females in the same ratio were used. All animals were regularly fed *ad libitum* and housed in a controlled lighting environment (12-h light/dark cycle), with an illumination level of less than 60 lux. All experiments were conducted under deep anesthesia by intraperitoneal (i.p.) injection of 20% urethane in saline buffer (0.9% NaCl) at a dose of 0.1 ml/10 g body weight. At the end of the experimental procedure, the mice were sacrificed by cervical dislocation while maintaining the deep anesthesia condition, and the tissues were collected for *ex vivo* analysis.

The treatment protocol used and the total number of animals divided by the experimental techniques are shown in **Figure 1**.

Treatment

The experimental protocols started when the animals were approximately 4–5 months old, in agreement with previous studies performed in the same mouse model (Piano et al., 2020). The individually housed animals were treated for 35 days with solutions of naringenin 100 mg/kg/day, quercetin 100 mg/kg/day, naringenin 50 + quercetin 100 mg/kg/day or vehicle (DMSO 0.025%).

The chosen dose of the single-administered molecules is derived from experimental evidence showing a reduced biological effect at lower doses (data not shown) and good efficacy at the doses proposed in previous studies conducted in the same laboratory (Piano et al., 2019, 2021) and by other colleagues (Testai et al., 2013). To evaluate a potential interaction between the two phenolic compounds, the ability of the less active (naringenin) to potentiate the effects of the most effective molecule (quercetin) has been analyzed. Therefore, quercetin is administered at the dose corresponding to that of the single treatment, while naringenin is administered at an ineffective dose (data not shown). The treatment was divided into two phases. During the first phase, Tvrm4 unexposed were pre-treated for 30 days; on day 30, they were exposed to light according to the protocol (Gargini et al., 2017); the second treatment phase lasted 5 additional days. The stock solutions of naringenin (45 mg/ml) and quercetin (10 mg/ml) were prepared in DMSO and added to the volume of the drinking water according to the bodyweight of the animal to achieve the expected daily dose.

Electroretinogram

The general procedure for animal preparation, anesthesia, electroretinogram (ERG) recording, light stimulation, and data analysis has been described in detail previously (Piano et al., 2021). Briefly, ERGs were recorded in complete darkness using coiled gold electrodes contacting the cornea moisturized by a thin layer of gel (Lacrinom, Farmigea), and the reference (earth) electrode was inserted at scalp level. The animal was placed inside the Ganzfeld sphere 30 cm in diameter, whose interior surface was coated with a highly reflective white paint and exposed to light stimulation. The light stimulation was carried out with a white light electric flash (SUNPACK B3600 DX, Tecad Company, Tokyo, Japan) and, to modulate the intensity, six calibrated neutral density filters were used. For scotopic ERG recordings, the mice were presented with a single flash of increasing intensity (1.71×10^{-5} to 377 cd*s/m^2, 0.6 log units steps), each repeated six times, with an inter-stimulus interval ranging from 20 s for dim flashes to 45 s for the brightest flashes. Isolated cone (photopic) components were obtained by superimposing the test flashes (0.016 to 377 cd*s/m^2), on a steady background of

A Treatment protocol

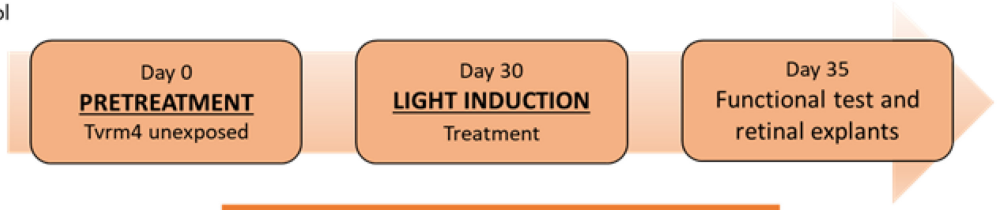

Pretreatment and treatment *x os*
Quercetin 100 mg/kg/day
Naringenin 100 mg/kg/day
Naringenin – Quercetin: 50 mg/kg/day - 100 mg/kg/day
Vehicle DMSO 0.025 %

B Total number of experimental animals

Treatment	N. animal treated	ERG n. animal	Western Blotting n. right retina	PCR – Real Time n. left retina	Immunohistochemistry n. Whole retina
Quercetin 100 mg/kg/day	12	6	6	6	6
Naringenin 100 mg/kg/day	12	6	11*	6	6
Naringenin – Quercetin: 50 mg/kg/day - 100 mg/kg/day	12	6	6	6	6
Vehicle DMSO 0.025 %	12	6	6	6	6
Unexposed/untreated healty control	7	6		6	1

FIGURE 1 | Treatment protocol and the number of animals used for the experimental plane. **(A)** Summary outline of the treatment protocol and the relative doses used for treatment with single molecules and treatment with molecules in combination. **(B)** Descriptive table of the total number of animals used for this study, with a detailed breakdown of how biological samples were used. *Due to the variability of the results of this treatment $n = 5$ contralateral retinas were taken from the animals designated for whole-mount retinal tissue preparation (right eye).

saturating intensity for rods (30 cd/m^2) after at least 15 min from background onset.

The amplitude of the scotopic a-wave was measured at 7 ms after the onset of the light stimulus and the b-wave was measured from the peak of the a-wave to the peak of the b-wave. The amplitude of the photopic b-wave was measured from the baseline to the peak of the b-wave. The data were analyzed with the LabVIEW 2019 program (National Instruments, Austin, TX, United States).

The mRNA Expression Analysis

The purification and extraction of total RNA from retina tissues were performed by miRNeasy Micro Kit (Qiagen, Hilden, Germany) according to the manufacturer's instructions. The extracted RNA was quantified by the Infinite M200 NanoQuant instrument (Tecan, Salzburg, Austria) and retro-transcribed by RT2 First Strand Kit (Qiagen, Hilden, Germany). The obtained cDNA was used for real-time polymerase chain reaction (PCR) expression analysis of multiple genes by using RT2 Profiler PCR Array (Mouse Oxidative Stress and Antioxidant Defense, #330231, PAMM-065Z, Qiagen, Hilden, Germany). The expression analysis was carried out by the Gene Globe Data Analysis Center ([1]Qiagen, Hilden, Germany). For the normalization step, the software automatically selected the most stable genes among those analyzed as the optimal set of reference genes. The geometric mean of these stable genes was used as a normalization factor.

In the same cDNA samples, the transcriptional levels of genes coding photoreceptors were further analyzed by real-time PCR by using specific primers RT^2 qPCR Primer Assay (Catalog No. 330001, Qiagen, Hilden, Germany) and RT2 SYBR® Green qPCR Mastermix (Qiagen, Hilden, Germany).

The selected primers were as follows: Guanine nucleotide-binding protein alpha transducing 1 (GNAT1): GeneGlobe ID – PPM03513A-200, Detected Transcript NM_008140; arrestin 3, retinal (ARR3): GeneGlobe ID – PPM04815A-200, Detected Transcripts NM_133205; guanine nucleotide-binding protein, alpha transducing 2 (GNAT2): GeneGlobe ID – PPM06964A-200, Detected Transcripts NM_008141; cyclic nucleotide-gated channel beta 1 (CNGB1): GeneGlobe ID – PPM06962A-200, Detected Transcripts NM_001195413. The obtained data were normalized over the same normalization factor used to analyze data from array experiments.

[1]https://geneglobe.qiagen.com

The normalized expression value is expressed as fold-change relative to the control group (DMSO-treated animals).

Western Blotting

After the ERG recordings, retinas were extracted and lysed with the modified RIPA buffer, described by Piano et al. (2013), and proteins were quantified with the Bradford assay. A 20-μg of total protein, mixed with 2× Laemmli, was loaded for each sample into pre-cast 4–20% polyacrylamide gels (Mini-PROTEAN TGX gel, Bio–Rad). After the electrophoretic run, the gel was activated using the ChemiDoc^{TM} XRS + instrument (Bio–Rad, California), and the separated proteins were transferred onto polyvinylidene fluoride (PVDF) membranes (Trans–Blot Turbo PVDF Transfer packs, Bio–Rad). The proteins were acquired to normalize the intensity of the investigated band with total protein (Gürtler et al., 2013). The blocking step was performed with EveryBlot Blocking Buffer solution (Biorad), 5 ml × 5 min at room temperature, to prevent non-specific antibody binding. The membrane was then incubated with the primary antibody (**Table 1**) diluted in 5 ml of the same solution, for 1 h at room temperature. After 5 × 5 min washes in t-TBS, the membrane was incubated with the secondary antibody conjugated to the peroxidase enzyme (HRP), in the same manner as the primary; washed (5 × 5 min) with t-TBS and then the immunoblot signal was visualized by using an enhanced chemiluminescence substrate detection system (LuminataTM Forte Western HRP Substrate, Millipore). The chemiluminescent images were acquired by Chemidoc XRS+ (Bio–Rad). The quantification was performed with Image Lab Software 6.0 (Bio–Rad). The proteins band intensities were normalized to amount of total protein in corresponding lane utilizing stain-free technology (Gürtler et al., 2013).

Immunohistochemistry

After the enucleation, the eye was marked dorsally, the anterior segment removed, to obtain the eyecup and fixed in 4% paraformaldehyde in phosphate saline buffer (PBS) for 20 min at room temperature, followed by 3 × 10 min washes in PBS. Subsequently, the retina was separated from the pigmented epithelium and placed in "free-floating." After that, the blocking step was performed in 5% bovine serum albumin (BSA) in PBS + Triton 0.1% at 4°C. The next day, the retina was incubated with the primary antibody (**Table 1**) in 1% BSA + Triton 0.1% for 3 days at 4°C. At the end of the 3 days, after 3 × 10 min washes in PBS, the retina was incubated with the secondary antibody for 2 more days. Finally, after an additional 3 × 10 min washes in PBS, the retina was mounted on the slide with the photoreceptor side up and covered with VECTASHIELD and coverslip. The images were acquired with a fluorescence microscope Nikon model, NiE with digital camera Nikon model, DS-Ri2. The several images acquired were joined through the use of Nis software to recreate the entire retinal surface and with the same software was also traced and measured the damaged area.

Statistical Analysis

The statistical comparisons for ERG registrations and WB results were carried out with one-way analysis of variance (ANOVA test), followed by *t*-tests with Bonferroni correlation, using the Origin Lab 8.0 program (MicroCal, Northampton, MA, United States). For mRNA expression analysis, the statistical comparisons were performed using Student's *t*-test of the normalized values for each gene in treatment groups compared to DMSO treated group. The *p*-values less than 0.05 were considered statistically significant.

RESULTS

The effectiveness of the sub-chronic treatment with naringenin or quercetin (100 mg/kg/day) and naringenin 50 + quercetin 100 mg/kg/day on the Tvrm4 induced mice (1 min 12,000 lux) retinal function was assessed by a variety of functional, morphological, and biochemical/molecular biological tests. **Figure 2** shows the daily intake of the solution and the effective dose of molecules taken for each group of mice treated.

First, the retinal function was assessed by scotopic and photopic ERG to evaluate the viability of rods and cones, respectively, in the three groups treated with nutraceutical molecules and compare with their respective controls Tvrm4 induced who received DMSO *per os* only. The tissues were then analyzed using immunohistological techniques for investigations regarding morphology and real-time PCR and western blot techniques for the determination of expression of photoreceptors and markers of oxidative stress to evaluate the presence of proteins essential for the survival of photoreceptors, oxidative stress, and apoptosis.

Functional and Morphological Recovery of Retinal Neurons After Administration of Natural Molecules

The alteration in retinal function and morphology, between the unexposed/untreated healthy control group and mice exposed to the light induction that triggers the genetic mutation that causes retinal degeneration, is shown in **Supplementary Figure 1**; **Figure 3A** shows the light intensity/response curves of the ERG after the sub-chronic treatments *per os* with naringenin 100 mg/kg/day, quercetin 100 mg/kg/day, naringenin 50 + quercetin 100 mg/kg/day, and of the control group, respectively, of the scotopic and photopic ERG. **Figure 3B** shows the histograms of the scotopic and photopic ERG's waves amplitude at the lowest luminance (0.36 cd*s/m^2, black bars) and the most intense light stimulus (377 cd*s/m^2, gray bars). From the graphs, it is possible to note, concerning the scotopic ERG, that in the case of the single treatment (naringenin 100 mg/kg/day or quercetin 100 mg/kg/day) the amplitude is significantly higher than in the group of animals treated with the vehicle alone. The combined treatment (naringenin 50 + quercetin 100 mg/kg/day) does not show the same trend. In this case, the scotopic ERG shows a greater response of the rods to less intense light stimuli (as if the light sensitivity were increased) compared to the control, this response; however, seems to reach saturation at lower light intensity also compared to the other experimental groups analyzed. In the photopic ERG, the effect obtained does not show statistically significant differences between the treatment and the control groups, except for the single treatment with quercetin 100 mg/kg/day.

TABLE 1 | List of antibodies for Western blotting and immunohistochemistry.

Antibody	Host	Company	Work dilution	Application
Anti-RHO	Mouse monoclonal	Sigma-Aldrich	1:1000	WB
Anti-opsin Red/Green	Rabbit polyclonal	Merck Millipore	1:500	WB
Anti-opsin Blue	Rabbit polyclonal	Merck Millipore	1:500	WB
Anti-Sod1	Rabbit polyclonal	Merck Millipore	1:1000	WB
Anti-Sod2	Goat polyclonal	Merck Millipore	1:1000	WB
Anti-Sod3	Mouse monoclonal	Merck Millipore	1:1000	WB
Anti-Caspase3	Rabbit polyclonal	Merck Millipore	1:1000	WB
Anti-Sirt1	Mouse monoclonal	Merck Millipore	1:1000	WB
Anti-cone arrestin	Rabbit polyclonal	Merck Millipore	1:500	IH
Anti-rabbit IgG HRP conjugated		Merck Millipore	1:5000	WB
Anti-mouse IgG HRP conjugated		Sigma-Aldrich	1:5000	WB
Anti-goat IgG HRP conjugated		Sigma-Aldrich	1:5000	WB
Anti-rabbit (Alexa Fluor 568)		Merck Millipore	1:500	IH

Intake of drinking solution (mean ± SD)

	DMSO group (n=12)	Naringenin group (n=12)	Quercetin group (n=12)	Naringenin + Quercetin group (n=12)
Week 1				
ml/die/animal	3,75 ± 0,22	3,54 ± 0,35	3,52 ± 0,29	3,73 ± 0,29
mg/kg/die/animal	-	87,06 ± 7,9	86,87 ± 5,81	137,32 ± 6,8
Week 2				
ml/die/animal	4,18 ± 1,02	3,86 ± 0,5	4,23 ± 0,84	3,65 ± 0,36
mg/kg/die/animal	-	96 ± 12,76	105,58 ± 21,00	140,48 ± 5,93
Week 3				
ml/die/animal	4,33 ± 1,21	3,76 ± 0,41	4,07 ± 0,51	4,03 ± 1,128
mg/kg/die/animal	-	89,92 ± 7,42	97,17 ± 6,83	144,84 ± 8,93
Week 4				
ml/die/animal	4,36 ± 1,25	3,71 ± 0,34	4,38 ± 1,08	4,85 ± 0,26
mg/kg/die/animal	-	88,86 ± 5,99	107,03 ± 15,23	150,51 ± 0,88
Week 5				
ml/die/animal	4,07 ± 0,99	3,72 ± 0,7	4,41 ± 0,88	6,58 ± 0,98
mg/kg/die/animal	-	89,11 ± 13,62	104,32 ± 14,49	150,94 ± 1,63

FIGURE 2 | Daily intake of drinking solution. The table shows the value expressed in mean ± SD of the relative intake for a week for each group of treatment.

Figure 4 shows the bar graph of gene expression specific for photoreceptors of mice treated with nutraceutical molecules, all samples of treated mice are normalized to the control (dashed line). The analyzed genes encode for proteins responsible for the proper functioning of photoreceptors: CNBG1 (light-sensitive channel), GNAT1 (transducin 1) present in the rods, and ARR3 (cone–arrestin), GNAT2 (transducin 2) present in the cones. The graph shows the ability of compounds to strongly modulate the transcriptional expression of genes present at the level of rods in mice: naringenin and quercetin induce an increase in the expression of CNGB1 and GNAT1.

Figure 5 shows the results obtained through morphological analysis of the retina and the assessment of protein levels (RHO and cone–opsins) essential for rods and cones. In panel A, are illustrated reconstructions of retinas labeled for cone–arrestin (red) and the pink line delineates the damaged areas (black areas) after photo-induction in treated animals compared to the group that received vehicle alone. In **Figure 5B**, the bar graph shows that the reduction in the percentage of damaged retinal area in treated mice is statistically significant compared with the control mice (*naringenin 100 vs. DMSO; # quercetin 100 vs. DMSO; $ naringenin 50 + quercetin 100 vs. DMSO). **Figure 5C** shows the results obtained by WB for the quantification of the protein levels of RHO (38 kDa) and cone–opsins blue + red/green (40 kDa). From the bar graph, it is possible to notice that RHO protein levels are higher in treated mice compared to the control (red

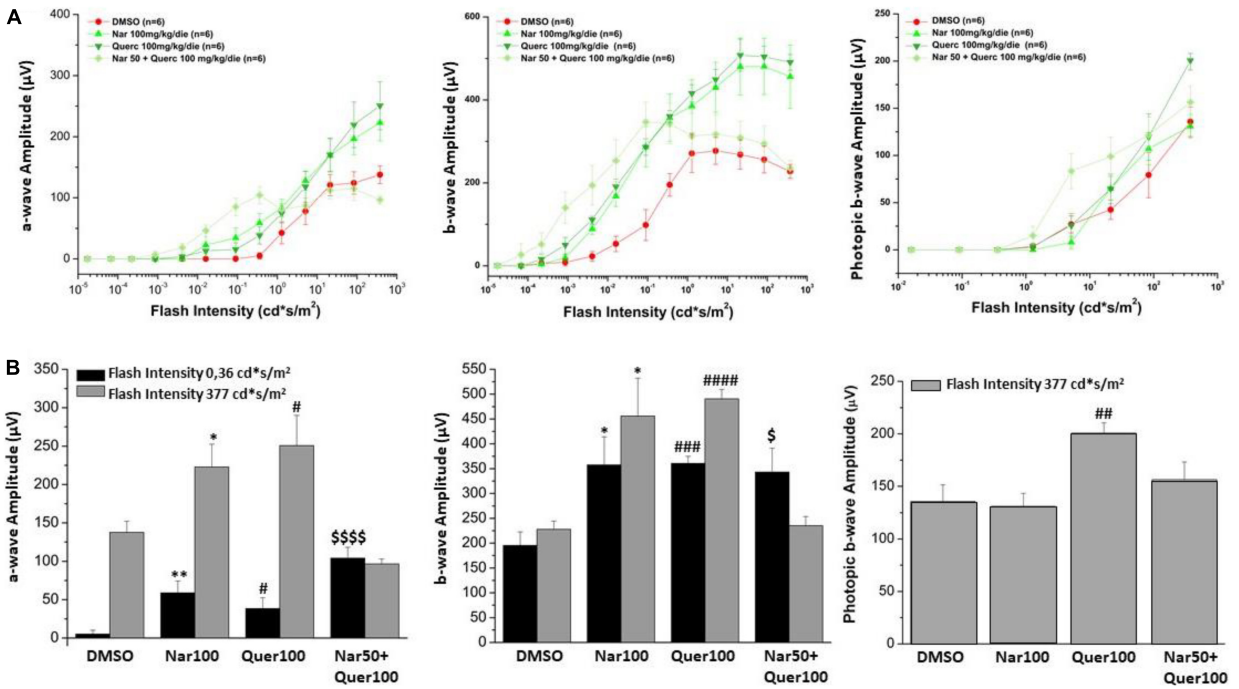

FIGURE 3 | Retinal function was assessed by scotopic and photopic ERG recording. **(A)** Scotopic a- and b-wave amplitude and photopic b-wave amplitude as a function of light stimulus intensity, in treatment (green scale line) and control groups (red line). **(B)** Histogram for the amplitude of scotopic a- and b-waves at a low light intensity (0.36 cd*s/m^2, black bars) and the highest (377 cd*s/m^2, gray bars); the amplitude of photopic b-wave at the highest light intensity (377 cd*s/m^2, gray bars). Bars represent mean ± SEM; statistical analysis was performed using one-way ANOVA test followed by Bonferroni test ($^*p \leq 0.05$, $^{**}p \leq 0.01$ naringenin 100 group vs. DMSO group; $^{\#}p \leq 0.05$, $^{\#\#}p \leq 0.01$, $^{\#\#\#}p \leq 0.001$, $^{\#\#\#\#}p \leq 0.0001$ quercetin 100 group vs. DMSO group; $^{\$}p \leq 0.05$, $^{\$\$\$}p \leq 0.001$, naringenin 50 + quercetin 100 group vs. DMSO group).

bar) with significant results for the single treatment quercetin (100 mg/kg/day) and the combined treatment (naringenin 50 + quercetin 100 mg/kg/day) (#quercetin 100 vs. DMSO; $ naringenin 50 + quercetin 100 vs. DMSO). On the other hand, the results obtained from the quantification of cone–opsins blue + red/green were not significant.

Efficacy of Natural Molecules in Modulating Oxidative Stress Defense and Apoptosis in Retinal Tissue

After verifying the viability and survival of photoreceptors following treatments with antioxidant nutraceuticals, the effect on markers of oxidative stress and apoptosis was evaluated. In RP, following the death of rods, triggered by the genetic mutation present, is created at the level of retinal tissue a condition of hyperoxia that causes an increase in the production of ROS (Yu et al., 2000, 2004). The presence of ROS and the consequent increase in oxidative stress is considered one of the factors leading to degeneration and secondary death of cones (Valter et al., 1998; Cingolani et al., 2006; Komeima et al., 2006, 2007, 2008; Lee et al., 2011). The previous studies in the rd10 animal model (autosomal recessive RP) showed a reduction in Sod1 and Sod2 following treatment with naturally occurring antioxidants (naringenin and quercetin) (Piano et al., 2019). Through the use of real-time PCR and WB technique, gene expression and protein levels of enzymes involved in cellular pathways aimed at counteracting oxidative stress were determined. As shown in **Figure 6**, the analysis of 84 genes, shows that the treatment with antioxidant molecules induces changes in the regulation of several genes involved in oxidative stress and antioxidant response. The gene regulation profile after naringenin and quercetin treatments shows a different color pattern in the heatmap (**Figure 6**), where quercetin seems to lead to greater changes than naringenin in the expression of genes involved in oxidative stress and antioxidant response. In detail, naringenin leads to upregulation of 10 genes (fold-change $\geq$ 2 vs. DMSO, used as pathological control; data not shown) and downregulation of 4 genes (fold-change $\leq$ 0.5 vs. DMSO; data not shown). The treatment with quercetin affected the expression of 32 genes, whose transcriptional levels appear strongly increased (fold-change $\geq$ 2 vs. DMSO; data not shown). Interestingly, the combined treatment appears able to affect the expression of almost all analyzed genes: 45 genes show a great increase in their expression levels (fold-change $\geq$ 2 vs. DMSO, data not shown), exhibiting an opposite profile of gene expression compared to DMSO treated group (**Figure 6**).

To better understand these modulations, the transcriptional levels of the same genes were analyzed also in healthy control (HC) mice. Compared to pathological control, the expression of 43 genes is strongly modulated (fold-change $\geq$ 2 or fold-change $\leq$ 0.5 vs. DMSO) in HC, suggesting a role of these genes in the pathogenesis of RP. As shown in **Figure 5**,

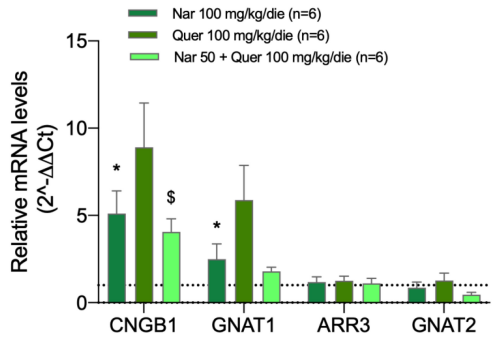

FIGURE 4 | Transcriptional levels of photoreceptor genes from the treated groups of animals compared to the pathological control. The transcriptional levels of four mRNAs coding for photoreceptor proteins were analyzed by real-time PCR. Specifically, the histogram shows the expression of CNBG1 coding light-sensitive channel, GNAT1 coding transducin 1, ARR3 coding cone-arrestin, and GNAT2 coding transducin 2 in the control group (DMSO treated animals) and in groups treated with naringenin 100 mg/kg/day, quercetin 100 mg/kg/day, and naringenin 50 + quercetin 100 mg/kg/day (n = 6, respectively). The data are representative of six animals ± SEM. The bars represent the value obtained after normalization of each value on the mean expression of the most stable genes among those analyzed (from array data) and are expressed as fold-change relative to the control group (made = 1). The statistical analysis was performed using Student's t-test of the normalized values for each gene in treatment groups ($^{*}p \leq 0.05$, naringenin 100 group vs. DMSO group; $^{\$}p \leq 0.05$, naringenin 50 + quercetin 100 group vs. DMSO group).

naringenin modulates the expression of some genes oppositely compared to HC. For example, dual oxidase 1 (Duox1), nitric oxide synthase 2 (Nos2) and Uncoupling Protein 3 (Ucp3) have an opposite trend. Instead, both quercetin and the combined treatment show an expression profile closer to that of HC compared to naringenin (**Figure 6**). For example, mice treated with quercetin and the combination show a similar expression profile of gene family coding glutathione peroxidases, lactoperoxidase, myeloperoxidase, and NADPH oxidases and their activators, compared to HC. Noteworthy, after the combined treatment, the transcriptional levels of several genes are strongly over-expressed compared to HC: the expression of genes coding glutathione peroxidases (Gpx), interleukin 19, recombination activating gene 2 (Rag2), and RecQ protein-like 4 (Recql4) is doubled. Furthermore, many genes (Gpx), lactoperoxidases (Lpo), prostaglandin–endoperoxide synthase 2 (Ptgs2), or myeloperoxidase (Mpo) are increased not only compared to HC but also to quercetin. Overall, quercetin appears the treatment closest to HC. **Figure 7A** shows the fold-change of the transcriptional expression of SOD1, SOD2, and SOD3 after treatment with antioxidants, normalized to the control group. **Figures 7B–D** show the protein levels of Sod1, Sod2, Sod3 enzymes, respectively, in treated mice compared with the control group treated with vehicle (red) **Figure 7E** shows a representative example of a WB experiment. The transcriptional expression of the SOD1 gene (A) is significantly upregulated after naringenin and the combined treatment (*naringenin 100 vs. DMSO; $naringenin 50 + quercetin 100 vs. DMSO;1.88 ± 0.64 and 2.18 ± 0.73-fold-increase, respectively). The SOD2 gene expression is increased after all treatments, as opposed to SOD3 expression (A). The results show reduced protein levels for Sod1 (B) in the combined and single treatment with quercetin compared to controls, in contrast, the single treatment with naringenin shows a significant increase in protein levels compared to the control (*naringenin 100 vs. DMSO; + naringenin 100 vs. quercetin 100; □ naringenin 50 + quercetin 100 vs. naringenin 100). The histogram for Sod2 (C) shows no statistically significant differences in the levels of the enzyme in the retina of treated mice compared to controls. The bar graph in D relative to Sod3, data showing, in all the various types of treatment, an increasing trend in the levels of the enzyme in treated animals compared to the control (red). Sod3 levels increased significantly ($DMSO vs. naringenin 50 + quercetin 100; □ naringenin 50 + Quercetin 100 vs. naringenin 100; ◊ naringenin 50 + Quercetin 100 vs. quercetin 100) in the group of animals that received the combined treatment (naringenin50 + quercetin 100 mg/kg/day) compared to the control group. To assess whether the administered nutraceutical molecules also could interfere with photoreceptor death, protein levels of markers of the apoptotic pathway were assessed (**Figures 8A,B**). In particular, Sirt-1, an anti-apoptotic factor, and Caspase-3, the ultimate effector of the cascade of apoptosis and common to the extrinsic and intrinsic pathways, were evaluated; the vehicle-treated control group (red bar), as shown by the histograms in **Figure 8B**, had high levels of the pro-apoptotic factor Caspase-3 and a low amount of the anti-apoptotic factor Sirt-1. From the histograms related to the treatments (green scales) it is evident a significant increase ($ DMSO vs. naringenin 50 + quercetin 100; □ naringenin 50 + quercetin 100 vs. naringenin 100; ◊ naringenin 50 + quercetin 100 vs. quercetin 100) of the anti-apoptotic factor Sirt-1 in the presence of the combined treatment (naringenin 50 + quercetin100 mg/kg/day) compared to the control while no significant variation is present following the single treatment with naringenin (100 mg/kg/day) or quercetin (100 mg/kg/day). Concerning the combined treatment, in accordance with the histogram relating to Sirt-1, there is a significant decrease ($DMSO vs. naringenin 50 + quercetin 100; □ naringenin 50 + quercetin 100 vs. naringenin 100; ◊ naringenin 50 + quercetin 100 vs. quercetin 100) of Caspase-3 compared to the control group (red); even in the single treatment, although not statistically significant, there is still a decrease of Caspase-3 compared to the diseased control.

DISCUSSION

The recent work in patients suggests that oxidative stress may promote blood–retinal barrier damage by modulating the production of vasoactive factors, and also accelerate the morphological damage of cone photoreceptors. Several studies in the literature have shown that too high concentrations of ROS lead to cellular damage in both animals and humans, in fact in their eyes, high levels of proteins resulting from oxidative damage were detected in the aqueous humor, compared with controls and

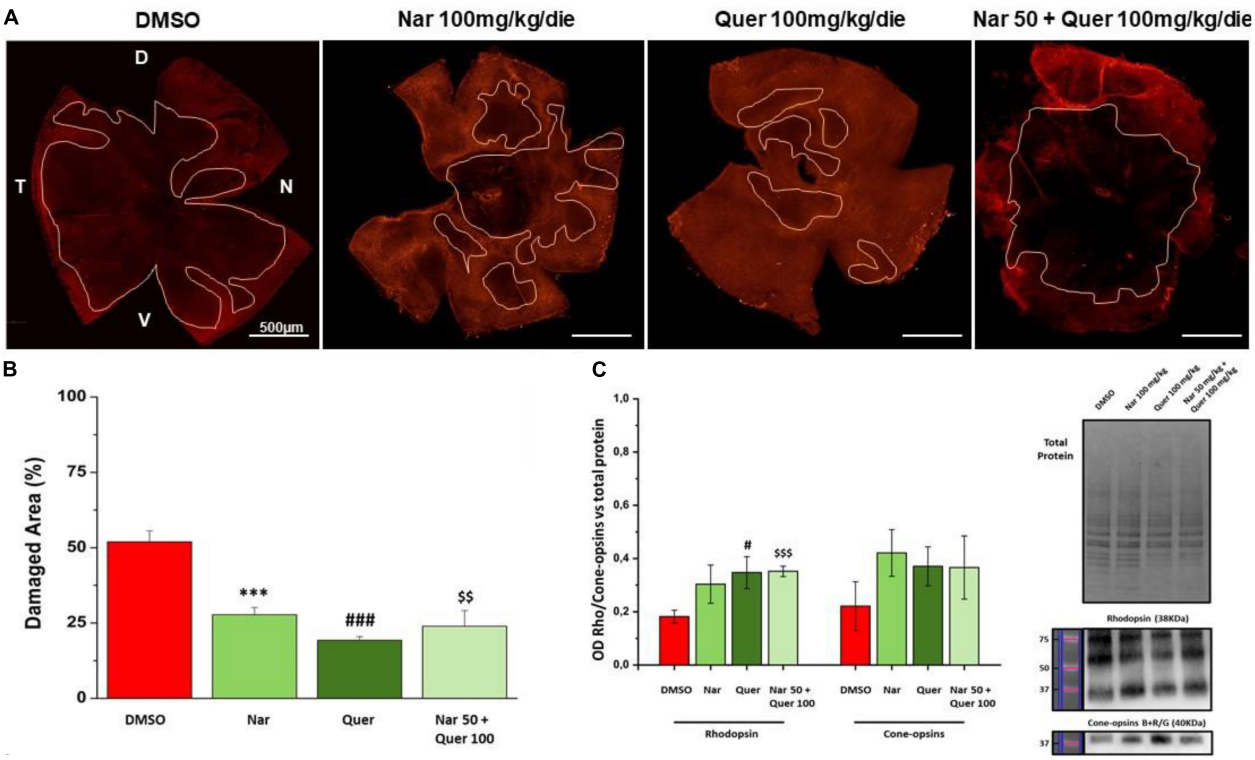

FIGURE 5 | Morphological assessment of the damaged area. **(A)** Morphology of whole-mount retina of naringenin 100 mg/kg/die, quercetin 100 mg/kg/die, naringenin 50 + quercetin 100 mg/kg/die treated groups and pathological control (cone-arrestin, red). The pink line delineates the damaged area after photo-induction. **(B)** Histogram for quantification of the damaged area as a percentage of total retinal area for each treatment and control. Each treatment group used to study retinal morphology consisted of $n = 6$ animals. The bars represent mean ± SEM; the statistical analysis was performed using one-way ANOVA test followed by Bonferroni test ($^{***}p \leq 0.001$, naringenin 100 group vs. DMSO group; $^{\#\#\#}p \leq 0.001$, quercetin 100 group vs. DMSO group; $^{\$\$}p \leq 0.01$, naringenin 50 + quercetin 100 group vs. DMSO group). **(C)** WB analysis for the treatment and control groups. On the right, the image of the bads related to total protein, RHO, and cone–opsins blue + red/green; on the left, the histogram related to the quantification, by optical densitometry, of RHO and cone–opsins. The number of animals used for WB analysis was, respectively, DMSO ($n = 6$); naringenin 100 mg/kg/die ($n = 11$); quercetin100 mg/kg/die ($n = 6$); naringenin 50 + quercetin 10 mg/kg/die ($n = 6$). The data are representative of animals ± SEM. The bars represent each value normalized with the total protein and then compared with the control group (DMSO only); the statistical analysis was performed using one-way ANOVA test followed by Bonferroni test ($^{\#}p \leq 0.05$, quercetin 100 group vs. DMSO group; $^{\$\$\$}p \leq 0.001$, naringenin 50 + quercetin 100 group vs. DMSO group).

how also the formation of cataracts in the eyes can be linked to oxidative stress (Campochiaro et al., 2015; Vingolo et al., 2022).

A previous study conducted in our laboratory has shown the predominant role of oxidative stress in secondary cone-photoreceptor death and the role in slowing down the degeneration of antioxidant molecules in an autosomal recessive model of RP (Piano et al., 2019). Further studies, conducted in different animal models of RP, confirmed the strong involvement of oxidative stress in cone degeneration by demonstrating how different therapeutic approaches, which target oxidative stress, are effective in slowing down the progressive degeneration of these cells (Assimopoulou et al., 2005; Shen et al., 2005; Komeima et al., 2006, 2007, 2008; Kanakis et al., 2007; Fernández-Sánchez et al., 2012; Xiong et al., 2015; Wang et al., 2016; Trouillet et al., 2018).

In the present study, we tested a therapeutic strategy using two flavonoids abundant in fruits and vegetables, naringenin and quercetin, to counteract the oxidative stress underlying RP progression. Indeed, these flavonoids show antioxidant properties that interact with the cellular detoxification enzyme system (Al-Dosari et al., 2017). Furthermore, it has been shown that the anti-oxidant and anti-apoptotic effects of flavonoids can limit neurodegeneration by providing neurotrophic support to prevent retinal damage in RP as in other types of retinal disorders, such as diabetic retinopathy (Al-Dosari et al., 2017) and age-related macular degeneration (AMD) (Maccarone et al., 2008; Falsini et al., 2010; Gopinath et al., 2018). Our findings confirm, and extend, previous data published by other groups on the pivotal role of increased oxidative stress in photoreceptor death and the beneficial effects of antioxidant molecules in slowing retinal degeneration. Specifically, we observed that sub-chronic non-invasive treatment with naturally derived molecules, frequently present in normal diets, can significantly slow disease progression in an animal model of autosomal dominant RP, Tvrm4. The single treatment with the two molecules is effective in preserving the functionality and morphology of the retina. Noteworthy, quercetin appears more effective to protect retinal function compared to naringenin. This less neuroprotection

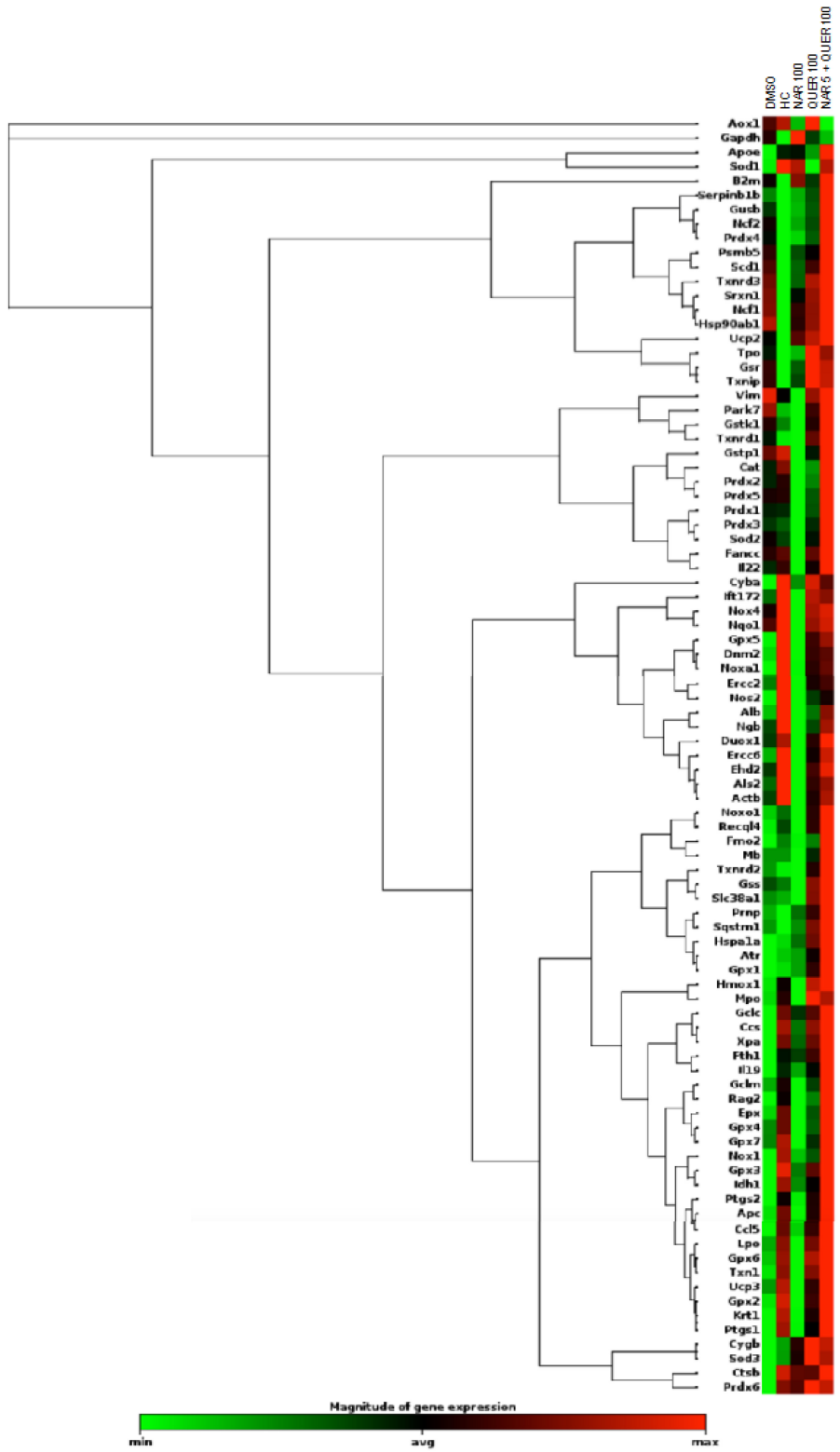

FIGURE 6 | Heatmap of genes (mRNAs) involved in oxidative stress and antioxidant response. Columns reports the transcriptional expression levels of 84 genes in groups treated with DMSO alone (control group), naringenin 100 mg/kg/day, quercetin 100 mg/kg/day, and naringenin 50 + quercetin 100 mg/kg/day (n = 6, respectively). Furthermore, the expression levels of the same genes in HC (n = 6). Each square represents the mean values of the values obtained after normalization on the mean expression of the most stable genes among those analyzed. Red color indicates the most upregulated expression levels, while green color indicates the least downregulated expression levels.

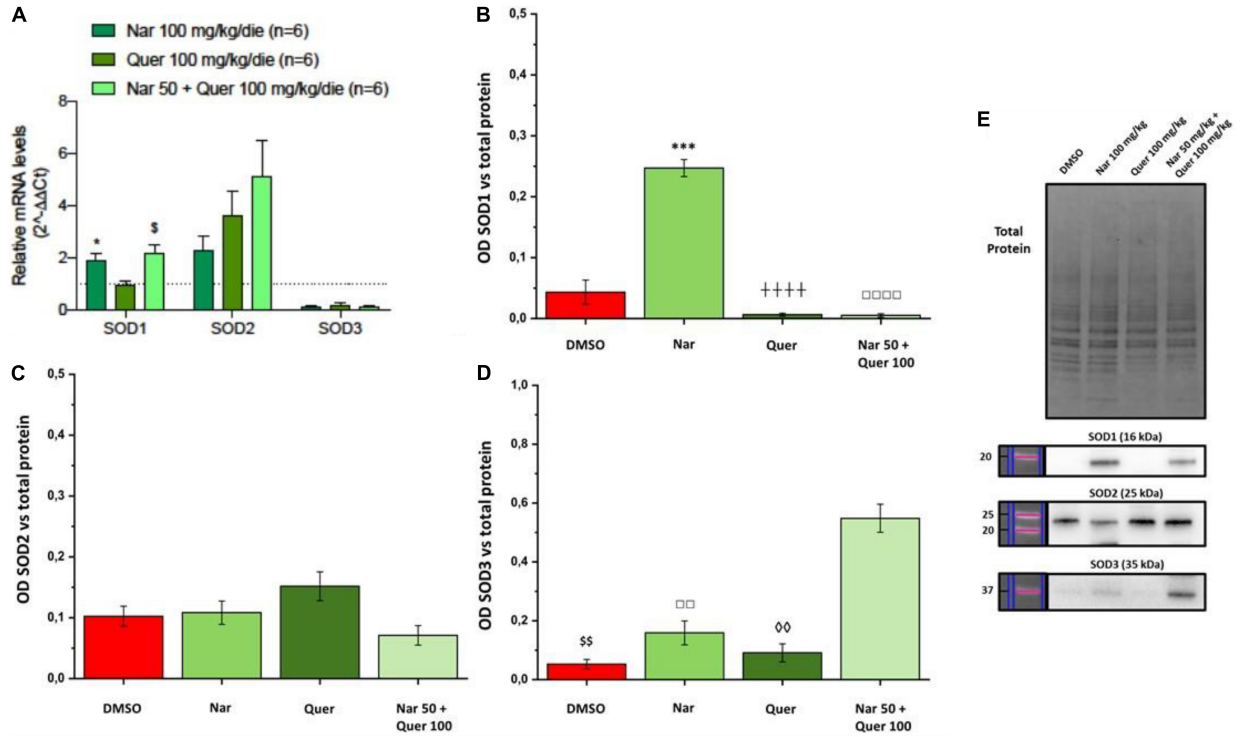

FIGURE 7 | Real-time PCR and WB analysis of oxidative stress markers. **(A)** Trend and statistical significance of transcriptional expression of Sod1, Sod2, and Sod3 genes (data from array analysis) in groups treated with naringenin 100 mg/kg/day, quercetin 100 mg/kg/day, and naringenin 50 + quercetin 100 mg/kg/day ($n = 6$, respectively) compared to the control group ($n = 6$). The data are extrapolated from the array analysis and are representative of six animals ± SEM. Bars represent the value obtained after normalization of each value on the mean expression of the most stable genes among those analyzed (from array analysis). The data are expressed as fold-change relative to the control group (made = 1). The statistical analysis was performed using Student's *t*-test of the normalized values for each gene in treatment groups ($^{*}p \leq 0.05$, naringenin 100 group vs. DMSO group; $^{\$}p \leq 0.05$, naringenin 50 + quercetin 100 group vs. DMSO group). **(B–D)** Quantification by WB of the protein levels of Sod1, Sod2, Sod3 in the groups treated with naringenin 100 mg/kg/day ($n = 10$), quercetin 100 mg/kg/day ($n = 6$) and naringenin 50 + quercetin 100 mg/kg/day ($n = 4$) compared with the control group (DMSO, $n = 6$). **(E)** Image of the bands related to Total Protein, Sod-1, Sod-2, and Sod-3. The data are representative of animals ± SEM. The bars represent each value normalized with the total protein and then compared with the control group (DMSO only); statistical analysis was performed using one-way ANOVA test followed by Bonferroni test ($^{***}p \leq 0.001$, naringenin 100 group vs. DMSO group; $^{\$\$}p \leq 0.01$, naringenin 50 + quercetin 100 group vs. DMSO group; $^{++++}p \leq 0{,}0001$, naringenin 100 group vs. quercetin 100 group; $^{\diamond\diamond}p \leq 0.01$, naringenin 50 + quercetin 100 group vs. quercetin 100 group; $^{\square\square}p \leq 0.01$, $^{\square\square\square\square}p \leq 0.0001$, naringenin 100 group vs. naringenin 50 + quercetin 100 group).

could be partly explained by the changes in transcriptional expression of genes involved in antioxidant defense regulation, where naringenin shows the expression profile is more different from HC. Furthermore, both gene and protein expression analysis showed an increase in SOD1 levels, as opposite to quercetin. Even if SOD1 has an important role in the antioxidant defense system in the retina (Dong et al., 2006), overexpression of SOD1 also showed increased oxidative damage and more rapid loss of cone function (Usui et al., 2011). Evidence reports that there is a discrepancy between the activity of the individual natural compound and the activity of whole fruit or vegetable from which they are extracted (Miller and Rice-Evans, 1997; Koss-Mikołajczyk et al., 2019; Baranowska et al., 2020). One of the possible explanations could be a pharmacological interaction between natural compounds. Therefore, we analyzed the potential effects of combined administration of the two flavonoids, evaluating the ability of the less active compound to potentiate the protective effects of the most active molecule. Un-expectedly, the combined treatment of the two molecules showed a different trend from single molecules. The expression analysis of genes involved in oxidative stress and antioxidant response suggests one possible explanation also to the unforeseen trend of the combined treatment: instead of restoring the physiological balance minimizing the levels of ROS, the co-treatment could lead to an excessive antioxidant response reducing also low levels of ROS that are involved in cell signaling and redox regulation, thus inducing an "anti-oxidative stress" (Poljsak and Milisav, 2012; Poljsak et al., 2013; Kornienko et al., 2019). Indeed, both anti-oxidative and oxidative stresses lead to the anti-oxidative imbalance that can be damaging (Poljsak et al., 2013). Moreover, the combined treatment induces a strong increase in the protein expression of SOD3 levels, as opposed to single treatments with naringenin and quercetin. Even if SOD3 protects from oxidative injury, its excessive increase can be deleterious (Ikelle et al., 2021).

Furthermore, from the results obtained it is possible to observe that the response to low luminance of the scotopic ERG, for animals treated with the combination of the two

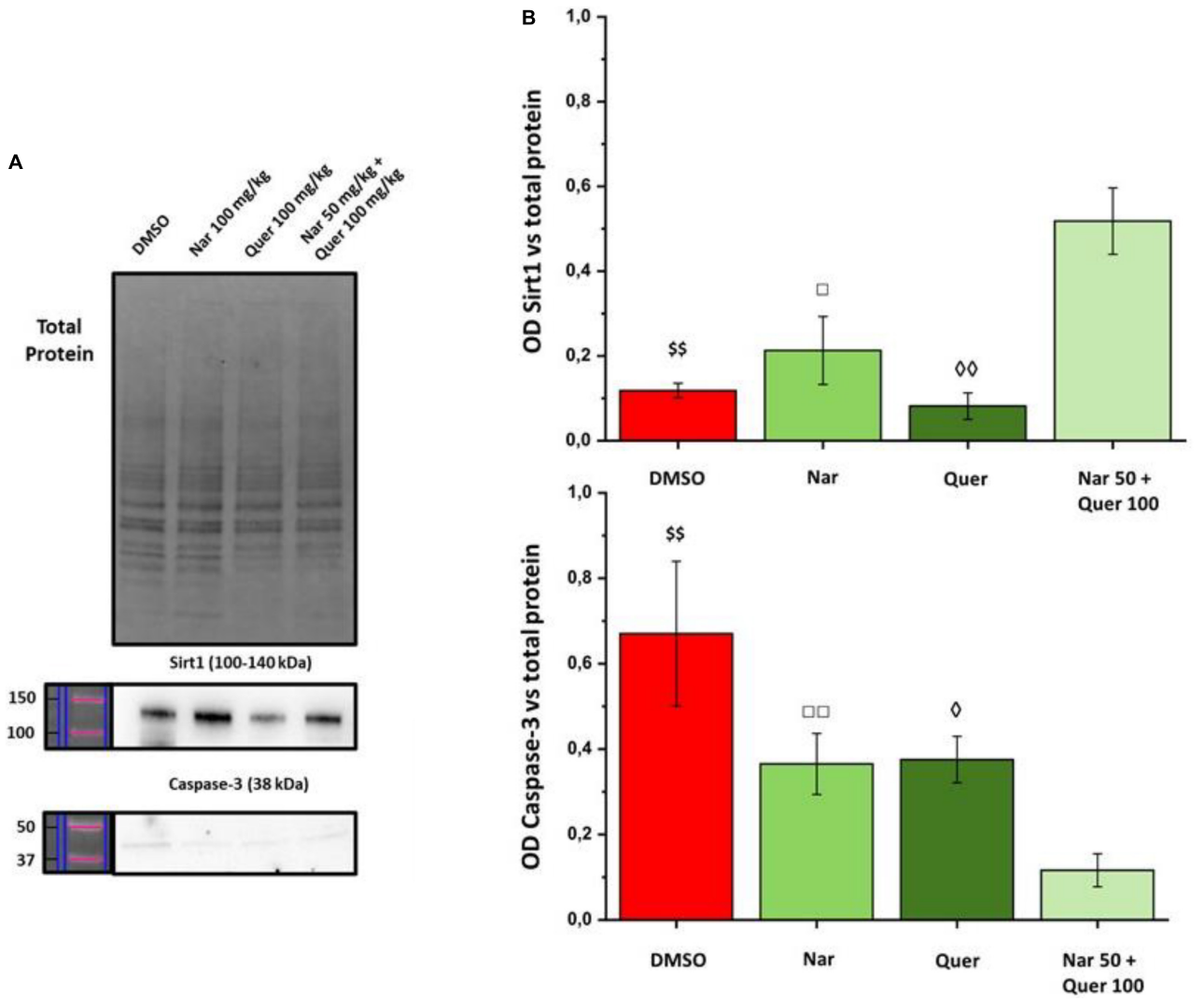

FIGURE 8 | WB analysis of apoptosis markers. **(A)** Image of the bands related to Total Protein, Caspase-3, and Sirt-1. **(B)** Histogram relative to the quantification, by optical densitometry, of Caspase-3 and Sirt-1. The number of animals used for WB analysis were, respectively: control group (DMSO, $n = 6$); naringenin 100 mg/kg/day ($n = 11$); quercetin 100 mg/kg/day ($n = 6$); naringenin 50 + quercetin 100 mg/kg/day ($n = 6$). The data are representative of animals ± SEM. The bars represent each value normalized with the total protein and then compared with the control group (DMSO only); the statistical analysis was performed using one-way ANOVA test followed by Bonferroni test ($^{\$\$}p \leq 0.01$, naringenin 50 + quercetin 100 group vs. DMSO group; $^{\diamond}p \leq 0.05$, $^{\diamond\diamond}p \leq 0.01$, naringenin 50 + quercetin 100 group vs. quercetin 100 group; $^{\square}p \leq 0.05$, $^{\square\square}p \leq 0.01$, naringenin 100 group vs. naringenin 50 + quercetin 100 group).

molecules, is greater than in pathological controls. This trend shows a drastic reduction at high light intensities, indicating a phenomenon of saturation of the photoreceptors and the lack of ability to recycle the photopigment (Lamb and Pugh, 2004; Kiser et al., 2012). This could be due to the ability of two molecules in combination to preserve cells from death (by modulation of the anti-apoptotic agent Sirt-1) and to stabilize the RHO molecules still available (Herrera-Hernández et al., 2017; Ortega et al., 2019) but inducing the antioxidant stress. As a result of this state within photoreceptors and RPE cells, which are responsible for recycling retinoid from RHO and are involved in phagocytosis of the tips of the outer segments of photoreceptors, there is an accumulation of toxic factors that do not allow the proper functioning of the photoreceptors. The development of anti-oxidative stress could cause metabolic deficits at the level of photoreceptors that hypothetically are no longer able to recycle and renew the proteins necessary for the proper functioning of the phototransduction machine (Ortega and Jastrzebska, 2019).

CONCLUSION

Overall, the data obtained from this study show that the anti-oxidant and anti-apoptotic effects of flavonoids may limit neurodegeneration by providing neurotrophic support to prevent retinal damage in an animal model of autosomal dominant

RP (Tvrm4 mice) as in other types of retinal diseases, such as diabetic retinopathy (Al-Dosari et al., 2017) and AMD (Maccarone et al., 2008; Falsini et al., 2010; Gopinath et al., 2018). In this work, we first used the Tvrm4 mouse model of RP to test the potential beneficial effects of two nutraceutical compounds, naringenin, and quercetin in single or combined administration, found in a typical Western diet, using a sub-chronic non-invasive treatment. In conclusion, our results demonstrate that supplementing the diet with sufficient doses of flavonoids could be an effective preventive, mutation-independent, non-invasive approach to slow retinal degeneration. This neuroprotective approach requires further investigation to estimate the true efficacy of the treatment to preserve vision in patients with various forms of RP and to establish the optimized regimen of exogenous antioxidant molecules especially when these are administered in combination.

DATA AVAILABILITY STATEMENT

The datasets presented in this study can be found in online repositories. The names of the repository/repositories and accession number(s) can be found in the article/ **Supplementary Material**.

ETHICS STATEMENT

The study was reviewed and approved by the Animal Welfare Organization (OPBA - Ethics Committee) of the University of Pisa and the Italian Ministry of Health (Protocol #653/2017-PR-DB173.3.EXT.0, Department of Pharmacy, University of Pisa). This study was conducted according to the guidelines of the Declaration of Helsinki and according to Italian and European institutional guidelines.

AUTHOR CONTRIBUTIONS

IP and CG conceptualized the study, contribute to the supervision, and wrote the original draft. IP, FC, and BP contributed to the data curation and formal analysis. CG and IP contributed to the funding acquisition. FC and BP contributed to the methodology. IP, FC, BP, and CG contributed to writing, reviewing, and editing the manuscript. All authors contributed to the article and approved the submitted version.

FUNDING

The work presented in this article was funded by Velux Stiftung (Grant No. 1236) and by the Research Projects of Ateneo 2020–2021 (Grant No. PRA2020_37), University of Pisa.

SUPPLEMENTARY MATERIAL

The Supplementary Material for this article can be found online at: https://www.frontiersin.org/articles/10.3389/fnins.2022.868750/full#supplementary-material

Supplementary Figure 1 | Retinal function and morphology. **(A)** Scotopic a- and b-wave amplitude and photopic b-wave amplitude as a function of light stimulus intensity, in Unexposed/untreated health control (black scale line) and Exposed groups (red line). **(B)** Representative ERG traces of scotopic and photopic ERG at the highest light intensity (377 cd*s/m^2 gray bars); **(C)** Whole-mount retina stained against cone–arrestin protein.

Supplementary Figure 2 | Specificity control of cone-arrestin antibody on retinal sections of unstressed/untreated Tvrm4 mice.

Supplementary Figure 3 | Control of the specificity of RHO **(A)** and cone–opsin **(B)** antibodies, respectively, on retinal protein lysates and on cell lysates of ARPE-19, a retinal pigment epithelium cell line that physiologically does not express photoreceptor-specific photopigments.

REFERENCES

Al-Dosari, D., Ahmed, M., Al-Rejaie, S., Alhomida, A., and Ola, M. (2017). Flavonoid naringenin attenuates oxidative stress, apoptosis and improves neurotrophic effects in the diabetic rat retina. *Nutrients* 9:1161. doi: 10.3390/nu9101161

Assimopoulou, A. N., Sinakos, Z., and Papageorgiou, V. P. (2005). Radical scavenging activity of *Crocus sativus* L. extract and its bioactive constituents. *Phytother. Res.* 19, 997–1000. doi: 10.1002/ptr.1749

Bacci, A., Runfola, M., Sestito, S., and Rapposelli, S. (2021). Beyond antioxidant effects: nature-based templates unveil new strategies for neurodegenerative diseases. *Antioxidants* 10:367. doi: 10.3390/antiox10030367

Baranowska, M., Suliborska, K., Todorovic, V., Kusznierewicz, B., Chrzanowski, W., Sobajic, S., et al. (2020). Interactions between bioactive components determine antioxidant, cytotoxic and nutrigenomic activity of cocoa powder extract. *Free Rad. Biol. Med.* 154, 48–61. doi: 10.1016/j.freeradbiomed.2020.04.022

Budzynski, E., Gross, A. K., McAlear, S. D., Peachey, N. S., Shukla, M., He, F., et al. (2010). Mutations of the *Opsin* Gene (Y102H and I307N) lead to light-induced degeneration of photoreceptors and constitutive activation of phototransduction in mice. *J. Biol. Chem.* 285, 14521–14533. doi: 10.1074/jbc.M110.112409

Campochiaro, P. A., and Mir, T. A. (2018). The mechanism of cone cell death in Retinitis pigmentosa. *Progr. Ret. Eye Res.* 62, 24–37. doi: 10.1016/j.preteyeres.2017.08.004

Campochiaro, P. A., Strauss, R. W., Lu, L., Hafiz, G., Wolfson, Y., Shah, S. M., et al. (2015). Is there excess oxidative stress and damage in eyes of patients with retinitis pigmentosa? *Antioxid. Redox Signal.* 23, 643–648. doi: 10.1089/ars.2015.6327

Castelli, V., Paladini, A., d'Angelo, M., Allegretti, M., Mantelli, F., Brandolini, L., et al. (2021). Taurine and oxidative stress in retinal health and disease. *CNS Neurosci. Ther.* 27, 403–412. doi: 10.1111/cns.13610

Cingolani, C., Rogers, B., Lu, L., Kachi, S., Shen, J., and Campochiaro, P. A. (2006). Retinal degeneration from oxidative damage. *Free Rad. Biol. Med.* 40, 660–669. doi: 10.1016/j.freeradbiomed.2005.09.032

D'Andrea, G. (2015). Quercetin: A flavonol with multifaceted therapeutic applications? *Fitoterapia* 106, 256–271. doi: 10.1016/j.fitote.2015.09.018

Dong, A., Shen, J., Krause, M., Akiyama, H., Hackett, S. F., Lai, H., et al. (2006). Superoxide dismutase 1 protects retinal cells from oxidative damage. *J. Cell. Physiol.* 208, 516–526. doi: 10.1002/jcp.20683

Falsini, B., Piccardi, M., Minnella, A., Savastano, C., Capoluongo, E., Fadda, A., et al. (2010). Influence of saffron supplementation on retinal flicker sensitivity in early age-related macular degeneration. *Invest. Ophthalmol. Vis. Sci.* 51:6118. doi: 10.1167/iovs.09-4995

Fernández-Sánchez, L., Lax, P., Esquiva, G., Martín-Nieto, J., Pinilla, I., and Cuenca, N. (2012). Safranal, a saffron constituent, attenuates retinal degeneration in P23H Rats. *PLoS One* 7:e43074. doi: 10.1371/journal.pone.0043074

Gargini, C., Novelli, E., Piano, I., Biagioni, M., and Strettoi, E. (2017). Pattern of retinal morphological and functional decay in a light-inducible, rhodopsin mutant mouse. *Sci. Rep.* 7, 5730. doi: 10.1038/s41598-017-06045-x

Gopinath, B., Liew, G., Kifley, A., Lewis, J. R., Bondonno, C., Joachim, N., et al. (2018). Association of dietary nitrate intake with the 15-year incidence of age-related macular degeneration. *J. Acad. Nutr. Diet.* 118, 2311–2314. doi: 10.1016/j.jand.2018.07.012

Gürtler, A., Kunz, N., Gomolka, M., Hornhardt, S., Friedl, A. A., McDonald, K., et al. (2013). Stain-Free technology as a normalization tool in Western blot analysis. *Anal. Biochem.* 433, 105–111. doi: 10.1016/j.ab.2012.10.010

Herrera-Hernández, M. G., Ramon, E., Lupala, C. S., Tena-Campos, M., Pérez, J. J., and Garriga, P. (2017). Flavonoid allosteric modulation of mutated visual rhodopsin associated with retinitis pigmentosa. *Sci. Rep.* 7:11167. doi: 10.1038/s41598-017-11391-x

Ikelle, L., Naash, M. I., and Al-Ubaidi, M. R. (2021). Modulation of SOD3 levels is detrimental to retinal homeostasis. *Antioxidants* 10:1595. doi: 10.3390/antiox10101595

Jeon, C.-J., Strettoi, E., and Masland, R. H. (1998). The major cell populations of the mouse retina. *J. Neurosci.* 18, 8936–8946. doi: 10.1523/JNEUROSCI.18-21-08936.1998

Kanakis, C. D., Tarantilis, P. A., Tajmir-Riahi, H. A., and Polissiou, M. G. (2007). Crocetin, dimethylcrocetin, and safranal bind human serum albumin: stability and antioxidative properties. *J. Agric. Food Chem.* 55, 970–977. doi: 10.1021/jf062638l

Kim, K.-A., Kang, S. W., Ahn, H. R., Song, Y., Yang, S. J., and Jung, S. H. (2015). Leaves of Persimmon (*Diospyros kaki* Thunb.) Ameliorate *N* -Methyl- *N* -nitrosourea (MNU)-induced retinal degeneration in mice. *J. Agric. Food Chem.* 63, 7750–7759. doi: 10.1021/acs.jafc.5b02578

Kiser, P. D., Golczak, M., Maeda, A., and Palczewski, K. (2012). Key enzymes of the retinoid (visual) cycle in vertebrate retina. *Biochim. Biophys. Acta* 1821, 137–151. doi: 10.1016/j.bbalip.2011.03.005

Komeima, K., Rogers, B. S., and Campochiaro, P. A. (2007). Antioxidants slow photoreceptor cell death in mouse models of retinitis pigmentosa. *J. Cell Physiol.* 213, 809–815. doi: 10.1002/jcp.21152

Komeima, K., Rogers, B. S., Lu, L., and Campochiaro, P. A. (2006). Antioxidants reduce cone cell death in a model of retinitis pigmentosa. *Proc. Natl. Acad. Sci. U.S.A.* 103, 11300–11305. doi: 10.1073/pnas.0604056103

Komeima, K., Usui, S., Shen, J., Rogers, B. S., and Campochiaro, P. A. (2008). Blockade of neuronal nitric oxide synthase reduces cone cell death in a model of retinitis pigmentosa. *Free Rad. Biol. Med.* 45, 905–912. doi: 10.1016/j.freeradbiomed.2008.06.020

Kornienko, J. S., Smirnova, I. S., Pugovkina, N. A., Ivanova, J. S., Shilina, M. A., Grinchuk, T. M., et al. (2019). High doses of synthetic antioxidants induce premature senescence in cultivated mesenchymal stem cells. *Sci. Rep.* 9:1296. doi: 10.1038/s41598-018-37972-y

Koss-Mikołajczyk, I., Kusznierewicz, B., and Bartoszek, A. (2019). The relationship between phytochemical composition and biological activities of differently pigmented varieties of berry fruits; comparison between embedded in food matrix and isolated anthocyanins. *Foods* 8:646. doi: 10.3390/foods8120646

Lamb, T. D., and Pugh, E. N. (2004). Dark adaptation and the retinoid cycle of vision. *Progr. Ret. Eye Res.* 23, 307–380. doi: 10.1016/j.preteyeres.2004.03.001

Lee, S. Y., Usui, S., Zafar, A., Oveson, B. C., Jo, Y.-J., Lu, L., et al. (2011). N-acetylcysteine promotes long-term survival of cones in a model of retinitis pigmentosa. *J. Cell. Physiol* 226, 1843–1849. doi: 10.1002/jcp.22508

Liu, X.-B., Liu, F., Liang, Y.-Y., Yin, G., Zhang, H.-J., Mi, X.-S., et al. (2021). Luteolin delays photoreceptor degeneration in a mouse model of retinitis pigmentosa. *Neural Regen. Res.* 16:2109. doi: 10.4103/1673-5374.303537

Maccarone, R., Di Marco, S., and Bisti, S. (2008). Saffron supplement maintains morphology and function after exposure to damaging light in mammalian retina. *Invest. Ophthalmol. Vis. Sci.* 49:1254. doi: 10.1167/iovs.07-0438

Miller, N. J., and Rice-Evans, C. A. (1997). The relative contributions of ascorbic acid and phenolic antioxidants to the total antioxidant activity of orange and apple fruit juices and blackcurrant drink. *Food Chem.* 60, 331–337. doi: 10.1016/s0308-8146(96)00339-1

Ortega, J. T., and Jastrzebska, B. (2019). The retinoid and non-retinoid ligands of the rod visual G Protein-coupled receptor. *Int. J. Mol. Sci.* 20:6218. doi: 10.3390/ijms20246218

Ortega, J. T., and Jastrzebska, B. (2021). Neuroinflammation as a therapeutic target in retinitis pigmentosa and quercetin as its potential modulator. *Pharmaceutics* 13:1935. doi: 10.3390/pharmaceutics13111935

Ortega, J. T., Parmar, T., and Jastrzebska, B. (2019). Flavonoids enhance rod opsin stability, folding, and self-association by directly binding to ligand-free opsin and modulating its conformation. *J. Biol. Chem.* 294, 8101–8122. doi: 10.1074/jbc.RA119.007808

Oveson, B. C., Iwase, T., Hackett, S. F., Lee, S. Y., Usui, S., Sedlak, T. W., et al. (2011). Constituents of bile, bilirubin and TUDCA, protect against oxidative stress-induced retinal degeneration: Bilirubin and retinitis pigmentosa. *J. Neurochem.* 116, 144–153. doi: 10.1111/j.1471-4159.2010.07092.x

Piano, I., D'Antongiovanni, V., Novelli, E., Biagioni, M., Dei Cas, M., Paroni, R. C., et al. (2020). Myriocin effect on Tvrm4 Retina, an autosomal dominant pattern of retinitis pigmentosa. *Front. Neurosci.* 14:372. doi: 10.3389/fnins.2020.00372

Piano, I., D'Antongiovanni, V., Testai, L., Calderone, V., and Gargini, C. (2019). A nutraceutical strategy to slowing down the progression of cone death in an animal model of retinitis pigmentosa. *Front. Neurosci.* 13:461. doi: 10.3389/fnins.2019.00461

Piano, I., Di Paolo, M., Corsi, F., Piragine, E., Bisti, S., Gargini, C., et al. (2021). Retinal neurodegeneration: correlation between nutraceutical treatment and animal model. *Nutrients* 13:770. doi: 10.3390/nu13030770

Piano, I., Novelli, E., Gasco, P., Ghidoni, R., Strettoi, E., and Gargini, C. (2013). Cone survival and preservation of visual acuity in an animal model of retinal degeneration. *Eur. J. Neurosci.* 37, 1853–1862. doi: 10.1111/ejn.12196

Poljsak, B., and Milisav, I. (2012). The neglected significance of "Antioxidative Stress". *Oxid. Med. Cell. Longev.* 2012:480895. doi: 10.1155/2012/480895

Poljsak, B., Šuput, D., and Milisav, I. (2013). Achieving the balance between ROS and antioxidants: when to use the synthetic antioxidants. *Oxid. Med. Cell. Longev.* 2013:956792. doi: 10.1155/2013/956792

Shen, J., Yang, X., Dong, A., Petters, R. M., Peng, Y.-W., Wong, F., et al. (2005). Oxidative damage is a potential cause of cone cell death in retinitis pigmentosa. *J. Cell. Physiol.* 203, 457–464. doi: 10.1002/jcp.20346

Testai, L., Martelli, A., Marino, A., D'Antongiovanni, V., Ciregia, F., Giusti, L., et al. (2013). The activation of mitochondrial BK potassium channels contributes to the protective effects of naringenin against myocardial ischemia/reperfusion injury. *Biochem. Pharmacol.* 85, 1634–1643. doi: 10.1016/j.bcp.2013.03.018

Trouillet, A., Dubus, E., Dégardin, J., Estivalet, A., Ivkovic, I., Godefroy, D., et al. (2018). Cone degeneration is triggered by the absence of USH1 proteins but prevented by antioxidant treatments. *Sci. Rep.* 8:1968. doi: 10.1038/s41598-018-20171-0

Usui, S., Oveson, B. C., Iwase, T., Lu, L., Lee, S. Y., Jo, Y.-J., et al. (2011). Overexpression of SOD in retina: Need for increase in H2O2-detoxifying enzyme in same cellular compartment. *Free Rad. Biol. Med.* 51, 1347–1354. doi: 10.1016/j.freeradbiomed.2011.06.010

Valter, K., Maslim, J., Bowers, F., and Stone, J. (1998). Photoreceptor dystrophy in the RCS rat: roles of oxygen, debris, and bFGF. *Invest. Ophthalmol. Vis. Sci.* 39, 2427–2442.

Vingolo, E. M., Casillo, L., Contento, L., Toja, F., and Florido, A. (2022). Retinitis Pigmentosa (RP):the role of oxidative stress in the degenerative process progression. *Biomedicines* 10:582. doi: 10.3390/biomedicines10030582

Viswanatha, G. L., Shylaja, H., and Moolemath, Y. (2017). The beneficial role of Naringin- a citrus bioflavonoid, against oxidative stress-induced neurobehavioral disorders and cognitive dysfunction in rodents: a systematic review and meta-analysis. *Biomed. Pharmacother.* 94, 909–929. doi: 10.1016/j.biopha.2017.07.072

Wang, J., Saul, A., Roon, P., and Smith, S. B. (2016). Activation of the molecular chaperone, sigma 1 receptor, preserves cone function in a murine model of inherited retinal degeneration. *Proc. Natl. Acad. Sci. U.S.A.* 113, E3764–E3772. doi: 10.1073/pnas.1521749113

Xiong, W., MacColl Garfinkel, A. E., Li, Y., Benowitz, L. I., and Cepko, C. L. (2015). NRF2 promotes neuronal survival in neurodegeneration and

acute nerve damage. *J. Clin. Invest.* 125, 1433–1445. doi: 10.1172/JCI79735

Yu, D. Y., Cringle, S. J., Su, E. N., and Yu, P. K. (2000). Intraretinal oxygen levels before and after photoreceptor loss in the RCS rat. *Invest. Ophthalmol. Vis. Sci.* 41, 3999–4006.

Yu, D.-Y., Cringle, S., Valter, K., Walsh, N., Lee, D., and Stone, J. (2004). Photoreceptor death, trophic factor expression, retinal oxygen status, and photoreceptor function in the P23H Rat. *Invest. Ophthalmol. Vis. Sci.* 45:2013.

Conflict of Interest: The authors declare that the research was conducted in the absence of any commercial or financial relationships that could be construed as a potential conflict of interest.

Publisher's Note: All claims expressed in this article are solely those of the authors and do not necessarily represent those of their affiliated organizations, or those of the publisher, the editors and the reviewers. Any product that may be evaluated in this article, or claim that may be made by its manufacturer, is not guaranteed or endorsed by the publisher.

frontiers | Frontiers in Neuroscience

ORIGINAL RESEARCH
published: 04 May 2022
doi: 10.3389/fnins.2022.869137

Novel Machine-Learning Based Framework Using Electroretinography Data for the Detection of Early-Stage Glaucoma

Mohan Kumar Gajendran[1], *Landon J. Rohowetz*[2], *Peter Koulen*[2,3] *and Amirfarhang Mehdizadeh*[1,2]*

[1] Department of Civil and Mechanical Engineering, School of Computing and Engineering, University of Missouri-Kansas City, Kansas City, MO, United States, [2] Vision Research Center, Department of Ophthalmology, University of Missouri-Kansas City, Kansas City, MO, United States, [3] Department of Biomedical Sciences, University of Missouri-Kansas City, Kansas City, MO, United States

OPEN ACCESS

Edited by:
Rafael Linden,
Federal University of Rio de Janeiro, Brazil

Reviewed by:
Marc Sarossy,
The University of Melbourne, Australia
Flora Hui,
Centre for Eye Research Australia, Australia

***Correspondence:**
Amirfarhang Mehdizadeh
mehdizadeha@umkc.edu

Specialty section:
This article was submitted to Neurodegeneration, a section of the journal Frontiers in Neuroscience

Received: 03 February 2022
Accepted: 28 March 2022
Published: 04 May 2022

Citation:
Gajendran MK, Rohowetz LJ, Koulen P and Mehdizadeh A (2022) Novel Machine-Learning Based Framework Using Electroretinography Data for the Detection of Early-Stage Glaucoma. Front. Neurosci. 16:869137. doi: 10.3389/fnins.2022.869137

Purpose: Early-stage glaucoma diagnosis has been a challenging problem in ophthalmology. The current state-of-the-art glaucoma diagnosis techniques do not completely leverage the functional measures' such as electroretinogram's immense potential; instead, focus is on structural measures like optical coherence tomography. The current study aims to take a foundational step toward the development of a novel and reliable predictive framework for early detection of glaucoma using machine-learning-based algorithm capable of leveraging medically relevant information that ERG signals contain.

Methods: ERG signals from 60 eyes of DBA/2 mice were grouped for binary classification based on age. The signals were also grouped based on intraocular pressure (IOP) for multiclass classification. Statistical and wavelet-based features were engineered and extracted. Important predictors (ERG tests and features) were determined, and the performance of five machine learning-based methods were evaluated.

Results: Random forest (bagged trees) ensemble classifier provided the best performance in both binary and multiclass classification of ERG signals. An accuracy of 91.7 and 80% was achieved for binary and multiclass classification, respectively, suggesting that machine-learning-based models can detect subtle changes in ERG signals if trained using advanced features such as those based on wavelet analyses.

Conclusions: The present study describes a novel, machine-learning-based method to analyze ERG signals providing additional information that may be used to detect early-stage glaucoma. Based on promising performance metrics obtained using the proposed machine-learning-based framework leveraging an established ERG data set, we conclude that the novel framework allows for detection of functional deficits of early/various stages of glaucoma in mice.

Keywords: glaucoma, machine learning, electroretinography, ERG, wavelet transform, early stage, AI

1. INTRODUCTION

Glaucoma, a chronic neurodegenerative disease affecting the retina and optic nerve, and a leading cause of blindness, is characterized by a progressive, irreversible loss of vision. As currently available treatment paradigms focus primarily on a predisposing factor, elevated intraocular pressure (IOP), and do not allow for repair of the retina and optic nerve once the disease has progressed and damage has occurred, technologies enabling an early diagnosis of glaucoma are needed urgently. Consequently, such new diagnostic modalities enabling early therapeutic intervention would significantly improve treatment outcomes. Current methods of glaucoma diagnosis are based on psychophysical techniques and the assessment of structural changes to the retina and optic nerve (Bussel et al., 2014). Standard automated perimetry testing, including the widely used Humphrey visual field testing, currently represents the most commonly utilized technique for glaucoma diagnosis and monitoring of disease progression and therapy outcomes (Ernest et al., 2012; Fidalgo et al., 2015). Recent efforts to employ machine-learning (ML) approaches to improve the analysis of behavioral psychophysical testing approaches produced moderate improvements over conventional analysis algorithms (Saeedi et al., 2021). However, significant damage to the retina and optic nerve, including loss of retinal ganglion cells (RGCs) has often already occurred before changes can be detected with standard automated perimetry testing (Turalba and Grosskreutz, 2010).

Recently, automated retinal image analysis (ARIA) systems have been developed for the diagnosis of complex diseases such as diabetic retinopathy and glaucoma (Sim et al., 2015; Lee et al., 2017). The development of these ARIA systems involved ML-based methods to detect structural changes determined with optical coherence tomography (OCT) imaging resulting in high analytical accuracy in automatically classifying disease phenotypes based on structural characteristics (Zhu et al., 2014; Asaoka et al., 2016; An et al., 2019). Despite such significant progress, early detection of glaucoma is still a challenge (Brandao et al., 2017), given the highly significant limitations of early detection of glaucoma based on structural methods. Systems employing the analysis of structural changes for glaucoma diagnosis are based on measuring retinal nerve fiber layer (RNFL) thickness in OCT images of the retina, which is highly variable and weakly correlated with RGC counts despite RNFL thickness being a surrogate marker of RGC degeneration and optic nerve fiber loss, hallmarks of glaucoma pathogenesis (Ledolter et al., 2015). Further, RGC loss often occurs early during pathogenesis in the absence of measurable RNFL thinning, prompting an urgent clinical need for methods with higher sensitivity, such as functional measures including ERG (Harwerth et al., 2002; Fortune et al., 2003; Takagi et al., 2012; Ledolter et al., 2015; Brandao et al., 2017). In contrast, functional measures such as visual field and ERG are sensitive to subtle changes in RGC function and RGC damage, which suggest a significant potential to enable early detection of glaucoma, even in the absence of elevated IOP, as seen in patients with normotensive glaucoma (Fortune et al., 2003; Aldebasi et al., 2004; Brandao et al., 2017). Therefore, this study aims to investigate such potential considering ERG signals.

Consequently, interventions could be initiated before irreversible damage occurs, allowing for the optimization of treatment strategies based on the improvement of RGC function (Ventura and Porciatti, 2006). This is of high clinical importance as determining the efficacy of therapies aimed at lowering IOP in open-angle glaucoma (Palmberg, 2002; Leske et al., 2007) requires early validation of therapy success (An et al., 2019), but will also be of importance for the development of novel alternative and complementary glaucoma therapies based on neuroprotective strategies (Rohowetz et al., 2018). Recently, in a study conducted by Tang et al. (2020) photopic negative response (PhNR) was used to assess the short-term changes in inner retinal function following intraocular pressure (IOP) decrease in glaucoma using eyedrops. Hui et al. (2020) showed that Nicotinamide supplementation helps improve the function of the inner retina in glaucoma.

Recent advances in the acquisition of complex neuroscience data have a significant innovative potential to progress toward more effective diagnostic systems (Kononenko, 2001). The adequate, timely, and clinically relevant analysis of such data has potentially high clinical impact (Lisboa, 2002). However, while such data sets can be readily acquired and technologies to further improve and simplify data acquisition continue to emerge (McPadden et al., 2019), critical barriers to implement the effective use of such novel data in clinical diagnostics and therapy delivery remain (Lee and Yoon, 2017). While the analysis of complex biomedical data is often part of medical diagnostics, current expert analysis standards and algorithms are limited by pattern recognition in few dimensions, which results in less than optimal identification or even exclusion of potentially relevant diagnostic features (Hannun et al., 2019). Machine learning could significantly augment medical diagnostics and increase their efficacy by analyzing aspects of complex and multi-dimensional biomedical data that are either not being considered adequately or that are not accessible to current analysis methods (Holzinger, 2014). Such machine-learning based diagnostic approaches have been developed and are being actively used for the detection of cardiovascular diseases (Al'Aref et al., 2019), and cancer (Cruz and Wishart, 2006).

ERG data are one such type of complex and multi-dimensional biomedical data that are potentially relevant to the diagnosis of glaucoma, but are currently not considered during routine clinical practice or in clinical research. Historically, this is due to multiple barriers related to clinical ERG data acquisition, such as limitations in reproducibility, high costs of both equipment and of individual tests, long test duration and complex test administration resulting in reduced patient acceptance and compliance, and the need for highly trained experts to administer tests. With the advent of novel ERG technologies, most of these barriers related to clinical ERG data acquisition have been removed (Nakamura et al., 2016; Asakawa et al., 2017; Kato et al., 2017; Hobby et al., 2018; Liu et al., 2018; Man et al., 2020), opening up the possibility to effectively use ERG data for glaucoma diagnostics, calling the

necessity for the development of novel approaches (e.g., M-L-based ones) that is capable to quickly and thoroughly analyze such data.

Machine learning is based on statistical techniques to learn from data and develop predictive models (Jordan and Mitchell, 2015). Recently, there has been a surge of interest in machine learning as significant advancements in computational hardware (Shi et al., 2016) facilitate the development of novel machine learning approaches as solutions to problems in various disciplines from financial forecasting to public transportation and healthcare (Trafalis and Ince, 2000; Omrani, 2015; Ahmad et al., 2018). There are several predictive techniques in machine learning with various complexities, ranging from simple linear models to advanced non-linear models such as those based on deep learning algorithms (Shailaja et al., 2018; Khan et al., 2021; Saxe et al., 2021). Currently, available ERG analysis methods, such as those developed by Hood et al. (2000), Ventura and Porciatti (2006), have contributed to a significantly improved understanding of the relationship between ERG signals and vision loss. These methods are limited to frequency domain analysis (Miguel-Jiménez et al., 2010; Luo et al., 2011; Palmowski-Wolfe et al., 2011; Ledolter et al., 2013) and the analyses of differences in amplitude and latency of ERG (Fortune et al., 2002; Thienprasiddhi et al., 2003; Stiefelmeyer et al., 2004; Chu et al., 2007; Todorova and Palmowski-Wolfe, 2011; Ho et al., 2012; Hori et al., 2012). In addition, these methods are often time-consuming, labor-intensive, and focused on parameters developed to address a small subset of mostly genetic diseases of the eye affecting predominantly pediatric patient populations (Frishman et al., 2000; Graham et al., 2000; Dale et al., 2010). To achieve higher accuracy and a more detailed understanding of disease progression and of the impact of therapeutic intervention, more sophisticated features such as those obtained from wavelet analysis are required (Forte et al., 2008; Barraco et al., 2014). Additionally, currently available methods are often not suitable for analyzing large data sets and databases, rendering them incapable of taking advantage of complex and rich datasets (Consejo et al., 2019; Armstrong and Lorch, 2020). These drawbacks prompted others (Bowd et al., 2014; Yousefi et al., 2015; Atalay et al., 2016; Verma et al., 2017) and us to design and develop novel methods capable of handling complex and large datasets and ultimately to provide a unique approach for diagnosing early-stage glaucoma. However, it should be noted that early detection of glaucoma is not possible with currently available techniques during the early stages of glaucoma pathogenesis, when cellular changes occur that do not result in structural damage or visual impairment yet. Such early-onset factors predisposing to glaucoma development include processes preceding the onset of ocular hypertension, for example, the onset of iris pigment dispersion preceding IOP elevation in the DBA/2 mouse model. However, and more importantly, we identified cellular changes resulting in altered ERG signals, such as changes in oscillatory potentials, that currently cannot be detected with other functional or structural measures.

Boquete and colleagues developed a method to automate glaucoma diagnosis based on ERG signals using neural networks and structural pattern analysis (Boquete et al., 2012). They utilized thirteen features (morphological and transitional characteristics) for training the model and achieved a testing accuracy of 80.7% (Boquete et al., 2012). This study was limited to basic morphological characteristics of mfERG recordings (Boquete et al., 2012). Miguel-Jiménez et al. (2015) also employed neural networks for ERG-based glaucoma diagnosis but used continuous wavelet transformed coefficients and achieved a binary classification accuracy of 86.90% (Miguel-Jiménez et al., 2015). Although a higher accuracy was achieved, this analysis was limited to wavelet features only (Miguel-Jiménez et al., 2015). Nevertheless, both studies showed that machine learning-based methods trained even on compact data sets provide powerful tools to analyze ERG signals and provide potentially new information relevant for the early detection of glaucoma. Sarossy and colleagues investigated the relationship between a compact set of features and glaucoma that can be analyzed with machine learning approaches; however, the study was limited to the analysis of the photopic negative response (PhNR) and five additional features (Sarossy et al., 2021).

The goal of the present study was to comprehensively assess the capability of machine-learning-based methods to detect early-stage glaucoma using time-series ERG signals. In particular, the following points are addressed during method development:

1. Develop a framework to extract and identify important predictors (features) from ERG signals.
2. Compare the predictive capability of statistical and wavelet-based features for binary and multiclass classification.
3. Develop a robust ML-based model to diagnose glaucoma (binary classification).
4. Develop a robust ML-based model capable of distinguishing various stages of glaucoma progression (multiclass classification).
5. Develop a robust ML-based model to provide a quantitative assessment of visual function by predicting retinal ganglion cell count from ERG signals for the first time.

2. METHODS

2.1. Overview

ML based algorithms have been applied to Electrocardiogram (ECG) signals in order to develop predictive models for diagnosing heart diseases (Li et al., 2014; Al'Aref et al., 2019). Recently machine learning-based Artificial Neural Networks (ANN) have been applied to ERG signals for obesity diagnosis (Yapici et al., 2021). However, to date, machine learning-based methods have not been applied systematically to analyze ERG signals for glaucoma detection. Therefore, the potential of ERG signals in glaucoma diagnosis has not been fully utilized. The present work aims to develop a predictive model for early glaucoma diagnosis based on machine-learning algorithms by utilizing advanced features from ERG signals as predictors. The steps involved in developing a machine-learning-based predictive model for ERG analysis are shown in **Figure 1**. Each of these steps is explained in detail below.

FIGURE 1 | Machine learning workflow using ERG signals. *ERG Database:* the ERG database contains the input ERG data used to train the predictive model. *Pre-processing of data:* this step ensures data quality by transforming the data to a common baseline, accounting for missing data, and handling outliers. *Feature extraction:* mathematical operations are performed on the data to extract features/parameters that indicate functional deficits in the eye. *Predictive Model Development:* algorithms can determine trends and patterns in data from statistical analysis of extracted features during training; these models can predict either class or value from the input data are called classifier and regression models, respectively. *Deployment of Model into medical devices:* successful predictive models can be included with ERG testing devices to provide real-time prognosis and diagnosis.

2.2. ERG: A Biomarker

Electroretinography measures the electrical responses of different types of cells in the retina, such as ganglion cells. These signals are usually measured in microvolts. Oscillatory Potential (OP) and Scotopic Threshold Response (STR) represent important ERG components indicative of RGC cell function (Saszik et al., 2002; Dong et al., 2004; Hancock and Kraft, 2004; Lei et al., 2006). OPs are small rhythmic wavelets superimposed on the ascending b-wave of the ERG and STR are negative corneal deflection elicited in the fully dark-adapted eye to dim stimuli. An International Society for Clinical Electrophysiology of Vision (ISCEV) standardized ERG protocol (Marmor et al., 2009) included several tests to measure the function of various retinal cell types, including the rod response, standard rod-cone response, Hi-intensity rods, and cones response, cone response, Hi-intensity cone response, flicker, and Hi flicker (Grillo et al., 2018). A visualization of nine ERG signals resulting from two ERG components (OP and STR) and seven ERG test responses is provided in **Figure 2**. The dynamics of ERG signals vary in people with various conditions and can therefore aid in differentiating individuals with glaucoma (Grillo et al., 2018), schizophrenia (Demmin et al., 2018), obesity (Yapici et al., 2021), and bipolar disorder (Hébert et al., 2020). ERG can also help in evaluating the effectiveness of new or existing drugs and therapy modalities (Lai et al., 2006, 2009; Nebbioso et al., 2009; da Silva et al., 2020).

2.3. Ganzfeld Flash Electroretinography

The development of pigmentary glaucomatous optic neuropathy in the DBA/2 mouse model had several similarities to glaucoma pathogenesis in human patients, including loss of vision and RGC (McKinnon et al., 2009; Burroughs et al., 2011; Grillo et al., 2013; de Lara et al., 2014; Kaja et al., 2014; Grillo and Koulen, 2015; Montgomery et al., 2016). The Ganzfeld flash electroretinography (fERG) procedures in mice were conducted under dim red light that was followed by an overnight dark adaptation (>12 h). Isoflurane at 3 and 1.5% was used respectively, to anesthetize mice and maintain anesthesia. The pupils were dilated using 1 drop of 1% tropicamide and were allowed to dilate for 10 min. Rectal temperature was monitored and maintained at 37°C using a heating pad. Silver-embedded thread electrodes were placed over the cornea in 1% methylcellulose with mini-contact lenses fitted preventing the corneal dehydration (Ocuscience LLC, Henderson, NV). The head was placed inside the Ganzfeld dome, and fERG with 2 recording channels was performed using an HMsERG system (Ocuscience LLC) equipped with an amplifier with a band pass from 0.3 to 300 Hz. Mice were subjected to the International Society for Clinical Electrophysiology of Vision (ISCEV) standardized ERG protocol [29], whose implementation is described in detail in Marmor et al. (2009). ERGView 4.380V software (OcuScience LLC) was used to perform statistical analyses including averaging multiple flashes recorded at each intensity and stored for further analysis. Additionally, mice were tested using a scotopic flash intensity series in the range of −4.5 to 1.5 log cd s/m^2. Further, a 1:1,000 neutral density filter (ND3) was used to control the 7 lowest flash intensities; data were averaged from 10 flashes (−4.5 to −3.5 log cd s/m^2), 4 flashes (−3 to 0.5 log cd s/m^2) at the lower intensities or measured from 1 flash at the 2 highest intensities (1 to 1.5 log cd s/m^2). Following the light adaptation (1.5 log cd s/m^2 for 10 min), responses from a photopic series (−2 to 1.5 log cd s/m^2; 32 flashes per intensity) were recorded in a separate fashion. Further details about data acquisition can be found in Grillo et al. (2018).

2.4. ERG Dataset

Ganzfeld fERG tests were performed on 4 months old ($n = 15$) and 11 months old ($n = 15$) male DBA/2 mice. Each animal had two sets of test data, one for each eye. Therefore, a total of 60 data sets for individual eyes were included in this study. Each data set comprised of nine different ERG signals (OP, STR, and seven signals from ERG testing protocols), as shown in **Figure 2** (OPs are small rhythmic wavelets superimposed on the ascending b-wave of the ERG and STR are negative corneal deflection elicited in the fully dark-adapted eye to dim stimuli). Therefore, 540 recordings were utilized in this study. Intraocular pressure (IOP) and retinal ganglion cell (RGC) count measurements were also utilized in this study. Although IOP data was available for all animals, RGC counts were only available for 10 (20 eyes). The animals were grouped in a binary group (healthy and glaucomatous) based on age and multiclass group based on IOP as (normal, <12 mm Hg; high, [≥12 mm Hg <17 mm Hg]; glaucomatous, ≥17 mm Hg). All the data used in this study was well-balanced for respective groups.

2.5. Pre-processing of Data

ERG raw data may contain several anomalies such as different start times, missing data, different sampling frequencies, noise, and unequal lengths of the signal recordings. In Machine learning-based modeling, the quality of the training data can significantly impact the model performance. Therefore, pre-processing (data preparation and screening) is crucial to ensure

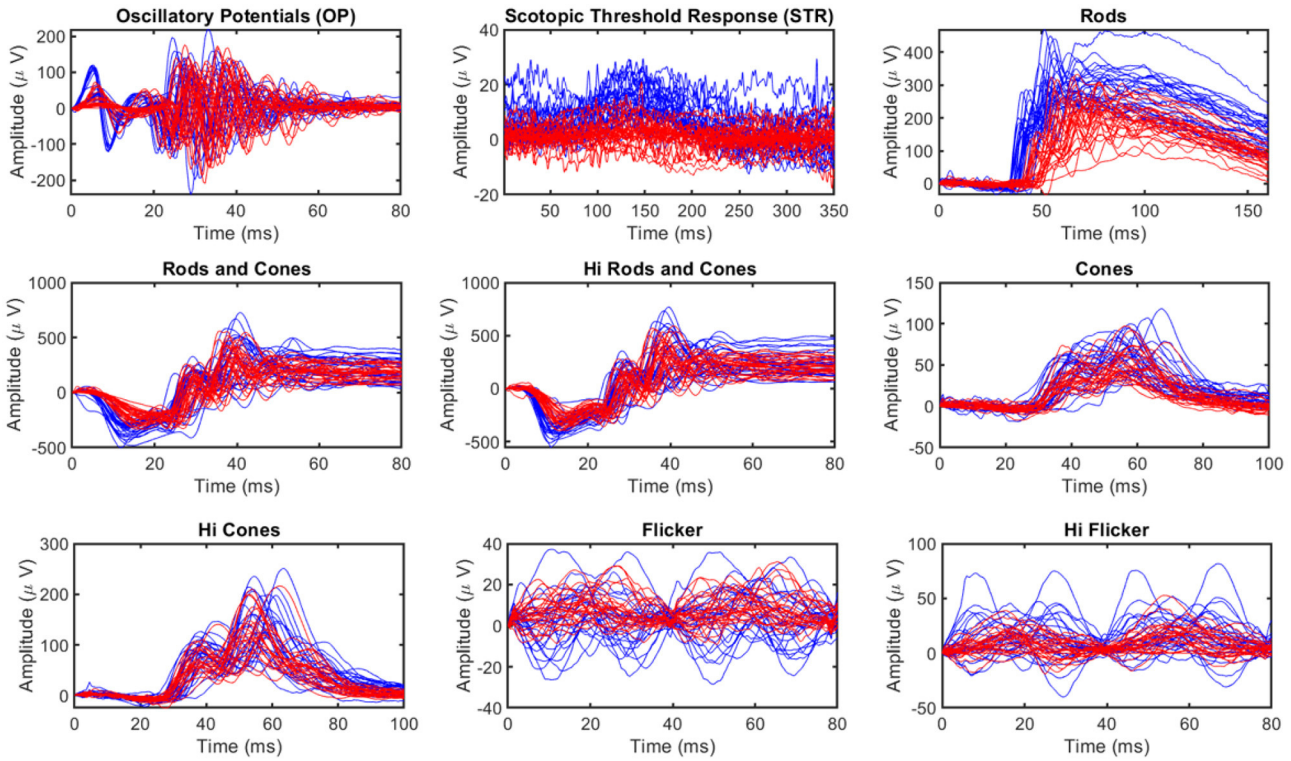

FIGURE 2 | Visualization of ERG Signals manifesting their complex nature. The blue lines correspond to healthy and red lines correspond to glaucomatous Signals. Signals resulting from ERG tests include *OP* (Oscillatory Potential: small rhythmic wavelets superimposed on the ascending b-wave of the ERG), *STR* (Scotopic Threshold Response: negative corneal deflection elicited in the fully dark-adapted eye to dim stimuli), *Rods* (rod response), *Rods and cones* (standard rod-cone response), *Hi Rods and cones* (Hi-intensity rods and cones response), *Cones* (cone response), *Hi cones* (Hi-intensity cone response), *Flicker* (Flicker response), and *Hi flicker* (Hi-intensity flicker response).

the quality of the training dataset (Jambukia et al., 2015). Pre-processing steps considered in the present study include,

1. Baseline adjustment
2. Feature extraction
3. Handling missing data
4. Handling outliers
5. Feature scaling
6. Feature selection

The signal's baseline (start time) can be different for different animals and testing protocols. Therefore, all the measurements were brought to a common baseline (start time was offset to zero) during baseline adjustment (Jambukia et al., 2015). Feature extraction involves computing a reduced set of values from a high-dimensional signal capable of summarizing most of the information contained in the signal (Khalid et al., 2014). The missing data were replaced with mean values (Graham et al., 2013). For handing outliers, values more than three scaled median absolute deviations (MAD) away from the median were detected as outliers and replaced with threshold values used in outlier detection (Aguinis et al., 2013). The feature's values vary widely, even by orders of magnitude. Therefore, it is important to bring the feature values to a similar range (feature scaling), especially when using distance-based machine learning algorithms (Wan, 2019). Feature selection is further dimensionality reduction from the extracted features. It is performed to reduce the computational cost of modeling, to achieve a better generalized, high-performance model that is simple and easy to understand (Aha and Bankert, 1996). Feature extraction and selection are explained in detail in the following sections.

2.6. Feature Extraction

ERG signals are complex high-dimensional data, and training a model with many variables requires significant computational resources. Feature extraction reduces the dimensionality of the data by computing a reduced set of values from a high-dimensional signal capable of summarizing most of the information contained in the signal (Guyon et al., 2008). In the present study, feature extraction was performed in two phases. First, common statistical features were extracted from the signal, followed by the extraction of advanced wavelet-based features. **Figure 3** provides an overview of the feature extraction process and is explained below.

2.6.1. Statistical Feature Extraction

A total of 17 Statistical features capable of describing the general behavior of ERG signals were extracted from the signal. These features were grouped as follows.

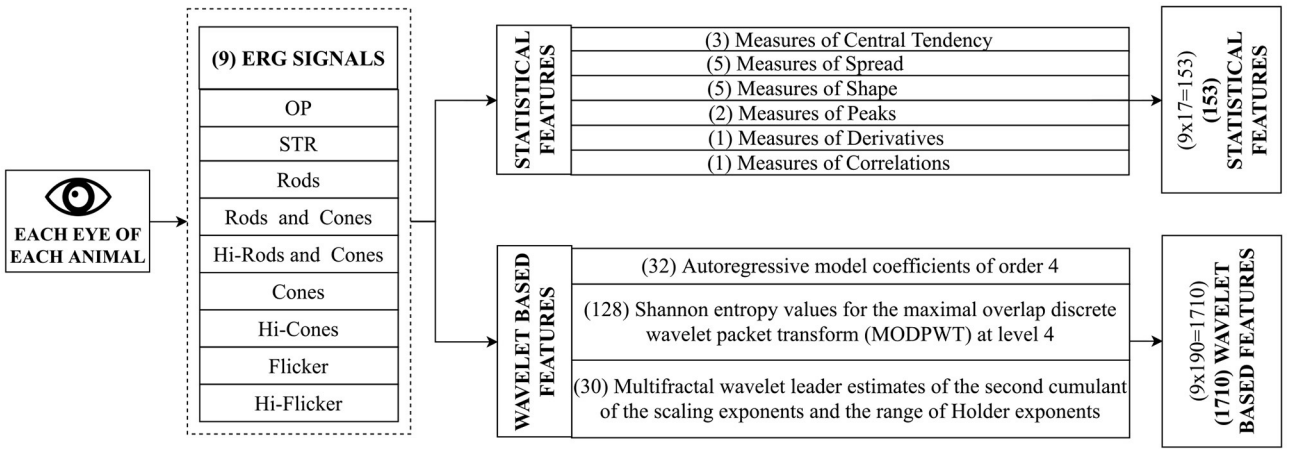

FIGURE 3 | Feature Extraction. During this process, mathematical operations are performed on the data to extract features. This step is crucial for discovering features indicative of functional deficits in the eye. ERG test on each eye leads to nine signals, as shown in **Figure 2**. Two sets of features (Standard features and advanced features) are extracted from each of the nine signals. The standard set of features include common statistical features such as mean, quartiles, and entropies. In contrast, the advanced set of features include sophisticated features such as autoregressive coefficients, Shannon entropy, and wavelet features.

1. Measures of Central Tendency
2. Measures of Spread
3. Measures of Shape
4. Measures of Peaks
5. Measures of Derivatives
6. Measures of Correlation

Measures of central tendency included mean, median, trimmed mean. Measures of spread included range, standard deviation, variance, mean absolute deviation, and interquartile range. Measures of the shape include skewness, kurtosis, central moments of the second and third-order, and aspect ratio. Measures of peaks included the number of peaks and troughs in the signal. Measures of derivatives include the first-order derivative of the signal with respect to time. Measures of correlation included the correlation coefficient of the signal with respect to time. The equations for the computation of these quantities can be found in Asgharzadeh-Bonab et al. (2020); Yapici et al. (2021).

2.6.2. Advanced Feature Extraction

Advanced features capable of capturing subtle changes were extracted from the signal. Each signal was split into 32 blocks (∼ 2000 samples/block) to further capture subtle changes in the signal (Martis et al., 2014). Daubechies least-asymmetric wavelet with four vanishing moments (Symlets 4) was used as mother wavelet to derive the wavelet coefficients (Daubechies, 1992). The following features (190 features in total as shown in **Figure 3**) were extracted from each block of the signal:

AR coefficients: The signal $x[n]$ at time instant n in an AR process of order p can be described as a linear combination of p earlier values of the same signal. The procedure is modeled as follows:

$$x[n] = \sum_{i=1}^{p} a[i]x[n-i] + e[n] \quad (1)$$

where $a[i]$ is the AR model's i^{th} coefficient, $e[n]$ denotes white noise with mean zero, and p denotes the AR order. The AR coefficients for each block were estimated using the Burg method (Zhao and Zhang, 2005); the order was determined using the ARfit model order selection method (Neumaier and Schneider, 2001) as 4th order. Therefore a 4-order AR model is chosen to represent each of the ERG signal components.

Wavelet based Shannon Entropy: The Shannon entropy is an information-theoretic measure of a signal. Shannon entropy (denoted as SE) values for the maximal overlap discrete wavelet packet transform (MOD- PWT) using four-level wavelet decomposition was computed on the terminal nodes of the wavelet (Li and Zhou, 2016). Mathematical expression for Shannon entropy using wavelet packet transform is as follows:

$$SE_j = -\sum_{k=1}^{N} p_{j,k} * \log p_{j,k} \quad (2)$$

where N is the number of coefficients in the j^{th} node and $p_{j,k}$ are the normalized squares of the wavelet packet coefficients in the j^{th} terminal node of the wavelet.

Multifractal wavelet leader estimates and multiscale wavelet variance estimates: The multifractal measure of the ERG signal was obtained using two wavelet methods (wavelet leader and cumulant of the scaling exponents). Wavelet leaders are time/space-localized suprema of the discrete wavelet coefficients' absolute value. These suprema are used to calculate the Holder exponents, which characterize the local regularity. In addition, second cumulant of the scaling exponents were obtained. Scaling

exponents are scale-dependent exponents that describe the signal's power-law behavior at various resolutions. The second cumulant basically depicts the scaling exponents' divergence from linearity (Leonarduzzi et al., 2010). Wavelet variance of ERG signals were also obtained as features. Wavelet variance quantifies the degree of variability in a signal by scale, or more precisely, the degree of variability in a signal between octave-band frequency intervals (Maharaj and Alonso, 2014).

2.7. Feature Selection

Feature extraction discussed previously was performed in order to reduce the dimensionality of the signals; however, the resulting number of features was still higher than the number of training data. Therefore, further reduction in the dimensionality of the data was performed using the feature selection method to identify relevant features for classification and regression. It should be noted that feature selection was necessary to reduce the computational cost of modeling, prevent the generation of a complex and over-fitted model with high generalization error, and generate a high-performance model that is simple and easy to understand (Saeys et al., 2007). In particular, the Minimum Redundancy Maximum Relevance (MRMR) sequential feature selection algorithm was used in the present study because this algorithm is specifically designed to drop redundant features [see (Darbellay and Vajda, 1999; Ding and Peng, 2005) for mathematical details/formulations], which was required to design a compact and efficient machine-learning-based model (Zhao et al., 2019). It is worth noting that other available dimensionality reduction techniques such as Principal component analysis (PCA) were not considered in this study as such techniques do not allow for direct tracing and understanding the relevance of each feature (Aha and Bankert, 1996).

2.8. Predictive Model Development

ML models are mathematical algorithms that provide predictions based on an inference derived from the generalizable predictive patterns of the training data (Bzdok et al., 2018). Several machine learning models were employed and evaluated in order to identify the best one to classify the ERG signals. These included decision trees, discriminant, support vector machine, nearest neighbor, and ensemble classifiers. Most of these models can perform both classification and regression. Decision tree-based models predict the target variable by learning simple decision rules (Navada et al., 2011). Discriminant classifiers are based on the assumption that each class has different Gaussian distributions of data, and the classification is performed based on Gaussian distribution parameters estimated by the fitting function (Cawley and Talbot, 2003). Support vector machine (SVM) is based on Vapnik–Chervonenkis theory, where a hyperplane separating the classes is determined. SVMs are efficient algorithms suitable for compact datasets (Noble, 2006). The nearest neighbor algorithm is based on the assumption that similar things exist nearby. It is a simple yet versatile model with high computational cost (Zhang and Zhou, 2007). Ensemble methods such as bagged trees (or random forest) combine the predictions of several learning algorithms with improving generalization. Although these methods are also computationally expensive, they are unlikely to over-fit (Dietterich, 2000). Regression analysis based on the above techniques was also performed alongside classification.

2.9. Performance Evaluation

Various performance evaluation metrics were utilized to compare different machine learning algorithms. The metrics used in this study include accuracy, sensitivity, specificity, precision, recall, f-score, root mean squared error, and their corresponding mathematical formulations are given below.

The abbreviations used in the following expressions include True Positive (TP) which are the cases the model correctly predicted the positive (glaucomatous) class. True Negative (TN) are the cases the model correctly predicted the negative (non-glaucomatous) class. False Positive (FP) are the cases the model incorrectly predicted the positive (glaucomatous) class. False Negative (FN) are the cases the model incorrectly predicted the negative (non-glaucomatous) class.

2.9.1. Accuracy

Accuracy is the percentage of correctly classified observations, as shown below.

$$\text{Accuracy}(\%) = \frac{\text{TP} + \text{FP}}{\text{TP} + \text{TN} + \text{FP} + \text{FN}} \tag{3}$$

2.9.2. Sensitivity

Sensitivity/Recall estimates the proportion of actual positives (e.g., actual glaucomatous) was identified correctly.

$$\text{Sensitivity/Recall (RE)} = \frac{\text{TP}}{\text{TP} + \text{FN}} \tag{4}$$

2.9.3. Specificity

Recall estimates the model's ability to correctly reject healthy patients without a Glaucoma.

2.9.4. Precision

Precision estimates the proportion of positive predictions (e.g., glaucomatous predictions) that was actually correct.

$$\text{Precision (PR)} = \frac{\text{TP}}{\text{TP} + \text{FP}} \tag{5}$$

2.9.5. F-Score

The F-Score estimates the harmonic mean of the precision and recall.

$$\text{F- Score} = \frac{\text{PR} \times \text{RE}}{\text{PR} + \text{RE}} \tag{6}$$

2.9.6. Root Mean Square Error (RMSE)

The Root Mean Square Error (RMSE) was used as the performance evaluation metric for regression analysis. RSME is the standard deviation of the prediction errors (residuals).

$$\text{RMSE} = \sqrt{\frac{\sum_{i=1}^{N} \left(\text{Actual } x_i - \text{ Predicted } \hat{x}_i \right)^2}{N}} \tag{7}$$

Where N is the number of observations.

3. RESULTS

A machine learning-based approach was developed and trained using the balanced ERG data previously published by Grillo et al. (2018). Although a compact dataset of 60 observations and 540 signals was used in this study, the current framework was able to consistently detect features (**Figures 6**, **9**) that are known to be medically relevant such as OP, STR, Flicker reported in various studies (Tyler, 1981; Saszik et al., 2002; de Lara et al., 2014, 2015; Porciatti, 2015; Grillo et al., 2018). In particular, studies conducted by Wilsey and Fortune (2016), Hermas (2019), Beykin et al. (2021) investigating the variability of PhNR in glaucomatous and healthy subjects in PERG and fERG have found that PhNR to be an important biomarkers for detection of glaucoma. It is worth noting that in fERG analysis (ERG protocol for this study), pSTR, nSTR, PhNR are extracted from STR.

Therefore, we were able to demonstrate that the proposed framework for early-stage glaucoma diagnosis can be reproducibly evaluated and validated even on such a compact database. Furthermore, we would like to note that there are other investigations that successfully applied ML-based method in different fields, including biomedical (Seo et al., 2020) and material science (Zhang and Ling, 2018) using compact datasets. The procedure employed for the development of the predictive modeling framework is summarized below.

- **Data Split:** Hold out (80% training, k-fold cross-validation, 20% testing).
- **Dimensionality reduction:** Feature Extraction.
- **Feature selection:** MRMR.
- **Hyper-parameter tuning:** k-fold cross-validation ($k = 10$).
- **Model Evaluation:** Performance metrics evaluated on the unseen testing set.

The dataset was divided into two parts; 80% of the data was used for training and validation, and the remaining 20% was set aside for testing. The hold-out testing strategy ensured that the test data was never a part of the training process (Yadav and Shukla, 2016). Dimensionality reduction was performed using feature extraction and feature selection. MRMR feature selection algorithm was used to identify the important predictors. K-fold ($K = 10$) cross-validation was used for training and hyper-parameter tuning (Duan et al., 2003). The cross-validation technique significantly reduces bias when working with small datasets (Varma and Simon, 2006). The loss function was the objective minimization function for both classification regressions during hyper-parameter optimization. The hyper-parameters associated with corresponding ML algorithms (Feurer and Hutter, 2019), as shown in **Table 1**, were optimized through nested cross-validation. Next, the trained model with optimized hyper-parameters was evaluated using test data that was not a part of training. To further ensure that the machine learning models compared in this investigation were not over-fitted, given the compact dataset used in the present study, the behavior of training and testing error vs. training cycles was monitored. Different techniques, including Tree, Discriminant, SVM, Naive Bayes, Tree Ensemble, and KNN, were applied, and their performances were assessed. The performance of each technique was assessed based on the accuracy (discussed in section 2.9) is tabulated in **Table 2**. Considering binary and multiclass classifications, it can be seen that the Ensemble-based technique (bagged tree) was consistently outperforming other techniques. Additionally, other performance metrics for ensemble bagged trees (discussed in section 2.9) are summarized in **Table 3**.

TABLE 1 | Hyperparameters tested/optimized.

Method	Hyperparameter search range	Optimized hyperparameters
Ensemble	**Ensemble method:** Bag, GentleBoost, LogitBoost, AdaBoost, RUSBoost **Number of learners:** 10–500 **Learning rate:** 0.001-1 **Maximum number of splits:** 1–47 **Number of predictors to sample:** 1–5	**Ensemble method:** Bag **Maximum number of splits:** 1 **Number of learners:** 52 **Number of predictors-to sample:** 1
Knn	**Number of neighbors:** 1-24 **Distance metric:** City block, Chebyshev, Correlation, Cosine, Euclidean, Hamming, Jaccard, Mahalanobis, Minkowski (cubic), Spearman **Distance weight:** Equal, Inverse, Squared inverse **Standardize data:** true, false	**Number of neighbors:** 24 **Distance metric:** Correlation **Distance weight:** Inverse **Standardize data:** true
NaiveBayes	**Distribution names:** Gaussian, Kernel **Kernel type:** Gaussian, Box, Epanechnikov, Triangle	**Distribution names:** Gaussian **Kernel type:** Epanechnikov
Discriminant	**Discriminant type:** Linear, Quadratic, Diagonal Linear, Diagonal Quadratic	**Discriminant type:** Diagonal Linear
SVM	**Multiclass method:** One-vs-All, One-vs.-One **Box constraint level:** 0.001-1000 **Kernel scale:** 0.001–1000 **Kernel function:** Gaussian, Linear, Quadratic, **Cubic Standardize data:** true, false	**Kernel function:** Linear **Box constraint level:** 2.4185 **Multiclass method:** One-vs.-All **Standardize data:** false
Tree	**Maximum number of splits:** 1–47 **Split criterion:** Gini's diversity index, Maximum deviance reduction	**Maximum number of splits:** 5 **Split criterion:** Maximum deviance reduction

3.1. Binary Classification

For binary classification (classifying animals with/without glaucoma) based on statistical features, the correlation of cones,

TABLE 2 | Testing accuracy obtained using various machine learning techniques.

		Tree	Discriminant	SVM	Naive Bayes	Ensemble (Bagged)	KNN
Binary	**Statistical**	75	80	**83.33**	80	**83.33**	66.70
	Wavelet	83.33	83.33	**91.70**	83.33	**91.70**	75
Multiclass	**Statistical**	33.33	41.70	50	16.70	**53.33**	33.33
	Wavelet	41.70	50	64.66	33.33	**80**	50

Values in bold font indicate the accuracies of best-performing classifier.

TABLE 3 | Performance metrics for ensemble classifier.

		Accuracy	F-measure	Precision	Sensitivity	Specificity
Binary	**Statistical**	80	80	80.36	80.36	80.36
	Wavelet	91.67	91.61	92.86	91.67	91.67
Multi-class	**Statistical**	53.33	50.74	53.18	51.67	75.48
	Wavelet	80	79.63	83.81	83.333	90.30

mean of flicker, median, and skewness of Hi Rods and cones, and standard deviation of cones were identified as important among the statistical features as shown in **Figure 4**. Moreover, the box plot demonstrates variations of each feature for each class (with/without glaucoma), respectively. Several models, including SVM and ensemble-based classifiers were used for training, and their performances were assessed. It turned out that the SVM and ensemble bagged tree provide the best performance with a testing accuracy of 83.33%, as shown in **Table 2**.

Next, the binary classification was performed using wavelet-based features. Among the extracted wavelet features, Shannon Entropy Values for Maximal Overlap Discrete Wavelet Packet Transform (MOD-PWT) were identified as important features from Rods and cones, Rods, STR, and OP, as shown in **Figure 5**. The utilization of the selected advanced features improved the accuracy to 91.70% by the ensemble bagged tree algorithm.

It should be noted that the MRMR method selects features based on statistical relevance while dropping redundant features and thus, is computationally efficient (Darbellay and Vajda, 1999; Ding and Peng, 2005). **Figure 6** demonstrates this for binary classification. It can be observed that correlation feature from cones, Moment of order three and trimmed mean feature from Oscillatory Potentials (OP) and Range and aspect ratio from Scotopic Threshold Response (STR) are highly correlated; Therefore, only the feature cones correlation was picked by the MRMR algorithm as inclusion of the other three did not increase/decrease the models predictability.

Figure 7 compares the predictive importance scores obtained based on the statistical and wavelet-based features. Predictive importance scores describe the predictive capability of selected features (Kuhn and Johnson, 2013). It can be observed that wavelet-based features can distinguish healthy and glaucomatous animals suggesting that they are more sensitive to subtle changes in ERG signals due to glaucoma. It should be noted that the feature selection algorithm MRMR (Maximum Relevance and Minimum Redundancy) ignores highly correlated features for model simplicity. Therefore, only uncorrelated sets of features that improved predictability across the animals were chosen, i.e., for a set of correlated features, one representing the correlated set gets picked by the algorithm. **Figure 6** demonstrates the list of important but highly correlated features that were dropped. The scatter plot inside the **Figure 6** shows the correlation coefficients confirming the high degree of the correlation between them.

3.2. Multiclass Classification

For multiclass classification (classifying animals to different stages, normal, high, and glaucomatous as mentioned in section 2.4) based on statistical features, the correlation of cones, number of troughs in Hi cones, kurtosis of STR and mean of flicker were identified as important among the statistical features as shown in **Figure 8**. Several models, including SVM and ensemble-based classifiers, were used for training, and their performances were assessed. It turned out that the ensemble-based classifiers, specifically the bagged trees model, provided the best performance with a testing accuracy of 53.33%, as shown in **Table 2**.

Next, the multiclass classification was performed using wavelet-based features. Among the extracted wavelet features, Wavelet variance of rods and Shannon Entropy Values and AR coefficients for Maximal Overlap Discrete Wavelet Packet Transform (MOD-PWT) were identified as important features from Hi-Flicker, Flicker, Hi-cones, and STR as shown in **Figure 9**. The identification of flicker as an important distinguishing feature in diagnosing early-stage glaucoma was consistent with previous studies (Tyler, 1981; Lachenmayr and Drance, 1992; Horn et al., 1997; Yoshiyama and Johnson, 1997). In fact, flicker measurements in eyes with early-stage glaucoma exhibited a loss in sensitivity around 30–40 Hz (Tyler, 1981). It is worth noting that the flicker measurements used in this study were recorded using flashes at 30 Hz. The identification of the flicker ERG test and the corresponding features, among other tests, reconfirmed the capability of the current approach in identifying the relevant features. Training the ensemble bagged trees model, utilizing the selected advanced features, improved the multiclass classification

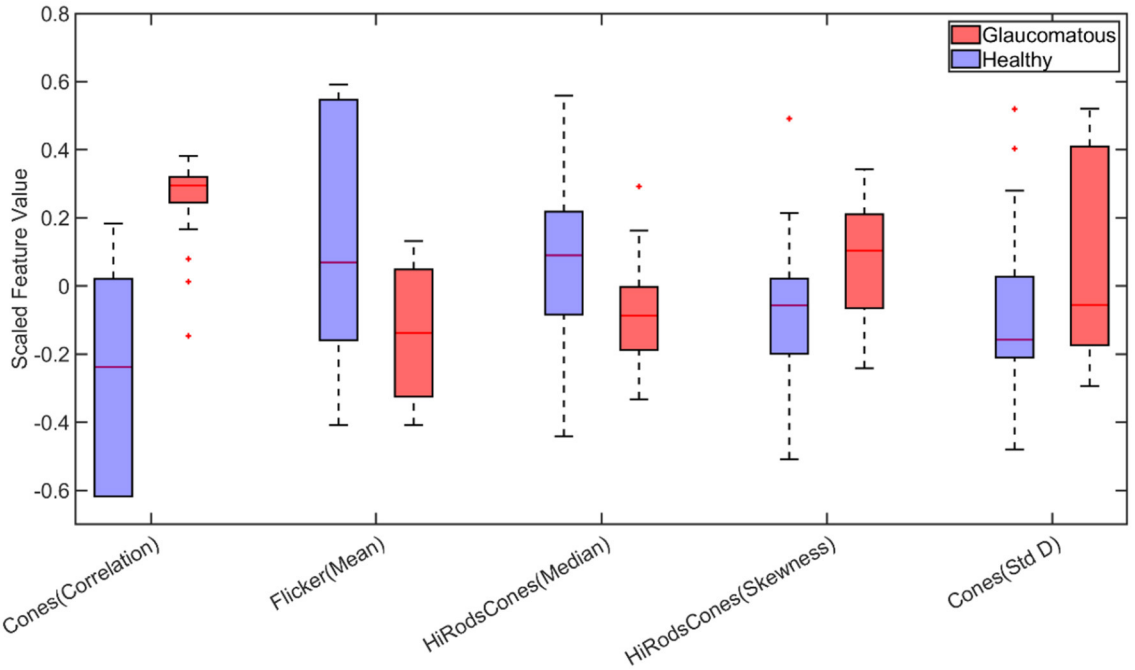

FIGURE 4 | Boxplot of statistical features selected by Minimum Redundancy and Maximum Relevance (MRMR) feature selection algorithm for binary classification (Std D, Standard Deviation). On each box, the central mark indicates the median, and the bottom and top edges of the box indicate the 25th and 75th percentiles, respectively. The whiskers extend to the most extreme data points not considered outliers, and the outliers are plotted individually using the "+" marker symbol.

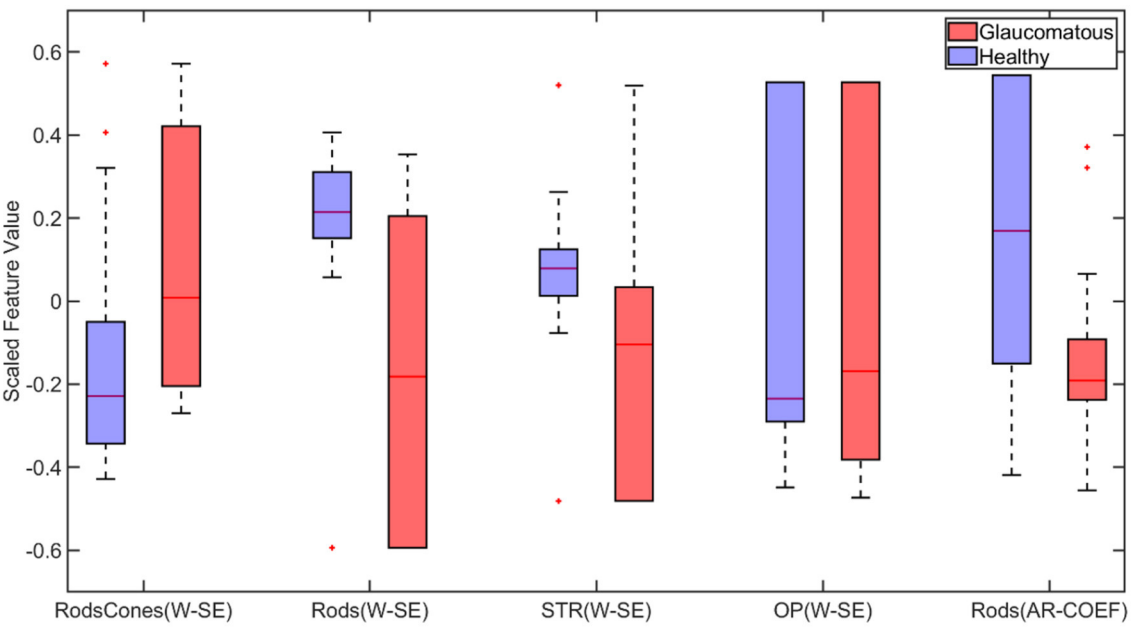

FIGURE 5 | Box plot of wavelet-based features selected by Minimum Redundancy and Maximum Relevance (MRMR) feature selection algorithm for binary classification (W-SE, Wavelet based Shannon Entropy; AR-COEF, Autoregressive Coefficient). On each box, the central mark indicates the median, and the bottom and top edges of the box indicate the 25th and 75th percentiles, respectively. The whiskers extend to the most extreme data points not considered outliers, and the outliers are plotted individually using the "+" marker symbol.

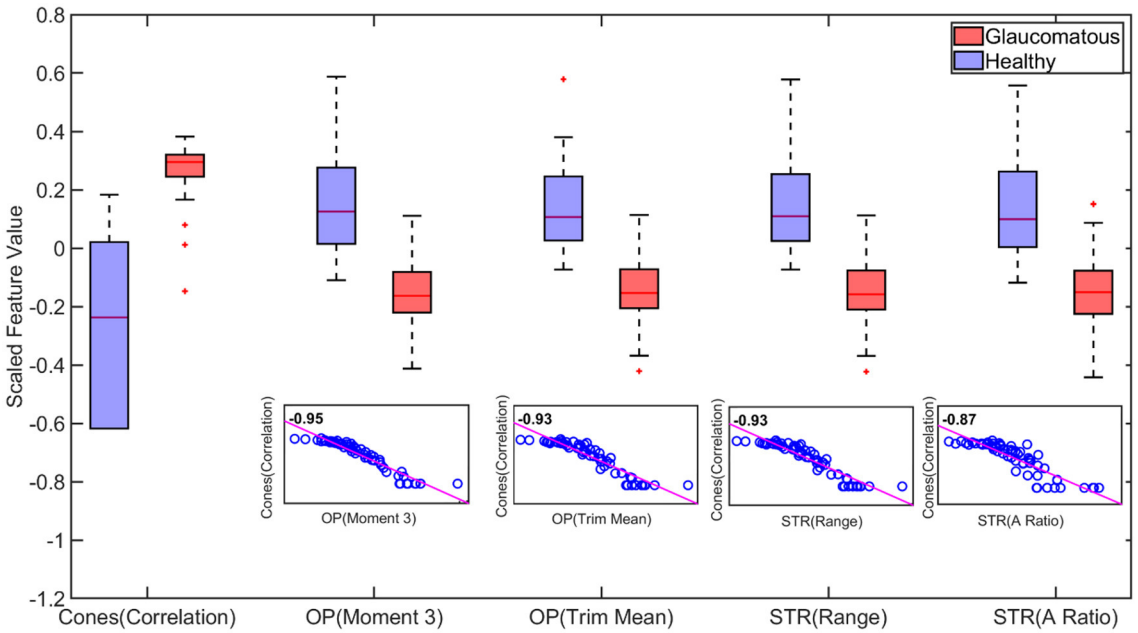

FIGURE 6 | Boxplot of statistically important features for binary classification. The important features capable of distinguishing healthy and glaucomatous are correlated feature from Cones, third order Moment and trimmed mean feature from Oscillatory Potentials (OP) and Range and aspect ratio from Scotopic Threshold Response (STR). However, the high similarity between these features quantified by the correlation scores in the scatter plot create redundancy (inclusion cones(correlation) feature alone vs inclusion all five features does not improve accuracy). Therefore, utilizing the cones correlation feature alone captures the behavior of the other four features. This dropping of redundant features and choosing Cones (correlation) feature alone is achieved by using Minimum Redundancy and Maximum Relevance (MRMR) algorithm (On each box, the central mark indicates the median, and the bottom and top edges of the box indicate the 25th and 75th percentiles, respectively. The whiskers extend to the most extreme data points not considered outliers, and the outliers are plotted individually using the "+" marker symbol.).

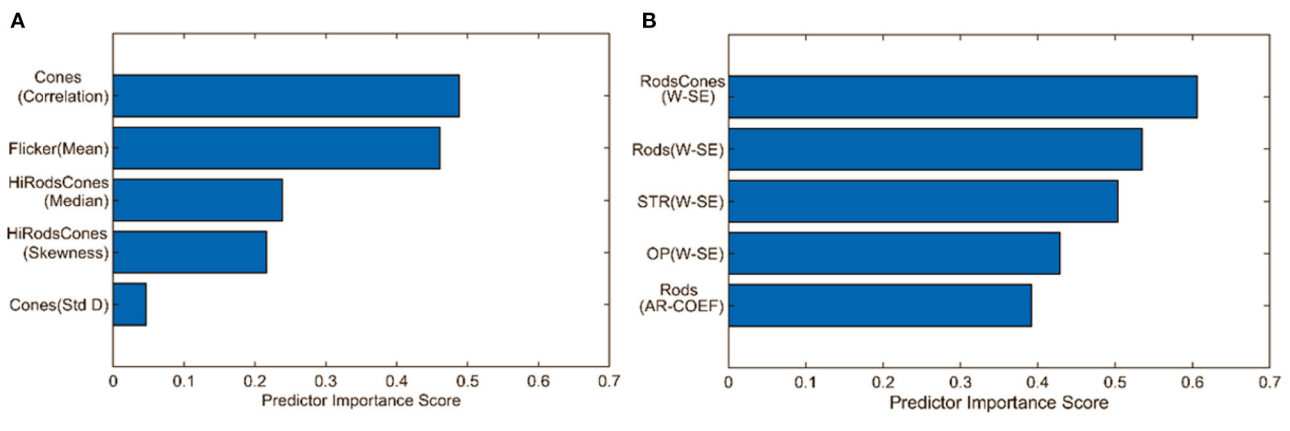

FIGURE 7 | Comparison of predictive importance scores for binary classification using **(A)** statistical features and **(B)** wavelet-based features. This bar chart illustrates the superior predictive capability of wavelet-based features. Std D, Standard Deviation; W-SE, Wavelet based Shannon entropy; AR-COEF, Autoregressive coefficient.

accuracy to 80%, as shown in **Table 2**. This improvement in accuracy indicated that wavelet-based features can distinguish healthy and glaucomatous animals suggesting that they are more sensitive to subtle changes in ERG signals due to glaucoma. The multiclass classification ability of this framework reaffirmed the rich and complex nature of ERG signals in assessing the disease progression.

3.3. RGC Regression

Regression analysis was performed to predict retinal ganglion cell count from ERG signals. Feature selection for regression was performed using MRMR sequential feature selection. RGC values of the animals ranged between 8 and 120. RSME for RGC regression was 15.64 and 11.20 for models trained with statistical features and wavelet-based features, respectively. Regression

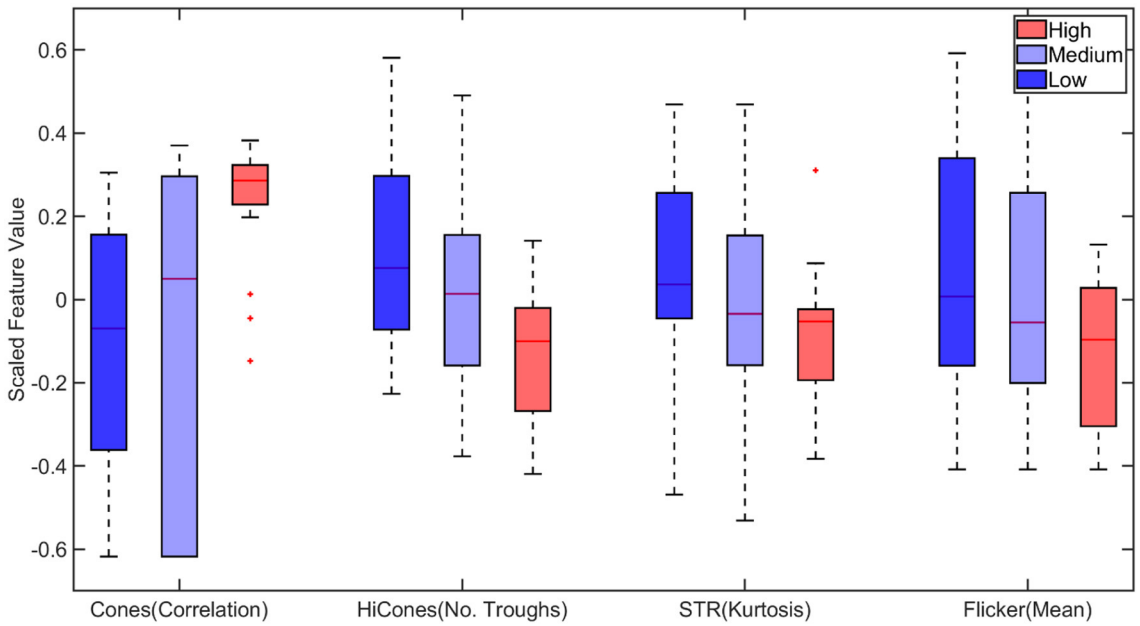

FIGURE 8 | Boxplot of statistical features selected by Minimum Redundancy and Maximum Relevance (MRMR) feature selection algorithm for multiclass classification. STR, Scotopic Threshold Response. On each box, the central mark corresponds to the median, and the bottom and top edges of the box correspond to the 25th and 75th percentiles, respectively. The dashed lines (whiskers) extend to the most extreme data points not considered outliers, and the outliers are plotted individually using the "+" marker symbol.

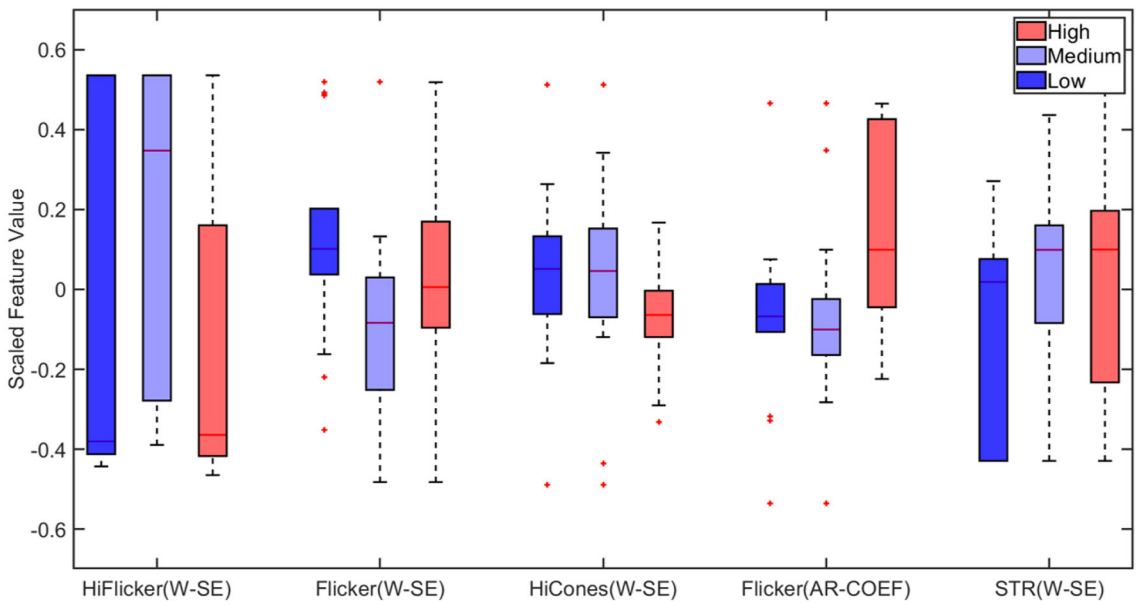

FIGURE 9 | Boxplot of wavelet-based features selected by Minimum Redundancy and Maximum Relevance (MRMR) feature selection algorithm for multiclass classification. STR, Scotopic Threshold Response; W-SE, Wavelet based Shannon Entropy; AR-COEF, Autoregressive Coefficient. On each box, the central mark indicates the median, and the bottom and top edges of the box indicate the 25th and 75th percentiles, respectively. The whiskers extend to the most extreme data points not considered outliers, and the outliers are plotted individually using the "+" marker symbol.

results using wavelet-based features are shown in **Figure 10**. The results in Grillo et al. (2018) indicate that RGC counts had a strong correlation with STR and OPs. The dominant features selected for RGC regression (from STR and OP) were in agreement with the findings in Grillo et al. (2018). **Table 4** compares performance of various ML based regression models

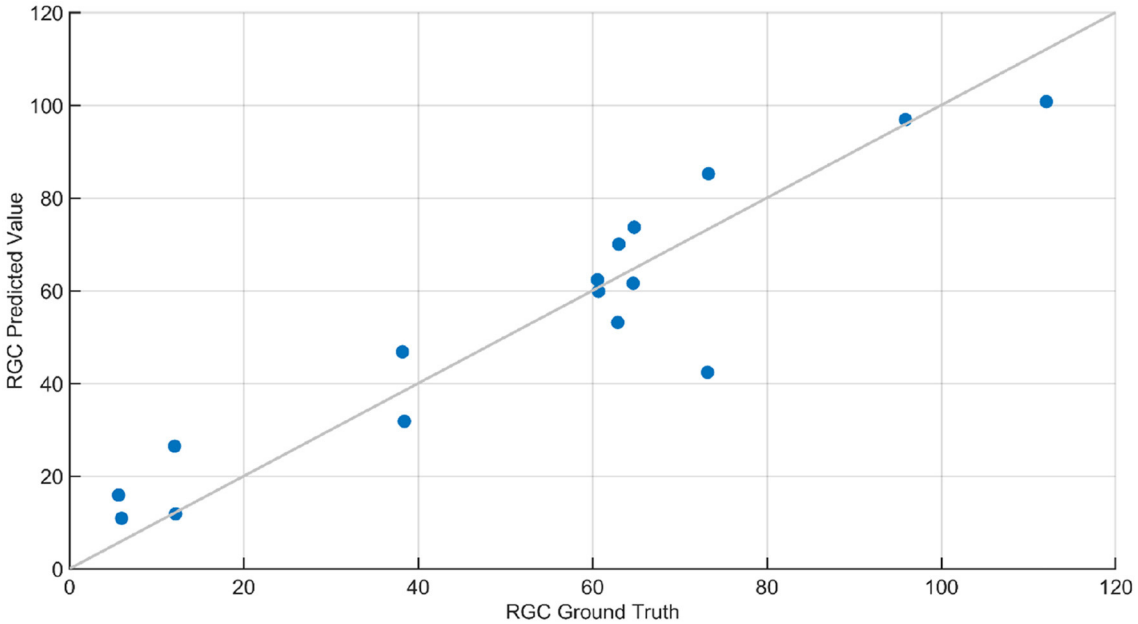

FIGURE 10 | RGC count regression plot. This plot contains the ground truth and predicted response of RGC count predicted using Gaussian Process Regression (GPR). The squared exponential GPR model was trained using both standard and advanced features. The RGC count of the animals ranged between 8 and 120, and the root mean squared error in the prediction of RGC was 11.2. The line in this plot denotes when the predicted values are equal to ground truth values.

TABLE 4 | Performance metrics for retinal ganglion cells (RGCs) Regression.

Machine learning algorithm	RSME	
	Statistical	Wavelet
Tree	31.716	17.852
SVM	17.177	13.82
Ensemble (Bagged)	29.129	24.387
Logistic regression	44.622	24.873
Gaussian process regression	**15.644**	**11.201**

Bold font indicate the best performing regression model and its corresponding RSME.

in predicting retinal ganglion cells (RGCs) counts: The higher error (RSME) with statistical features compared with the wavelet-based advanced features emphasized the need for sophisticated features to predict RGC count accurately. SVM- and GPR-based models provided the most accurate prediction of RGC numbers from ERG signals. Specifically, squared exponential and rational quadratic models of GPR provided the least error.

4. DISCUSSION

Our goal was to determine the feasibility of applying ML-based methods to the analysis of ERG signals for glaucoma detection at different stages of the disease. In the present study, we systematically applied machine-learning-based methods for the first time to detect glaucoma and predict RGC loss based on ERG signals. The present study utilized ERGs measured in mice rather than from human patients, because the use of data from a preclinical model allowed us to validate "ground truth" data sets with a range of complimentary and alternative experimental strategies, which is not possible in human clinical studies. These include histology, biochemical, and immunochemical assays, as well as optomotor reflex measurements. We were able to determine for the first time that advanced features (wavelet-based features) are capable of detecting subtle changes in the ERG signal and perform multiclass classification based on the progression level of the disease with 80% accuracy. In particular, we found that Shannon Entropy Values for Maximal Overlap Discrete Wavelet Packet Transform (MOD-PWT) and AR coefficients represent important features capable of detecting early-stage glaucoma. Among the nine available ERG signals, Flicker, STR, OP, and Rod-Cone appear integral for such successful detection. This is in agreement with the results published in Lei et al. (2006). However, given that these features are highly correlated, the ML-based algorithm picks only one for each set of highly correlated features to reduce the model complexity as shown in **Figure 6**.

In addition, the method proposed here performs ERG analysis in a wavelet domain instead of a frequency domain, which allows to capture subtle changes in the signals. In addition, various intricate features such as multiscale wavelet variance estimates, Shannon entropy, and autoregressive coefficients are incorporated in the method, compared to basic features such as differences in amplitude and latency in previous studies (Hood et al., 2000; Fortune et al., 2002; Thienprasiddhi et al., 2003; Stiefelmeyer et al., 2004; Ventura and Porciatti, 2006; Chu et al., 2007; Miguel-Jiménez et al., 2010; Luo et al., 2011; Palmowski-Wolfe et al., 2011; Todorova and Palmowski-Wolfe, 2011; Ho

et al., 2012; Hori et al., 2012; Ledolter et al., 2013; Consejo et al., 2019). The results strongly suggest that such advanced features in the wavelet domain are necessary for detection of early-stage glaucoma. Moreover, in contrast to the recent study that leverages ML-based technique to analyze ERG using solely the photopic negative response (PhNR) component (Armstrong and Lorch, 2020), the current method uses all ERG components in the analysis to fully utilize the capability of the ML-based technique to crunch large data sets and draw complicated relationships. Therefore, the proposed framework is not limited to a small subset of genetic eye diseases like previous studies (Fortune et al., 2002; Thienprasiddhi et al., 2003; Stiefelmeyer et al., 2004; Chu et al., 2007; Miguel-Jiménez et al., 2010; Luo et al., 2011; Palmowski-Wolfe et al., 2011; Todorova and Palmowski-Wolfe, 2011; Ho et al., 2012; Hori et al., 2012; Ledolter et al., 2013; Consejo et al., 2019); instead, it is capable of mapping ERG signals to various eye diseases.

5. CONCLUSION

Results obtained in the present study strongly suggest that the methods employed can reproducibly identify dominant features for classification and regression from STR, Oscillatory potentials (OPs), and other ERG tests consistent with the results reported in previously published work on the sensitivity of and OPs and flicker to subtle changes in RGC function and viability (Tyler, 1981; Brandao et al., 2017). Further, our approach identified additional dominant distinguishing features such as Shannon Entropy Values for Maximal Overlap Discrete Wavelet Packet Transform (MOD-PWT) and AR coefficients, which are not distinguishable by traditional methods used in Grillo et al. (2018). This strongly suggests that the current machine-learning-based algorithm has significant potential in distinguishing subtle changes in ERG signals corresponding to different stages of glaucoma disease development. This capability of the technique could be used as a foundational step to create a reliable framework for the early detection of glaucoma and to monitor efficacy of therapeutic intervention in both clinical practice and novel drug development for glaucoma. In addition, the inclusion of various ERG protocols in this framework, such as cones, rods and cones, STR, and oscillatory potentials, represent responses from different cell types in the eye. Therefore, ERG response can be mapped to diseases specific to those cell types. It should be noted that this study was based on mice and with 12 h of dark adaptation. The promising results obtained here suggest the great potential for this method to help detect early stage, pre-symptomatic glaucoma. However, an additional study on adaptation requirements would be required before extending this framework to humans.

DATA AVAILABILITY STATEMENT

The datasets generated for this study are available on request to the corresponding author. Requests to access these datasets should be directed to mehdizadeha@umkc.edu.

AUTHOR CONTRIBUTIONS

MG contributed in machine learning framework development, formal analysis, investigation, validation, visualization, and writing—original draft. LR contributed in writing—review and editing. PK contributed in providing the data, conceptualization, supervision, and writing—review and editing. AM contributed in conceptualization, supervision, and writing—review and editing. All authors contributed to the article and approved the submitted version.

FUNDING

Research reported in this publication was supported by the Felix and Carmen Sabates Missouri Endowed Chair in Vision Research, the Vision Research Foundation of Kansas City, and in part by National Eye Institute grant EY031248 of the National Institutes of Health (PK). The content is solely the responsibility of the authors and does not necessarily represent the official views of the National Institutes of Health. The publication cost was covered by PK.

REFERENCES

Aguinis, H., Gottfredson, R. K., and Joo, H. (2013). Best-practice recommendations for defining, identifying, and handling outliers. *Organ. Res. Methods* 16, 270–301. doi: 10.1177/1094428112470848

Aha, D. W., and Bankert, R. L. (1996). "A comparative evaluation of sequential feature selection algorithms," in *Learning from Data*, eds. D. Fisher and H.-J. Lenz (New York, NY: Springer), 199–206. doi: 10.1007/978-1-4612-2404-4_19

Ahmad, M. A., Eckert, C., and Teredesai, A. (2018). "Interpretable machine learning in healthcare," in *Proceedings of the 2018 ACM International Conference on Bioinformatics, Computational Biology, and Health Informatics* (Washington, DC), 559–560. doi: 10.1145/3233547.3233667

Al'Aref, S. J., Anchouche, K., Singh, G., Slomka, P. J., Kolli, K. K., Kumar, A., et al. (2019). Clinical applications of machine learning in cardiovascular disease and its relevance to cardiac imaging. *Eur. Heart J.* 40, 1975–1986. doi: 10.1093/eurheartj/ehy404

Aldebasi, Y. H., Drasdo, N., Morgan, J. E., and North, R. V. (2004). S-cone, l+ m-cone, and pattern, electroretinograms in ocular hypertension and glaucoma. *Vision Res.* 44, 2749–2756. doi: 10.1016/j.visres.2004.06.015

An, G., Omodaka, K., Hashimoto, K., Tsuda, S., Shiga, Y., Takada, N., et al. (2019). Glaucoma diagnosis with machine learning based on optical coherence tomography and color fundus images. *J. Healthcare Eng.* 2019, 4061313. doi: 10.1155/2019/4061313

Armstrong, G. W., and Lorch, A. C. (2020). A (eye): a review of current applications of artificial intelligence and machine learning in ophthalmology. *Int. Ophthalmol. Clin.* 60, 57–71. doi: 10.1097/IIO.0000000000000298

Asakawa, K., Amino, K., Iwase, M., Kusayanagi, Y., Nakamura, A., Suzuki, R., et al. (2017). New mydriasis-free electroretinogram recorded with skin electrodes in healthy subjects. *Biomed. Res. Int.* 2017, 8539747. doi: 10.1155/2017/8539747

Asaoka, R., Murata, H., Iwase, A., and Araie, M. (2016). Detecting preperimetric glaucoma with standard automated perimetry using a deep learning classifier. *Ophthalmology* 123, 1974–1980. doi: 10.1016/j.ophtha.2016.05.029

Asgharzadeh-Bonab, A., Amirani, M. C., and Mehri, A. (2020). Spectral entropy and deep convolutional neural network for ECG beat classification. *Biocybernet. Biomed. Eng*. 40, 691–700. doi: 10.1016/j.bbe.2020.02.004

Atalay, E., Nongpiur, M. E., Yap, S. C., Wong, T. T., Goh, D., Husain, R., et al. (2016). Pattern of visual field loss in primary angle-closure glaucoma across different severity levels. *Ophthalmology* 123, 1957–1964. doi: 10.1016/j.ophtha.2016.05.026

Barraco, R., Adorno, D. P., Brai, M., and Tranchina, L. (2014). A comparison among different techniques for human ERG signals processing and classification. *Phys. Med*. 30, 86–95. doi: 10.1016/j.ejmp.2013.03.006

Beykin, G., Norcia, A. M., Srinivasan, V. J., Dubra, A., and GoldbERG, J. L. (2021). Discovery and clinical translation of novel glaucoma biomarkers. *Prog. Retinal Eye Res*. 80, 100875. doi: 10.1016/j.preteyeres.2020.100875

Boquete, L., Miguel-Jiménez, J. M., Ortega, S., Rodriguez-Ascariz, J., Pérez-Rico, C., and Blanco, R. (2012). Multifocal electroretinogram diagnosis of glaucoma applying neural networks and structural pattern analysis. *Expert Syst. Appl*. 39, 234–238. doi: 10.1016/j.eswa.2011.07.013

Bowd, C., Weinreb, R. N., Balasubramanian, M., Lee, I., Jang, G., Yousefi, S., et al. (2014). Glaucomatous patterns in frequency doubling technology (FDT) perimetry data identified by unsupervised machine learning classifiers. *PLoS ONE* 9, e85941. doi: 10.1371/journal.pone.0085941

Brandao, L. M., Monhart, M., Schötzau, A., Ledolter, A. A., and Palmowski-Wolfe, A. M. (2017). Wavelet decomposition analysis in the two-flash multifocal ERG in early glaucoma: a comparison to ganglion cell analysis and visual field. *Document. Ophthalmol*. 135, 29–42. doi: 10.1007/s10633-017-9593-y

Burroughs, S. L., Kaja, S., and Koulen, P. (2011). Quantification of deficits in spatial visual function of mouse models for glaucoma. *Investig. Ophthalmol. Visual Sci*. 52, 3654–3659. doi: 10.1167/iovs.10-7106

Bussel, I. I., Wollstein, G., and Schuman, J. S. (2014). Oct for glaucoma diagnosis, screening and detection of glaucoma progression. *Brit. J. Ophthalmol*. 98(Suppl 2), ii15–ii19. doi: 10.1136/bjophthalmol-2013-304326

Bzdok, D., Altman, N., and Krzywinski, M. (2018). Points of significance: statistics versus machine learning. *Nat. Methods* 2018, 1–7. doi: 10.1038/nmeth.4642

Cawley, G. C., and Talbot, N. L. (2003). Efficient leave-one-out cross-validation of kernel fisher discriminant classifiers. *Pattern Recogn*. 36, 2585–2592. doi: 10.1016/S0031-3203(03)00136-5

Chu, P. H., Chan, H. H., and Brown, B. (2007). Luminance-modulated adaptation of global flash mfERG: fellow eye losses in asymmetric glaucoma. *Investig. Ophthalmol. Visual Sci*. 48, 2626–2633. doi: 10.1167/iovs.06-0962

Consejo, A., Melcer, T., and Rozema, J. J. (2019). "Introduction to machine learning for ophthalmologists," in *Seminars in Ophthalmology*, Vol. 34 (Taylor & Francis), 19–41. doi: 10.1080/08820538.2018.1551496

Cruz, J. A., and Wishart, D. S. (2006). Applications of machine learning in cancer prediction and prognosis. *Cancer Inform*. 2, 117693510600200030. doi: 10.1177/117693510600200030

da Silva, C. N., Dourado, L. F. N., de Lima, M. E., and da Silva Cunha, A. Jr. (2020). Pnpp-19 peptide as a novel drug candidate for topical glaucoma therapy through nitric oxide release. *Transl. Vision Sci. Technol*. 9, 33–33. doi: 10.1167/tvst.9.8.33

Dale, E. A., Hood, D. C., Greenstein, V. C., and Odel, J. G. (2010). A comparison of multifocal ERG and frequency domain oct changes in patients with abnormalities of the retina. *Document. Ophthalmol*. 120, 175–186. doi: 10.1007/s10633-009-9210-9

Darbellay, G. A., and Vajda, I. (1999). Estimation of the information by an adaptive partitioning of the observation space. *IEEE Trans. Inform. Theory* 45, 1315–1321. doi: 10.1109/18.761290

Daubechies, I. (1992). *Ten Lectures on Wavelets*. New York, NY: Society for Industrial and Applied Mathematics.

de Lara, M. J. P., Guzmán-Aránguez, A., de la Villa, P., Diaz-Hernández, J. I., Miras-Portugal, M. T., and Pintor, J. (2015). Increased levels of extracellular ATP in glaucomatous retinas: possible role of the vesicular nucleotide transporter during the development of the pathology. *Mol. Vis*. 21, 1060.

de Lara, M. J. P., Santano, C., Guzmán-Aránguez, A., Valiente-Soriano, F. J., Avilés-Trigueros, M., Vidal-Sanz, M., et al. (2014). Assessment of inner retina dysfunction and progressive ganglion cell loss in a mouse model of glaucoma. *Exp. Eye Res*. 122, 40–49. doi: 10.1016/j.exer.2014.02.022

Demmin, D. L., Davis, Q., Roché, M., and Silverstein, S. M. (2018). Electroretinographic anomalies in schizophrenia. *J. Abnormal Psychol*. 127, 417. doi: 10.1037/abn0000347

Dietterich, T. G. (2000). "Ensemble methods in machine learning," in *International Workshop on Multiple Classifier Systems* (Berlin, Heidelberg: Springer), 1–15. doi: 10.1007/3-540-45014-9_1

Ding, C., and Peng, H. (2005). Minimum redundancy feature selection from microarray gene expression data. *J. Bioinform. Comput. Biol*. 3, 185–205. doi: 10.1142/S0219720005001004

Dong, C.-J., Agey, P., and Hare, W. A. (2004). Origins of the electroretinogram oscillatory potentials in the rabbit retina. *Vis. Neurosci*. 21, 533–543. doi: 10.1017/S0952523804214043

Duan, K., Keerthi, S. S., and Poo, A. N. (2003). Evaluation of simple performance measures for tuning SVM hyperparameters. *Neurocomputing* 51, 41–59. doi: 10.1016/S0925-2312(02)00601-X

Ernest, P. J., Schouten, J. S., Beckers, H. J., Hendrikse, F., Prins, M. H., and Webers, C. A. (2012). The evidence base to select a method for assessing glaucomatous visual field progression. *Acta Ophthalmol*. 90, 101–108. doi: 10.1111/j.1755-3768.2011.02206.x

Feurer, M., and Hutter, F. (2019). "Hyperparameter optimization," in *Automated Machine Learning*, eds. F. Hutter, L. Kotthoff, and J. Vanschoren (Cham: Springer), 3–33. doi: 10.1007/978-3-030-05318-5_1

Fidalgo, B. M., Crabb, D. P., and Lawrenson, J. G. (2015). Methodology and reporting of diagnostic accuracy studies of automated perimetry in glaucoma: evaluation using a standardised approach. *Ophthal. Physiol. Opt*. 35, 315–323. doi: 10.1111/opo.12208

Forte, J. D., Bui, B. V., and Vingrys, A. J. (2008). Wavelet analysis reveals dynamics of rat oscillatory potentials. *J. Neurosci. Methods* 169, 191–200. doi: 10.1016/j.jneumeth.2007.12.007

Fortune, B., Bearse, M. A., Cioffi, G. A., and Johnson, C. A. (2002). Selective loss of an oscillatory component from temporal retinal multifocal ERG responses in glaucoma. *Investig. Ophthalmol. Visual Sci*. 43, 2638–2647.

Fortune, B., Wang, L., Bui, B. V., Cull, G., Dong, J., and Cioffi, G. A. (2003). Local ganglion cell contributions to the macaque electroretinogram revealed by experimental nerve fiber layer bundle defect. *Investig. Ophthalmol. Visual Sci*. 44, 4567–4579. doi: 10.1167/iovs.03-0200

Frishman, L. J., Saszik, S., Harwerth, R. S., Viswanathan, S., Li, Y., Smith, E. L., et al. (2000). Effects of experimental glaucoma in macaques on the multifocal ERG. *Document. Ophthalmol*. 100, 231–251. doi: 10.1023/A:1002735804029

Graham, J. W., Cumsille, P. E., and Shevock, A. E. (2013). Methods for handling missing data. doi: 10.1002/9781118133880.hop202004

Graham, S. L., Klistorner, A. I., Grigg, J. R., and Billson, F. A. (2000). Objective VEP perimetry in glaucoma: asymmetry analysis to identify early deficits. *J. Glaucoma* 9, 10–19. doi: 10.1097/00061198-200002000-00004

Grillo, S. L., Keereetaweep, J., Grillo, M. A., Chapman, K. D., and Koulen, P. (2013). N-palmitoylethanolamine depot injection increased its tissue levels and those of other acylethanolamide lipids. *Drug Design Dev. Therapy* 7, 747. doi: 10.2147/DDDT.S48324

Grillo, S. L., and Koulen, P. (2015). Psychophysical testing in rodent models of glaucomatous optic neuropathy. *Exp. Eye Res*. 141, 154–163. doi: 10.1016/j.exer.2015.06.025

Grillo, S. L., Montgomery, C. L., Johnson, H. M., and Koulen, P. (2018). Quantification of changes in visual function during disease development in a mouse model of pigmentary glaucoma. *J. Glaucoma* 27, 828. doi: 10.1097/IJG.0000000000001024

Guyon, I., Gunn, S., Nikravesh, M., and Zadeh, L. A. (2008). *Feature Extraction: Foundations and Applications*, Vol. 207. Springer.

Hancock, H. A., and Kraft, T. W. (2004). Oscillatory potential analysis and ERGs of normal and diabetic rats. *Investig. Ophthalmol. Visual Sci*. 45, 1002–1008. doi: 10.1167/iovs.03-1080

Hannun, A. Y., Rajpurkar, P., Haghpanahi, M., Tison, G. H., Bourn, C., Turakhia, M. P., et al. (2019). Cardiologist-level arrhythmia detection and classification in ambulatory electrocardiograms using a deep neural network. *Nat. Med*. 25, 65–69. doi: 10.1038/s41591-018-0268-3

Harwerth, R. S., Crawford, M., Frishman, L. J., Viswanathan, S., Smith, E. L. III, and Carter-Dawson, L. (2002). Visual field defects and neural losses from experimental glaucoma. *Prog Retinal Eye Res*. 21, 91–125. doi: 10.1016/S1350-9462(01)00022-2

Hébert, M., Mérette, C., Gagné, A.-M., Paccalet, T., Moreau, I., Lavoie, J., et al. (2020). The electroretinogram may differentiate schizophrenia from bipolar disorder. *Biol. Psychiatry* 87, 263–270. doi: 10.1016/j.biopsych.2019.06.014

Hermas, A. (2019). *Sensitivity and specificity of the uniform field ERG in glaucoma detection* (Ph.D. thesis). University of Ottawa, Ottawa, ON, Canada.

Ho, W.-C., Wong, O.-Y., Chan, Y.-C., Wong, S.-W., Kee, C.-S., and Chan, H. H.-L. (2012). Sign-dependent changes in retinal electrical activity with positive and negative defocus in the human eye. *Vision Res*. 52, 47–53. doi: 10.1016/j.visres.2011.10.017

Hobby, A. E., Kozareva, D., Yonova-Doing, E., Hossain, I. T., Katta, M., Huntjens, B., et al. (2018). Effect of varying skin surface electrode position on electroretinogram responses recorded using a handheld stimulating and recording system. *Document. Ophthalmol*. 137, 79–86. doi: 10.1007/s10633-018-9652-z

Holzinger, A. (2014). Trends in interactive knowledge discovery for personalized medicine: cognitive science meets machine learning. *IEEE Intell. Inform. Bull*. 15, 6–14. doi: 10.1007/978-3-662-43968-5_1

Hood, D. C., Greenstein, V. C., Holopigian, K., Bauer, R., Firoz, B., Liebmann, J. M., et al. (2000). An attempt to detect glaucomatous damage to the inner retina with the multifocal ERG. *Investig. Ophthalmol. Visual Sci*. 41, 1570–1579.

Hori, N., Komori, S., Yamada, H., Sawada, A., Nomura, Y., Mochizuki, K., et al. (2012). Assessment of macular function of glaucomatous eyes by multifocal electroretinograms. *Document. Ophthalmol*. 125, 235–247. doi: 10.1007/s10633-012-9351-0

Horn, F. K., Jonas, J. B., Korth, M., Jünemann, A., and Gründler, A. (1997). The full-field flicker test in early diagnosis of chronic open-angle glaucoma. *Am. J. Ophthalmol*. 123, 313–319. doi: 10.1016/S0002-9394(14)70126-6

Hui, F., Tang, J., Williams, P. A., McGuinness, M. B., Hadoux, X., Casson, R. J., et al. (2020). Improvement in inner retinal function in glaucoma with nicotinamide (vitamin b3) supplementation: a crossover randomized clinical trial. *Clin. Exp. Ophthalmol*. 48, 903–914. doi: 10.1111/ceo.13818

Jambukia, S. H., Dabhi, V. K., and Prajapati, H. B. (2015). "Classification of ECG signals using machine learning techniques: a survey," in *2015 International Conference on Advances in Computer Engineering and Applications* (Ghaziabad, India: IEEE), 714–721. doi: 10.1109/ICACEA.2015.7164783

Jordan, M. I., and Mitchell, T. M. (2015). Machine learning: trends, perspectives, and prospects. *Science* 349, 255–260. doi: 10.1126/science.aaa8415

Kaja, S., Naumchuk, Y., Grillo, S. L., Borden, P. K., and Koulen, P. (2014). Differential up-regulation of vesl-1/homer 1 protein isoforms associated with decline in visual performance in a preclinical glaucoma model. *Vision Res*. 94, 16–23. doi: 10.1016/j.visres.2013.10.018

Kato, K., Kondo, M., Nagashima, R., Sugawara, A., Sugimoto, M., Matsubara, H., et al. (2017). Factors affecting mydriasis-free flicker ERGs recorded with real-time correction for retinal illuminance: study of 150 young healthy subjects. *Investig. Ophthalmol. Visual Sci*. 58, 5280–5286. doi: 10.1167/iovs.17-22587

Khalid, S., Khalil, T., and Nasreen, S. (2014). "A survey of feature selection and feature extraction techniques in machine learning," in *2014 Science and Information Conference* (London, UK: IEEE), 372–378. doi: 10.1109/SAI.2014.6918213

Khan, M. Z., Gajendran, M. K., Lee, Y., and Khan, M. A. (2021). Deep neural architectures for medical image semantic segmentation. *IEEE Access*. 83002–83024. doi: 10.1109/ACCESS.2021.3086530

Kononenko, I. (2001). Machine learning for medical diagnosis: history, state of the art and perspective. *Artif. Intell. Med*. 23, 89–109. doi: 10.1016/S0933-3657(01)00077-X0

Kuhn, M., and Johnson, K. (2013). "Measuring predictor importance," in *Applied Predictive Modeling* (New York, NY: Springer), 463–485. doi: 10.1007/978-1-4614-6849-3_18

Lachenmayr, B., and Drance, S. (1992). The selective effects of elevated intraocular pressure on temporal resolution. *German J. Ophthalmol*.1, 26–31.

Lai, T., Ngai, J., Lai, R., and Lam, D. (2009). Multifocal electroretinography changes in patients on ethambutol therapy. *Eye* 23, 1707–1713. doi: 10.1038/eye.2008.361

Lai, T. Y., Ngai, J. W., Chan, W.-M., and Lam, D. S. (2006). Visual field and multifocal electroretinography and their correlations in patients on hydroxychloroquine therapy. *Document. Ophthalmol*. 112, 177–187. doi: 10.1007/s10633-006-9006-0

Ledolter, A. A., Kramer, S. A., Todorova, M. G., Schötzau, A., and Palmowski-Wolfe, A. M. (2013). The effect of filtering on the two-global-flash mfERG: identifying the optimal range of frequency for detecting glaucomatous retinal dysfunction. *Document. Ophthalmol*. 126, 117–123. doi: 10.1007/s10633-012-9364-8

Ledolter, A. A., Monhart, M., Schoetzau, A., Todorova, M. G., and Palmowski-Wolfe, A. M. (2015). Structural and functional changes in glaucoma: comparing the two-flash multifocal electroretinogram to optical coherence tomography and visual fields. *Document. Ophthalmol*. 130, 197–209. doi: 10.1007/s10633-015-9482-1

Lee, A., Taylor, P., Kalpathy-Cramer, J., and Tufail, A. (2017). Machine learning has arrived! *Ophthalmology* 124, 1726–1728. doi: 10.1016/j.ophtha.2017.08.046

Lee, C. H., and Yoon, H.-J. (2017). Medical big data: promise and challenges. *Kidney Res. Clin. Pract*. 36, 3. doi: 10.23876/j.krcp.2017.36.1.3

Lei, B., Yao, G., Zhang, K., Hofeldt, K. J., and Chang, B. (2006). Study of rod-and cone-driven oscillatory potentials in mice. *Investig. Ophthalmol. Visual Sci*. 47, 2732–2738. doi: 10.1167/iovs.05-1461

Leonarduzzi, R. F., Schlotthauer, G., and Torres, M. E. (2010). "Wavelet leader based multifractal analysis of heart rate variability during myocardial ischaemia," in *2010 Annual International Conference of the IEEE Engineering in Medicine and Biology* (Buenos Aires, Argentina: IEEE), 110–113. doi: 10.1109/IEMBS.2010.5626091

Leske, M. C., Heijl, A., Hyman, L., Bengtsson, B., Dong, L., Yang, Z., et al. (2007). Predictors of long-term progression in the early manifest glaucoma trial. *Ophthalmology* 114, 1965–1972. doi: 10.1016/j.ophtha.2007.03.016

Li, Q., Rajagopalan, C., and Clifford, G. D. (2014). A machine learning approach to multi-level ECG signal quality classification. *Comput. Methods Prog. Biomed*. 117, 435–447. doi: 10.1016/j.cmpb.2014.09.002

Li, T., and Zhou, M. (2016). ECG classification using wavelet packet entropy and random forests. *Entropy* 18, 285. doi: 10.3390/e18080285

Lisboa, P. J. (2002). A review of evidence of health benefit from artificial neural networks in medical intervention. *Neural Netw*. 15, 11–39. doi: 10.1016/S0893-6080(01)00111-3

Liu, H., Ji, X., Dhaliwal, S., Rahman, S. N., McFarlane, M., Tumber, A., et al. (2018). Evaluation of light-and dark-adapted ERGs using a mydriasis-free, portable system: clinical classifications and normative data. *Document. Ophthalmol*. 137, 169–181. doi: 10.1007/s10633-018-9660-z

Luo, X., Patel, N. B., Harwerth, R. S., and Frishman, L. J. (2011). Loss of the low-frequency component of the global-flash multifocal electroretinogram in primate eyes with experimental glaucoma. *Investig. Ophthalmol. Visual Sci*. 52, 3792–3804. doi: 10.1167/iovs.10-6667

Maharaj, E. A., and Alonso, A. M. (2014). Discriminant analysis of multivariate time series: application to diagnosis based on ECG signals. *Comput. Stat. Data Anal*. 70, 67–87. doi: 10.1016/j.csda.2013.09.006

Man, T. T., Yip, Y. W., Cheung, F. K., Lee, W. S., Pang, C. P., and Brelén, M. E. (2020). Evaluation of electrical performance and properties of electroretinography electrodes. *Transl. Vis. Sci. Technol*. 9, 45–45. doi: 10.1167/tvst.9.7.45

Marmor, M., Fulton, A., Holder, G., Miyake, Y., Brigell, M., and Bach, M. (2009). Iscev standard for full-field clinical electroretinography (2008 update). *Document. Ophthalmol*. 118, 69–77. doi: 10.1007/s10633-008-9155-4

Martis, R. J., Chakraborty, C., and Ray, A. K. (2014). "Wavelet-based machine learning techniques for ECG signal analysis," in *Machine Learning in Healthcare Informatics*, eds. S. Dua, U. R. Acharya, and P. Dua (Berlin, Heidelberg: Springer), 25–45. doi: 10.1007/978-3-642-40017-9_2

McKinnon, S. J., Schlamp, C. L., and Nickells, R. W. (2009). Mouse models of retinal ganglion cell death and glaucoma. *Exp. Eye Res*. 88, 816–824. doi: 10.1016/j.exer.2008.12.002

McPadden, J., Durant, T. J., Bunch, D. R., Coppi, A., Price, N., Rodgerson, K., et al. (2019). Health care and precision medicine research: analysis of a scalable data science platform. *J. Med. Internet Res*. 21, e13043. doi: 10.2196/13043

Miguel-Jiménez, J., Boquete, L., Ortega, S., Rodriguez-Ascariz, J., and Blanco, R. (2010). Glaucoma detection by wavelet-based analysis of the global flash multifocal electroretinogram. *Med. Eng. Phys*. 32, 617–622. doi: 10.1016/j.medengphy.2010.02.019

Miguel-Jiménez, J. M., Blanco, R., De-Santiago, L., Fernandez, A., Rodriguez-Ascariz, J. M., Barea, R., et al. (2015). Continuous-wavelet-transform analysis of

the multifocal ERG waveform in glaucoma diagnosis. *Med. Biol. Eng. Comput.* 53, 771–780. doi: 10.1007/s11517-015-1287-6

Montgomery, C. L., Keereetaweep, J., Johnson, H. M., Grillo, S. L., Chapman, K. D., and Koulen, P. (2016). Changes in retinal n-acylethanolamines and their oxylipin derivatives during the development of visual impairment in a mouse model for glaucoma. *Lipids* 51, 857–866. doi: 10.1007/s11745-016-4161-x

Nakamura, N., Fujinami, K., Mizuno, Y., Noda, T., and Tsunoda, K. (2016). Evaluation of cone function by a handheld non-mydriatic flicker electroretinogram device. *Clin. Ophthalmol.* 10, 1175. doi: 10.2147/OPTH.S104721

Navada, A., Ansari, A. N., Patil, S., and Sonkamble, B. A. (2011). "Overview of use of decision tree algorithms in machine learning," in *2011 IEEE Control and System Graduate Research Colloquium* (Shah Alam, Malaysia: IEEE), 37–42. doi: 10.1109/ICSGRC.2011.5991826

Nebbioso, M., Grenga, R., and Karavitis, P. (2009). Early detection of macular changes with multifocal ERG in patients on antimalarial drug therapy. *J. Ocular Pharmacol. Therapeut.* 25, 249–258. doi: 10.1089/jop.2008.0106

Neumaier, A., and Schneider, T. (2001). Estimation of parameters and eigenmodes of multivariate autoregressive models. *ACM Trans. Math. Softw.* 27, 27–57. doi: 10.1145/382043.382304

Noble, W. S. (2006). What is a support vector machine? *Nat. Biotechnol.* 24, 1565–1567. doi: 10.1038/nbt1206-1565

Omrani, H. (2015). Predicting travel mode of individuals by machine learning. *Transport. Res. Proc.* 10, 840–849. doi: 10.1016/j.trpro.2015.09.037

Palmberg, P. (2002). Answers from the ocular hypertension treatment study. *Arch. Ophthalmol.* 120, 829–830. doi: 10.1001/archopht.120.6.829

Palmowski-Wolfe, A., Todorova, M., and Orgül, S. (2011). Multifocal oscillatory potentials in the "two global flash" mferg in high and normal tension primary open-angle glaucoma. *J. Clin. Exp. Ophthalmol.* 2, 167. doi: 10.4172/2155-9570.1000167

Porciatti, V. (2015). Electrophysiological assessment of retinal ganglion cell function. *Exp. Eye Res.* 141, 164–170. doi: 10.1016/j.exer.2015.05.008

Rohowetz, L. J., Kraus, J. G., and Koulen, P. (2018). Reactive oxygen species-mediated damage of retinal neurons: drug development targets for therapies of chronic neurodegeneration of the retina. *Int. J. Mol. Sci.* 19, 3362. doi: 10.3390/ijms19113362

Saeedi, O., Boland, M. V., D'Acunto, L., Swamy, R., Hegde, V., Gupta, S., et al. (2021). Development and comparison of machine learning algorithms to determine visual field progression. *Transl. Vis. Sci. Technol.* 10, 27–27. doi: 10.1167/tvst.10.7.27

Saeys, Y., Inza, I., and Larranaga, P. (2007). A review of feature selection techniques in bioinformatics. *Bioinformatics* 23, 2507–2517. doi: 10.1093/bioinformatics/btm344

Sarossy, M., Kumar, D., and Wu, Z. (2021). "Relationship between glaucoma and complexity measures of the electroretinogram," in *2021 Seventh International conference on Bio Signals, Images, and Instrumentation (ICBSII)* (Chennai, India: IEEE), 1–4. doi: 10.1109/ICBSII51839.2021.9445121

Saszik, S. M., Robson, J. G., and Frishman, L. J. (2002). The scotopic threshold response of the dark-adapted electroretinogram of the mouse. *J. Physiol.* 543, 899–916. doi: 10.1113/jphysiol.2002.019703

Saxe, A., Nelli, S., and Summerfield, C. (2021). If deep learning is the answer, what is the question? *Nat. Rev. Neurosci.* 22, 55–67. doi: 10.1038/s41583-020-00395-8

Seo, H., Badiei Khuzani, M., Vasudevan, V., Huang, C., Ren, H., Xiao, R., et al. (2020). Machine learning techniques for biomedical image segmentation: An overview of technical aspects and introduction to state-of-art applications. *Med. Phys.* 47, e148–e167. doi: 10.1002/mp.13649

Shailaja, K., Seetharamulu, B., and Jabbar, M. (2018). "Machine learning in healthcare: a review," in *2018 Second International Conference on Electronics, Communication and Aerospace Technology (ICECA)* (Coimbatore, India: IEEE), 910–914. doi: 10.1109/ICECA.2018.8474918

Shi, S., Wang, Q., Xu, P., and Chu, X. (2016). "Benchmarking state-of-the-art deep learning software tools," in *2016 7th International Conference on Cloud Computing and Big Data (CCBD)* (Macau, China: IEEE), 99–104. doi: 10.1109/CCBD.2016.029

Sim, D. A., Keane, P. A., Tufail, A., Egan, C. A., Aiello, L. P., and Silva, P. S. (2015). Automated retinal image analysis for diabetic retinopathy in telemedicine. *Curr. Diabetes Rep.* 15, 14. doi: 10.1007/s11892-015-0577-6

Stiefelmeyer, S., Neubauer, A. S., Berninger, T., Arden, G. B., and Rudolph, G. (2004). The multifocal pattern electroretinogram in glaucoma. *Vision Res.* 44, 103–112. doi: 10.1016/j.visres.2003.08.012

Takagi, S. T., Kita, Y., Yagi, F., and Tomita, G. (2012). Macular retinal ganglion cell complex damage in the apparently normal visual field of glaucomatous eyes with hemifield defects. *J. Glaucoma* 21, 318–325. doi: 10.1097/IJG.0b013e31820d7e9d

Tang, J., Hui, F., Hadoux, X., Soares, B., Jamieson, M., van Wijngaarden, P., et al. (2020). Short-term changes in the photopic negative response following intraocular pressure lowering in glaucoma. *Investig. Ophthalmol. Visual Sci.* 61, 16–16. doi: 10.1167/iovs.61.10.16

Thienprasiddhi, P., Greenstein, V. C., Chen, C. S., Liebmann, J. M., Ritch, R., and Hood, D. C. (2003). Multifocal visual evoked potential responses in glaucoma patients with unilateral hemifield defects. *Am. J. Ophthalmol.* 136, 34–40. doi: 10.1016/S0002-9394(03)00080-1

Todorova, M. G., and Palmowski-Wolfe, A. M. (2011). MfERG responses to long-duration white stimuli in glaucoma patients. *Document. Ophthalmol.* 122, 87–97. doi: 10.1007/s10633-011-9263-4

Trafalis, T. B., and Ince, H. (2000). "Support vector machine for regression and applications to financial forecasting," in *Proceedings of the IEEE-INNS-ENNS International Joint Conference on Neural Networks. IJCNN 2000* (Como, Italy: IEEE), 348–353. doi: 10.1109/IJCNN.2000.859420

Turalba, A. V., and Grosskreutz, C. (2010). "A review of current technology used in evaluating visual function in glaucoma," in *Seminars in Ophthalmology*, Vol. 25 (Taylor & Francis), 309–316. doi: 10.3109/08820538.2010.518898

Tyler, C. W. (1981). Specific deficits of flicker sensitivity in glaucoma and ocular hypertension. *Investig. Ophthalmol. Visual Sci.* 20, 204–212.

Varma, S., and Simon, R. (2006). Bias in error estimation when using cross-validation for model selection. *BMC Bioinform.* 7, 91. doi: 10.1186/1471-2105-7-91

Ventura, L. M., and Porciatti, V. (2006). Pattern electroretinogram in glaucoma. *Curr. Opin. Ophthalmol.* 17, 196–202. doi: 10.1097/01.icu.0000193082.44938.3c

Verma, S., Nongpiur, M. E., Atalay, E., Wei, X., Husain, R., Goh, D., et al. (2017). Visual field progression in patients with primary angle-closure glaucoma using pointwise linear regression analysis. *Ophthalmology* 124, 1065–1071. doi: 10.1016/j.ophtha.2017.02.027

Wan, X. (2019). Influence of feature scaling on convergence of gradient iterative algorithm. *J. Phys.* 1213, 032021. doi: 10.1088/1742-6596/1213/3/032021

Wilsey, L. J., and Fortune, B. (2016). Electroretinography in glaucoma diagnosis. *Curr. Opin. Ophthalmol.* 27, 118. doi: 10.1097/ICU.0000000000000241

Yadav, S., and Shukla, S. (2016). "Analysis of k-fold cross-validation over hold-out validation on colossal datasets for quality classification," in *2016 IEEE 6th International Conference on Advanced Computing (IACC)* (Bhimavaram, India: IEEE), 78–83. doi: 10.1109/IACC.2016.25

Yapici, İ. S., Erkaymaz, O., and Arslan, R. U. (2021). A hybrid intelligent classifier to estimate obesity levels based on ERG signals. *Phys. Lett. A* 399, 127281. doi: 10.1016/j.physleta.2021.127281

Yoshiyama, K. K., and Johnson, C. A. (1997). Which method of flicker perimetry is most effective for detection of glaucomatous visual field loss? *Investig. Ophthalmol. Visual Sci.* 38, 2270–2277.

Yousefi, S., Goldbaum, M. H., Varnousfaderani, E. S., Belghith, A., Jung, T.-P., Medeiros, F. A., et al. (2015). Detecting glaucomatous change in visual fields: analysis with an optimization framework. *J. Biomed. Inform.* 58, 96–103. doi: 10.1016/j.jbi.2015.09.019

Zhang, M.-L., and Zhou, Z.-H. (2007). ML-KNN: a lazy learning approach to multi-label learning. *Pattern Recogn.* 40, 2038–2048. doi: 10.1016/j.patcog.2006.12.019

Zhang, Y., and Ling, C. (2018). A strategy to apply machine learning to small datasets in materials science. *NPJ Comput. Mater.* 4, 1–8. doi: 10.1038/s41524-018-0081-z

Zhao, Q., and Zhang, L. (2005). "ECG feature extraction and classification using wavelet transform and support vector machines," in *2005 International Conference on Neural Networks and Brain* (Beijing, China: IEEE), 1089–1092.

Zhao, Z., Anand, R., and Wang, M. (2019). "Maximum relevance and minimum redundancy feature selection methods for a marketing machine learning platform," in *2019 IEEE International Conference on Data Science and Advanced Analytics (DSAA)* (Washington, DC: IEEE), 442–452. doi: 10.1109/DSAA.2019.00059

Zhu, H., Poostchi, A., Vernon, S. A., and Crabb, D. P. (2014). Detecting abnormality in optic nerve head images using a feature extraction analysis. *Biomed. Opt. Express* 5, 2215–2230. doi: 10.1364/BOE.5.002215

Author Disclaimer: The content is solely the responsibility of the authors and does not necessarily represent the official views of the National Institutes of Health.

Conflict of Interest: PK, AM, and MG have a patent-pending based on this study.

The remaining author declares that the research was conducted in the absence of any commercial or financial relationships that could be construed as a potential conflict of interest.

Publisher's Note: All claims expressed in this article are solely those of the authors and do not necessarily represent those of their affiliated organizations, or those of the publisher, the editors and the reviewers. Any product that may be evaluated in this article, or claim that may be made by its manufacturer, is not guaranteed or endorsed by the publisher.

frontiers | Frontiers in Neuroscience

REVIEW
published: 04 May 2022
doi: 10.3389/fnins.2022.890021

Molecular Mechanisms Underlying the Therapeutic Role of Vitamin E in Age-Related Macular Degeneration

*Genea Edwards, Caroline G. Olson, Carlyn P. Euritt and Peter Koulen**

Department of Ophthalmology, Vision Research Center, School of Medicine, University of Missouri-Kansas City, Kansas City, MO, United States

The eye is particularly susceptible to oxidative stress and disruption of the delicate balance between oxygen-derived free radicals and antioxidants leading to many degenerative diseases. Attention has been called to all isoforms of vitamin E, with α-tocopherol being the most common form. Though similar in structure, each is diverse in antioxidant activity. Preclinical reports highlight vitamin E's influence on cell physiology and survival through several signaling pathways by activating kinases and transcription factors relevant for uptake, transport, metabolism, and cellular action to promote neuroprotective effects. In the clinical setting, population-based studies on vitamin E supplementation have been inconsistent at times and follow-up studies are needed. Nonetheless, vitamin E's health benefits outweigh the controversies. The goal of this review is to recognize the importance of vitamin E's role in guarding against gradual central vision loss observed in age-related macular degeneration (AMD). The therapeutic role and molecular mechanisms of vitamin E's function in the retina, clinical implications, and possible toxicity are collectively described in the present review.

Keywords: age-related macular degeneration (AMD), antioxidant, retina, tocopherol, tocotrienol, vitamin E

OPEN ACCESS

Edited by:
Yasushi Kitaoka, St. Marianna University School of Medicine, Japan

Reviewed by:
Masaki Tanito, Shimane University, Japan
Ilaria Piano, University of Pisa, Italy

***Correspondence:**
Peter Koulen
koulenp@umkc.edu

Specialty section:
This article was submitted to Neurodegeneration, a section of the journal Frontiers in Neuroscience

Received: *05 March 2022*
Accepted: *21 March 2022*
Published: *04 May 2022*

Citation:
Edwards G, Olson CG, Euritt CP and Koulen P (2022) Molecular Mechanisms Underlying the Therapeutic Role of Vitamin E in Age-Related Macular Degeneration. Front. Neurosci. 16:890021. doi: 10.3389/fnins.2022.890021

INTRODUCTION

Nutrition has a significant influence on ocular health. Certain vitamins may prevent or slow the risk of several eye diseases like age-related macular degeneration (AMD), glaucoma, diabetic retinopathy (DR), and cataracts. Supplementation is oftentimes beneficial and necessary if dietary intake is below recommended guidelines. Compared to other organs of the body, the eye is particularly susceptible to oxidative stress. Finding a balance between free oxygen radicals and antioxidant vitamins E, A, and C may lower the threat of retinopathy. Of the fat-soluble vitamins, vitamin E is a powerful antioxidant occurring organically in foods that protect the body from free radicals that damage cellular processes. Vitamin E exists naturally in eight chemical forms: α (alpha), β (beta), γ (gamma) and δ (delta)-tocopherol and α (alpha), β (beta), γ (gamma) and δ (delta)-tocotrienol. Of all the forms, γ-tocopherol is the most common form found in a Western diet of plant oils, though α-tocopherol [D-α-tocopherol (RRR-α-tocopherol)

configuration] is the most biologically active. Tocopherols are subject to oxidation, hence tocopheryl acetate (DL-α-tocopheryl acetate), tocopheryl succinate (DL-α-tocopheryl succinate), and tocopheryl nicotinate (DL-α-tocopheryl nicotinate)were created for their stability under oxidative conditions by converting the phenol group of the vitamin to an ester while tocopheryl nicotinate is esterified to a niacin (vitamin B3) molecule.

Tocotrienols are the less understood and considerably less widespread form of vitamin E. Tocotrienols differ in their side chains by containing three trans double bonds, making them much more flexible, putting greater stress on phospholipid membranes. They are found in cereal grains like barley, rice, and wheat. Palm oil is a great source of antioxidants that contains a significant amount of tocotrienols. Half of the natural vitamin E family are represented by tocotrienols, yet there are major gaps in the literature regarding the non-α-tocopherol forms. The biological actions of the differing homologs of vitamin E are diverse though they are structurally similar. The unsaturated side chains of tocotrienols appear to allow for more efficient tissue penetration and distribution (Sen et al., 2006). Research into tocotrienols has gained momentum in the last several decades and has changed the trend in research of vitamin E.

The focus of this review is to shed light on the molecular mechanisms involved in vitamin E signaling pathways as a potential therapy for AMD, a progressive and irreversible worsening of central vision, using a search of peer-reviewed articles in the PubMed® database for biomedical literature focusing on the key words of the present review article and covering the literature published prior to submission of the present review article. Current treatments such as anti-angiogenic drugs or laser therapy slow down the progression but there is no cure. Results from population-based studies report no improvement with vitamin E supplementation (Taylor et al., 2002) while others tout the benefits for intermediate or advanced AMD (Lindblad et al., 1999; Chew et al., 2012). A synopsis of important preclinical and clinical studies involving vitamin E's benefit toward preserving vision are presented here with the optimism that it will attract more research attention to its mechanism of action.

THERAPEUTIC ROLE OF VITAMIN E IN RETINAL DISEASE

Since its discovery a century ago (Evans and Bishop, 1922; Evans, 1925), vitamin E's antioxidant, anti-inflammatory, and anti-apoptotic properties have made it a therapeutic option for neurodegenerative diseases. Its antioxidant properties were discovered in the 1930s from studies directed at animal fats (Olcott and Emerson, 1937). In addition to its ability to delay cellular injury, vitamin E also regulates inflammatory cytokines and cell-signaling mechanisms. Evidence indicating that the neurodegenerative process is associated with oxidative stress and inflammation has led to the idea that neurological conditions, especially retinal neurodegeneration may be prevented with vitamin E.

Dietary Supplementation

Antioxidants take part in the crucial role of maintaining the health of retinal tissue, as the retina is highly susceptible to oxidative damage and free radicals. It naturally has a high amount of blood supply with extensive oxidative metabolism which can lead to increased amounts of free radical production and lipid peroxidation (Muller, 1992; Winkler et al., 1999). The therapeutic role of vitamin E in retinal disease pathogenesis has been widely explored yet the focus of the data has been on clinical studies in limiting the progression of retinal disease with vitamin E treatment, especially dry AMD. The molecular mechanisms of its therapeutic activity on degenerative retinal diseases like AMD remain lesser-known. Vitamin E's importance, alone or in combination with additional vitamins such as vitamins A and C has been shown to maintain retinal structure and function. The most prevalent form of synthetic vitamin E is tocopheryl acetate, found commonly in supplements, especially widely popular ocular supplements containing the Age-Related Eye Disease Study (AREDS) and AREDS2 formulation which introduced zeaxanthin and lutein into the supplement (Lindblad et al., 1999; Chew et al., 2012). These studies are important clinical trials funded by the National Eye Institute and considered to be the gold standard in promoting eye health. These supplements have been clinically shown to slow the progression of advanced AMD (Snodderly, 1995). Additional intake of lutein, zeaxanthin, and other carotenoids with the reduction in zinc and the absence of beta-carotene from the original AREDS formulation has shown to be beneficial alongside vitamin E (**Table 1**; Cho et al., 2008; Abdel-Aal el et al., 2013; Yang S. F. et al., 2016). A recent comparative study looked at the concentrations of vitamin E in national name brand vitamin supplements recommended for patients at risk for macular degeneration and concluded that levels were slightly higher than the label indicated, but not enough to cause systemic toxicity (Fleissig et al., 2021).

Dietary supplementation with antioxidants can inhibit complications of diabetes due to oxidative stress and abnormal ATPase activity in the retina (Kowluru et al., 1996, 1999, 2001). Retinal blood flow improvement in patients with diabetes as evidenced by diabetes-induced electroretinogram (ERG) and retinal vascular permeability (RVP) abnormalities have been seen with vitamin E supplementation (Kunisaki et al., 1995, 1998; Timothy et al., 2004). Other serious retinal diseases and injuries of importance in which vitamin E has been shown to also provide a protective effect include photic injury, oxidative injury, retinal edema, uveitis-associated macular edema, and glaucomatous damage (Tanito et al., 2002; Ohira et al., 2003; Aydemir et al., 2004a,b; Nussenblatt et al., 2006; Engin et al., 2007; Zapata et al., 2008).

Macular Degeneration and Vitamin E

The highest concentrations of vitamin E are found inside the retinal pigment epithelium (RPE) followed by the outer segments of the photoreceptor cells (Stephens et al., 1988). Photoreceptor cell death (Dunaief et al., 2002), lipofuscin accumulation (Dorey et al., 1989; Finnemann et al., 2002), and

TABLE 1 | Comparison of AMD nutritional supplements.

	Commercially available formulas								
Nutrient	**AREDS***	**AREDS2**	**B&L Preservision AREDS**	**B&L Preservision AREDS2**	**B&L Ocuvite Eye Health**	**Alcon Systane I-Caps AREDS**	**Alcon Systane I-Caps AREDS 2**	**Biosyntrx Eye and Body Complete**	**Eye Science Macular Health Formula**
Vitamin C	400 mg	400 mg	226 mg (ascorbic acid)	250 mg (ascorbic acid)	150 mg (ascorbic acid)	2226 mg (ascorbic acid)	250 mg (ascorbic acid)	251 mg (ascorbic acid and ascorbyl palmitate)	500 mg (ascorbic acid)
Vitamin E	400 IU	400 IU	90 mg (dl-alpha tocopherol acetate)	90 mg (dl-alpha tocopherol acetate)	20 mg (d-alpha tocopherol)	120 IU (dl-alpha tocopheryl acetate)/80 IU (d-alpha -tocopheryl acetate)	200 IU (d-alpha tocopherol acetate)	15 IU (d-alpha tocopheryl succinate and mixed tocopherols), 15 mg mixed tocotrienols	400 IU (d-alpha tocopheryl succinate)
Beta-carotene*	15 mg	–	4296 mcg	–	–	14320 IU	–	1000 IU (retinyl palmitate)	–
Copper (cupric oxide)**	2 mg	2 mg	0.8 mg (cupric oxide)	1 mg (cupric oxide)	1 mg (copper oxide)	0.8 mg (cupric oxide)	1 mg (cupric gluconate)	0.25 mg (copper sebacate)	2 mg (copper gluconate)
Lutein	–	10 mg	–	5 mg (marigold flower extract)	5 mg (marigold flower extract)	–	5 mg	10 mg	10 mg
Zeaxanthin	–	2 mg	–	1 mg (marigold flower extract or paprika fruit extract)	1 mg (marigold flower extract)	–	1 mg	3.13 mg zeaxanthin isomers, 2.13 mg zeaxanthin 3R, 3′R	2 mg
Zinc	80 mg	80 mg	34.8 mg (zinc oxide)	40 mg (zinc oxide)	9 mg (zinc oxide)	34.8 mg (zinc oxide)	12.5 mg (zinc oxide)	12.5 mg (zinc monomethionine)	40 mg (zinc oxide)
Omega-3 fatty acids	–	–	–	–	250 mg (160 mg EPA, 90 mg DHA)	–	–	–	–

**Not recommended for smokers. **Added to avoid zinc-related copper deficiency. Formulas are based on the NEI-funded Age-Related Eye Diseases Studies (AREDS and AREDS2). Supplements that are made from entirely natural sources contain d-alpha-tocopherol. This also is referred to as RRR-alpha-tocopherol. D-alpha-tocopherol is the most bioavailable form of alpha-tocopherol, meaning it's the type that is preferred for use by your body and is better absorbed and utilized than other forms. Dl-alpha-tocopherol is a synthetic form of alpha-tocopherol. This synthetic form of alpha-tocopherol is less bioavailable than the d-alpha-tocopherol and is only half as potent, notes the Oregon State University, Linus Pauling Institute. This form of alpha-tocopherol is frequently found in nutritional supplements and fortified foods. Conversion: 1 mg of alpha-tocopherol is equivalent to 1.49 international units (IU) of the natural form (d-alpha tocopherol) or 2.22 IU of the synthetic form (dl-alpha tocopherol), 1 mg of beta carotene equals 1667 IU.*

metabolic dysfunction of RPE are the main contributing factors in AMD (Brown et al., 2019). Oxidative stress is known to play a part in photoreceptor cell death and overall damage in many retinal diseases including retinitis pigmentosa (RP), diabetic retinopathy (DR), AMD, and glaucoma. Research studies report that macular degeneration developed in monkeys after a diet deficient in vitamin E. Lesions were characterized by large, focal disruption of photoreceptor outer rod segments (Hayes, 1974b). Indication of mitochondrial oxidative stress in RPE linked metabolic dysfunction between photoreceptors and RPE suggesting a possible mechanism for AMD in superoxide dismutase 2 (Sod2)-KO mice (Brown et al., 2019). Photoreceptor outer segment degeneration was reported in rats that were given a diet lacking vitamin E due to enhanced activity of lysosomal enzymes in the RPE (Amemiya, 1981). These studies call attention to the consequences of a diet deficient in vitamin E to guard against oxidative stress induced by lipid peroxidation and suggest vitamin E's role as a treatment strategy in preserving retinal function in AMD.

Scientific literature has also identified an inflammatory role in AMD (Ambati et al., 2013; Kauppinen et al., 2016). Inflammatory cytokines, complement system, macrophage involvement, and more recently, inflammasomes of the innate immune system have been shown to be involved in the pathogenesis of AMD (Liu et al., 2011; Chen and Smith, 2012; Shin and Bayry, 2013; Knickelbein et al., 2015; Yang Y. et al., 2016). Oxidative stress coupled with inflammation performs a role in disease progression to the intermediate state characterized by accumulation of drusen, lipofuscin deposits that build up in the Bruch's membrane. Constituents of drusen such as amyloid-β,7-ketocholesterol, carboxyethylpyrrole protein (CEP)-adducts, and advanced glycation end products (AGE)-adducts may elicit local complement activation (Crabb et al., 2002; Dentchev et al., 2003; Glenn and Stitt, 2009; Rodríguez and Larrayoz, 2010). Of those with early to intermediate AMD, 15–20% will develop into late-stage AMD (Sunness et al., 1997). Evidence of increased levels a marker of inflammation, high-sensitivity C-reactive protein (hsCRP), may predict the risk of macular degeneration. A study from 2013 looked at hsCRP in blood samples of men and women and observed a significantly increased risk of AMD for high versus low hsCRP levels (Mitta et al., 2013). CRP potentially mediates complement activation and may have significant roles in therapeutic intervention in AMD. Activation of complement by CRP was demonstrated with exogenous addition of CRP by the formation of complement component iC3b in A2E-laden RPE cells bathed in normal human serum (Zhou et al., 2009). The fluorophore molecule A2E (N-retinylidene-N-retinylethanolamine) is short for two all-trans-retinal molecules (vitamin A aldehyde) and one ethanolamine molecule (Lamb and Simon, 2004). In Sparrow et al. (2012), they showed that pre-treatment with 100 μM of vitamin E for 24-h suppressed complement activation evident by reduction of iC3b production in mature retinal pigment epithelium-19 (ARPE-19) cells with A2E accumulation (Sparrow et al., 2012).

Tocotrienols have been shown to inhibit angiogenesis, the development of new capillaries from established blood vessel networks (Miyazawa et al., 2008). Excessive and abnormal growth of new blood vessels frequently occurs in neovascular or "wet" AMD. Research performed with human umbilical vein endothelial cells (HUVECs) by Miyazawa et al., 2008 concluded that tocotrienols halted proliferation induced by growth factors, cellular migration, and tube formation. Tocotrienols also displayed suppression of tumor cell-induced angiogenesis in mouse dorsal air sac (DOS) assay, tocopherols did not (Miyazawa et al., 2008). Evidently, the differences in the biological activity of the two forms of vitamin E are not redundant and the different isoforms of vitamin E should be individually considered.

VITAMIN E DEFICIENCY

Our bodies need regular consumption and supply of vitamin E stores. In 2000, the Food and Nutrition Board of the Institute of Medicine recommended a 15 mg typical daily allowance of vitamin E for adults (Medicine, 2000). Vitamin E is lipid soluble, so any deficiencies are likely caused by dietary fat absorption or metabolism.

Symptoms

Deficiency in vitamin E leads to characteristic, irreversible changes in retinal structure and function. Described changes include progressive neurological syndrome, pigmentary retinopathy, cerebellar ataxia, loss of position and vibration sense, pes cavus, scoliosis, and generalized muscle weakness (Hayton et al., 2003). Factors leading to deficiency in vitamin E can include environmental or nutritional influences, genetic entities, iatrogenic, or experimentally induced sources. Mutations found in α-tocopherol transfer protein (α-TTP) lead to ataxia, a decline in the coordination of voluntary muscle movements, with isolated vitamin E deficits (Ouahchi et al., 1995). Vitamin E deficiencies are rare, but cases have been seen in children diagnosed with abetalipoproteinemia and familial hypobetalipoproteinaemia. These syndromes are lipoprotein deficiency disorders causing a large amount of fat to build up in the blood due to a lack of a protein that breaks down the fat molecules (Lloyd, 1973). A very small study of children diagnosed with chronic cholestasis and low blood serum vitamin E and A concentrations all developed abnormal flash ERGs and half had abnormal visual evoked potentials (VEPs; Bishara et al., 1982). Patients with abetalipoproteinemia and severe vitamin E deficiency demonstrated abnormal visual electrophysiology (Bishara et al., 1982). Clinical retinal manifestations include the development of progressive pigmentary retinopathy and subnormal mixed cone-rod ERG amplitudes. Initial treatment with oral vitamins E and A is advised (Alvarez et al., 1983; Chowers et al., 2001). Cystic fibrosis and cholestatic liver disease are also implicated in vitamin E deficiency with ocular findings largely revealing a decrease of the ERG b-wave, abnormalities of eye movement, and retinal degenerative changes (Alvarez et al., 1983).

Retinopathy of Prematurity

Infants, especially premature babies, have an increased susceptibility to oxidative damage due to their exposure to large amounts of free radicals during the birth process as their lungs adapt to their new environment as well as having vitamin

deficiencies (Muller, 1992). This is exacerbated in premature babies with respiratory distress syndrome of the newborn, in which they are administered supportive oxygen in the hospital, causing further free radical formation (Muller, 1992). Premature infants can have vitamin E deficiency which can manifest as hemolytic anemia and impaired coordination. Retinopathy of prematurity (ROP) is often treated with vitamin E supplementation in order to scavenge free radicals created in the hypoxic birth process. In most newborns, vitamin E is derived from breastmilk and reaches normal levels after a few weeks. Vitamin E is easily found in a balanced diet, however, a diet high in processed foods or low in fat can lead to a deficiency in vitamin E. This was studied in lactating women and those with diets high in processed foods had lower vitamin E levels in their breastmilk (Amorim et al., 2021).

Bioavailability

Absorption of vitamin E is controlled by transporters including the multidrug resistance protein 1 (MDR1) and ATP-binding cassette transporter B1 (ABCB1) expressed on the apical surface of enterocytes. Drug interactions can occur at this point in the process as certain medications and herbal supplements including St. John's wort can alter expression of these transporters (Podszun and Frank, 2014). Delivery of vitamin E to its target tissues is a necessary process that involves a number of lipoproteins for transport of vitamin E's hydrophobic characteristics, and binding proteins which allow for transport intracellular and extracellularly (**Table 2**). Although γ-tocopherol is the most abundant isoform, its bioavailability is limited. Studies demonstrated that concentrations of γ-tocopherol, but not α-tocopherol, declined dramatically in plasma and lipoproteins of normal individuals 24-h after ingestion. Moreover, studies in patients post-surgical for gall bladder procedures, revealed secretion of γ-tocopherol in bile is preferential, suggesting the liver distinguishes between α- and γ-tocopherol secretion (Traber and Kayden, 1989). The discrimination of γ- in favor of α-tocopherol is due, in part, to a higher affinity for transfer protein. The mechanism of transport that is specific to α-tocopherol occurs in the liver by a 32 kDa protein, α-tocopherol transfer protein (α-TTP), that facilitates its secretion from hepatocytes to extrahepatic tissues (Thakur et al., 2010). α-TTP was first reported in rat liver by Catignani and Bieri (1977). Originally thought to only be present in the liver, it is now widely accepted to be found in the brain, kidney, lung, and spleen (Hosomi et al., 1998; Copp et al., 1999; Yamaoka et al., 2008; Tamura et al., 2020). Additionally, it has also been found to be localized to human placenta and mouse uterus (Kaempf-Rotzoll et al., 2002, 2003; Rotzoll et al., 2008). Distribution of vitamin E intracellularly has been identified to be controlled by a novel, cytosolic 46-kDa α-tocopherol associated protein (α-TAP), which binds α-tocopherol by chylomicron formation and lipids in the liver (Stocker et al., 1999; Zimmer et al., 2000) and acts as a metabolizing enzyme by increasing the uptake and absorption of vitamin E and hence facilitates an anti-proliferative effect most notably in prostate cancer and as a tumor suppressor in cancer through a non-vitamin E mechanism. The highest amounts of the human homolog hTAP have been found in the liver, brain, prostate, and breast epithelial cells (Upadhyay and Misra, 2009; Tam et al., 2013). α-TTP and α-TAP are expected to be found in the retina since this neural tissue and its circuitry is an extension of the brain and nervous system (London et al., 2013; De Groef and Cordeiro, 2018).

Transport Across Blood Barriers

Transport of vitamins and essential nutrients through the blood-retinal barrier (BRB) is facilitated by membrane permeability and

TABLE 2 | Vitamin E binding and transport proteins.

Vascular transport		
Protein	**Gene**	**Function**
Chylomicron/Apolipoprotein B-48	APOB	transport under normal physiological conditions
High density lipoprotein/Apolipoprotein AI	APOA1	transport under normal physiological conditions
Low density lipoprotein/Apolipoprotein B	APOB	transport under fasting conditions
Very low density lipoprotein/several apolipoproteins	APOB, APOC1, APOC2, APOE	transport under normal physiological conditions
Afamin	AFM	binds hydrophobic molecules and may be involved in the transport of vitamin E across the blood-brain barrier
Intracellular binding proteins		
Protein	**Gene**	**Function**
Alpha-tocopherol transfer protein	TTPA (known as TPP1)	intracellular transport protein
Scavenger receptor class B type 1 (SR-B1)	SCARB1	transfers vitamin E into the cell
ATP-binding cassette transporter A1	ABCA1	excretes vitamin E out of the cell
SEC14-like protein 2 [known as alpha-tocopherol-associated protein (short names: TAP, hTAP), squalene transfer protein, supernatant protein factor (short name: SPF)]	SEC14L2 (synonyms:C22orf6, KIAA1186, KIAA1658)	associates with α-tocopherol by binding hydrophobic molecules for intracellular transport
SEC14-like protein 3 (aka Tocopherol-associated protein 2), SEC14-like protein 4 (aka Tocopherol-associated protein 3)	SEC14L3 (synonym:TAP2), SEC14L4 (synonym:TAP3)	not investigated thoroughly
Saposin B	PSAP	has specific binding site for γ tocopherol

regulation of tight junctions of the retinal capillary endothelial cells (inner BRB), analogous to the blood-brain barrier (BBB; Campbell and Humphries, 2012), and RPE cells (outer BRB). Inward and outward movement of fluid and molecules between blood and retina is restricted by these structures. DR and AMD are directly linked with alterations of the BRB (Cunha-Vaz et al., 2011). To circumvent the BRB, intravitreal injection of steroids and anti-vascular endothelial growth factor (VEGF) treatments have become more widely administered in recent years. Modulation of the inner BRB to enhance systemic therapeutic intervention may lead to better options in controlling retinal diseases (Campbell and Humphries, 2012). Aeschimann et al. (2017) has shown that vitamin E delivery can be effectively transported to tissues protected by an endothelial barrier utilizing HUVECs. α-TTP displays a tendency to aggregate into stable high molecular weight oligomers which then transport α-tocopherol across endothelial barriers but not through epithelial barriers.

Experimentally induced vitamin E deficiency is a way of evaluating the effects of decreased levels of vitamin E found in the retina. Interrelationships of vitamin E and A have been studied and was found that a diet fed to rats lacking in both vitamin E and A accelerated loss of photoreceptor cells but the amount of cell death varied according to the quantity of vitamin A provided in the diet (Robison et al., 1980). Dietary vitamin E must cross the BRB from the circulating blood to be effective in protecting the retina. Lipid transport by high-density lipoprotein (HDL) via scavenger receptor class B type I (SR-BI) in the retina has been identified in the transport process (Tachikawa et al., 2007). Tserentsoodol et al. (2006) showed an internal lipid transport mechanism that involves HDL-like particles and SR-BI proteins are found in retinal pigment epithelium/choriocapillaris (CC) regions, Müller cells, ganglion cells, and as well as primate photoreceptors. Experimental evidence using α-TTP null mice fed a diet deficient in vitamin E leads to a severe deficiency of vitamin E (a rare condition), enhances lipid peroxidation in the retina, and accelerates degenerative changes in the retina with age (Tanito et al., 2007).

Animal Models of Retinal Vitamin E Deficiency

Rodent models of experimental vitamin E deficiency can provide clues to vitamin E's role in disease processes of the retina (Elizabeth Rakoczy et al., 2006). Through disease models, we have learned that vitamin E and A maintain various structures of the retinal tissue, yet in their absence, results in lipofuscin deposits in the RPE and loss of rod nuclei in rats fed a diet lacking vitamin E and A (Robison et al., 1979, 1980). Studies using frog retinal outer rod segments revealed stabilization of membrane fluidity due to α-tocopherol (Moran et al., 1987). Alterations in membrane fluidity, lipid peroxidation, and irreversible loss of long-chain polyunsaturated fatty acids (LC-PUFAs) were also indicated in the rat (Goss-Sampson et al., 1998). Other models of experimentally induced vitamin E deficiency include monkey and bovine, which show similar alterations in loss of structural integrity to rod outer segment membranes (Hayes, 1974a; Farnsworth and Dratz, 1976; Guajardo et al., 1999). The symbiotic relationship between the structures of the outer BRB that include the RPE/Bruch's membrane/choriocapillaris (CC) complex is lost in AMD and suggest vitamin E's transport mechanism is ultimately compromised (Bhutto and Lutty, 2012; Hosoya and Kubo, 2014; Tisi et al., 2021).

MOLECULAR MECHANISMS OF VITAMIN E SIGNALING IN THE RETINA

Vitamin E is known to activate kinases and transcription factors that regulate gene expression (**Figure 1**). Signaling pathways that are associated with the pathophysiology of macular degeneration such as the mitogen-activated protein kinase (MAPK) signaling pathway, which is stimulated by mitogens, hormones, growth factors, cytokines, oxidative stress (Kyosseva, 2016), and the transcription factor, nuclear factor erythroid 2-related factor 2 (Nrf2), regulates genes involved in the oxidative stress response (He et al., 2020). The most widely known signaling pathway associated with the retina and macular degeneration is the vascular endothelial growth factor (VEGF) signaling pathway (Kowanetz and Ferrara, 2006).

Distribution of Vitamin E in Ocular Tissues

Much is still not understood on the signaling mechanism of vitamin E's neuroprotective and cytoprotective effects in the retina. It has been shown that levels of α-tocopherol are higher in the retina than in the vitreous and choroid. These findings correlate with serum levels of α-tocopherol (Bhat, 1986). Results from a comparative study to determine distribution differences in rat eye tissue by administration of a 5 μL eye drop of either tocopherol or tocotrienol concluded that the α-tocotrienol concentration increased in all ocular tissues. Results showed that α-tocopherol did not increase significantly nor did γ-tocopherol and γ-tocotrienol differ significantly. Noteworthy increases in total vitamin E were found in the neural retina, eyecup, and crystalline lens (Tanito et al., 2004).

Role of Vitamin E in Retinal Layers

Photoreceptors and especially the outer rod segments are the most vulnerable to oxidative damage through peroxidation because more than 65% of the membrane fatty acids are poly-unsaturated (Muller, 1992). Scavengers including glutathione peroxidase are upregulated in the photoreceptor outer segments in response to light exposure (Ohira et al., 2003). Levels of α-tocopherol in retinal cytosol also have a positive correlation with the antioxidant ability of vitamin A, suggesting a compounding effect (Guajardo et al., 1999). This part of the retina also sustains phototoxic damage due to intense light exposure over time which can be seen as lipofuscin granules (Muller, 1992; Winkler et al., 1999). Vitamin E can be beneficial to decreasing phototoxic damage because of its ability to decrease lipid peroxidation. Vitamin E deficiency accelerates RPE autofluorescent pigment deposition rates, possibly by

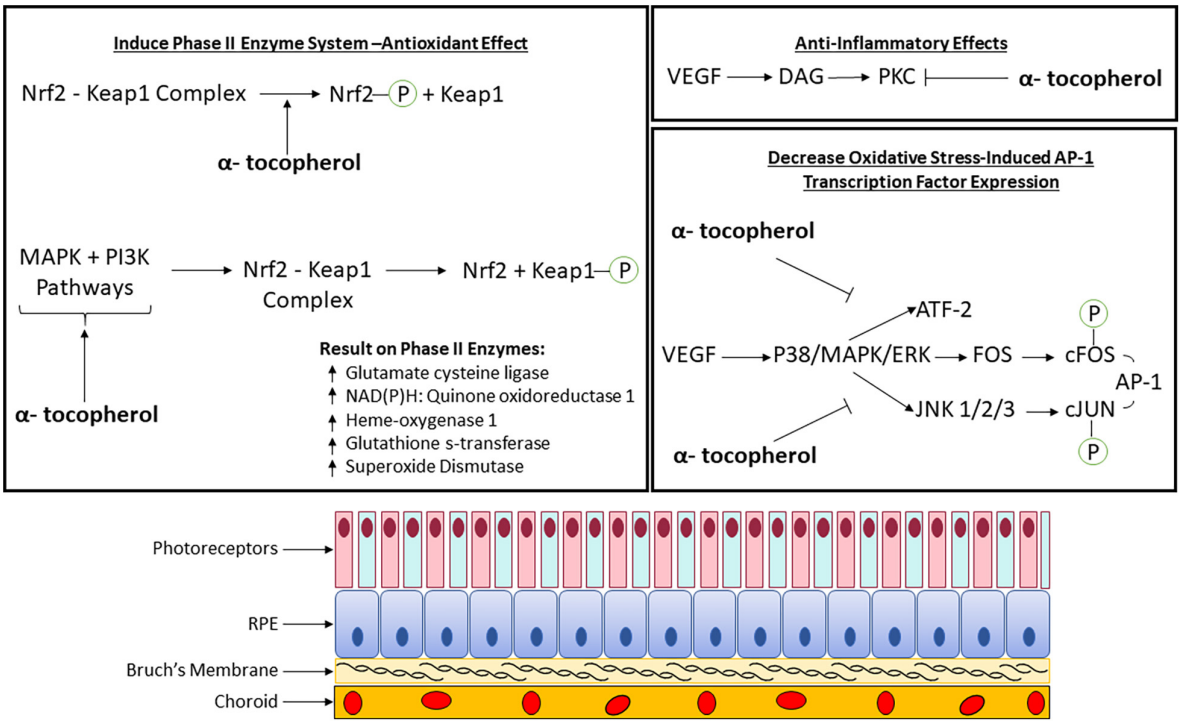

FIGURE 1 | Molecular pathomechanism of vitamin E (α-tocopherol) with phase II enzyme system, anti-inflammatory, and oxidative stress involvement in the retina. AP-1, Activator protein-1; ATF-2, activating transcription factor 2; DAG, diacylglycerol; ERK, extracellular-signal-regulated kinase; FOS, proto-oncogene c-Fos; JNK, c-Jun N-terminal protein kinase; Keap1, kelch-like ECH-associated protein 1; MAPK, mitogen-activated protein kinase; Nrf2, nuclear factor erythroid 2-related factor 2; P, phosphate group; PI3K, phosphoinositide 3-kinase; PKC, protein kinase C; VEGF, vascular endothelial growth factor.

enhancing the conversion of phagocytosed photoreceptor outer segment components into autofluorescent pigment granules (Muller, 1992; Winkler et al., 1999). This is likely a similar mechanism to age-related lipofuscin formation. Both are formed by autooxidation of photoreceptor disk membrane components.

The choroid and CC region can be affected by oxidative damage in AMD so there is potential for vitamin E to ameliorate these effects. As red blood cells pass through the CC region, hemoglobin precursors may undergo photoactivation (Winkler et al., 1999). Activating these precursors may generate reactive oxygen species which can then damage the RPE and Bruch's membrane (Winkler et al., 1999). A deficiency of vitamin E in rats triggered an increase of lipofuscin content in melanocytes and fibroblasts of the choroid (Herrmann et al., 1984). These changes were not seen in the endothelial cells of the CC (Chapy et al., 2015).

Interconnected Signaling Pathways

In addition to vitamin E's oxygen scavenging properties, inhibition of cell growth and protein kinase C (PKC) activity has been observed (Saishin et al., 2003; Xu et al., 2004; Betti et al., 2006; Kim et al., 2010; Titchenell et al., 2012). It has also been shown to alter expression of transcription factors involved in gene expression (Zingg, 2015; He et al., 2020). More research is needed to demonstrate that vitamin E mediates signal transduction involved in macular degeneration pathology (**Figure 1**). A summary of these pathways as determined by published experimental studies is described in the sub-sections below.

Models to Study Vitamin E Signaling

A common experimental model to study AMD and oxidative stress is the use of the ARPE-19 cell line, immortalized human RPE cells, and human telomerase reverse transcriptase (hTERT)-RPE. In Duncan et al., 2022 they demonstrate that α-tocopherol, γ-tocopherol, δ-tocopherol, and α-tocotrienol all exhibited similar, but not identical, antioxidant activity. In addition, exposure time is important for its protective properties against oxidative stress. Synthesis of new proteins was also found to be partially required with α-tocopherol, but not γ-tocopherol, within a 24-h period and before exposure to tertiary butyl hydroperoxide (tBHP) for optimal cytoprotection (Duncan et al., 2022). In another study, ARPE-19 cells were subjected to pre-treatment of ≥2.5 mM α-tocopherol, which significantly decreased oxidative stress-induced activator protein-1 (AP1) transcription factor expression at 14 h but was not further reduced with higher levels of α-tocopherol (Yin et al., 2011). The major AP1 transcription factor family of genes include JUN, FOS, and ATF, which are important regulators of redox, cellular homeostasis, and proliferation that can activate nuclear factor kappa-light-chain-enhancer of activated B cells (NFκB) and MAPK/extracellular-signal-regulated kinase (ERK) signaling

pathways (**Figure 1**). Vitamin E pre-treatment also significantly improved viability in APRE-19 cells exposed to oxidative stress and quenched blue light induced lipofuscin autofluorescent pigment accumulations of A2E-epoxidation causing DNA damage and cell death in macular degeneration etiology, respectively (Sparrow et al., 2003; Kagan et al., 2012). It was also determined α -tocopherol, in combination with either zeaxanthin or lutein, provided better protection to A2E photooxidation than single antioxidant treatment (Kim et al., 2006).

Animal models are crucial for studying the mechanism of AMD pathogenesis and evaluating therapeutic options to prevent or slow disease progression. The features and stages of AMD are not all replicated in non-human primates due to the lack of a macula, but instead, horizontal visual streaks through the retina have similarities to the primate macula (Hughes, 1985). Researchers are still able to tease out valuable information on mechanistic and novel treatments. A table of commonly utilized models is listed in the following reviews (Pennesi et al., 2012; Fletcher et al., 2014). Vitamin E therapeutics can be administered to animals either systemically or topically to assess its effects on disease phenotypes. There is scope for further investigation here as this area is unexplored or currently under exploration during the writing of this review.

Phase II Enzyme Inducer

Vitamin E has been shown experimentally to induce the phase II enzyme system. These enzymes are involved in drug metabolism in the liver and conjugate oxidized intermediates to form hydrophilic products that can be more easily excreted by the body. An upstream promoter regulatory element called the antioxidant-response element (ARE) regulates the expression of these enzymes. The ARE regulator is activated by Nrf2 transcription factors. A study using an acrolein (oxidant) model of AMD in human retinal pigment epithelium cells showed that α-tocopherol has been found to activate the nuclear factor erythroid 2-related factor 2 (Nrf2) pathway (Feng et al., 2010). This is done through cysteine residue oxidative modification within kelch-like ECH-associated protein 1 (Keap1) or phosphorylating Nrf2 (Feng et al., 2010). Activating this pathway upregulates phase II enzymes (Feng et al., 2010). Alternately, the same pathway can be activated by α-tocopherol by activating phosphoinositide 3-kinase (PI3K) and mitogen-activated protein kinase (MAPK) pathways which cause Keap1 phosphorylation (**Figure 1**; Feng et al., 2010). The importance of Nrf2 and upregulation of phase II genes has potential for neuroprotective application in AMD.

MOLECULAR MECHANISMS OF VITAMIN E SIGNALING OUTSIDE OF THE RETINA

Signal transduction pathways are modulated by vitamin E through several mechanisms relevant for its absorption, distribution, metabolism, and molecular functions. These include modulation of a variety of enzymes involved in signal transduction like cyclooxygenase-2 (COX-2), diacylglycerol kinase (DGK), 5-, 12-, and 15-lipoxygenases (LO), protein kinase B (PKB), PKC, protein tyrosine kinases (PTK), phospholipase A2 (PLA2), protein phosphatase 2A (PP2A), and protein tyrosine phosphatase (PTP) (Zingg, 2015, 2019).

Modulation of Vitamin E

It is highly unlikely that one antioxidant is proven to be effective in absence of other members of a supporting team like vitamin C, selenium, vitamin A, CoQ10, and calcium to work efficiently (Golumbic and Mattill, 1941). Calcium plays a significant role in the metabolism of vitamin E. In studies of hepatocytes, calcium was shown to modulate vitamin E metabolism. Decreasing intracellular calcium levels led to a decrease in α-tocopherol levels (Pascoe and Reed, 1987).

Peroxyl Radical-Scavenging System

Vitamin E's antioxidant activity can scavenge reactive oxygen and nitrogen species. This can protect mono-unsaturated fatty acids (MUFAs/PUFAs) and their lipid mediators which are important for cellular functions (Zingg, 2019). The unusually high content of PUFAs in the membrane lipids are susceptible to oxygen damage when vitamin E is low. These fatty acids can play beneficial roles in preventing cancer, insulin resistance, non-alcoholic steatohepatitis (NASH), cardiovascular, and neurodegenerative disease (Zingg, 2019). It has been shown that mixed tocopherols as seen in a typical diet had more effect on several of the observed effects of tocopherol including decreasing lipid peroxidation, attenuating platelet aggregation, and decreasing arterial thrombosis than α-tocopherol alone (Liu et al., 2002). Modulation by vitamin E can also affect the stability and properties of the cell membrane, which can indirectly modulate the signaling properties of proteins in the membrane (Zingg, 2019). The different vitamin E analogs affect cellular signaling differently through signal transduction enzymes and influencing the translocation of receptors to the plasma membrane (Zingg, 2019). Supplementation with vitamin E succinate was shown to increase activity of glutathione reductase and thus increase glutathione concentrations (Rego et al., 1998). In addition, vitamin E has been demonstrated to affect oxidative actions related to stress. Stress-induced increase in lipid peroxidation caused by nitric oxide production is a process that can be decreased by vitamin E (Yargiçoğlu et al., 2003). Choroidal neovascularization, observed in "wet" AMD, is vulnerable to sub-retinal hemorrhages which may induce retinal degeneration by promoting lipid peroxidation from iron released from hemorrhages as oxyhemoglobin (HbO2) or methemoglobin (metHb). When porcine retinal homogenates were incubated with α-tocopherol or docosahexaenoic acid (DHA), a major fatty acid, α-tocopherol was more rapidly decomposed than DHA with metHb versus HbO2. α-tocopherol scavenged hemoglobin-induced lipid peroxyl radicals and was consumed in the process (Ito et al., 1995).

Mitochondrial Dysfunction

Mitochondria are the primary user of oxygen for energy synthesis and reactive oxygen species (ROS) produced there can go to the cytosol, be neutralized by antioxidants, or remain within the

mitochondria and interact with mitochondrial lipids, proteins, and DNA. These interactions can alter mitochondrial function by deactivating enzymes involved in the respiratory chain and citric acid cycle. Mitochondrial dysfunction has been implicated in diseases including aging, dementia, type 2 diabetes, and obesity (Napolitano et al., 2019). As the major antioxidant present in mitochondrial membranes, vitamin E can respond with peroxyl radicals and protect mitochondrial membranes from oxidative stress (Napolitano et al., 2019). This effect can also be seen from studies in allergic asthma. Interleukin-4 (IL-4) and 12/15 lipoxygenase (12/15-LOX) contribute to mitochondrial dysfunction in allergic asthma and can be reduced by vitamin E supplementation (Mabalirajan et al., 2009). The mechanism of IL-4 inhibition is thought to inhibit the binding of NF-κB and transcription factor Sp-1 with binding sites of the IL-4 promoter region (Mabalirajan et al., 2009). Interestingly, administration of vitamin E increased mice longevity by slowing mitochondrial degeneration (Mabalirajan et al., 2009).

Vitamin E Signaling in Systemic Disease

In addition to Vitamin E's antioxidant properties, vitamin E is known to have other beneficial effects in various disease processes including being anti-thrombotic, anti-neoplastic, anti-angiogenic, anti-inflammatory, and on levels of cholesterol (Pearce et al., 1992; Singh et al., 2005; Song and DeBose-Boyd, 2006; Zingg, 2019; Ziegler et al., 2020). Anti-proliferative and apoptotic properties have also been observed through studies examining its inhibitory effects on mouse mammary cells. This effect is thought to be due to its ability to reduce PKC activation and can be extrapolated to modulating general mammary gland development, function, and modification (McIntyre et al., 2000). Anti-neoplastic actions of tocopherol have been described in breast, colon, and prostate cancer cells (Betti et al., 2006). This is thought to be due to a decrease in PKC-α activity and decreased expression of cell cycle-related proteins (Betti et al., 2006). This PKC-α effect can also decrease activation of MAPK/ERK (Betti et al., 2006) and modulate gene expression, including certain proteins that control cell cycle progression, including cyclin D, cyclin E1, p27, and p53 (Betti et al., 2006). γ-tocopherol may have stronger anti-inflammatory and anti-neoplastic effects than α-tocopherol through increased inhibition of COX2 (Betti et al., 2006).

Vitamin E can be anti-inflammatory through inhibition of the PKC pathway (Lloret et al., 2019). It can activate protein phosphatase 2A (PP2A) that deactivates PKC and modulates diacylglycerol kinase (DGK) activity (Lloret et al., 2019). α- and β-tocopherol have different effects on PKC. α- tocopherol has a significant inhibitory effect on PKC in vascular smooth muscle causing arrest of cell growth but β-tocopherol does not (Betti et al., 2006; Lloret et al., 2019). This effect has been studied with regards to Alzheimer's disease, as there is thought to be an oxidative stress and inflammatory component.

Vitamin E is thought to have anti-thrombotic properties and has been studied in myocardial infarction prevention. Separate from its antioxidant properties, α-tocopherol regulates genes and enzyme activity involved in vitamin E uptake and metabolism in addition to regulating lipoprotein uptake and inflammation (Ziegler et al., 2020). A study of patients with myocardial infarction, showed decreased levels of vitamin E in a significant number of patients (Ziegler et al., 2020). Anti-inflammatory properties including decreasing the release of proinflammatory cytokines including interleukin-8 (IL-8) and plasminogen activator inhibitor-1 (PAI-1) as well as decreasing CRP levels have been observed (Singh et al., 2005).

Vascular Endothelial Growth Factor Signaling

Studies indicate vitamin E to have regulatory effects on angiogenesis through the modulation of VEGF (Zingg, 2019). The exact regulatory pathways are unclear, as in some settings vitamin E can activate or inhibit VEGF but it is thought to block effector mechanisms (Nussenblatt et al., 2006). Studies have been done in human microvascular endothelial cells (HMVECs), HUVECs, and cultured endothelial cells with varying effects on VEGF receptors (Zingg, 2019). It has been observed that expectant ewes given vitamin E showed enhanced angiogenesis and formation of the vascular network in the placenta, thought to be due to increased VEGF (Zingg, 2019). On the other hand, in a comparative study, tocotrienols inhibited bovine aortic endothelial cell proliferation and tube formation of which δ-tocotrienol appeared to have the highest activity. δ-tocotrienol reduced VEGF-activated tube formation in HUVECs and halted new blood vessel formation shown by a chorioallantoic membrane assay to assess *in vivo* angiogenesis on the growing chick embryo (Miyazawa et al., 2004).

MOLECULAR MECHANISMS OF VITAMIN E TOXICITY

Toxic amounts of vitamin E do not concentrate in the body as it is metabolized and transported out of the liver through bile and urine. This prevents accumulating α-tocopherol levels and eliminates toxic effects in most healthy individuals. Although rare, there are some circumstances where exogenous vitamin supplementation is not due to diet alone or conditions that prevent excess vitamin E from being eliminated from the body. Ideally, vitamin E supplementation should be kept to a lower dosage.

Hypervitaminosis

As with many vitamins, an excess of vitamin E can cause potential health complications. Many individuals consume vitamin E supplements for its antioxidant or immune-boosting properties. An accumulation of vitamin is a pathological condition known as hypervitaminosis. It may take months for a vitamin to substantially accumulate in the tissues, especially if the body is unable to eliminate it (Kitagawa and Mino, 1989; Handelman et al., 1994). The daily tolerable upper limit dose is 1000 mg (Miller et al., 2005). An upsurge in mortality from all causes has been reported with excessive doses of vitamin E (Miller et al., 2005). Toxic amounts of vitamin E can alter liver and kidney function and cause muscle weakness or bleeding problems (Tsai et al., 1978). In addition, as vitamin E is metabolized in

the liver by cytochrome P450 (CYP) enzyme system, it can interact with many other commonly used medications that share this pathway.

Cardiovascular Disease

The link between high doses of vitamin E and heart failure has been extensively studied in several randomized control trials including most notably the HOPE and HOPE-TOO trials. These trials found greater risk of heart failure related to high doses of vitamin E (≥400 IU/d) (Lonn et al., 2005). The cause for this effect is unclear but has been postulated to be due to disruption of the natural balance of antioxidant systems or reduction of HDL cholesterol (Lonn et al., 2005). This effect was redemonstrated by a similar trial, finding a 50% increase in risk to develop congestive heart failure (CHF) after administration of α-tocopherol (Brigelius-Flohé, 2007). A study examining the effects of megadoses of vitamin E showed an increase in serum triglyceride levels most pronounced in female subjects (Tsai et al., 1978). Heart failure can result in microvascular dysfunction in the retina where dilation responses of both arteriolar and venular retinal microvessels were significantly reduced to a flicker stimulus (Grassi and Mancia, 2018; Nägele et al., 2018). Concern about this effect may limit the usefulness of vitamin E in large doses in patients with extensive cardiovascular risk factors or diabetes, both of which are common in the elderly population where AMD would be seen. On the other hand, Bursell et al. (1999) described in early stages of type I diabetes, high doses of vitamin E controlled retinal blood flow with minimal to no diabetic retinopathy.

Thyroid Homeostasis

Tocopherol has been shown to affect the hypothalamus-pituitary-thyroid axis (Tsai et al., 1978). Prolonged vitamin E deficiency has shown a reduction in function of this system, while large doses of vitamin E have been shown to lower concentrations of thyroid hormone T3 and T4 (Tsai et al., 1978). However, studies with a longer duration have shown that this may be a transitory effect (Tsai et al., 1978). Low thyroid levels can cause hypertriglyceridemia and may contribute to this observed effect (Tsai et al., 1978). Thyroid hormones are known to regulate visual functions in human and mouse studies (Takeda et al., 1994, 1996; Ittermann et al., 2014). Data indicate that cultured human RPE cells are a direct target of thyroid hormones (THs; Duncan et al., 1999). Ma et al. (2014) looked at cone cell viability and whether TH signaling affects retinal degeneration mouse models. TH signaling has been shown to be important for cone visual pigment expression and pattern formation while an overabundance of TH signaling causes cone degeneration (Ng et al., 2010). In contrast, Ma's study discovered when TH signaling was suppressed in rodent cone-rod dystrophy models, preservation of cones was found, a novel approach to macular degeneration therapy (Ma et al., 2014). A link between thyroid hormone, vitamin E, and macular degeneration has not been thoroughly investigated and can only be speculated at this time.

Bleeding Disorders

The most well-known symptom of vitamin E toxicity is bleeding. Vitamin E inhibits vitamin K dependent activation of clotting factors, tissue factor, and inhibits aggregation of platelets with an oxidative stress mediated mechanism (Handelman et al., 1994; Chapy et al., 2015). Intracranial hemorrhagic stroke with higher than recommended doses of vitamin E has been reported (Le et al., 2020). This is especially important to consider in patients using warfarin (a vitamin K antagonist) for anticoagulation. A retrospective cohort study found that serum vitamin E levels could predict bleeding events in patients on warfarin (Chapy et al., 2015).

Drug Interactions

Vitamin E supplementation can also potentially interact with medications such as simvastatin (Zocor) and niacin, chemotherapy and radiotherapy, and anticoagulants and antiplatelet medications (Brown et al., 2001; Cheung et al., 2001; Doyle et al., 2006; Block et al., 2007; Lawenda et al., 2008; Violi et al., 2010; Pastori et al., 2013). Decreased concentrations of mRNA for hepatic organic anion transporting polypeptide 3 (OATP3) transport proteins have been found in rats that were injected with α-tocopherol (Podszun and Frank, 2014). These transport proteins are important for uptake of statin medications into circulation. Several cases have implicated the use of niacin with cystoid macular edema (CME; Millay et al., 1988; Fraunfelder et al., 1995; Callanan et al., 1998; Domanico et al., 2015). The CYP enzyme family can also be affected by vitamin E. These enzymes are responsible for metabolism of xenobiotics and 60% of prescription medications (Brigelius-Flohé, 2007). In rat studies using vitamin E supplementation, a vitamin E deficient diet reduced CYP enzyme concentrations. The mechanism behind this is thought to be vitamin E activation of a nuclear pregnane X receptor (PXR) driven chloramphenicol acetyltransferase (CAT) reporter in HepG2 cells, a human hepatoma cell line that is typically used in drug metabolism and hepatotoxicity studies which can mediate and induce CYP functions (Brigelius-Flohé, 2007). This can decrease the efficacy of common drugs. RRR-α-tocopherol did not alter hepatic mRNA expression of CYP enzymes, however, high doses of all racemic α-tocopherol acetate induced hepatic mRNA expression 3-4x (Podszun and Frank, 2014). At normal doses, vitamin E does not appear to have significant effects on CYP expression. There is evidence to suggest a link between CYP27A1, a broadly expressed mitochondrial sterol 27-hydroxylase, AMD, and cholesterol maintenance in the retinal. Retinal lesions developed in Cyp27a1$^{-/-}$ mice were characterized by cholesterol containing drusen, neovascularization, and activated Müller cells (Omarova et al., 2012). Müller cells are the first to reveal changes in metabolic processes due to retinal stress or disease. Cholesterol buildup is associated with macular degeneration (Sarks et al., 1999; Curcio et al., 2011). It is conceivable that the AREDS formulation containing vitamin E reduces the progression of drusen in AMD, but this is not proven and remains to be seen.

Fetal Health and Birth Defects

Research investigating teratogenic effects triggered by vitamin E on fetal health has been investigated in rat models where no obvious teratogenic effects, survival rate, or size and weight of litters were observed (Martin and Hurley, 1977). In mothers treated daily with 500 mg of vitamin E, results showed a delay

in opening eyelids and other ocular complications, however, nothing statistically significant in comparison to control animals (Martin and Hurley, 1977). It has been shown in several studies that vitamin E protects against birth defects in the presence of nicotine use, sparing malformations, embryonic bone development (Güler et al., 2022), decreased the rate of embryo malformations, and increased size and maturation of streptozotocin-induced diabetic animals (Viana et al., 1996). Folic acid and vitamin E taken together with antiepileptic, antihypertensive, and anti-allergic drugs prevented mortality and teratogenic effects in mice (Wahid et al., 2014). Teratogenicity due to zinc deficiency is not ameliorated by vitamin E, suggesting that fatty acid metabolism may be impeded by zinc causing an increase in the lipid peroxidation rate (Hurley et al., 1983). With this, it cannot be assumed that vitamin E's antioxidant effects are entirely beneficial.

Ocular Drug Delivery to Bypass Systemic Effects

While significant doses of systemic vitamin E have demonstrated a toxic effect (Abdo et al., 1986), there is less pre-clinical evidence to show that accumulations of ocular vitamin E are toxic. Intravitreal injection of high concentrations of an ocular therapeutic allows for the bypass of systemic effects (Peyman et al., 2009). Results from intravitreal injection of vitamin E in rabbits suggest that α-tocopherol in doses of 0.05, 0.10, and 0.20 mL failed to show any toxic effects following injection at 1 week, 1 month, and 3 months (Fallor et al., 1984).

CONCLUSION AND FUTURE RESEARCH

Vitamin E influences cell physiology and survival by several signaling pathways. The molecular mechanisms by which it achieves uptake, transport, metabolism, and cellular action to promote neuroprotective effects in the retina are still being elucidated. Clinical studies suggest that supplements containing vitamin E may benefit individuals with moderate to severe AMD in contrast to only a nominal protective effect in early disease progression. Reducing the risk of AMD vision loss must begin prior to detection. Supplementing our diet with vitamin E, recommended by medical professionals, is beneficial to our health and survival but current literature also warns us against adverse effects. The long-term supplementation of vitamin E to counteract the progressive effects of AMD deserves further pre-clinical research.

AUTHOR CONTRIBUTIONS

PK conceived and designed the review. All authors performed the literature review, wrote, edited, and reviewed the manuscript.

FUNDING

This publication was supported in part by a grant from the National Eye Institute (EY030747) of the National Institutes of Health (PK). The content is solely the responsibility of the authors and does not necessarily represent the official views of the National Institutes of Health. Additional support by the Felix and Carmen Sabates Missouri Endowed Chair in Vision Research and a Challenge Grant from Research to Prevent Blindness is gratefully acknowledged.

ACKNOWLEDGMENTS

Support by the Vision Research Foundation of Kansas City is gratefully acknowledged.

REFERENCES

Abdel-Aal el, S. M., Akhtar, H., Zaheer, K., and Ali, R. (2013). Dietary sources of lutein and zeaxanthin carotenoids and their role in eye health. *Nutrients* 5, 1169–1185. doi: 10.3390/nu5041169

Abdo, K. M., Rao, G., Montgomery, C. A., Dinowitz, M., and Kanagalingam, K. (1986). Thirteen-week toxicity study of d-alpha-tocopheryl acetate (vitamin E) in Fischer 344 rats. *Food Chem. Toxicol.* 24, 1043–1050. doi: 10.1016/0278-6915(86)90287-5

Aeschimann, W., Staats, S., Kammer, S., Olieric, N., Jeckelmann, J. M., Fotiadis, D., et al. (2017). Self-assembled α-Tocopherol Transfer Protein Nanoparticles Promote Vitamin E Delivery Across an Endothelial Barrier. *Sci. Rep.* 7:4970. doi: 10.1038/s41598-017-05148-9

Alvarez, F., Landrieu, P., Laget, P., Lemonnier, F., Odièvre, M., and Alagille, D. (1983). Nervous and ocular disorders in children with cholestasis and vitamin A and E deficiencies. *Hepatology.* 3, 410–414. doi: 10.1002/hep.1840030321

Ambati, J., Atkinson, J. P., and Gelfand, B. D. (2013). Immunology of age-related macular degeneration. *Nat. Rev. Immunol.* 13, 438–451. doi: 10.1038/nri3459

Amemiya, T. (1981). Photoreceptor outer segment and retinal pigment epithelium in vitamin E deficient rats. An electron microscopic and electron histochemical study. *Albrecht Von. Graefes Arch. Klin. Exp. Ophthalmol.* 216, 103–109. doi: 10.1007/BF00414577

Amorim, N. C. M., Silva, A. G. C. L. D., Rebouças, A. S., Bezerra, D. S., Lima, M. S. R., Medeiros, J. F. P., et al. (2021). Dietary share of ultra-processed foods and its association with vitamin E biomarkers in Brazilian lactating women. *Br. J. Nutr.* 2021, 1–8. doi: 10.1017/S0007114521001963

Aydemir, O., Celebi, S., Yilmaz, T., Yekeler, H., and Kükner, A. S. (2004a). Protective effects of vitamin E forms (alpha-tocopherol, gamma-tocopherol and d-alpha-tocopherol polyethylene glycol 1000 succinate) on retinal edema during ischemia-reperfusion injury in the guinea pig retina. *Int. Ophthalmol.* 25, 283–289. doi: 10.1007/s10792-005-2034-z

Aydemir, O., Nazıroğlu, M., Celebi, S., Yılmaz, T., and Kükner, A. S. (2004b). Antioxidant effects of alpha-, gamma- and succinate-tocopherols in guinea pig retina during ischemia-reperfusion injury. *Pathophysiology* 11, 167–171. doi: 10.1016/j.pathophys.2004.08.001

Betti, M., Minelli, A., Canonico, B., Castaldo, P., Magi, S., Aisa, M. C., et al. (2006). Antiproliferative effects of tocopherols (vitamin E) on murine glioma C6 cells: homologue-specific control of PKC/ERK and cyclin signaling. *Free Radic Biol. Med.* 41, 464–472. doi: 10.1016/j.freeradbiomed.2006.04.012

Bhat, R. (1986). Serum, retinal, choroidal vitreal vitamin E concentrations in human infants. *Pediatrics* 78, 866–870. doi: 10.1542/peds.78.5.866

Bhutto, I., and Lutty, G. (2012). Understanding age-related macular degeneration (AMD): relationships between the photoreceptor/retinal pigment epithelium/Bruch's membrane/choriocapillaris complex. *Mol. Aspects Med.* 33, 295–317. doi: 10.1016/j.mam.2012.04.005

Bishara, S., Merin, S., Cooper, M., Azizi, E., Delpre, G., and Deckelbaum, R. J. (1982). Combined vitamin A and E therapy prevents retinal

electrophysiological deterioration in abetalipoproteinaemia. *Br. J. Ophthalmol.* 66, 767–770. doi: 10.1136/bjo.66.12.767

Block, K. I., Koch, A. C., Mead, M. N., Tothy, P. K., Newman, R. A., and Gyllenhaal, C. (2007). Impact of antioxidant supplementation on chemotherapeutic efficacy: a systematic review of the evidence from randomized controlled trials. *Cancer Treat Rev.* 33, 407–418. doi: 10.1016/j.ctrv.2007.01.005

Brigelius-Flohé, R. (2007). Adverse effects of vitamin E by induction of drug metabolism. *Genes Nutr.* 2, 249–256. doi: 10.1007/s12263-007-0055-0

Brown, B. G., Zhao, X. Q., Chait, A., Fisher, L. D., Cheung, M. C., Morse, J. S., et al. (2001). Simvastatin and niacin, antioxidant vitamins, or the combination for the prevention of coronary disease. *N. Engl. J. Med.* 345, 1583–1592. doi: 10.1056/NEJMoa011090

Brown, E. E., DeWeerd, A. J., Ildefonso, C. J., Lewin, A. S., and Ash, J. D. (2019). Mitochondrial oxidative stress in the retinal pigment epithelium (RPE) led to metabolic dysfunction in both the RPE and retinal photoreceptors. *Redox Biol.* 24:101201. doi: 10.1016/j.redox.2019.101201

Bursell, S. E., Clermont, A. C., Aiello, L. P., Aiello, L. M., Schlossman, D. K., Feener, E. P., et al. (1999). High-dose vitamin E supplementation normalizes retinal blood flow and creatinine clearance in patients with type 1 diabetes. *Diabetes Care* 22, 1245–1251. doi: 10.2337/diacare.22.8.1245

Callanan, D., Blodi, B. A., and Martin, D. F. (1998). Macular edema associated with nicotinic acid (niacin). *JAMA* 279:1702. doi: 10.1001/jama.279.21.1702-b

Campbell, M., and Humphries, P. (2012). The blood-retina barrier: tight junctions and barrier modulation. *Adv. Exp. Med. Biol.* 763, 70–84. doi: 10.1007/978-1-4614-4711-5_3

Catignani, G. L., and Bieri, J. G. (1977). Rat liver alpha-tocopherol binding protein. *Biochim Biophys Acta* 497, 349–357. doi: 10.1016/0304-4165(77)90192-1

Chapy, H., André, P., Declèves, X., Scherrmann, J. M., and Cisternino, S. A. (2015). polyspecific drug/proton antiporter mediates diphenhydramine and clonidine transport at the mouse blood-retinal barrier. *Br. J. Pharmacol.* 172, 4714–4725. doi: 10.1111/bph.13246

Chen, J., and Smith, L. E. (2012). Protective inflammasome activation in AMD. *Nat. Med.* 18, 658–660. doi: 10.1038/nm.2761

Cheung, M. C., Zhao, X. Q., Chait, A., Albers, J. J., and Brown, B. G. (2001). Antioxidant supplements block the response of HDL to simvastatin-niacin therapy in patients with coronary artery disease and low HDL. *Arterioscler. Thromb. Vasc. Biol.* 21, 1320–1326. doi: 10.1161/hq0801.095151

Chew, E. Y., Clemons, T., SanGiovanni, J. P., Danis, R., Domalpally, A., et al. (2012). The Age-Related Eye Disease Study 2 (AREDS2): study design and baseline characteristics (AREDS2 report number 1). *Ophthalmology* 119, 2282–2289. doi: 10.1016/j.ophtha.2012.05.027

Cho, E., Hankinson, S. E., Rosner, B., Willett, W. C., and Colditz, G. A. (2008). Prospective study of lutein/zeaxanthin intake and risk of age-related macular degeneration. *Am. J. Clin. Nutr.* 87, 1837–1843. doi: 10.1093/ajcn/87.6.1837

Chowers, I., Banin, E., Merin, S., Cooper, M., and Granot, E. (2001). Long-term assessment of combined vitamin A and E treatment for the prevention of retinal degeneration in abetalipoproteinaemia and hypobetalipoproteinaemia patients. *Eye* 15(Pt 4), 525–530. doi: 10.1038/eye.2001.167

Copp, R. P., Wisniewski, T., Hentati, F., Larnaout, A., Ben Hamida, M., and Kayden, H. J. (1999). Localization of alpha-tocopherol transfer protein in the brains of patients with ataxia with vitamin E deficiency and other oxidative stress related neurodegenerative disorders. *Brain Res.* 822, 80–87. doi: 10.1016/s0006-8993(99)01090-2

Crabb, J. W., Miyagi, M., Gu, X., Shadrach, K., West, K. A., Sakaguchi, H., et al. (2002). Drusen proteome analysis: an approach to the etiology of age-related macular degeneration. *Proc. Natl. Acad. Sci. U S A.* 99, 14682–14687. doi: 10.1073/pnas.222551899

Cunha-Vaz, J., Bernardes, R., and Lobo, C. (2011). Blood-retinal barrier. *Eur. J. Ophthalmol.* 21(Suppl. 6), S3–S9. doi: 10.5301/EJO.2010.6049

Curcio, C. A., Johnson, M., Rudolf, M., and Huang, J. D. (2011). The oil spill in ageing Bruch membrane. *Br. J. Ophthalmol.* 95, 1638–1645. doi: 10.1136/bjophthalmol-2011-300344

De Groef, L., and Cordeiro, M. F. (2018). Is the Eye an Extension of the Brain in Central Nervous System Disease? *J. Ocul. Pharmacol. Ther.* 34, 129–133. doi: 10.1089/jop.2016.0180

Dentchev, T., Milam, A. H., Lee, V. M., Trojanowski, J. Q., and Dunaief, J. L. (2003). Amyloid-beta is found in drusen from some age-related macular degeneration retinas, but not in drusen from normal retinas. *Mol. Vis.* 9, 184–190.

Domanico, D., Verboschi, F., Altimari, S., Zompatori, L., and Vingolo, E. M. (2015). Ocular Effects of Niacin: a Review of the Literature. *Med. Hypothesis Discov. Innov. Ophthalmol.* 4, 64–71.

Dorey, C. K., Wu, G., Ebenstein, D., Garsd, A., and Weiter, J. J. (1989). Cell loss in the aging retina. Relationship to lipofuscin accumulation and macular degeneration. *Invest Ophthalmol. Vis. Sci.* 30, 1691–1699.

Doyle, C., Kushi, L. H., Byers, T., Courneya, K. S., Demark-Wahnefried, W., and Grant, B. (2006). Nutrition, Physical Activity and Cancer Survivorship Advisory Committee; American Cancer Society. Nutrition and physical activity during and after cancer treatment: an American Cancer Society guide for informed choices. *CA Cancer J. Clin.* 56, 323–353. doi: 10.3322/canjclin.56.6.323

Dunaief, J. L., Dentchev, T., Ying, G. S., and Milam, A. H. (2002). The role of apoptosis in age-related macular degeneration. *Arch. Ophthalmol.* 120, 1435–1442. doi: 10.1001/archopht.120.11.1435

Duncan, K. G., Bailey, K. R., Baxter, J. D., and Schwartz, D. M. (1999). The human fetal retinal pigment epithelium: a target tissue for thyroid hormones. *Ophthalmic. Res.* 31, 399–406. doi: 10.1159/000055564

Duncan, R. S., Hurtado, D. T., Hall, C. W., and Koulen, P. (2022). Differential Mechanisms of Action and Efficacy of Vitamin E Components in Antioxidant Cytoprotection of Human Retinal Pigment Epithelium. *Front. Pharmacol.* 12:798938. doi: 10.3389/fphar.2021.798938

Elizabeth Rakoczy, P., Yu, M. J., Nusinowitz, S., Chang, B., and Heckenlively, J. R. (2006). Mouse models of age-related macular degeneration. *Exp. Eye Res.* 82, 741–752. doi: 10.1016/j.exer.2005.10.012

Engin, K. N., Engin, G., Kucuksahin, H., Oncu, M., Engin, G., and Guvener, B. (2007). Clinical evaluation of the neuroprotective effect of alpha-tocopherol against glaucomatous damage. *Eur. J. Ophthalmol.* 17, 528–533. doi: 10.1177/112067210701700408

Evans, H. M. (1925). Invariable Occurrence of Male Sterility with Dietaries Lacking Fat Soluble Vitamine E. *Proc. Natl. Acad. Sci. U S A.* 11, 373–377. doi: 10.1073/pnas.11.7.373

Evans, H. M., and Bishop, K. S. (1922). On the existence of a hitherto unrecognized dietary factor essential for reproduction. *Science* 56, 650–651. doi: 10.1126/science.56.1458.650

Fallor, M. K., Silverman, C. A., and Yoshizumi, M. O. (1984). Ocular toxicity of experimental intravitreal vitamin E. *J. Toxicol.* 3, 337–344. doi: 10.3109/15569528409036286

Farnsworth, C. C., and Dratz, E. A. (1976). Oxidative damage of retinal rod outer segment membranes and the role of vitamin E. *Biochim. Biophys. Acta* 443, 556–570. doi: 10.1016/0005-2736(76)90473-9

Feng, Z., Liu, Z., Li, X., Jia, H., Sun, L., Tian, C., et al. (2010). α-Tocopherol is an effective Phase II enzyme inducer: protective effects on acrolein-induced oxidative stress and mitochondrial dysfunction in human retinal pigment epithelial cells. *J. Nutr. Biochem.* 21, 1222–1231. doi: 10.1016/j.jnutbio.2009.10.010

Finnemann, S. C., Leung, L. W., and Rodriguez-Boulan, E. (2002). The lipofuscin component A2E selectively inhibits phagolysosomal degradation of photoreceptor phospholipid by the retinal pigment epithelium. *Proc. Natl. Acad. Sci. U S A* 99, 3842–3847. doi: 10.1073/pnas.052025899

Fleissig, E., Apenbrinck, E., Zhang, X., and Barr, C. C. (2021). Vitamin Analysis Comparison Study. *Am. J. Ophthalmol.* 222, 202–205. doi: 10.1016/j.ajo.2020.08.028

Fletcher, E. L., Jobling, A. I., Greferath, U., Mills, S. A., Waugh, M., Ho, T., et al. (2014). Studying age-related macular degeneration using animal models. *Optom. Vis. Sci.* 91, 878–886. doi: 10.1097/OPX.0000000000000322

Fraunfelder, F. W., Fraunfelder, F. T., and Illingworth, D. R. (1995). Adverse ocular effects associated with niacin therapy. *Br. J. Ophthalmol.* 79, 54–56. doi: 10.1136/bjo.79.1.54

Glenn, J. V., and Stitt, A. W. (2009). The role of advanced glycation end products in retinal ageing and disease. *Biochim. Biophys. Acta* 1790, 1109–1116. doi: 10.1016/j.bbagen.2009.04.016

Golumbic, C., and Mattill, H. A. (1941). Antioxidants and the autoxidation of fats. XIII. The antioxygenic action of ascorbic acid in association with tocopherols, hydroquinones and related compounds. *J. Am. Chem. Soc.* 63, 1279–1280. doi: 10.1021/ja01850a037

Goss-Sampson, M. A., Kriss, T., and Muller, D. P. (1998). Retinal abnormalities in experimental vitamin E deficiency. *Free Radic Biol. Med.* 25, 457–462. doi: 10.1016/s0891-5849(98)00096-3

Grassi, G., and Mancia, G. (2018). 'Keep an eye' on the heart: retinal microcirculation disarray in congestive heart failure. *Eur Heart J.* 39, 57–59. doi: 10.1093/eurheartj/ehx664

Guajardo, M., Terrasa, A., and Catalá, A. (1999). The effect of alpha tocopherol, all-trans retinol and retinyl palmitate on the non enzymatic lipid peroxidation of rod outer segments. *Mol. Cell Biochem.* 197, 173–178. doi: 10.1023/a:1006926605402

Güler, H., Aycan, K., Yilmaz, S., Nisari, M., Ertekin, T., Özge, A. L., et al. (2022). The Protective Role of Vitamin E Against Teratogenic Effects of Nicotine on Embryonic Bone Development. *Med. Rec.* 4, 7–15.

Handelman, G. J., Epstein, W. L., Peerson, J., Spiegelman, D., Machlin, L. J., and Dratz, E. A. (1994). Human adipose alpha-tocopherol and gamma-tocopherol kinetics during and after 1 y of alpha-tocopherol supplementation. *Am. J. Clin. Nutr.* 59, 1025–1032. doi: 10.1093/ajcn/59.5.1025

Hayes, K. C. (1974b). Retinal degeneration in monkeys induced by deficiencies of vitamin E or A. *Invest Ophthalmol.* 13, 499–510.

Hayes, K. C. (1974a). Pathophysiology of vitamin E deficiency in monkeys. *Am. J. Clin. Nutr.* 27, 1130–1140. doi: 10.1093/ajcn/27.8.1130

Hayton, S. M., Kriss, A., Wade, A., and Muller, D. P. (2003). The effects of different levels of all-rac- and RRR-alpha-tocopheryl acetate (vitamin E) on visual function in rats. *Clin. Neurophysiol.* 114, 2124–2131. doi: 10.1016/s1388-2457(03)00214-1

He, F., Ru, X., and Wen, T. (2020). NRF2, a Transcription Factor for Stress Response and Beyond. *Int. J. Mol. Sci.* 21:4777. doi: 10.3390/ijms21134777

Herrmann, R. K., Robison, W. G. Jr., and Bieri, J. G. (1984). Deficiencies of vitamins E and A in the rat: lipofuscin accumulation in the choroid. *Invest. Ophthalmol. Vis. Sci.* 25, 429–433.

Hosomi, A., Goto, K., Kondo, H., Iwatsubo, T., Yokota, T., Ogawa, M., et al. (1998). Localization of alpha-tocopherol transfer protein in rat brain. *Neurosci. Lett.* 256, 159–162. doi: 10.1016/s0304-3940(98)00785-x

Hosoya, K. I., and Kubo, Y. (2014). "Vitamin Transport Across the Blood–Retinal Barrier: Focus on Vitamins C, E, and Biotin," in *Handbook of nutrition, diet and the eye*, ed. V. R. Preedy (Cambridge, MA: Academic Press), 321–329. doi: 10.1016/b978-0-12-401717-7.00032-0

Hughes, A. (1985). New perspectives in retinal organisation. *Prog. Ret. Res.* 4, 243–313. doi: 10.1016/0278-4327(85)90011-2

Hurley, L. S., Dungan, D. D., Keen, C. L., and Lönnerdal, B. (1983). The effects of vitamin E on zinc deficiency teratogenesis in rats. *J. Nutr.* 113, 1875–1877. doi: 10.1093/jn/113.9.1875

Medicine (2000). *Institute of Medicine (Us) Panel on Dietary Antioxidants and Related Compounds Dietary Reference Intakes for Vitamin C, Vitamin E, Selenium, and Carotenoids*. Washington, DC: National Academies Press.

Ito, T., Nakano, M., Yamamoto, Y., Hiramitsu, T., and Mizuno, Y. (1995). Hemoglobin-induced lipid peroxidation in the retina: a possible mechanism for macular degeneration. *Arch. Biochem. Biophys.* 316, 864–872. doi: 10.1006/abbi.1995.1116

Ittermann, T., Dörr, M., Völzke, H., Tost, F., Lehmphul, I., Köhrle, J., et al. (2014). High serum thyrotropin levels are associated with retinal arteriolar narrowing in the general population. *Thyroid.* 24, 1473–1478. doi: 10.1089/thy.2014.0190

Kaempf-Rotzoll, D. E., Horiguchi, M., Hashiguchi, K., Aoki, J., Tamai, H., Linderkamp, O., et al. (2003). Human placental trophoblast cells express alpha-tocopherol transfer protein. *Placenta.* 24, 439–444. doi: 10.1053/plac.2002.0966

Kaempf-Rotzoll, D. E., Igarashi, K., Aoki, J., Jishage, K., Suzuki, H., Tamai, H., et al. (2002). Alpha-tocopherol transfer protein is specifically localized at the implantation site of pregnant mouse uterus. *Biol. Reprod.* 67, 599–604. doi: 10.1095/biolreprod67.2.599

Kagan, D. B., Liu, H., and Hutnik, C. M. (2012). Efficacy of various antioxidants in the protection of the retinal pigment epithelium from oxidative stress. *Clin. Ophthalmol.* 6, 1471–1476. doi: 10.2147/OPTH.S35139

Kauppinen, A., Paterno, J. J., Blasiak, J., Salminen, A., and Kaarniranta, K. (2016). Inflammation and its role in age-related macular degeneration. *Cell Mol. Life Sci.* 73, 1765–1786. doi: 10.1007/s00018-016-2147-8

Kim, J. H., Kim, J. H., Jun, H. O., Yu, Y. S., and Kim, K. W. (2010). Inhibition of protein kinase C delta attenuates blood-retinal barrier breakdown in diabetic retinopathy. *Am. J. Pathol.* 176, 1517–1524. doi: 10.2353/ajpath.2010.090398

Kim, S. R., Nakanishi, K., Itagaki, Y., and Sparrow, J. R. (2006). Photooxidation of A2-PE, a photoreceptor outer segment fluorophore, and protection by lutein and zeaxanthin. *Exp. Eye Res.* 82, 828–839. doi: 10.1016/j.exer.2005.10.004

Kitagawa, M., and Mino, M. (1989). Effects of elevated d-alpha(RRR)-tocopherol dosage in man. *J. Nutr. Sci. Vitaminol.* 35, 133–142. doi: 10.3177/jnsv.35.133

Knickelbein, J. E., Chan, C. C., Sen, H. N., Ferris, F. L., and Nussenblatt, R. B. (2015). Inflammatory Mechanisms of Age-related Macular Degeneration. *Int. Ophthalmol. Clin.* 55, 63–78. doi: 10.1097/IIO.0000000000000073

Kowanetz, M., and Ferrara, N. (2006). Vascular endothelial growth factor signaling pathways: therapeutic perspective. *Clin. Cancer Res.* 12, 5018–5022. doi: 10.1158/1078-0432.CCR-06-1520

Kowluru, R. A., Engerman, R. L., and Kern, T. S. (1999). Abnormalities of retinal metabolism in diabetes or experimental galactosemia. VI. Comparison of retinal and cerebral cortex metabolism, and effects of antioxidant therapy. *Free Radic Biol. Med.* 26, 371–378. doi: 10.1016/s0891-5849(98)00210-x

Kowluru, R. A., Kern, T. S., Engerman, R. L., and Armstrong, D. (1996). Abnormalities of retinal metabolism in diabetes or experimental galactosemia. III. Effects of antioxidants. *Diabetes* 45, 1233–1237. doi: 10.2337/diab.45.9.1233

Kowluru, R. A., Tang, J., and Kern, T. S. (2001). Abnormalities of retinal metabolism in diabetes and experimental galactosemia. VII. Effect of long-term administration of antioxidants on the development of retinopathy. *Diabetes* 50, 1938–1942. doi: 10.2337/diabetes.50.8.1938

Kunisaki, M., Bursell, S. E., Clermont, A. C., Ishii, H., Ballas, L. M., Jirousek, M. R., et al. (1995). Vitamin E prevents diabetes-induced abnormal retinal blood flow via the diacylglycerol-protein kinase C pathway. *Am. J. Physiol.* 269(2 Pt 1), E239–E246. doi: 10.1152/ajpendo.1995.269.2.E239

Kunisaki, M., Bursell, S. E., Umeda, F., Nawata, H., and King, G. L. (1998). Prevention of diabetes-induced abnormal retinal blood flow by treatment with d-alpha-tocopherol. *Biofactors* 7, 55–67. doi: 10.1002/biof.5520070109

Kyosseva, S. V. (2016). Targeting MAPK Signaling in Age-Related Macular Degeneration. *Ophthalmol. Eye Dis.* 8, 23–30. doi: 10.4137/OED.S32200

Lamb, L. E., and Simon, J. D. (2004). A2E: a component of ocular lipofuscin. *Photochem. Photobiol.* 79, 127–136. doi: 10.1562/0031-86552004079<0127:aacool<2.0.co;2

Lawenda, B. D., Kelly, K. M., Ladas, E. J., Sagar, S. M., Vickers, A., and Blumberg, J. B. (2008). Should supplemental antioxidant administration be avoided during chemotherapy and radiation therapy? *J. Natl. Cancer Inst.* 100, 773–783. doi: 10.1093/jnci/djn148

Le, N. K., Kesayan, T., Chang, J. Y., and Rose, D. Z. (2020). Cryptogenic Intracranial Hemorrhagic Strokes Associated with Hypervitaminosis E and Acutely Elevated α-Tocopherol Levels. *J. Stroke Cerebrovasc. Dis.* 29:104747. doi: 10.1016/j.jstrokecerebrovasdis.2020.104747

Liu, B., Wei, L., Meyerle, C., Tuo, J., Sen, H. N., Li, Z., et al. (2011). Complement component C5a promotes expression of IL-22 and IL-17 from human T cells and its implication in age-related macular degeneration. *J. Transl. Med.* 9, 1–12. doi: 10.1186/1479-5876-9-111

Liu, M., Wallin, R., Wallmon, A., and Saldeen, T. (2002). Mixed tocopherols have a stronger inhibitory effect on lipid peroxidation than alpha-tocopherol alone. *J. Cardiovasc. Pharmacol.* 39, 714–721. doi: 10.1097/00005344-200205000-00012

Lindblad, A. S., Kassoff, A., Kieval, S., Mehu, M., Buehler, J., Eglow, M., et al. (1999). The Age-Related Eye Disease Study (AREDS): design implications AREDS report no. 1. *Control. Clin. Trials* 20, 573–600. doi: 10.1016/s0197-2456(99)00031-8

Lloret, A., Esteve, D., Monllor, P., Cervera-Ferri, A., and Lloret, A. (2019). The Effectiveness of Vitamin E Treatment in Alzheimer's Disease. *Int. J. Mol. Sci.* 20:879. doi: 10.3390/ijms20040879

Lloyd, J. K. (1973). Lipoprotein deficiency disorders. *Clin. Endocrinol. Metab.* 2, 127–147. doi: 10.1016/s0300-595x(73)80030-1

London, A., Benhar, I., and Schwartz, M. (2013). The retina as a window to the brain-from eye research to CNS disorders. *Nat. Rev. Neurol.* 9, 44–53. doi: 10.1038/nrneurol.2012.227

Lonn, E., Bosch, J., Yusuf, S., Sheridan, P., Pogue, J., Arnold, J. M., et al. (2005). HOPE and HOPE-TOO Trial Investigators. Effects of long-term vitamin E supplementation on cardiovascular events and cancer: a randomized controlled trial. *JAMA* 293, 1338–1347. doi: 10.1001/jama.293.11.1338

Ma, H., Thapa, A., Morris, L., Redmond, T. M., Baehr, W., and Ding, X. Q. (2014). Suppressing thyroid hormone signaling preserves cone photoreceptors in mouse models of retinal degeneration. *Proc. Natl. Acad. Sci. U S A.* 111, 3602–3607. doi: 10.1073/pnas.1317041111

Mabalirajan, U., Aich, J., Leishangthem, G. D., Sharma, S. K., Dinda, A. K., and Ghosh, B. (2009). Effects of vitamin E on mitochondrial dysfunction and asthma features in an experimental allergic murine model. *J. Appl. Physiol.* 107, 1285–1292. doi: 10.1152/japplphysiol.00459.2009

Martin, M. M., and Hurley, L. S. (1977). Effect of large amounts of vitamin E during pregnancy and lactation. *Am. J. Clin. Nutr.* 30, 1629–1637. doi: 10.1093/ajcn/30.10.1629

McIntyre, B. S., Briski, K. P., Tirmenstein, M. A., Fariss, M. W., Gapor, A., and Sylvester, P. W. (2000). Antiproliferative and apoptotic effects of tocopherols and tocotrienols on normal mouse mammary epithelial cells. *Lipids* 35, 171–180. doi: 10.1007/BF02664767

Millay, R. H., Klein, M. L., and Illingworth, D. R. (1988). Niacin maculopathy. *Ophthalmology* 95, 930–936. doi: 10.1016/s0161-6420(88)33073-3

Miller, E. R. III, Pastor-Barriuso, R., Dalal, D., Riemersma, R. A., Appel, L. J., and Guallar, E. (2005). Meta-analysis: high-dosage vitamin E supplementation may increase all-cause mortality. *Ann. Intern. Med.* 142, 37–46. doi: 10.7326/0003-4819-142-1-200501040-00110

Mitta, V. P., Christen, W. G., Glynn, R. J., Semba, R. D., Ridker, P. M., Rimm, E. B., et al. (2013). reactive protein and the incidence of macular degeneration: pooled analysis of 5 cohorts. *JAMA Ophthalmol.* 131, 507–513. doi: 10.1001/jamaophthalmol.2013.2303

Miyazawa, T., Shibata, A., Nakagawa, K., and Tsuzuki, T. (2008). Anti-angiogenic function of tocotrienol. *Asia Pac. J. Clin. Nutr.* 17(Suppl. 1), 253–256.

Miyazawa, T., Tsuzuki, T., Nakagawa, K., and Igarashi, M. (2004). Antiangiogenic potency of vitamin E. *Ann. N. Y. Acad. Sci.* 1031, 401–404. doi: 10.1196/annals.1331.057

Moran, J., Salazar, P., and Pasantes-Morales, H. (1987). Effect of tocopherol and taurine on membrane fluidity of retinal rod outer segments. *Exp. Eye Res.* 45, 769–776. doi: 10.1016/s0014-4835(87)80094-5

Muller, D. P. (1992). Vitamin E therapy in retinopathy of prematurity. *Eye* 6(Pt 2), 221–225. doi: 10.1038/eye.1992.43

Nägele, M. P., Barthelmes, J., Ludovici, V., Cantatore, S., von Eckardstein, A., Enseleit, F., et al. (2018). Retinal microvascular dysfunction in heart failure. *Eur. Heart J.* 39, 47–56. doi: 10.1093/eurheartj/ehx565

Napolitano, G., Fasciolo, G., Di Meo, S., and Venditti, P. (2019). Vitamin E Supplementation and Mitochondria in Experimental and Functional Hyperthyroidism: a Mini-Review. *Nutrients* 11:2900. doi: 10.3390/nu11122900

Ng, L., Lyubarsky, A., Nikonov, S. S., Ma, M., Srinivas, M., Kefas, B., et al. (2010). Type 3 deiodinase, a thyroid-hormone-inactivating enzyme, controls survival and maturation of cone photoreceptors. *J. Neurosci.* 30, 3347–3357. doi: 10.1523/JNEUROSCI.5267-09.2010

Nussenblatt, R. B., Kim, J., Thompson, D. J., Davis, M. D., Chew, E., Ferris, F. L., et al. (2006). Vitamin E in the treatment of uveitis-associated macular edema. *Am. J. Ophthalmol.* 141, 193–194. doi: 10.1016/j.ajo.2005.07.036

Ohira, A., Tanito, M., Kaidzu, S., and Kondo, T. (2003). Glutathione peroxidase induced in rat retinas to counteract photic injury. *Invest Ophthalmol. Vis. Sci.* 44, 1230–1236. doi: 10.1167/iovs.02-0191

Olcott, H. S., and Emerson, O. H. (1937). Antioxidants and the autoxidation of fats. IX. The antioxidant properties of the tocopherols. *J. Am. Chem. Soc.* 59, 1008–1009. doi: 10.1021/ja01285a013

Omarova, S., Charvet, C. D., Reem, R. E., Mast, N., Zheng, W., Huang, S., et al. (2012). Abnormal vascularization in mouse retina with dysregulated retinal cholesterol homeostasis. *J. Clin. Invest.* 122, 3012–3023. doi: 10.1172/JCI63816

Ouahchi, K., Arita, M., Kayden, H., Hentati, F., Ben Hamida, M., Sokol, R., et al. (1995). Ataxia with isolated vitamin E deficiency is caused by mutations in the alpha-tocopherol transfer protein. *Nat. Genet.* 9, 141–145. doi: 10.1038/ng0295-141

Pascoe, G. A., and Reed, D. J. (1987). Relationship between cellular calcium and vitamin E metabolism during protection against cell injury. *Arch. Biochem. Biophys.* 253, 287–296. doi: 10.1016/0003-9861(87)90181-0

Pastori, D., Carnevale, R., Cangemi, R., Saliola, M., Nocella, C., Bartimoccia, S., et al. (2013). Vitamin E serum levels and bleeding risk in patients receiving oral anticoagulant therapy: a retrospective cohort study. *J. Am. Heart Assoc.* 2:e000364. doi: 10.1161/JAHA.113.000364

Pearce, B. C., Parker, R. A., Deason, M. E., Qureshi, A. A., and Wright, J. J. (1992). Hypocholesterolemic activity of synthetic and natural tocotrienols. *J. Med. Chem.* 35, 3595–3606. doi: 10.1021/jm00098a002

Pennesi, M. E., Neuringer, M., and Courtney, R. J. (2012). Animal models of age related macular degeneration. *Mol. Aspects Med.* 33, 487–509. doi: 10.1016/j.mam.2012.06.003

Peyman, G. A., Lad, E. M., and Moshfeghi, D. M. (2009). Intravitreal injection of therapeutic agents. *Retina.* 29, 875–912. doi: 10.1097/IAE.0b013e3181a94f01

Podszun, M., and Frank, J. (2014). Vitamin E-drug interactions: molecular basis and clinical relevance. *Nutr. Res. Rev.* 27, 215–231. doi: 10.1017/S0954422414000146

Rego, A. C., Santos, M. S., Proenca, M. T., and Oliveira, C. R. (1998). Influence of vitamin E succinate on retinal cell survival. *Toxicology* 128, 113–124. doi: 10.1016/s0300-483x(98)00054-7

Robison, W. G. Jr., Kuwabara, T., and Bieri, J. G. (1979). Vitamin E deficiency and the retina: photoreceptor and pigment epithelial changes. *Invest. Ophthalmol. Vis. Sci.* 18, 683–690.

Robison, W. G. Jr., Kuwabara, T., and Bieri, J. G. (1980). Deficiencies of vitamins E and A in the rat. Retinal damage and lipofuscin accumulation. *Invest. Ophthalmol. Vis. Sci.* 19, 1030–1037.

Rodríguez, I. R., and Larrayoz, I. M. (2010). Cholesterol oxidation in the retina: implications of 7KCh formation in chronic inflammation and age-related macular degeneration. *J. Lipid. Res.* 51, 2847–2862. doi: 10.1194/jlr.R004820

Rotzoll, D. E., Scherling, R., Etzl, R., Stepan, H., Horn, L. C., and Pöschl, J. M. (2008). Immunohistochemical localization of alpha-tocopherol transfer protein and lipoperoxidation products in human first-trimester and term placenta. *Eur. J. Obstet Gynecol. Reprod. Biol.* 140, 183–191. doi: 10.1016/j.ejogrb.2008.03.013

Saishin, Y., Saishin, Y., Takahashi, K., Melia, M., Vinores, S. A., and Campochiaro, P. A. (2003). Inhibition of protein kinase C decreases prostaglandin-induced breakdown of the blood-retinal barrier. *J. Cell Physiol.* 195, 210–219. doi: 10.1002/jcp.10238

Sarks, S. H., Arnold, J. J., Killingsworth, M. C., and Sarks, J. P. (1999). Early drusen formation in the normal and aging eye and their relation to age related maculopathy: a clinicopathological study. *Br. J. Ophthalmol.* 83, 358–368. doi: 10.1136/bjo.83.3.358

Sen, C. K., Khanna, S., and Roy, S. (2006). Tocotrienols: vitamin E beyond tocopherols. *Life Sci.* 78, 2088–2098. doi: 10.1016/j.lfs.2005.12.001

Shin, J. I., and Bayry, J. A. (2013). role for IL-17 in age-related macular degeneration. *Nat. Rev. Immunol.* 13:701. doi: 10.1038/nri3459-c1

Singh, U., Devaraj, S., and Jialal, I. (2005). Vitamin E, oxidative stress, and inflammation. *Annu. Rev. Nutr.* 25, 151–174. doi: 10.1146/annurev.nutr.24.012003.132446

Snodderly, D. M. (1995). Evidence for protection against age-related macular degeneration by carotenoids and antioxidant vitamins. *Am. J. Clin. Nutr.* 62(6 Suppl.), 1448S–1461S. doi: 10.1093/ajcn/62.6.1448S

Song, B. L., and DeBose-Boyd, R. A. (2006). Insig-dependent ubiquitination and degradation of 3-hydroxy-3-methylglutaryl coenzyme a reductase stimulated by delta- and gamma-tocotrienols. *J. Biol. Chem.* 281, 25054–25061. doi: 10.1074/jbc.M605575200

Sparrow, J. R., Ueda, K., and Zhou, J. (2012). Complement dysregulation in AMD: RPE-Bruch's membrane-choroid. *Mol. Aspects Med.* 33, 436–445. doi: 10.1016/j.mam.2012.03.007

Sparrow, J. R., Vollmer-Snarr, H. R., Zhou, J., Jang, Y. P., Jockusch, S., Itagaki, Y., et al. (2003). A2E-epoxides damage DNA in retinal pigment epithelial cells. Vitamin E and other antioxidants inhibit A2E-epoxide formation. *J. Biol. Chem.* 278, 18207–18213. doi: 10.1074/jbc.M300457200

Stephens, R. J., Negi, D. S., Short, S. M., van Kuijk, F. J., Dratz, E. A., and Thomas, D. W. (1988). Vitamin E distribution in ocular tissues following long-term dietary depletion and supplementation as determined by microdissection and gas chromatography-mass spectrometry. *Exp. Eye Res.* 47, 237–245. doi: 10.1016/0014-4835(88)90007-3

Stocker, A., Zimmer, S., Spycher, S. E., and Azzi, A. (1999). Identification of a novel cytosolic tocopherol-binding protein: structure, specificity, and tissue distribution. *IUBMB Life* 48, 49–55. doi: 10.1080/713803478

Sunness, J. S., Rubin, G. S., Applegate, C. A., Bressler, N. M., Marsh, M. J., Hawkins, B. S., et al. (1997). Visual function abnormalities and prognosis in eyes with age-related geographic atrophy of the macula and good visual acuity. *Ophthalmology* 104, 1677–1691. doi: 10.1016/s0161-6420(97)30079-7

Tachikawa, M., Okayasu, S., and Hosoya, K. (2007). Functional involvement of scavenger receptor class B, type I, in the uptake of alpha-tocopherol using cultured rat retinal capillary endothelial cells. *Mol. Vis.* 29, 2041–2047.

Takeda, M., Kakegawa, T., and Suzuki, M. (1996). Effect of thyroidectomy on photoreceptor cells in adult rat retina. *Life Sci.* 58, 631–637. doi: 10.1016/0024-3205(95)02331-3

Takeda, M., Onoda, N., and Suzuki, M. (1994). Characterization of thyroid hormone effect on the visual system of the adult rat. *Thyroid* 4, 467–474. doi: 10.1089/thy.1994.4.467

Tam, K. W., Ho, C. T., Lee, W. J., Tu, S. H., Huang, C. S., Chen, C. S., et al. (2013). Alteration of α-tocopherol-associated protein (TAP) expression in human breast epithelial cells during breast cancer development. *Food Chem.* 138, 1015–1021. doi: 10.1016/j.foodchem.2012.09.147

Tamura, T., Otulakowski, G., Post, M., and Kavanagh, B. P. (2020). α-Tocopherol Transfer Protein Enhances α-Tocopherol Protective Effects in Lung A549 Cells. *Am. J. Respir. Cell Mol. Biol.* 62, 810–813. doi: 10.1165/rcmb.2019-0404LE

Tanito, M., Itoh, N., Yoshida, Y., Hayakawa, M., Ohira, A., and Niki, E. (2004). Distribution of tocopherols and tocotrienols to rat ocular tissues after topical ophthalmic administration. *Lipids* 39, 469–474. doi: 10.1007/s11745-004-1252-0

Tanito, M., Masutani, H., Nakamura, H., Ohira, A., and Yodoi, J. (2002). Cytoprotective effect of thioredoxin against retinal photic injury in mice. *Invest. Ophthalmol. Vis. Sci.* 43, 1162–1167.

Tanito, M., Yoshida, Y., Kaidzu, S., Chen, Z. H., Cynshi, O., Jishage, K., et al. (2007). Acceleration of age-related changes in the retina in alpha-tocopherol transfer protein null mice fed a Vitamin E-deficient diet. *Invest. Ophthalmol. Vis. Sci.* 48, 396–404. doi: 10.1167/iovs.06-0872

Taylor, H. R., Tikellis, G., Robman, L. D., McCarty, C. A., and McNeil, J. J. (2002). Vitamin E supplementation and macular degeneration: randomised controlled trial. *BMJ* 325:11. doi: 10.1136/bmj.325.7354.11

Thakur, V., Morley, S., and Manor, D. (2010). Hepatic α-tocopherol transfer protein: ligand-induced protection from proteasomal degradation. *Biochemistry* 49, 9339–9344. doi: 10.1021/bi100960b

Timothy, N. H., Clermont, A. C., Della Vecchia, K. M., King, G. L., Aiello, L. P., and Bursell, S. E. (2004). d—-Tocopherol Reduces Diabetes–Induced Retinal Vascular Leakage and ERG Abnormalities in the Rat. *Investig. Ophthalmol. Vis. Sci.* 45, 1099–1099.

Tisi, A., Feligioni, M., Passacantando, M., Ciancaglini, M., and Maccarone, R. (2021). The Impact of Oxidative Stress on Blood-Retinal Barrier Physiology in Age-Related Macular Degeneration. *Cells* 10:64. doi: 10.3390/cells10010064

Titchenell, P. M., Lin, C. M., Keil, J. M., Sundstrom, J. M., Smith, C. D., and Antonetti, D. A. (2012). Novel atypical PKC inhibitors prevent vascular endothelial growth factor-induced blood-retinal barrier dysfunction. *Biochem. J.* 446, 455–467. doi: 10.1042/BJ20111961

Traber, M. G., and Kayden, H. J. (1989). Preferential incorporation of alpha-tocopherol vs gamma-tocopherol in human lipoproteins. *Am. J. Clin. Nutr.* 49, 517–526. doi: 10.1093/ajcn/49.3.517

Tsai, A. C., Kelley, J. J., Peng, B., and Cook, N. (1978). Study on the effect of megavitamin E supplementation in man. *Am. J. Clin. Nutr.* 31, 831–837. doi: 10.1093/ajcn/31.5.831

Tserentsoodol, N., Gordiyenko, N. V., Pascual, I., Lee, J. W., Fliesler, S. J., and Rodriguez, I. R. (2006). Intraretinal lipid transport is dependent on high density lipoprotein-like particles and class B scavenger receptors. *Mol. Vis.* 12, 1319–1333.

Upadhyay, J., and Misra, K. (2009). Towards the interaction mechanism of tocopherols and tocotrienols (vitamin E) with selected metabolizing enzymes. *Bioinformation* 3, 326–331. doi: 10.6026/97320630003326

Viana, M., Herrera, E., and Bonet, B. (1996). Teratogenic effects of diabetes mellitus in the rat. *Prev. Vit. Diabet.* 39, 1041–1046. doi: 10.1007/BF00400652

Violi, F., Pignatelli, P., and Basili, S. (2010). Nutrition, supplements, and vitamins in platelet function and bleeding. *Circulation* 121, 1033–1044. doi: 10.1161/CIRCULATIONAHA.109.880211

Wahid, S., Khan, R. A., and Feroz, Z. (2014). Reduction in mortality and teratogenicity following simultaneous administration of folic acid and vitamin E with antiepileptic, antihypertensive and anti-allergic drugs. *J. Pharm. Bioallied. Sci.* 6, 185–191. doi: 10.4103/0975-7406.130955

Winkler, B. S., Boulton, M. E., Gottsch, J. D., and Sternberg, P. (1999). Oxidative damage and age-related macular degeneration. *Mol. Vis.* 5:32.

Xu, X., Zhu, Q., Xia, X., Zhang, S., Gu, Q., and Luo, D. (2004). Blood-retinal barrier breakdown induced by activation of protein kinase C via vascular endothelial growth factor in streptozotocin-induced diabetic rats. *Curr. Eye Res.* 28, 251–256. doi: 10.1076/ceyr.28.4.251.27834

Yamaoka, S., Kim, H. S., Ogihara, T., Oue, S., Takitani, K., Yoshida, Y., et al. (2008). Severe Vitamin E deficiency exacerbates acute hyperoxic lung injury associated with increased oxidative stress and inflammation. *Free Radic. Res.* 42, 602–612. doi: 10.1080/10715760802189864

Yang, S. F., Roberts, J. E., Liu, Q. H., Pang, J., and Sarna, T. (2016). Zeaxanthin and Lutein in the Management of Eye Diseases. *J. Ophthalmol.* 2016:4915916. doi: 10.1155/2016/4915916

Yang, Y., Liu, F., Tang, M., Yuan, M., Hu, A., Zhan, Z., et al. (2016). Macrophage polarization in experimental and clinical choroidal neovascularization. *Sci. Rep.* 4:30933. doi: 10.1038/srep30933

Yargiçoğlu, P., Yaraş, N., Ağar, A., Gümüşlü, S., Bilmen, S., and Ozkaya, G. (2003). The effect of vitamin E on stress-induced changes in visual evoked potentials (VEPs) in rats exposed to different experimental stress models. *Acta Ophthalmol. Scand.* 81, 181–187. doi: 10.1034/j.1600-0420.2003.00040.x

Yin, J., Thomas, F., Lang, J. C., and Chaum, E. (2011). Modulation of oxidative stress responses in the human retinal pigment epithelium following treatment with vitamin C. *J. Cell Physiol.* 226, 2025–2032. doi: 10.1002/jcp.22532

Zapata, G. L., Guajardo, M. H., and Terrasa, A. M. (2008). The in vitro protective effect of alpha-tocopherol on oxidative injury in the dog retina. *Vet. J.* 177, 266–272. doi: 10.1016/j.tvjl.2007.04.005

Zhou, J., Kim, S. R., Westlund, B. S., and Sparrow, J. R. (2009). Complement activation by bisretinoid constituents of RPE lipofuscin. *Invest. Ophthalmol. Vis. Sci.* 50, 1392–1399. doi: 10.1167/iovs.08-2868

Ziegler, M., Wallert, M., Lorkowski, S., and Peter, K. (2020). Cardiovascular and Metabolic Protection by Vitamin E: A Matter of Treatment Strategy? *Antioxidants* 9:935. doi: 10.3390/antiox9100935

Zimmer, S., Stocker, A., Sarbolouki, M. N., Spycher, S. E., Sassoon, J., and Azzi, A. (2000). A novel human tocopherol-associated protein: cloning, in vitro expression, and characterization. *J. Biol. Chem.* 275, 25672–25680. doi: 10.1074/jbc.M000851200

Zingg, J. M. (2015). Modulation of Signal Transduction and Gene Expression by Vitamin E via PI3Kγ/PKB and hTAP1/SEC14L2-Mediated Lipid Exchange. *J. Nutr. Sci. Vitaminol.* 61(Suppl.), S76–S77. doi: 10.3177/jnsv.61.S76

Zingg, J. M. (2019). Vitamin E: Regulatory Role on Signal Transduction. *IUBMB Life* 71, 456–478. doi: 10.1002/iub.1986

Conflict of Interest: The authors declare that the research was conducted in the absence of any commercial or financial relationships that could be construed as a potential conflict of interest.

Publisher's Note: All claims expressed in this article are solely those of the authors and do not necessarily represent those of their affiliated organizations, or those of the publisher, the editors and the reviewers. Any product that may be evaluated in this article, or claim that may be made by its manufacturer, is not guaranteed or endorsed by the publisher.

frontiers | Frontiers in Neuroscience

ORIGINAL RESEARCH
published: 05 May 2022
doi: 10.3389/fnins.2022.858049

Neuronal Dysfunction Is Linked to the Famine-Associated Risk of Proliferative Retinopathy in Patients With Type 2 Diabetes

*Olena Fedotkina[1†], Ruchi Jain[2†], Rashmi B. Prasad[2], Andrea Luk[3], Marta García-Ramírez[4], Türküler Özgümüs[1], Liubov Cherviakova[5], Nadiya Khalimon[6], Tetiana Svietleisha[7], Tetiana Buldenko[8], Victor Kravchenko[9], Deepak Jain[2], Allan Vaag[10], Juliana Chan[3], Mykola D. Khalangot[9,11], Cristina Hernández[4], Peter M. Nilsson[2], Rafael Simo[4], Isabella Artner[2] and Valeriya Lyssenko[1,2]**

[1] Department of Clinical Science, Center for Diabetes Research, University of Bergen, Bergen, Norway, [2] Department of Clinical Sciences, Lund University Diabetes Center, Skane University Hospital, Malmö, Sweden, [3] Prince of Wales Hospital, Hong Kong Institute of Diabetes and Obesity, The Chinese University of Hong Kong, Hong Kong, Hong Kong SAR, China, [4] Vall d'Hebron Research Institute and CIBERDEM, Barcelona, Spain, [5] Chernihiv Regional Hospital, Chernihiv, Ukraine, [6] City Hospital No. 2, Chernihiv, Ukraine, [7] City Hospital No. 1, Chernihiv, Ukraine, [8] Department of Health Care of Chernihiv Regional State Administration, Chernihiv, Ukraine, [9] Komisarenko Institute of Endocrinology and Metabolism, Kyiv, Ukraine, [10] Steno Diabetes Center Copenhagen, Copenhagen, Denmark, [11] Shupyk National Healthcare University of Ukraine, Kyiv, Ukraine

Persons with type 2 diabetes born in the regions of famine exposures have disproportionally elevated risk of vision-threatening proliferative diabetic retinopathy (PDR) in adulthood. However, the underlying mechanisms are not known. In the present study, we aimed to investigate the plausible molecular factors underlying progression to PDR. To study the association of genetic variants with PDR under the intrauterine famine exposure, we analyzed single nucleotide polymorphisms (SNPs) that were previously reported to be associated with type 2 diabetes, glucose, and pharmacogenetics. Analyses were performed in the population from northern Ukraine with a history of exposure to the Great Ukrainian Holodomor famine [the Diagnostic Optimization and Treatment of Diabetes and its Complications in the Chernihiv Region (DOLCE study), n = 3,583]. A validation of the top genetic findings was performed in the Hong Kong diabetes registry (HKDR, n = 730) with a history of famine as a consequence of the Japanese invasion during WWII. In DOLCE, the genetic risk for PDR was elevated for the variants in *ADRA2A*, *PCSK*9, and *CYP2C19*2* loci, but reduced at *PROX1* locus. The association of *ADRA2A* loci with the risk of advanced diabetic retinopathy in famine-exposed group was further replicated in HKDR. The exposure of embryonic retinal cells to starvation for glucose, mimicking the perinatal exposure to famine, resulted in sustained increased expression of *Adra2a* and *Pcsk9*, but decreased *Prox1*. The exposure to starvation exhibited a lasting inhibitory effects on neurite outgrowth, as determined by neurite length. In conclusion, a consistent genetic findings on the

OPEN ACCESS

Edited by:
Giovanni Casini,
University of Pisa, Italy

Reviewed by:
Leandro Cabral Zacharias,
University of São Paulo, Brazil
Rosario Amato,
University of Pisa, Italy

***Correspondence:**
Valeriya Lyssenko
Valeriya.Lyssenko@uib.no

[†] These authors have contributed equally to this work

Specialty section:
This article was submitted to Neurodegeneration, a section of the journal Frontiers in Neuroscience

Received: 19 January 2022
Accepted: 28 March 2022
Published: 05 May 2022

Citation:
Fedotkina O, Jain R, Prasad RB, Luk A, García-Ramírez M, Özgümüs T, Cherviakova L, Khalimon N, Svietleisha T, Buldenko T, Kravchenko V, Jain D, Vaag A, Chan J, Khalangot MD, Hernández C, Nilsson PM, Simo R, Artner I and Lyssenko V (2022) Neuronal Dysfunction Is Linked to the Famine-Associated Risk of Proliferative Retinopathy in Patients With Type 2 Diabetes. Front. Neurosci. 16:858049. doi: 10.3389/fnins.2022.858049

famine-linked risk of *ADRA2A* with PDR indicate that the nerves may likely to be responsible for communicating the effects of perinatal exposure to famine on the elevated risk of advanced stages of diabetic retinopathy in adults. These results suggest the possibility of utilizing neuroprotective drugs for the prevention and treatment of PDR.

Keywords: diabetic retinopathy, intrauterine exposure, famine, neuronal function, neurodegeneration

INTRODUCTION

Patients with type 2 diabetes are at high risk of vision-threatening proliferative diabetic retinopathy (PDR) leading to blindness. The diabetic retinopathy (DR) remains a leading cause of the vision loss and preventable blindness in adults aged 20–74 years (Wong et al., 2016). The crude prevalence of the visual impairment and blindness caused by the DR has increased in recent years, mainly due to the increase of type 2 diabetes in low- and middle-income countries (Flaxman et al., 2017). Today, the laser therapy and anti-vascular endothelial growth factor (VEGF) intravitreous injections targeting neovascularization are the most commonly used treatments, despite that the recent clinical and research evidence advocate the important role of a tight cellular interaction between the different compartments of the neurovascular unit in the pathogenesis of PDR (Dodson, 2007; Simó et al., 2014; Simo et al., 2018). However, not all patients can afford and/or respond to these therapies and still effective preventive modalities are far to be optimal because the underlying causal mechanisms are not completely understood. Besides the modifying role of metabolic risk factors in diabetes, it is becoming evident that early life events such as intrauterine nutritional deprivation and stress exposures might contribute to the compromised programming of vasculature during fetal development and thereby increase susceptibility to the micro- and macro-vascular diseases in adults (Kistner et al., 2002; Mitchell et al., 2008; Gopinath et al., 2010). Thus, a perinatal exposure to famine was suggested to contribute to the rapid increase of type 2 diabetes prevalence in China—the current epicenter of the global diabetes epidemic (Zimmet et al., 2017). The Dutch hunger winter (1944–1945), the Chinese (1959–1961), and the Great Ukrainian (1932–1933) famine studies reported the link between the famine exposure at birth and the long-term adverse consequences in adults such as hyperglycemia, obesity, and dyslipidemia, but also cardiovascular disease and kidney dysfunction (Roseboom et al., 2001; Lumey et al., 2015; Zimmet et al., 2017). Our observations in individuals with type 2 diabetes, who experienced perinatal exposure to famine, demonstrated disproportionally elevated risk for PDR as compared to patients with type 2 diabetes that were born unexposed in two populations from Ukraine and Hong Kong (Fedotkina et al., 2021a).

In the present study, we investigated the possible underlying molecular mechanisms of the famine-associated risk of PDR by using genetic markers previously linked to glycemia or drug metabolism in the exposed to famine populations from Ukraine and Hong Kong. The changes in the expression of genes associated with PDR in the exposed to famine population were studied in the experimental primary cell culture model of embryonic retinal cells exposed to starvation for glucose and helped to confirm a molecular link between perinatal exposure to famine and PDR.

MATERIALS AND METHODS

Study Populations

The Diabetes and Its Complications in the Chernihiv Region Study

The Diagnostic Optimization and Treatment of Diabetes and its Complications in the Chernihiv Region (DOLCE) is a population-based study of the patients with diabetes of all ages and their relatives in the Chernihiv region of northern Ukraine. Patients with diabetes and their first-degree relatives (parents, siblings, or children) were invited to participate. The recruitment started in November 2011 and ended in December 2014 (Fedotkina et al., 2021b). With the help of an endocrinologist and diabetes nurse, all participants completed a questionnaire covering their medical history, including the information on the family history of diabetes, anthropometric measurements (weight, height, and blood pressure), alcohol intake, smoking, medication for diabetes, hypertension, and hyperlipidemia. The information on co-morbidities was provided by primary care physicians, using the participants' hospital discharge records as a primary source. Overall, 6,095 patients with diabetes (n = 785 type 1 diabetes, n = 4,297 type 2 diabetes, n = 62 unspecified, n = 951 healthy relatives) were enrolled in the study. The severity of DR was assessed using fundus photography. The PDR outcome was defined as proliferative retinopathy, or laser-treated DR, or blindness. The fasting samples were withdrawn for plasma glucose measurements and HbA1c; plasma and serum samples were stored at –80°C for further determinations of C-peptide, insulin, and lipid levels. All blood measurements were performed at the Department of Clinical Chemistry, Scania University Hospital Diabetes, Malmoe, Sweden (Laboratoriemedicin, 2020). Insulin resistance (HOMA2-IR) and beta-cell function (HOMA-B) were estimated based on C-peptide concentrations calculated using the HOMA calculator (Levy et al., 1998; HOMACalculator, 2021). Fasting blood-ethylenediaminetetraacetic acid (EDTA) samples were taken at the examination and were stored for DNA extraction from all patients with diabetes and their relatives. Genotyping was carried out at the Lund University Diabetes Center (LUDC), Department of Clinical Sciences, Diabetes and Endocrinology (Lund, Sweden). All participants provided a written informed consent. The study was approved by the local

ethics committee (approval number for Ukraine: Dnr17/2011-09-14, for Norway: 2019/28968).

The Hong Kong Diabetes Register: Validation Cohort for Genetic Findings

The Hong Kong Diabetes Registry (HKDR) was established in 1994 at the Diabetes and Endocrine Center, the Prince of Wales Hospital, Hong Kong Special Administrative Region (Luk et al., 2017; Fedotkina et al., 2021a). Patients with physician-diagnosed diabetes who attended the center for a comprehensive evaluation of diabetes complications were consecutively recruited. The referral sources included hospital- and community-based clinics. The detailed information including demographics, co-morbidities, and medication use was documented. The physical measurements, including vital signs and anthropometric parameters, were collected. The presence of diabetic retinopathy was examined by fundus photography and interpreted by trained endocrinologists. To keep the consistency with the previous report (Fedotkina et al., 2021a), advanced diabetic retinopathy was defined by fulfilling one or more of the following: Reduced visual acuity, PDR, pre-PDR, history of laser photocoagulation or presence of laser scar, and history of vitrectomy. Anti-VEGF treatment was not routinely used at the time that patients were recruited; hence it was not considered as advanced diabetic retinopathy. The fasting blood samples were obtained for plasma glucose, HbA1c, lipids, and renal function tests. A written informed consent was obtained from the patients at study enrollment. The HKDR was approved by the New Territories East Cluster Clinical Research Ethics Committee (reference number: 2007.339). The current dataset included 3,021 eligible participants from HKDR, 730 of them with available genetic information, and the selection of individuals was described in **Supplementary Figure 1**. The clinical characteristics of HKDR individuals are presented in **Supplementary Table 1A**. During the WWII period (1941–1945), Hong Kong experienced the famine exposure as a consequence of the Japanese invasion, which lasted for 3 years and 8 months.

Genetics

We performed gene-environment interaction to study the molecular susceptibility of PDR attributed to type 2 diabetes, which is more detrimental in the individuals at risk for type 2 diabetes after intrauterine undernutrition as a consequence of famine exposure (Fedotkina et al., 2021a). We analyzed a panel of 76 SNPs associated with type 2 diabetes, plasma glucose, and pharmacogenetics as a part of previously designed ANDIS panel of genetic loci reproducibly associated with risk of T2D in the 3,583 DOLCE participants (Ahlqvist et al., 2018). In DOLCE, the genotyping was performed using Mass Array iPLEX, and the Illumina Omni express array; genotyping of the individuals in HKDR was described elsewhere (van Zuydam et al., 2018). The schematic overview of genetic analyses flow in the DOLCE cohort was represented on the **Supplementary Figure 2**. Allele frequencies of SNPs used in the final analyses did not differ between groups that had or had not been perinatally exposed to famine, ruling out the contributing effects of at risk alleles to the excessive loss of susceptible individuals ($p > 0.01$) (**Supplementary Table 2**).

In vitro Expression Measurements in Human Retinal Tissue

To rule out the effect of type 2 diabetes *per se* on expression of identified genes in the human retina in the patients without PDR, we obtained and analyzed postmortem retinal tissue from the Blood and Tissue Bank of Vall d'Hebron University Hospital, Barcelona, Spain. The procedure for eye cup donation and for the handling of this biologic material is rigorously regulated by the protocol of donations of the Blood and Tissue Bank of the Catalan Department of Health and was approved by the ethics committee of Vall d'Hebron University Hospital (PR-AG-4/2010). The methods for RNA extraction and reverse-transcription quantitative polymerase chain reaction (RT–qPCR) have been previously reported (Hernández et al., 2016). A total of 10 donors with diabetes and 5 donors without diabetes matched by age and sex were included in the study. One eye cup was harvested to separate neuroretina from retinal pigment epithelium, and samples of both tissues were immediately frozen with liquid nitrogen and stored at -80°C. The tissue samples derived from this eye cup were used for the studies of gene expression in the neuroretina. The time from death to eye enucleation was less than 4 h.

RNA Quality Assessment

The concentration and purity of RNAs were obtained by spectrophotometry in the NanoDrop instrument (Thermo Fisher Scientific), which specifically measure absorbance using small sample volumes. The quality of the samples was validated by the RIN assessment. *RT–PCR*. The PCRs were performed with the cDNA obtained with a High Capacity Kit (Applied Biosystems, Madrid, Spain) with random hexamer primers in a Thermal Cycler 2720 (Applied Biosystems, Madrid, Spain). Also, TaqMan Assays exon–exon boundary (Applied Biosystems, Madrid, Spain) were used for amplification of ADRA2A Hs01099503_s1; CYP2C19 Hs00426380_m1; PCSK9 Hs00545399_m1; PROX_m1; Hs00896293_m1 and β-Actin housekeeping gene assay (Hs01060665_g1) also purchased from Applied Biosystems (Applied Biosystems, Madrid, Spain). The PCR was performed in a 7.900 HT Thermal Cycler Sequence Detection System with 384-well optical plates (Applied Biosystems, Madrid, Spain). Then it was noticed that CYP2C19 Hs00426380_m1 and PCSK9 Hs00545399_m1 measurements (Applied Biosystems, Madrid, Spain) were higher than 35 CTs, and therefore they were not considered for the analysis. The rest of the measurements (<33 CTs) were obtained by calculating relative quantifications (R.Q.) using the Ct method.

In vitro Starvation Experiments of Embryonic Retinal Cells

Ethical Permits

The study was approved by the local ethics committee (2018–579, 2016/891), and the experiments were performed in compliance with the animals in research: reporting *in vivo* experiments (ARRIVE) guidelines (Kilkenny et al., 2010). Given that glucose

is an essential nutrient needed for cell growth and proliferation, we designed *ex vivo* exposure experiments in embryonic retinal cells starved for glucose. The mice retinas were isolated from E18.5 embryos, and retinal cells were starved for glucose in a neurobasal medium for 6 h, followed by culturing in normal glucose medium for 6 days. We investigated the acute effects of starvation and analyzed expression of genes associated with DR using RT–qPCR and measured axonal length 1 day after the end of starvation. The measurements were repeated 6 days after the end of starvation to obtain information on the long-term effects of starvation exposure.

Isolation and Culture of Retinal Cells

First, C57BL/6J mice were purchased from Charles River. The retinas were isolated from E18.5 mouse embryos and digested with 0.05% trypsin (ready-made, Gibco) for 15 min at 37°C. The digestion was terminated by adding Dulbecco's modified Eagle's medium (Gibco) supplemented with 25-mM sodium bicarbonate (Gibco), 25-mM 4-(2-hydroxyethyl)-1-piperazineethanesulfonic acid (HEPES) (Gibco), 10% fetal bovine serum (v/v, Hyclone), and 1% penicillin and streptomycin solution (v/v, Gibco). The cell suspension was filtered through 70-μM filter and centrifuged at 1,300 rpm for 5 min, resuspended in medium, and centrifuged. This was repeated twice and the cells were plated on poly L-lysine coated plates at a density of 2.0×10^6 cell/cm^2. Second, on the next day, the cells were washed 2 times with phosphate-buffered saline (PBS) and starved for glucose in neurobasal medium supplemented with B27 supplement lacking insulin, with 0.06 g/L-glutamine, 1% penicillin–streptomycin (v/v, Gibco), and 11-mM HEPES for 6 h. Finally, the cells were further cultured for 6 days in the complete neurobasal medium.

The RNA Isolation and RT-qPCR

Total RNA was isolated using the miRNeasy micro kit (Qiagen). Reverse transcription was carried out using the RevertAid First Strand cDNA synthesis kit (Thermo Fischer Scientific), following the manufacturer's instructions using 500-ng total RNA. Taqman RT–qPCR system was used for gene expression quantification (ThermoFischer Scientific). The gene expression data were normalized against the expression of hypoxanthine-guanine phosphoribosyltransferase (HPRT). The experiments were repeated for $n = 4–5$, each in duplicate. The data were shown as a mean expression with SEM and were analyzed with Student's *t*-test.

Immunocytochemistry

Cells were fixed with 4% paraformaldehyde for 15 min at room temperature and permeabilized with 0.2% Triton X-100 in PBS for 10 min. The cells were then blocked for 1 h in 5% fetal bovine serum in PBS, and incubated with a primary antibody—rabbit anti-β III tubulin antibody (Covance; 1:1,000, Catalog No. PRB-435P-100), chicken anti-β III tubulin antibody (Abcam; 1:1,000, Catalog No. ab117716), rabbit anti-Pcsk9 antibody (Abcam; 1:100, Catalog No. ab31762), rabbit anti-Adra2a antibody (Sigma-Aldrich; 1:100, Catalog No. A271) and mouse anti-Nestin antibody (Chemicon; 1:500), overnight at 4°C. The next day, the cells were rinsed 3 times with PBS and incubated with a secondary antibody [donkey anti-rabbit IgG Alexa 488 (ThermoFischer Scientific); goat anti-rabbit IgG Alexa 568 (ThermoFischer Scientific) or donkey anti-rabbit IgG Cy5 (Jackson ImmunoResearch)] 1:250 for 1 h at the room temperature. The nuclei were stained with 2 μg/ml Hoechst 33342. The cells were imaged using Zeiss LSM 780 laser scanning microscope (LSM) using either 20 × or 40 × objective.

Image Analysis

Bright-field images of the isolated retinal cells on day 2 were acquired using an Olympus IX73 microscope. The fluorescent images on day 7 were acquired using the LSM (Zeiss LSM 780) using the 20 × objective and ZEN software (Zeiss). Four images of the retinal cultures were acquired per sample, and the neurite extensions were quantified using Fiji with simple neurite tracer plug-in (Longair et al., 2011; Schindelin et al., 2012). The representative bright-field images were also acquired using LSM (Zeiss LSM 780).

Global DNA Methylation

Genome-wide DNA methylation analyses were performed using DNA extracted from peripheral blood lymphocytes (Gentra Autopure, Qiagene) of the DOLCE study participants using the Illumina Infinium 450 Bead Chip with Infinium assay (Illumina iScan) and the standard Infinium HD assay methylation protocol guide (part number 15019519, Illumina). The DNA was quantified using picogreen (DNA assay kit 2000, Invitrogen, Tecan Infinitie); 1-μg DNA was bisulfite-treated using the EZ DNA Methylation^{TM} kit (Zymo Research), following the manufacturer's instructions. The modified DNA was hybridized with the Illumina 450 K beadchips and scanned using Illumina iScan, according to the manufacturer's protocol. The samples were randomly distributed on the arrays. The Infinium HumanMethylation450 BeadChip contains 485 577 probes with 99% coverage of RefSeq genes with the capacity for 12 samples per chip (Bibikova et al., 2011).

The GenomeStudio methylation module software of the Genome studio Genome Browser (NCBI build 37) was used to calculate the raw methylation score for each DNA methylation site, represented as the methylation β-value. The β-values were calculated as follows: β = intensity of the methylated allele (M) ÷ (Intensity of the unmethylated allele (U) + intensity of the methylated allele [(M) + 100]). All samples passed the GenomeStudio quality control steps based on the built-in control probes for staining, hybridization, extension, and specificity, and displayed high-quality bisulfite conversion efficiency with an intensity signal above 4,000 (Bibikova et al., 2011). The probes detected at $p > 0.01$, less than three beads in at least 5% samples per probe, non-CpG probes, single nucleotide polymorphism (SNP)-related probes, multi-hit probes, and allosomal CpG probes were filtered out. Overall, DNA methylation data were obtained for 411,923 probes. The background correction and beta mixture quantile normalization (BMIQ) to normalize the type I and type II probes was implemented using ChAMP (Teschendorff et al., 2012). The singular value decomposition

(SVD) method was used to assess batch effect, and ComBat was implemented to correct multiple batch effects (Johnson et al., 2007; Teschendorff et al., 2009). Since genome-wide methylation analysis was performed using DNA obtained from the whole blood, the methylation status could potentially reflect the combination of blood cell types. Then RefbaseEWAS was hence implemented to correct for changes in the distribution of white blood cells between different subpopulations using DNA methylation signatures in combination with a previously obtained external validation set consisting of signatures from purified leukocyte samples (Houseman et al., 2015). To reduce the heteroscedasticity for highly methylated or unmethylated sites, β-values were converted to *M*-values in the lumi package for further analysis calculated as $M = \log_2[\beta/(1 - \beta)]$ (Du et al., 2008, 2010).

Statistical Analysis

A flowchart for the quality control and preparation of the DOLCE dataset for the statistical analysis is represented in **Supplementary Figure 3**. All subsequent episodes of famine exposure in Ukraine were combined into decades of births before 1950 (exposed to famine) and after 1950 (unexposed) as previously described (Fedotkina et al., 2021b). To study the association of genetic variants and perinatal exposure to famine on the risk of PDR in adulthood, the interaction term between SNPs and famine exposure (year of birth before or after 1950) was fitted using generalized estimation equation using sex, age at visit, diabetes duration, and HbA1c as covariates, and corrected for family relationships (R-package "gee" version 4.13–19; defining families as clusters and correlation structure as exchangeable) (VanderWeele and Knol, 2014; Carey and Ripley, 2019). The association of the genetic variants and the risk of PDR in individuals that had been born perinatally exposed or unexposed to famine was also assessed using effect size heterogeneity Q-statistics and quantified using I^2-value. Bonferroni correction was used to adjust for multiple testing in genetic association tests, $p < 0.05$ was considered statistically significant. The relationship between the risk variants and famine exposure and degree of methylation, quantified as *M*-value, was calculated using linear regression. The relationship between the risk variants and type 2 diabetes was analyzed using logistic regression using sex and age as covariates, *p*-values were adjusted for multiple testing correction using the false discovery rate method. All reported *p*-values are two-sided. All analyses were performed using R software, plink v. 1.07 (Purcell et al., 2007; R Core Team, 2013).

RESULTS

Genetic Variants and the Risk of Proliferative Diabetic Retinopathy in Offspring of Individuals With Perinatal Exposure to Famine

Discovery of Genetic Variants in the Diabetes and Its Complications in the Chernihiv Region Cohort

To gain understanding into the putative biology of the previously reported link between exposure to famine and the risk of PDR (Fedotkina et al., 2021a), we analyzed a panel of type 2 diabetes susceptibility genetic loci in 3,583 patients with type 2 diabetes from the DOLCE study. Among these patients, 1,758 (30% men) individuals had been perinatally exposed to famine, and 1,825 (35% men) were born during modern times and had not been perinatally exposed to famine. Among them, 67 (3.8%) and 41 (2.2%) individuals had PDR, respectively. The clinical characteristics of the participants in the DOLCE cohort are shown in **Supplementary Table 1B**.

We found four SNPs to be significantly associated with PDR in offspring to famine-exposed individuals in the DOLCE study (**Table 1**). The risk loci linked to increased risk of PDR were glucose-rising genotypes of *ADRA2A* rs10885122 ($OR_{exposed vs. unexposed}$, 95% CI, 3.67, 1.77–7.63 vs. 0.45, 0.28-0.71, $p_{interaction} = 0.003$); genotypes associated with pharmacogenetic response to statin therapy at *PCSK9* rs2479409 (2.27, 1.26–4.06 vs. 0.59, 0.37–0.94, $p_{interaction} = 0.021$); and genotypes associated with reduced function of drug-metabolizing gene *CYP2C19*2* rs4244285 (2.87, 1.23–6.68 vs. 0.48, 0.23–0.99, $p_{interaction} = 0.040$). By contrast, alleles linked to elevated glucose levels at *PROX1* rs340874 showed a reduced risk of PDR (0.54, 0.32–0.89 vs. 1.57, 1.05–2.35, $p_{interaction} = 0.045$) (**Table 1**). However, only rs10885122 on *ADRA2A* remained significant after Bonferroni correction in heterogeneity analysis ($p_{heterogeneity} = 6.0 \times 10^{-5}$). To rule out the potential associations of genotypes with the poor glycemic control of diabetes, heterogeneity analyses were also

TABLE 1 | Genetic variants and the risk of PDR for offspring to parents exposed and unexposed to famine in the DOLCE cohort.

Gene	SNP	Risk allele	RAF	Exposed to famine	Unexposed	Interaction	Effect size heterogeneity	
				OR (90% CI)	OR (90% CI)	*p*	I^2	Qep
ADRA2A	rs10885122	G	0.86	3.67 (1.77–7.63)	0.45 (0.28–0.71)	0.003	94	0.00006*
PCSK9	rs2479409	G	0.35	2.27 (1.26–4.06)	0.59 (0.37–0.94)	0.021	89	0.00313
PROX1	rs340874	C	0.50	0.54 (0.32–0.89)	1.57 (1.05–2.35)	0.045	87	0.00642
*CYP2C19*2*	rs4244285	A	0.13	2.87 (1.23–6.68)	0.48 (0.23–0.99)	0.040	86	0.00826

*All subsequent episodes of exposure to famine were combined covering the period before 1950 (exposed to famine) and after 1950 (unexposed). The odds ratios are obtained from interaction analyses of risk variants (additive model) and famine exposure adjusted for sex, age, and diabetes duration. The influence of genetic variants on the risk of advanced diabetic retinopathy in individuals that had been born exposed or not exposed to famine was verified using odds-ratio heterogeneity Q-statistics and quantified using I^2-value. RAF, risk allele frequency. *Significant after adjustment for the multiple testing using Bonferroni correction ($p < 0.05$).*

TABLE 2 | Genetic variants and the risk of ADVDR for offspring to parents exposed and unexposed to famine in the HKDR cohort.

Gene	SNP	Risk allele	RAF	Exposed to famine		Unexposed		Interaction
				OR (90% CI)	*p*	OR (90% CI)	*p*	*p*
ADRA2A	rs10885122	G	0.94	3.13 (1.12–13.2)	0.0265	0.94 (0.18–17.4)	0.953	0.368
PCSK9	rs2479409	G	0.68	0.91 (0.59–1.42)	0.674	1.48 (0.46–5.37)	0.522	0.455
PROX1	rs340874	C	0.41	0.78 (0.51–1.17)	0.236	1.26 (0.44–3.69)	0.661	0.401
*CYP2C19*2*	rs4244285	A	0.31	0.61 (0.37–0.96)	0.0325	0.51 (0.08–1.71)	0.308	0.814

The odds ratios are obtained from interaction analyses of risk variants (additive model) and famine exposure adjusted for sex, age, and diabetes duration. ADVDR, advanced diabetic retinopathy; RAF, risk allele frequency.

adjusted for the HbA1c level, and the results did not change (**Supplementary Table 3**).

Replication of Genetic Findings in the Hong Kong Diabetes Register Cohort

Replication of the top variants in the HKDR conferred significantly increased risk of *ADRA2A* rs10885122 for advanced diabetic retinopathy in persons with type 2 diabetes who were born during famine, while no risk was observed in unexposed individuals (OR, 95% CI, 3.13, 1.12–13.2, p_{famine} = 0.026 vs. 0.94, 0.18–17.4, $p_{nonfamine}$ = 0.953) (**Table 2**).

Gene Expression in Human Retina of Patients With and Without Diabetes

Notably, expression level of the *ADRA2A* and *PROX1* genes did not significantly differ in the retinas from non-famine type 2 diabetes patients with mild non-proliferative DR and non-diabetic donors (Blood and Tissue Bank of Vall d'Hebron University Hospital) (**Supplementary Table 4**), ruling out the impact of diabetes condition *per se* on expression level of identified genetic variants in the human retina. Together, these results point at presence of hyperglycemia independent molecular mechanisms driving progression to PDR in people who were exposed to famine-related insults at birth.

Exposure of Embryonic Retinal Cells to Starvation and Gene Expression

Establishment and Evaluation of a Primary Cell Culture Model

The priming for future diseases during fetal development most likely includes modulation of gene expression. To study the potential mechanisms by which starvation could influence gene expression, we developed a primary cell culture model of starvation for glucose using mice embryonic retinal cells, since the human and mice retinal transcriptomes have shown remarkable similarity during development (Hoshino et al., 2017). As a proof-of-concept that our primary cell culture model mimics essential pathophysiological events implicated in the development of PDR (Aiello et al., 1994), we evaluated the expression of the pro-angiogenic genes *VegfA* and *Vegfr2* (**Figure 1**). These genes encode vascular endothelial growth factor A and its tyrosine kinase receptor, vascular endothelial growth factor 1R—the well-established pathogenic markers of PDR. We confirmed the upregulation of *VegfA* gene expression in response to glucose deprivation (**Figure 1**). Additionally, we analyzed expression of *Txnip*—a thioredoxin interaction protein ascribed a pathogenic role in diabetes and related complications, whose expression is strongly up-regulated by glucose in normal physiology (Parikh et al., 2007). As anticipated, *Txnip* expression was significantly reduced upon 6-h glucose deprivation (**Supplementary Figure 4B**). These observations confirmed that the primary cell culture model mimicking embryonic retinal cell starvation for glucose exhibit key pathogenic features (elevated VEGF) associated with PDR in humans.

Effects of Short Term (6-h) and Long-Term (6-Days) Starvation for Glucose on Gene Expression

In this model, short-term 6-h exposure to starvation for glucose resulted in the up-regulation of expression of *Adra2a* and *Pcsk9* (**Figures 1A,B**). Further, the expression of *Adra2a* and *Pcsk9* genes continued to be elevated in starved cells cultured in normal glucose medium for 6 days after the end of starvation, while the expression of the *Prox1* gene was significantly reduced in comparison with untreated (control) cells (**Figures 1C,D**).

Effect of Starvation for Glucose on Morphology of Neurons

We also evaluated the effect of starvation on morphology of neurons using our primary cell culture model. We used the axonal length as a proxy for outgrowth capacity, serving as an indirect measurement of the ability of neurons to form extended connections—a hallmark of plasticity and adaptive processes in brain development (Prince, 1998). On average, the length of the longest neurite was 11-μm shorted 1 day after exposure to starvation, while the mean length of starved neurites was not significantly affected (**Supplementary Figure 5**). Long-term effects, nevertheless, revealed 3.7-μm shortening ($p < 0.01$) of the mean axonic length of starved retinal neurons (**Supplementary Figure 5**), suggesting sustained inhibitory effects of starvation on neurite outgrowth (**Figure 2**). Immunohistochemistry revealed that *ADRA2A* was expressed in both the neuron body and the axon, while the expression of *PCSK9* was higher at the plasma membrane of the neurons than at axon (**Figure 3**). Collectively, these observations suggested persistent effects of starvation exposure on the morphological properties of the neurons.

Effects of Risk Variants on Methylation and Gene Expression

Methylation QTLs and Expression QTLs

A potential mechanism affecting changes in gene expression might involve epigenetic modifications of the DNA (Tobi et al., 2018). In a limited subset of DOLCE participants exposed and unexposed to famines (n = 51), we performed genome-wide methylation genotyping for exploratory analyses. Methylome analysis of DNA revealed differential methylation of the *ADRA2A* gene ($p < 0.05$) in famine-exposed compared with unexposed individuals (**Supplementary Table 5A**). To investigate the potential methylome QTL effects of identified SNPs, we performed look up in the publicly available mother-child ALSPAC database, which supported the association of methylome with genetic variants for all four genes (*ADRA2A*, *PCSK9*, *CYP2C19*2*, and *PROX1)* (**Supplementary Table 6**; Golding et al., 2001). Additionally, to investigate expression QTL effects, we performed look-up in the GTEX database, which deposited tissue biobank to study relationship between genetic variants and gene expression in diverse tissues in humans. These analyses showed effects of retinopathy-associated genotypes on increased gene expression for *PCSK9* (rs2479409) in skin fibroblasts, for *CYP2C19*2* (rs4244285) in skin fibroblasts, liver, and stomach, and for *PROX1* (rs340874) in the brain (**Supplementary Table 7**; Consortium, 2015). The genotypes of *ADRA2A* or its proxies were not present in the GTEX database. Although expression of the gene in the retinal cells is not present in the GTEX database, observed eQTL effects emphasize the potential role of the identified genetic variants in the different organs and tissues, and thus plausible in the retina.

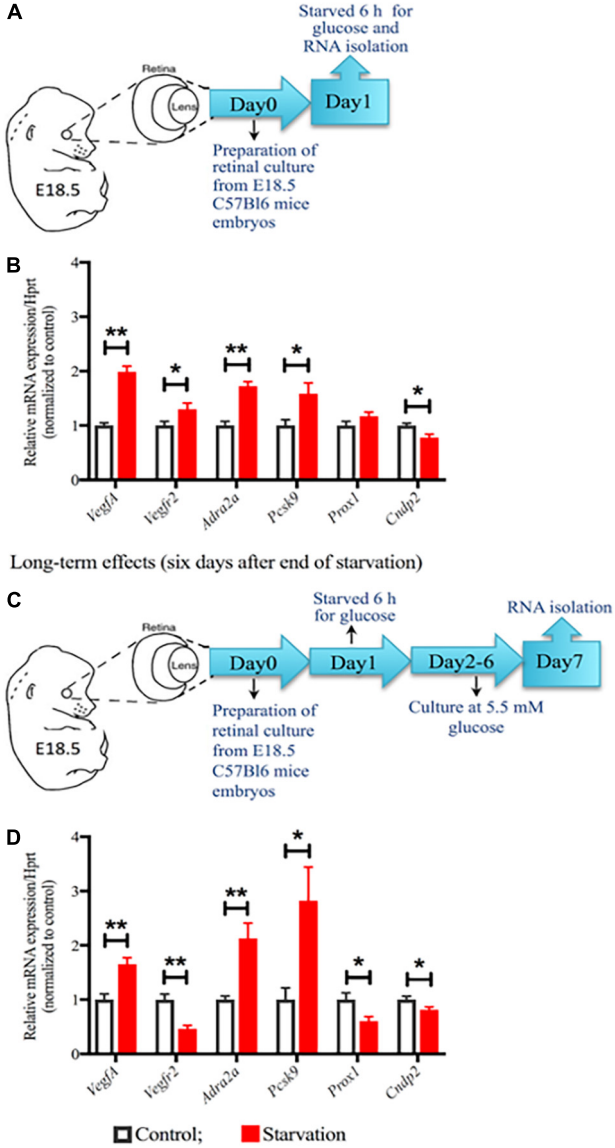

FIGURE 1 | The impact of exposure to starvation for glucose on gene expression in embryonic retinal cells. **(A,C)** Schematic overview of the established and validated *in vitro* model of embryonic retinal cells exposed to glucose starvation to mimic the perinatal exposure to famine. Dissociated retinal cell cultures were prepared from E18.5 mouse embryos and plated on dishes coated with poly-L-lysine (day 0; as described in **Supplementary Methods**). The culture was starved for glucose for 6 h on day 1. RNA was isolated after the end of starvation on day 1 **(A)** or day 7 **(C)**. **(B,D)** Relative mRNA levels on day 1 **(B)** and day 7 **(D)**, determined by RT–qPCR (n = 5–6). Untreated cells were used as controls. $^{**}p < 0.01$, $^{*}p < 0.05$ (two-tailed paired Student's t-test). All values are means + S.E.M.

DISCUSSION

The results of this study highlight the importance of the neuronal dysfunction as a potential early event in the pathogenesis of microcirculatory abnormalities in adult type 2 diabetes patients with PDR whom, as children, were exposed to perinatal famine at birth. In this regard, the genetic and molecular immunohistochemistry findings of embryonic retinal cells support the idea that starvation for glucose insults during early retinogenesis might exhibit a lasting effect and act as triggers of subsequent diabetes-associated changes in the neurovascular unit in adults.

The findings of this study are in line with emerging evidence suggesting that neuroprotection could play a role in the treatment of early stages of DR, although current treatments for DR are mostly addressed to advanced disease (Simo et al., 2018, 2019). The central role for the neurovascular unit in the pathogenesis of DR has been previously discussed, but the exact pathogenic mechanisms are not entirely understood (Abcouwer and Gardner, 2014; Simo et al., 2014). The present study reveals a number of genes with neuronal and vascular functions that might influence risk of adult PDR, with *ADRA2A* being the strongest. The genetic association results from the two independent populations of Ukraine and Hong Kong exposed to famine at birth illuminated the most significant locus rs10885122 resided in the *ADRA2A* gene linked to function of nervous tissues. In the neuronal development of neonatal and adult hippocampus, α2ARA activity has been shown to regulate proliferation and survival of neural precursor cells (Jhaveri et al., 2014). These findings are in line with the

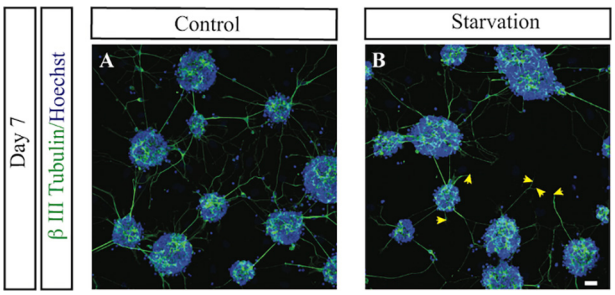

FIGURE 2 | The impact of exposure to starvation for glucose on neurite outgrowth in embryonic retinal cells. Representative confocal LSM images of untreated (control) **(A)** and starved primary retinal cells **(B)** on day 7 of the experiment described in this figure, showing neurons (β III tubulin) and cell nuclei (Hoechst). The images are representative of 3–4 replicates. Scale bar, 20 μm. *n* = 3–4. Arrows indicate loss of neurite outgrowth.

reported neuroprotective effects of α2ARA agonist on Müller cells function after injury and also inhibition of apoptosis of the retinal ganglion cells (Nizari et al., 2016; Harun-Or-Rashid and Hallböök, 2018). This indicated the important role of neurons in the starvation-associated mechanisms linked to diabetic retinopathy and informed the ensuing experiments in the animal model. In this study, a significant and stable up-regulation of *Adra2a* expression was observed in the primary cell culture of embryonic retinal cells after starvation for glucose. Further, differential DNA methylation of *ADRA2A* upstream of SNP rs10885122 observed almost 70 years after perinatal exposure to famine could partly explain the long-lasting effects of famine on gene expression. It might be important to comment that we detected increased *ADRA2A* methylation in famine-exposed individuals, which could be referred as linked with transcriptional repression. However, there are plenty of examples of other forms of gene regulation as a function of CpG modulation, including transcriptional activation, which depends on the site and gene locus (Tirado-Magallanes et al., 2017). The results from this study support the previous observations and may pave the way for targeting α2ARA in the retina for the treatment of DR (Simo et al., 2019).

One possible mechanism by which early life exposure may exert programming effects on the risk of neuronal dysfunction later in life can involve impaired function of the stem cell progenitors (Dyer et al., 2003). In line with this, we found that the type 2 diabetes risk variant in the neuronal progenitor *PROX1* gene was associated with decreased risk of severe DR in offspring of individuals exposed to famine, while this variant increased the PDR risk in the unexposed group. The associations of *PROX1* variant showed same directionality of the effects in famine-exposed group from HKDR, even though did not reach statistical significance. Although our methylation studies might be underpowered to detect *PROX1* mQTL effects, in the publically available ALSPAC cohort, the risk variant in *PROX1* was associated with increased methylation as well as increased methylation of *PROX1* was seen in type 2 diabetes individuals as compared to healthy controls. Expression of

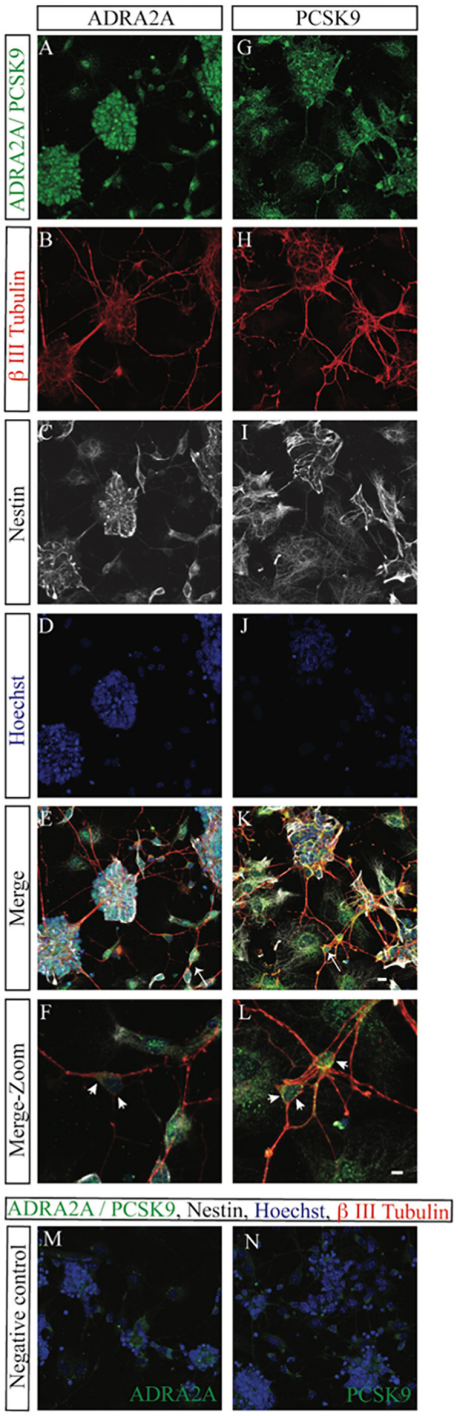

FIGURE 3 | Immunocytochemistry of *ADRA2A* and *PCSK9* levels in control (untreated) primary mouse retinal cells on day 7. Representative confocal LSM images of primary mouse retinal cultures at day 7 showing expression of *ADRA2A* **(A)**, β III tubulin **(B)**, Nestin **(C)**, cell nuclei (Hoechst), **(D)** a merge image **(E)**, and a zoomed merge image **(F)**. **(G–L)** LSM images of primary mouse retinal cultures at day 7 showing expression of *PCSK9* **(G)**, β III tubulin **(H)**, Nestin **(I)**, cell nuclei (Hoechst) **(J)**, a merge image **(K)** and a zoomed merge image **(L)**. **(M,N)** Negative controls were treated without primary antibody and are shown as merge images. Scale bar = 10 μm or scale bar = 5 μm for zoomed images.

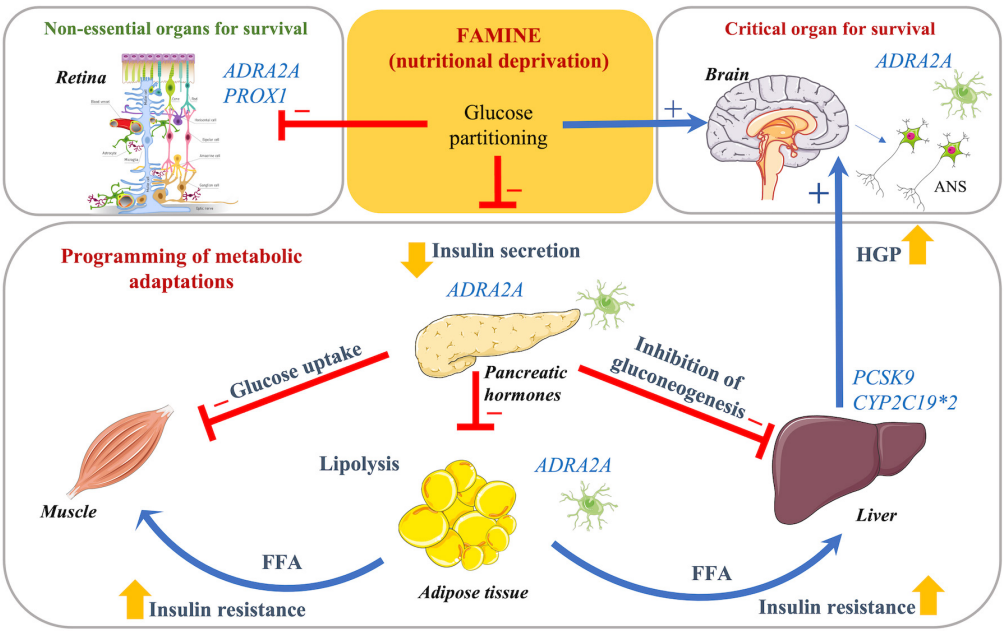

FIGURE 4 | Schematic representation of the suggested mechanisms underlying association between perinatal famine exposure and the risk of proliferative retinopathy in adults with type 2 diabetes. An exposure to starvation induces a situation of nutritional deficits confronting the body to maintain metabolic balance by shunting the energy, i.e., glucose being the main source, from non-essential peripheral organs (including retina) to critical for survival organs (brain). Insulin secretion from the pancreas is reduced to slow down uptake of glucose in the periphery (muscle, liver, and adipose tissue), while endogenous hepatic glucose production (liver) is increased to partition and supply glucose to the brain. In addition to the adaptive insulin resistance, lipolysis is induced to release free fatty acids as backup system to be used as energy sources by non-essential organs and tissues; *ADRA2A* is abandonedly expressed in the neuronal tissues surrounding pancreatic islets, adipocytes, hepatocytes, and neuroretinal glial cells. This supports the concept of the metabolic re-programming of insulin secretion and action as well elevated lipolysis during early life as an adaptive mechanism to nutritional deprivation. The nerves may mediate these programming effects of increased predisposition to the risk of proliferative retinopathy in adults.

PROX1 is shown to be downregulated in islets from type 2 diabetes donors as compared to controls (Fadista et al., 2014). It is therefore tempting to speculate that methylation changes of *PROX1* gene during starvation could contribute to the increased gene expression, also acting as a protective mechanism to restore the pool of the stem cells.

One possibility to aid clinical management of PDR is that existing drugs will be beneficial for another disease. Interestingly, we found that variants of the *PCSK9* gene that affect lipid metabolism in the liver were associated with an increased risk of severe DR in individuals with famine exposure at birth (Zhang et al., 2016). Similarly, in the *ex vivo* model, the developmental changes induced by starvation exposure resulted in permanent up-regulation of *Pcsk9* expression in the retinal cells. A potential explanation could be that the *PCSK9* gene is methylated during starvation exposure and epigenetically regulated (Lohoff et al., 2017; Tobi et al., 2018). The manifestation of programmed fetal effects on adult phenotypes, nevertheless, may not be unmasked until later in life, after triggering by subsequent environmental factors (Gluckman et al., 2008). Therefore, this link is likely to be missed in most genetic studies conducted in populations of developed nations without subsequently experienced repeat exposure to famine. While *PCSK9* inhibitors have been introduced for the treatment of cardiovascular diseases, other potential effects of *PCSK9* inhibitors, such as DR treatment, should be explored.

It is important to note that the primary cell cultures were prepared from embryos at E18.5. At this stage, the retina constitutes not only retinal neurons but also Müller cells and endothelial cells (Blackshaw et al., 2004; Dakubo et al., 2008). In the present study, the immunostaining experiments displayed some isolated immunopositive profile of *ADRA2A*, *PCSK9* and *PROX 1* not colocalizing with beta3 tubulin. Notably, our recently published data on the global mRNA sequencing analyses from the same cellular model indicated that starvation for glucose caused marked transcriptomics changes in various retinal markers including vascular markers and allowed us to generate hypothesis of potential detrimental reprogramming of the entire neurovascular unit (Özgümüs et al., 2021).

Several metabolic adaptations have been proposed to lie in the heart of fetal programming and developmental plasticity during intrauterine exposure to starvation (**Figure 4**). These are attributed to the situation when body is confronted with a nutritional challenge to maintain energy balance. The main mechanisms are centered around the goal of shunting energy resources derived using glucose from non-essential functions to the critical organs like brain, which accounts for greater than 80% of the body's metabolism in the newborn (Tanner, 1978). Given that the insulin stimulates the glucose uptake

by tissues throughout the body, the metabolic and signaling changes are required to modify insulin secretory capacity (de Rooij et al., 2006). To partition a glucose uptake between the brain and the insulin target organs (muscle, liver, and adipose tissue) mechanisms of inducing insulin resistance are taken place (Kuzawa, 2010). At the same time, the prolonged starvation leads to fat mobilization from the depots and releasing free fatty acids as backup system to be used as energy sources by these tissues (Kuzawa, 2010). Thereby, the neurons and the neuronal signaling network might play a central role in these energy partitioning mechanisms for developing brain as obligatory glucose user and nervous tissue as mediator of signals to the peripheral organs, e.g., lipolysis in the adipose tissue, insulin secretion from pancreatic beta cells, and inhibitory actions of insulin in the liver. In the study, the findings of genes involved in nervous tissues and lipid metabolism support the concepts of the metabolic re-programming of energy metabolism during early life as an adaptive mechanisms to nutritional deprivation, which may have lasting effects.

Strengths and Limitations

Our genetic analyses were based only on selected first reports of established and reproducible genetic variants linked to risk of T2D, which represented only a fraction of type 2 diabetes susceptibility variants reported in the literature (Ahlqvist et al., 2018). Further genome wide association study (GWAS) analyses should support and unravel novel genetic loci contributing to the famine-associated risk of retinopathy. Although the methylation analyses supported the potential effects of epigenetic changes in the *ADRA2A* gene on the famine-associated risk of PDR, the subset with methylation data was underpowered to detect, particularly, small effects and therefore increased sample size would be required. Although the population of Hong Kong represents a unique validation cohort, the sample size with available genotyping was limited. Nevertheless, the association of *ADRA2A* locus with the advanced stages of diabetic retinopathy in famine-exposed individuals in the HKDR was similar to that observed in the DOLCE study reassuring the link between famine-related exposure and elevated risk of severity of diabetic retinopathy. Finally, the records on macular edema were not available in the DOLCE cohort; however, only seven patients with laser-treated retinopathy did not have information on PDR, which is less likely being able to substantially influence the results. In HKDR, patients with macular edema were excluded from the analyses.

The DOLCE participants with type 2 diabetes were from the Chernihiv region of northern Ukraine, a population that was affected by the Great Holodomor famine (Fedotkina et al., 2021a). The famine exposed group was defined based on the year of birth as we have previously demonstrated significantly elevated odds ratios for PDR in people from the exposed regions born before 1950 as opposed to those born after 1950 as compared to similar groups in the unexposed regions (Fedotkina et al., 2021a). These results indicated that other factors than age contributed to the elevated risks of PDR in the regions affected by the historical famine. Thus, one potential methodological caveat in both populational cohorts from Ukraine and Hong Kong could be that we did not have genetic information in a control group from the neighboring geographical regions of the same ethnicity not exposed to the famines. Additionally, there might be other cultural changes explaining differences between patients with diabetes in the DOLCE study born before and after 1950 such as socio-economical and behavioral factors. Thus, the stress hormones during the periods of famine insults in patients born before 1950 could *per se* induce epigenetic modifications (Ewald et al., 2014). Further, some therapeutics that became available to patients born after 1950 could potentially interact with the genetic susceptibility and thereby modify risks of PDR linked to *ADRA2A*, *PSCK9*, and *CYP2C19*2* mutations or nurturing stemness effects of *PROX1* mutations. This enhances the importance of gene-environment and gene–drug interaction studies in discoveries of potential therapeutic mechanisms and drug targets.

In summary, we show the possible involvement of neuronal *ADRA2A*, *PCSK9*, and neuroprogenitor marker *PROX1* genes as molecular underpinnings in the pathogenesis of PDR. These findings may inform the development and testing of neuroprotective drugs relevant to the famine-exposed individuals or other individuals with progressive diabetes.

DATA AVAILABILITY STATEMENT

The datasets presented in this article are not readily available because of ethical considerations. Requests to access the datasets should be directed to corresponding author.

ETHICS STATEMENT

The studies involving human participants were reviewed and approved by the Dnr17/2011-09-14—approval number for Ukraine (UNDR study), 2019/28968—approval number for Norway (UNDR study); reference number 2007.339 (HKDR study); PR-AG-4/2010 (expression measurements in human retinal tissue). The patients/participants provided their written informed consent to participate in this study. The animal study was reviewed and approved by the local ethics committee (2018-579, 2016/891).

AUTHOR CONTRIBUTIONS

OF did the statistical, genetic, and methylome analyses, data interpretation, and drafted the manuscript. RJ developed an experimental *in vitro* model and carried out statistical analyses, data interpretation, and drafted the manuscript. RP performed analyses of methylome data. MG-R, TÖ, CH, and RS carried out gene expression analyses. LC, NK, TS, and TB developed the study design, and collected the data. DJ assisted in immunohistochemistry analyses. VK, AV, and MK contributed to acquisition of the data. IA was responsible for the mice acquisition. PN participated in the study design and contributed to the editing of the manuscript. VL conceived and designed the study, planned the analyses, supervised all parts of the study, interpreted the data, and wrote the manuscript. All authors

contributed to the interpretation of the data, and approved the final version of the manuscript.

FUNDING

This work was supported by the Swedish Research Council (Dnr2015-03574 and Dnr349-2006-237), Strategic Research Area Exodiab (Dnr2009-1039), the Novonordisk Foundation (NNF12OC1016467), Swedish Foundation for Strategic Research (DnrIRC15-0067), the Steno Diabetes Center Copenhagen, Bergen Research Foundation and Trond Mohn Foundation (BFS811294), and the University of Bergen.

ACKNOWLEDGMENTS

We thank the patients for their diligent and active participation, Anatoliy Lysenko and Valentina Burkhanova for their excellent management and technical assistance, and Emanuela Monni for discussions on the neuronal experiments.

SUPPLEMENTARY MATERIAL

The Supplementary Material for this article can be found online at: https://www.frontiersin.org/articles/10.3389/fnins.2022.858049/full#supplementary-material

REFERENCES

Abcouwer, S. F., and Gardner, T. W. (2014). Diabetic retinopathy: loss of neuroretinal adaptation to the diabetic metabolic environment. *Ann. N. Y. Acad. Sci.* 1311, 174–190. doi: 10.1111/nyas.12412

Ahlqvist, E., Storm, P., Karajamaki, A., Martinell, M., Dorkhan, M., Carlsson, A., et al. (2018). Novel subgroups of adult-onset diabetes and their association with outcomes: a data-driven cluster analysis of six variables. *Lancet Diabetes Endocrinol.* 6, 361–369. doi: 10.1016/S2213-8587(18)30051-2

Aiello, L. P., Avery, R. L., Arrigg, P. G., Keyt, B. A., Jampel, H. D., Shah, S. T., et al. (1994). Vascular endothelial growth factor in ocular fluid of patients with diabetic retinopathy and other retinal disorders. *N. Engl. J. Med.* 331, 1480–1487. doi: 10.1056/NEJM199412013312203

Bibikova, M., Barnes, B., Tsan, C., Ho, V., Klotzle, B., Le, J. M., et al. (2011). High density DNA methylation array with single CpG site resolution. *Genomics* 98, 288–295. doi: 10.1016/j.ygeno.2011.07.007

Blackshaw, S., Harpavat, S., Trimarchi, J., Cai, L., Huang, H., Kuo, W. P., et al. (2004). Genomic analysis of mouse retinal development. *PLoS Biol.* 2:e247. doi: 10.1371/journal.pbio.0020247

Carey, V. J., and Ripley, B. (2019). *Generalized Estimation Equation Solver (Version 4.13-20) [R-package]*. Available Online at: https://cran.r-project.org/web/packages/gee/gee.pdf (accessed October 26, 2020).

Consortium, G. T. (2015). Human genomics. The Genotype-Tissue Expression (GTEx) pilot analysis: multitissue gene regulation in humans. *Science* 348, 648–660. doi: 10.1126/science.1262110

Dakubo, G. D., Mazerolle, C., Furimsky, M., Yu, C., St-Jacques, B., McMahon, A. P., et al. (2008). Indian hedgehog signaling from endothelial cells is required for sclera and retinal pigment epithelium development in the mouse eye. *Dev. Biol.* 320, 242–255. doi: 10.1016/j.ydbio.2008.05.528

de Rooij, S. R., Painter, R. C., Phillips, D. I., Osmond, C., Michels, R. P., Godsland, I. F., et al. (2006). Impaired insulin secretion after prenatal exposure to the Dutch famine. *Diabetes Care* 29, 1897–1901. doi: 10.2337/dc06-0460

Dodson, P. M. (2007). Diabetic retinopathy: treatment and prevention. *Diab. Vasc. Dis. Res.* 4, S9–S11. doi: 10.3132/dvdr.2007.051

Du, P., Kibbe, W. A., and Lin, S. M. (2008). lumi: a pipeline for processing Illumina microarray. *Bioinformatics* 24, 1547–1548. doi: 10.1093/bioinformatics/btn224

Du, P., Zhang, X., Huang, C.-C., Jafari, N., Kibbe, W. A., Hou, L., et al. (2010). Comparison of Beta-value and M-value methods for quantifying methylation levels by microarray analysis. *BMC Bioinformatics* 11:587. doi: 10.1186/1471-2105-11-587

Dyer, M. A., Livesey, F. J., Cepko, C. L., and Oliver, G. (2003). Prox1 function controls progenitor cell proliferation and horizontal cell genesis in the mammalian retina. *Nat. Genet.* 34, 53–58. doi: 10.1038/ng1144

Ewald, E. R., Wand, G. S., Seifuddin, F., Yang, X., Tamashiro, K. L., Potash, J. B., et al. (2014). Alterations in DNA methylation of Fkbp5 as a determinant of blood-brain correlation of glucocorticoid exposure. *Psychoneuroendocrinology* 44, 112–122. doi: 10.1016/j.psyneuen.2014.03.003

Fadista, J., Vikman, P., Laakso, E. O., Mollet, I. G., Esguerra, J. L., Taneera, J., et al. (2014). Global genomic and transcriptomic analysis of human pancreatic islets reveals novel genes influencing glucose metabolism. *Proc. Natl. Acad. Sci. U.S.A.* 111, 13924–13929. doi: 10.1073/pnas.1402665111

Fedotkina, O., Luk, A., Jain, R., Prasad, R. B., Shungin, D., Simó-Servat, O., et al. (2021a). Perinatal famine is associated with excess risk of proliferative retinopathy in patients with type 2 diabetes. *Acta Ophthalmol.* 100, e539–e545. doi: 10.1111/aos.14948

Fedotkina, O., Sulaieva, O., Ozgumus, T., Cherviakova, L., Khalimon, N., Svietleisha, T., et al. (2021b). Novel reclassification of adult diabetes is useful to distinguish stages of beta-cell function linked to the risk of vascular complications: the DOLCE study from northern Ukraine. *Front. Genet.* 12:637945. doi: 10.3389/fgene.2021.637945

Flaxman, S. R., Bourne, R. R. A., Resnikoff, S., Ackland, P., Braithwaite, T., Cicinelli, M. V., et al. (2017). Global causes of blindness and distance vision impairment 1990-2020: a systematic review and meta-analysis. *Lancet Glob. Health* 5, e1221–e1234. doi: 10.1016/S2214-109X(17)30393-5

Gluckman, P. D., Hanson, M. A., Cooper, C., and Thornburg, K. L. (2008). Effect of in utero and early-life conditions on adult health and disease. *N. Engl. J. Med.* 359, 61–73. doi: 10.1056/NEJMra0708473

Golding, J., Pembrey, M., Jones, R., and Team, A. S. (2001). ALSPAC–the Avon longitudinal study of parents and children. I. study methodology. *Paediatr. Perinat. Epidemiol.* 15, 74–87. doi: 10.1046/j.1365-3016.2001.00325.x

Gopinath, B., Baur, L. A., Wang, J. J., Teber, E., Liew, G., Cheung, N., et al. (2010). Smaller birth size is associated with narrower retinal arterioles in early adolescence. *Microcirculation* 17, 660–668. doi: 10.1111/j.1549-8719.2010.00062.x

Harun-Or-Rashid, M., and Hallböök, F. (2018). Alpha 2-adrenergic receptor agonist brimonidine stimulates ERK1/2 and AKT signaling via transactivation of EGF receptors in the human MIO-M1 Müller cell line. *Curr. Eye Res.* 44, 34–45. doi: 10.1080/02713683.2018.1516783

Hernández, C., Bogdanov, P., Corraliza, L., García-Ramírez, M., Solà-Adell, C., Arranz, J. A., et al. (2016). Topical administration of GLP-1 receptor agonists prevents retinal neurodegeneration in experimental diabetes. *Diabetes* 65, 172–187. doi: 10.2337/db15-0443

HOMACalculator (2021). *HOMA Calculator*. Available Online at: https://www.dtu.ox.ac.uk/homacalculator/ (accessed October 20, 2020).

Hoshino, A., Ratnapriya, R., Brooks, M. J., Chaitankar, V., Wilken, M. S., Zhang, C., et al. (2017). Molecular anatomy of the developing human retina. *Dev. Cell* 43, 763–779.e4. doi: 10.1016/j.devcel.2017.10.029

Houseman, E. A., Kim, S., Kelsey, K. T., and Wiencke, J. K. (2015). DNA methylation in whole blood: uses and challenges. *Curr. Environ. Health Rep.* 2, 145–154. doi: 10.1007/s40572-015-0050-3

Jhaveri, D. J., Nanavaty, I., Prosper, B. W., Marathe, S., Husain, B. F., Kernie, S. G., et al. (2014). Opposing effects of α2-and β-adrenergic receptor stimulation on quiescent neural precursor cell activity and adult hippocampal neurogenesis. *PLoS One* 9:e98736. doi: 10.1371/journal.pone.0098736

Johnson, W. E., Li, C., and Rabinovic, A. (2007). Adjusting batch effects in microarray expression data using empirical Bayes methods. *Biostatistics* 8, 118–127. doi: 10.1093/biostatistics/kxj037

Kilkenny, C., Browne, W. J., Cuthill, I. C., Emerson, M., and Altman, D. G. (2010). Improving bioscience research reporting: the ARRIVE guidelines for reporting animal research. *PLoS Biol.* 8:e1000412. doi: 10.1371/journal.pbio.1000412

Kistner, A., Jacobson, L., Jacobson, S. H., Svensson, E., and Hellstrom, A. (2002). Low gestational age associated with abnormal retinal vascularization and increased blood pressure in adult women. *Pediatr. Res.* 51, 675–680. doi: 10.1203/00006450-200206000-00003

Kuzawa, C. W. (2010). "Beyond feast–famine: brain evolution, human life history, and the metabolic syndrome," in *Human Evolutionary Biology*, ed. M. P. Muehlenbein (Cambridge: Cambridge University Press).

Laboratoriemedicin (2020). *Laboratoriemedicin*. Skåne: Scania Regional Council.

Levy, J. C., Matthews, D. R., and Hermans, M. P. (1998). Correct homeostasis model assessment (HOMA) evaluation uses the computer program. *Diabetes Care* 21, 2191–2192. doi: 10.2337/diacare.21.12.2191

Lohoff, F. W., Sorcher, J. L., Rosen, A. D., Mauro, K. L., Fanelli, R. R., Momenan, R., et al. (2017). Methylomic profiling and replication implicates deregulation of PCSK9 in alcohol use disorder. *Mol. Psychiatry* 23, 1900–1910. doi: 10.1038/mp.2017.168

Longair, M. H., Baker, D. A., and Armstrong, J. D. (2011). Simple Neurite Tracer: open source software for reconstruction, visualization and analysis of neuronal processes. *Bioinformatics* 27, 2453–2454. doi: 10.1093/bioinformatics/btr390

Luk, A. O. Y., Lau, E. S. H., Cheung, K. K. T., Kong, A. P. S., Ma, R. C. W., Ozaki, R., et al. (2017). Glycaemia control and the risk of hospitalisation for infection in patients with type 2 diabetes: Hong Kong diabetes registry. *Diabetes Metab. Res. Rev.* 33:e2923. doi: 10.1002/dmrr.2923

Lumey, L. H., Khalangot, M. D., and Vaiserman, A. M. (2015). Association between type 2 diabetes and prenatal exposure to the Ukraine famine of 1932-33: a retrospective cohort study. *Lancet Diabetes Endocrinol.* 3, 787–794. doi: 10.1016/S2213-8587(15)00279-X

Mitchell, P., Liew, G., Rochtchina, E., Wang, J. J., Robaei, D., Cheung, N., et al. (2008). Evidence of arteriolar narrowing in low-birth-weight children. *Circulation* 118, 518–524. doi: 10.1161/circulationaha.107.747329

Nizari, S., Guo, L., Davis, B. M., Normando, E. M., Galvao, J., Turner, L. A., et al. (2016). Non-amyloidogenic effects of α2 adrenergic agonists: implications for brimonidine-mediated neuroprotection. *Cell Death Dis.* 7:e2514. doi: 10.1038/cddis.2016.397

Özgümüs, T., Sulaieva, O., Jain, R., Artner, I., and Lyssenko, V. (2021). Starvation to glucose reprograms development of neurovascular unit in embryonic retinal cells. *Front. Cell Dev. Biol.* 9:726852. doi: 10.3389/fcell.2021.726852

Parikh, H., Carlsson, E., Chutkow, W. A., Johansson, L. E., Storgaard, H., Poulsen, P., et al. (2007). TXNIP regulates peripheral glucose metabolism in humans. *PLoS Med.* 4:e158. doi: 10.1371/journal.pmed.0040158

Prince, M. (1998). Is chronic low-level lead exposure in early life an etiologic factor in Alzheimer's disease? *Epidemiology* 9, 618–621. doi: 10.1097/00001648-199811000-00009

Purcell, S., Neale, B., Todd-Brown, K., Thomas, L., Ferreira, M. A., Bender, D., et al. (2007). PLINK: a tool set for whole-genome association and population-based linkage analyses. *Am. J. Hum. Genet.* 81, 559–575. doi: 10.1086/519795

R Core Team (2013). *R: A Language and Environment for Statistical Computing*. Vienna: R Foundation for Statistical Computing.

Roseboom, T. J., van der Meulen, J. H., Ravelli, A. C., Osmond, C., Barker, D. J., and Bleker, O. P. (2001). Effects of prenatal exposure to the Dutch famine on adult disease in later life: an overview. *Mol. Cell. Endocrinol.* 185, 93–98. doi: 10.1016/s0303-7207(01)00721-3

Schindelin, J., Arganda-Carreras, I., Frise, E., Kaynig, V., Longair, M., Pietzsch, T., et al. (2012). Fiji: an open-source platform for biological-image analysis. *Nat. Methods* 9, 676–682. doi: 10.1038/nmeth.2019

Simo, R., Hernandez, C., and European Consortium for the Early Treatment of Diabetic Retinopathy (2014). Neurodegeneration in the diabetic eye: new insights and therapeutic perspectives. *Trends Endocrinol. Metab.* 25, 23–33. doi: 10.1016/j.tem.2013.09.005

Simo, R., Hernandez, C., Porta, M., Bandello, F., Grauslund, J., Harding, S. P., et al. (2019). Effects of topically administered neuroprotective drugs in early stages of diabetic retinopathy: results of the EUROCONDOR clinical trial. *Diabetes* 68, 457–463. doi: 10.2337/db18-0682

Simo, R., Stitt, A. W., and Gardner, T. W. (2018). Neurodegeneration in diabetic retinopathy: does it really matter? *Diabetologia* 61, 1902–1912. doi: 10.1007/s00125-018-4692-1

Simó, R., Sundstrom, J. M., and Antonetti, D. A. (2014). Ocular anti-VEGF therapy for diabetic retinopathy: the role of VEGF in the pathogenesis of diabetic retinopathy. *Diabetes Care* 37, 893–899. doi: 10.2337/dc13-2002

Tanner, F. F. M. (1978). *Postnatal Growth Neurobiology*. Boston, MA: Springer.

Teschendorff, A. E., Marabita, F., Lechner, M., Bartlett, T., Tegner, J., Gomez-Cabrero, D., et al. (2012). A beta-mixture quantile normalization method for correcting probe design bias in Illumina Infinium 450 k DNA methylation data. *Bioinformatics* 29, 189–196. doi: 10.1093/bioinformatics/bts680

Teschendorff, A. E., Menon, U., Gentry-Maharaj, A., Ramus, S. J., Gayther, S. A., Apostolidou, S., et al. (2009). An epigenetic signature in peripheral blood predicts active ovarian cancer. *PLoS One* 4:e8274. doi: 10.1371/journal.pone.0008274

Tirado-Magallanes, R., Rebbani, K., Lim, R., Pradhan, S., and Benoukraf, T. (2017). Whole genome DNA methylation: beyond genes silencing. *Oncotarget* 8, 5629–5637. doi: 10.18632/oncotarget.13562

Tobi, E. W., Slieker, R. C., Luijk, R., Dekkers, K. F., Stein, A. D., Xu, K. M., et al. (2018). DNA methylation as a mediator of the association between prenatal adversity and risk factors for metabolic disease in adulthood. *Sci. Adv.* 4:eaao4364. doi: 10.1126/sciadv.aao4364

van Zuydam, N. R., Ahlqvist, E., Sandholm, N., Deshmukh, H., Rayner, N. W., Abdalla, M., et al. (2018). A genome-wide association study of diabetic kidney disease in subjects with type 2 diabetes. *Diabetes* 67, 1414–1427. doi: 10.2337/db17-0914

VanderWeele, T. J., and Knol, M. J. (2014). A tutorial on interaction. *Epidemiol. Methods* 3, 33–72.

Wong, T. Y., Cheung, C. M., Larsen, M., Sharma, S., and Simo, R. (2016). Diabetic retinopathy. *Nat. Rev. Dis. Primers* 2:16012.

Zhang, L., Song, K., Zhu, M., Shi, J., Zhang, H., Xu, L., et al. (2016). Proprotein convertase subtilisin/kexin type 9 (PCSK9) in lipid metabolism, atherosclerosis and ischemic stroke. *Int. J. Neurosci.* 126, 675–680. doi: 10.3109/00207454.2015.1057636

Zimmet, P. Z., El-Osta, A., and Shi, Z. (2017). The diabetes epidemic in China is a public health emergency: the potential role of prenatal exposure. *J. Public Health Emerg.* 1:80. doi: 10.21037/jphe.2017.10.01

Conflict of Interest: The authors declare that the research was conducted in the absence of any commercial or financial relationships that could be construed as a potential conflict of interest.

frontiers | Frontiers in Neuroscience

BRIEF RESEARCH REPORT
published: 20 May 2022
doi: 10.3389/fnins.2022.912757

αA-Crystallin Mediated Neuroprotection in the Retinal Neurons Is Independent of Protein Kinase B

Madhu Nath[1] *and Patrice Elie Fort*[1,2]*

[1] Department of Ophthalmology and Visual Sciences, University of Michigan, Ann Arbor, MI, United States, [2] Department of Molecular and Integrative Physiology, University of Michigan, Ann Arbor, MI, United States

OPEN ACCESS

Edited by:
Peter Koulen,
University of Missouri–Kansas City, United States

Reviewed by:
Kyriaki Thermos,
University of Crete, Greece
Cristina Hernández,
Vall d'Hebron Research Institute (VHIR), Spain

***Correspondence:**
Patrice Elie Fort
patricef@umich.edu

Specialty section:
This article was submitted to Neurodegeneration, a section of the journal Frontiers in Neuroscience

Received: 04 April 2022
Accepted: 27 April 2022
Published: 20 May 2022

Citation:
Nath M and Fort PE (2022) αA-Crystallin Mediated Neuroprotection in the Retinal Neurons Is Independent of Protein Kinase B. Front. Neurosci. 16:912757. doi: 10.3389/fnins.2022.912757

Phosphatidylinositol 3-kinase (PI3K)/Akt signal pathway mediates pro-survival function in neurons. In the retina, PI3K/AKT/mTOR signaling pathway is related to the early pathogenesis of diabetic retinopathy. Signaling molecules in the membrane-initiated signaling pathway exhibiting neuroprotective function interacts with the PI3K/Akt pathway as an important survival pathway. Molecular chaperone α-crystallins are known to potentially interact and/or regulate various pro-survival and pro-apoptotic proteins to regulate cell survival. Among these demonstrated mechanisms, they are well-reported to regulate and inhibit apoptosis by interacting and sequestrating the proapoptotic proteins such as Bax and Bcl-Xs. We studied the importance of metabolic stress-induced enhanced Akt signaling and αA-crystallin interdependence for exhibiting neuroprotection in metabolically challenged retinal neurons. For the first time, this study has revealed that αA-crystallin and activated Akt are significantly neuroprotective in the stressed retinal neurons, independent of each other. Furthermore, the study also highlighted that significant inhibition of the PI3K-Akt pathway does not alter the neuroprotective ability of αA-crystallin in stressed retinal neurons. Interestingly, our study also demonstrated that in the absence of Akt activation, αA-crystallin inhibits the translocation of Bax in the mitochondria during metabolic stress, and this function is regulated by the phosphorylation of αA-crystallin on residue 148.

Keywords: αA-crystallin, protein kinase B, retinal neurons, apoptosis, neuroprotection

INTRODUCTION

Protein kinase B (Akt) is an essential signaling protein that can be activated by various growth factors such as platelet-derived growth factor, epidermal growth factor, basic fibroblast growth factor, and insulin-like growth factor as well as insulin (Fayard et al., 2005; Sale and Sale, 2008). Akt phosphorylation is one of the essential signaling events responsible for various physiological

functions, including metabolism, survival/apoptosis, differentiation, and proliferation (Brazil et al., 2004). Various studies have reported that many signaling molecules in the membrane-initiated signaling pathway exhibiting neuroprotective function interact with the PI3K/Akt pathway as an important survival pathway (Mannella and Brinton, 2006). Akt activation can also activate downstream signaling pathways involved in inflammation, such as the induction of phosphorylation and activation of IκB and the release of NF-κB (Ihekwaba et al., 2004). In addition, studies have reported that Akt activation exerts a neuroprotective effect in neuronal cells against ischemic brain damage (Ohba et al., 2004) and oxidative damages in the retina (Yu et al., 2006), besides enhancing the retina insulin receptor response through intraocular insulin growth factor-2 administration in diabetic rats (Zolov et al., 2021).

Pro-survival mechanisms are particularly important for neurons, as they often get exposed to environmental stressors. Retinal neurons consistently deal with external stimuli, which eventually cause oxidative and nutrient stresses, resulting in retinal pathology. Importantly, these noxious environmental stressors can originate from the retina, the adjacent vitreous body, the extracellular matrix, or the blood vessels and capillaries (Skeie and Mahajan, 2013; Thanos et al., 2014). Several groups, including ours, have reported the upregulation of the small heat shock proteins α-crystallins in the vitreous-retina complex of mice (Skeie and Mahajan, 2013) and diabetic donors (Ruebsam et al., 2018). Moreover, the upregulation of α-crystallins is believed to be a part of an adaptive response for promoting neuroprotection (Vazquez-Chona et al., 2004; Ying et al., 2008; Ruebsam et al., 2018). While believed to be associated with the chaperone function, α-crystallins specific neuroprotection mechanisms remain largely unclear.

α-Crystallins are known to potentially interact and/or regulate various pro-survival and pro-apoptotic proteins to regulate cell survival. Among these demonstrated mechanisms are the well-reported regulation and inhibition of apoptosis by interacting with and sequestrating proapoptotic proteins such as Bax and Bcl-Xs (Mao et al., 2004). In lens epithelial cells, αB-crystallin has also been reported to promote survival by activating RAF/MEK/ERK pathway (Liu et al., 2004). Despite demonstrating a strong neuroprotective role in the retina, αA-crystallin interaction with pro-survival signaling pathways is unclear. Since it has been previously shown to potentially regulate Akt signaling in lens epithelial cells, the current study was carried out to delineate the possible interaction of αA-crystallin with pro-survival Akt signaling molecule for its neuroprotective function in retinal neurons under metabolic stress.

MATERIALS AND METHODS

Cell Culture

Rat retinal neuronal cells (R28) were obtained from Applied Biological Materials Inc. (Richmond, BC, Canada). Cells were maintained in DMEM, 5 mM Glucose (DMEM-NG) supplemented with 10% FBS (Flow Laboratories) at 37°C, 5% CO_2 unless stated otherwise. For experiments, R28 cells were differentiated into neurons in DMEM with 8-(4-Chlorophenylthio)adenosine 3′,5′-cyclic monophosphate (8-CPT-cAMP, Catalog # C3912, Millipore Sigma, St. Louis, MO, United States) at a final concentration of 2.5 mM on laminin-coated plates as described earlier (Ruebsam et al., 2018).

Transfection and Experimental Protocol

Cells were transfected using the Neon Transfection System (Invitrogen, Waltham, MA, United States) following the manufacturer's instructions. Briefly, cells were trypsinized and washed in PBS before resuspending in suspension buffer and electroporated with targeted plasmids. Cells were then plated in six-well plates for protein expression studies. Post-transfection, cells were plated in DMEM with 5 or 25 mM glucose for 24 h. The cells were then incubated in either serum-free DMEM, 25 mM glucose, or 25 mM glucose with 100 ng/ml TNFα (R&D Systems, Catalog # 210-TA) for 4 h before analysis, whereas 5 mM DMEM served as the experimental control.

Cell Death Analysis

To investigate the effect of conditioned media on R28 cell viability, cell death rates were assessed using DNA Fragmentation ELISA (Roche Diagnostics, Indianapolis, IN, United States) according to the manufacturer's instructions and as previously described (Ruebsam et al., 2018). Transfected R28 cells were seeded in a 96 well plate at a density of 1×10^5 cells per well were incubated with or without stressors and either Akt Inhibitor V or Akt Inhibitor XII (30 μM; Millipore Sigma, Darmstadt, Germany) for 4 h. Following stress, cells were lysed in 100 μl of lysis buffer. Next, 20 μl of the supernatant and the positive and negative controls were transferred into the ELISA plate and the immunoreagent complex. Following incubation and washes, the colorimetric solution was added and incubated until the colorimetric reaction developed. After adding the stop solution, the colorimetric signal was measured with a fluorescence plate reader in a FLUOstar OMEGA plate reader (BMG LABTECH, Ortenberg, Germany) with excitation at 405 and 490 nm.

Caspase-3/7 Activity Assay

Caspase-3/7 activity was measured using the Apo-ONE Assay (Promega, Madison, WI, United States) described previously (Abcouwer et al., 2010). Briefly, R28 retinal neuron cells were seeded in a 96 well plate at a density of 1×10^5 cells per well were incubated with 100 μl of medium without serum for 4 h. Following incubation, caspase-3/7 activity was measured in the supernatants in a 96-well plate format, according to the manufacturer's protocol at 37°C.

Subcellular Fractionation

To assess Bax translocation in mitochondria, R28 retinal neuron cells were subjected for subcellular fractionation. Briefly, the cell pellets were resuspended in 100 μL of cytosolic buffer containing 1X PBS, 300 mM sucrose, 5 mM PMSF, and protease inhibitor cocktail and sonicated. After incubating the mixture at ice for 30 min, the lysates were centrifuged for 60 min at 10,000 × *g*

at 4°C, and the supernatant was collected containing cytosolic fraction. The pellet was then resuspended in mitochondrial buffer containing 1X PBS, 1% Triton X-100 150 nM NaCl, and protease inhibitor cocktail and sonicated. The resuspension was centrifuged at 10,000 × *g* for 30 min at 4°C, and the supernatant was collected containing mitochondrial fraction.

Immunoblot

Cells were homogenized by sonication in the previously described RIPA buffer (Ruebsam et al., 2018). Protein concentrations were measured with the Pierce BCA reagent, and all samples were adjusted for equal protein concentration. Whole lysates and subcellular fractions were immunoblotted using NuPage gels 4–12% and MES buffer following the manufacturer's instructions (Thermo Fisher Scientific, Waltham, MA, United States). Gels were run in MES buffer (Thermo Fisher Scientific, Waltham, MA, United States) per the manufacturer's instructions. Western blot transfer was carried out on Nitrocellulose membranes using the Mini Trans-Blot cell (Catalog # 1703930, Bio-Rad, Hercules, CA, United States) at 160 V for 1 h at 4°C. Cell lysates were screened for Akt (9272S, Cell Signaling Technology, Danvers, MA, United States), Bax (D2E11, Cell Signaling Technology, United States), HA Tag (C29F4, Cell signaling technology, United States), phosphorylated-FOXO3a (Cat no #9466, Cell Signaling Technology, United States), phosphorylated-S6 (D68F8, Cell Signaling Technology, United States), phosphorylated-4EBP1 (236B4, Cell Signaling Technology, United States), Total-4EBP1 (53H11, Cell Signaling Technology, United States), GAPDH (D16H11, Cell Signaling Technology, United States), COX-IV (Cat no #4844, Cell Signaling Technology, United States), αA-crystallin (sc-28306, Santa Cruz Biotechnology, Dallas, TX, United States) expression and β-actin (MAB-1501, Millipore, Burlington, MA, United States) as a loading control.

Statistics

The mean ± SEM and statistically significant differences are reported. Analyses were performed using non-repeated-measures ANOVA, followed by the Student–Newman–Keuls test for multiple comparisons. A *p*-value less than 0.05 was considered significant.

RESULTS

αA-Crystallin Protects Retinal Neurons From Metabolic Stress by a Mechanism Independent of the Pro-survival Akt Pathway

We have previously demonstrated that αA-crystallin is strongly neuroprotective for retinal neurons exposed to metabolic stress and that threonine 148 phosphorylation essentially controls the protective role of αA-crystallin (Ruebsam et al., 2018). We indeed reported that while the phosphomimetic form of αA-crystallin shows improved neuroprotective function, the non-phosphorylatable form showed an almost complete lack of protection, consistent with a key regulatory function of this phosphorylation (Ruebsam et al., 2018). Since αA-crystallin was previously shown to promote epithelial cell survival through modulation of the pro-survival Akt pathway, we aimed to test the existence of a similar relationship in retinal neurons. For this analysis, we have used differentiated retinal neurons from rat R28 retinal neuron cells overexpressing either myristoylated (Myr) or kinase-dead (KD) form of Akt with or without wild type (WT) phosphomimetic (T148D) or non-phosphorylatable form (T148A) of αA-crystallin (**Figure 1A**). Our data demonstrated that retinal neurons overexpressing the myristoylated (Myr-Akt) form of Akt or the wild type (WT) form of αA-crystallin alone had ∼50% reduction in cell death induced by serum starvation (**Figure 1B**) and "diabetic-like" stress (**Figure 1C**). No additional protection was observed in retinal neurons co-overexpressing Myr-Akt with either WT or the phosphomimetic form of αA-crystallin in either metabolic stress (**Figures 1B,C**). As expected, our data showed that retinal neurons overexpressing the non-phosphorylatable αA-crystallin mutant (not shown) or the kinase-dead form of Akt had cell death levels comparable to that of the empty vector-transfected cells. Suggestive of independent mechanisms, overexpression of the KD form of Akt did not impact the protective effect of αA-crystallin overexpression. In contrast, overexpression of the non-phosphorylatable αA-crystallin mutant did not impact the protective effect of the myristoylated Akt in either the serum starvation or "diabetic-like" stress conditions (**Figures 1B,C**).

Pan-Akt Inhibition Does Not Impact the Protective Effect of αA-Crystallin Overexpression

We then used a chemical inhibitor-based approach as a secondary method to assess the involvement of Akt in the regulation of αA-crystallin neuroprotective effect and its regulation by T148 phosphorylation. Because R28 retinal neurons endogenously express multiple Akt isoforms, differentiated R28 retinal neurons overexpressing the WT or phosphomimetic form of αA-crystallin were exposed to serum starvation or "diabetic-like" stress in the presence of a pan-Akt inhibitor (XII) that we previously characterized (Gardner et al., 2015). As we previously showed, this pan-Akt specific inhibitor dramatically reduced the phosphorylation of proteins downstream of Akt, including FOXO3a, S6, and 4E-BP1 (**Figure 2A**), confirming the significant inhibition of Akt signaling. Furthermore, specific Akt signaling inhibition by this treatment was confirmed by its effectiveness in suppressing the protective impact of Myr-Akt on cell death induced by either of these metabolic stress conditions (**Figure 2B**). Consistent with parallel effects of these protective pathways, our data further revealed that inhibition of Akt had no impact on the protective effect of overexpression of either the WT or phosphomimetic form of αA-crystallin (**Figure 2B**). Of note, while not impacting cell death, inhibition of endogenous Akt has led to increasing caspase 3/7 activity in all the groups and was comparable to the empty vector (**Figure 2C**), suggesting that the protective effect of αA-crystallin is at least partially caspase-independent.

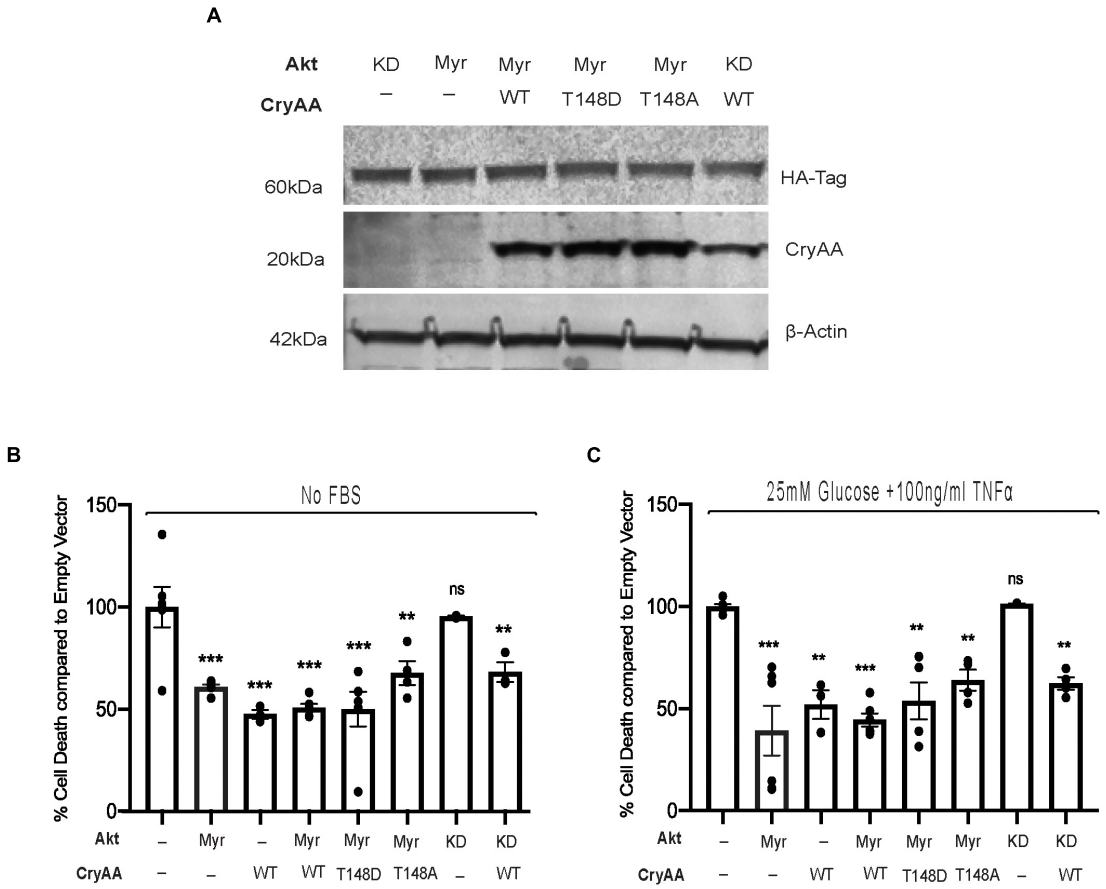

FIGURE 1 | αA-Crystallin protects retinal neurons in stress conditions, independent of the pro-survival Akt pathway. Rat retinal neuronal cells (R28) cells were transfected with either empty vector (EV), wild type αA-crystallin (WT), phosphomimetic form of αA-crystallin (T148D), or non-phosphorylatable form of αA-crystallin (T148A) with/without myristoylated (Myr) or kinase-dead (KD) form of protein kinase B (Akt). Post transfection, cells were either kept in serum starvation (No FBS) or exposed to diabetic-like stress (25 mM glucose + 10 ng/ml TNFα). The expression of αA-crystallin and Akt in cell lysates was assessed for stressed R28 cells **(A)** using immunoblotting. DNA fragmentation ELISA was performed as the endpoint on Rat retinal neuronal cells (R28), incubated with the No FBS **(B)** or diabetic-like stress **(C)** for 4 h. Each endpoint was measured on a minimum of three technical replicates in two independent experiments (n = 3/each condition). Statistical analysis was performed by one-way ANOVA followed by the Student–Newman–Keuls test. $^{**}p \leq 0.01$, $^{***}p \leq 0.001$. CryAA, αA-crystallin; Akt, protein kinase B; TNFα, tumor necrosis factor-alpha; HA-Tag, human influenza hemagglutinin tag; Myr, myristoylated form of protein kinase B; KD, a kinase-dead form of protein kinase B; WT, wild type αA-crystallin; T148D, phosphomimetic form of αA-crystallin; T148A, non-phosphorylatable form of αA-crystallin.

αA-Crystallin Phosphorylation at Residue T148 Inhibits Stress-Induced Bax Translocation to Mitochondria Independent of Pro-survival Akt Pathway

We previously reported that αA-crystallin prevents neuronal cells death through regulation of Bax translocation to the mitochondria. Thus, we next assessed how manipulation of Akt signaling might impact the regulation of the cellular localization of Bax by αA-crystallin. Differentiated R28 retinal neurons overexpressing dominant negative Akt with either WT, phosphomimetic, or non-phosphorylatable form of αA-crystallin exposed to metabolic stress was analyzed for Bax expression and subcellular localization (**Figure 3A**). We first confirmed that the presence of KD Akt with either form of αA-crystallin in metabolically stressed retinal neurons does not have any impact on the total Bax expression (**Figure 3B**). Consistent with a key role of T148 phosphorylation independent of Akt, the metabolic stress-induced translocation of Bax to the mitochondria was almost completely suppressed in retinal neurons overexpressing the phosphomimetic form of αA-crystallin, even when co-expressing the KD form of Akt (**Figures 3C,D**). Altogether this study demonstrates that αA-crystallin protects retinal neurons from metabolic stress-induced cell death by sequestrating Bax in a T148 phosphorylation-dependent manner independent of Akt signaling.

DISCUSSION

The current work studied the importance of metabolic stress-induced enhanced Akt signaling and αA-crystallin interdependence for exhibiting neuroprotection in metabolically challenged retinal neurons. For the first time, this study has

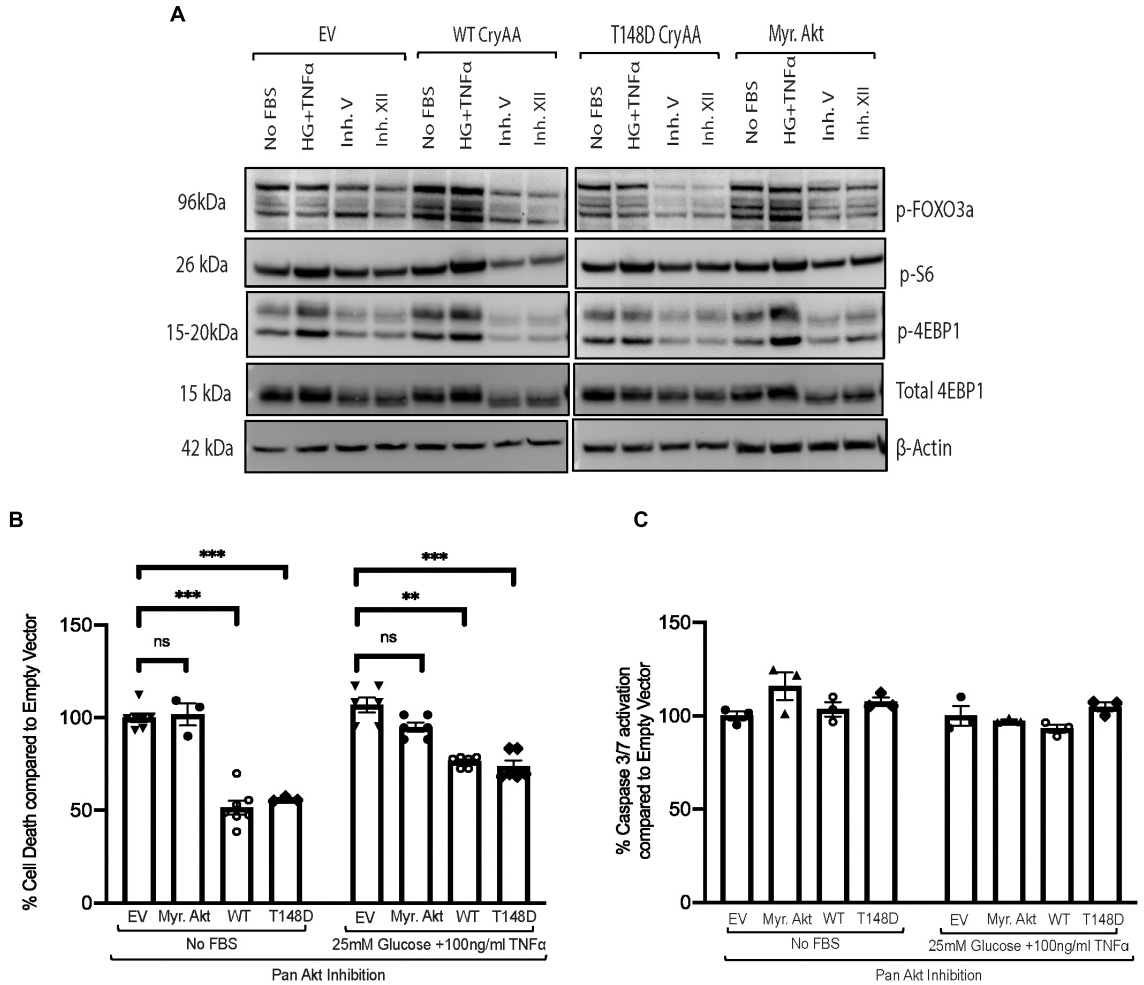

FIGURE 2 | Pan-Akt inhibition does not impact the protective effect of αA-crystallin on retinal neurons. Rat retinal neuronal cells (R28) cells were transfected with either empty vector (EV), wild type αA-crystallin (WT), phosphomimetic form of αA-crystallin (T148D), or myristoylated (Myr) form of protein kinase B (Myr-Akt). For pharmacological inhibition of Pan-Akt expression, post transfection, cells were either kept in serum starvation (No FBS) or exposed to diabetic-like stress (25 mM glucose + 10 ng/ml TNFα) with the pan-Akt inhibitor XII (30 μM conc.) for 4 h. The expression of downstream targets of the Akt pro-survival pathway in cell lysates was assessed for stressed R28 cells **(A)** using immunoblotting. DNA fragmentation ELISA **(B)** and caspase 3/7 activation **(C)** assay were performed as the endpoint on Rat retinal neuronal cells (R28), incubated with the No FBS or diabetic-like stress **(B,C)** for 4 h, respectively. Each endpoint was measured on a minimum of three technical replicates in two independent experiments (n = 3/each condition). Statistical analysis was performed by one-way ANOVA followed by the Student–Newman–Keuls test. $^{**}p \leq 0.01$, $^{***}p \leq 0.001$. CryAA, αA-crystallin; Akt, protein kinase B; TNFα, tumor necrosis factor-alpha; HA-Tag, human influenza hemagglutinin tag; Myr, myristoylated form of protein kinase B; KD, a kinase-dead form of protein kinase B; WT, wild type αA-crystallin; T148D, phosphomimetic form of αA-crystallin; T148A, non-phosphorylatable form of αA-crystallin; p-FOXO3a, phosphorylated forkhead box O-3; p-S6, phosphorylated ribosomal protein S6; p-4EBP1, phosphorylated factor 4E-binding protein 1.

revealed that αA-crystallin and activated Akt are significantly neuroprotective in the stressed retinal neurons, independent of each other. Furthermore, the study also highlighted that significant inhibition of the PI3K-Akt pathway does not alter the neuroprotective ability of αA-crystallin in stressed retinal neurons. Interestingly, our study also demonstrated that in the absence of Akt activation, αA-crystallin inhibits the translocation of Bax in the mitochondria during metabolic stress, and this function is regulated by the phosphorylation of αA-crystallin on residue 148. Overall, our study suggests that αA-crystallin and its phosphorylation on residue 148 plays an important role in regulating apoptosis in stressed retinal neurons and can exert this function independent of Akt signaling.

Phosphatidylinositol 3-kinase (PI3K)/Akt signal pathway is well known for mediating pro-survival function in neurons. In the retina, PI3K/AKT/mTOR signaling pathway is related to the early pathogenesis of diabetic retinopathy (Reiter et al., 2006; Fort et al., 2014; Zhang et al., 2019). This pathway is reported to play a major role in protecting against oxidative stress-induced apoptosis (Faghiri and Bazan, 2010) and high glucose-induced inflammatory injury in retinal pigment epithelial cells (Ran et al., 2019). Studies have also reported its active participation in oxidative stress-induced apoptosis in

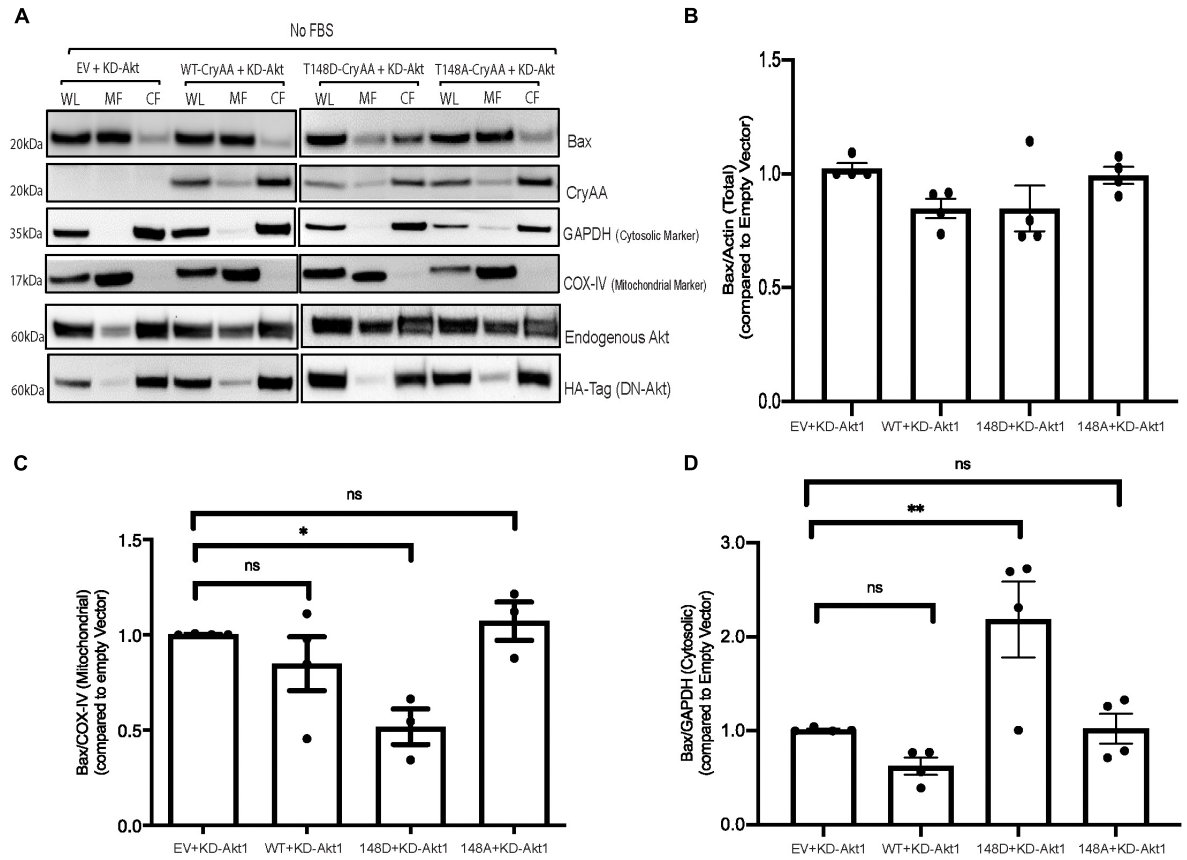

FIGURE 3 | αA-Crystallin phosphorylation at residue 148D is important for inhibiting stress-induced Bax translocation to mitochondria and does not depend on Akt to mediate this effect. Rat retinal neuronal cells (R28) cells were co-transfected with either empty vector (EV), wild type αA-crystallin crystallin (WT), phosphomimetic form of αA-crystallin (T148D), or non-phosphorylatable form of αA-crystallin (T148A) with kinase-dead (KD) form of Akt. Post transfection, cells were exposed to serum starvation (No FBS) for 4 h. Bax, CryAA, and kinase-dead Akt expression in cytosolic, mitochondrial, and whole lysates were assessed in stressed R28 cells **(A)** using immunoblotting. In addition, the expression of Bax in total lysates **(B)**, the mitochondrial fraction **(C)**, and cytosolic fractions **(D)** were analyzed using ImageJ software. Each endpoint was measured on a minimum of three technical replicates in two independent experiments (n = 3/each condition). Statistical analysis was performed by one-way ANOVA followed by the Student–Newman–Keuls test. $^{*}p \leq 0.05$, $^{**}p \leq 0.01$. CryAA, αA-crystallin; Akt, protein kinase B; GAPDH, glyceraldehyde 3-phosphate dehydrogenase; COX-IV, cytochrome c oxidase complex IV; HA-Tag, human influenza hemagglutinin tag; KD, a kinase-dead form of protein kinase B; WT, wild type αA-crystallin; T148D, phosphomimetic form of αA-crystallin; T148A, non-phosphorylatable form of αA-crystallin.

retinal neurons (Yu et al., 2006) and a cytoprotective role in response to the local redox environment of human RPE cells (Kim et al., 2010).

Previous reports, including ours, have demonstrated that the small heat shock chaperone protein αA-crystallin is considerably neuroprotective to the metabolically stressed neurons (Thanos et al., 2014; Ruebsam et al., 2018; Zhu and Reiser, 2018). While studying αA-crystallin possible interaction with the Akt pathway in demonstrating its neuroprotective ability, our current study revealed that it is neuroprotective to metabolically stress retinal neurons, and this function is independent of Akt activation. α-Crystallins were recently proposed to prevent the oxidative stress-related injury to retinal ganglion cells *via* regulation of the Akt/BAD pathway (Hua Wang et al., 2020), and αB-crystallin was reported to be effectively promoting astrocytes viability through phosphatidylinositol 3-kinase (PI3K)/protein kinase B (Akt) signaling pathways under serum-deprivation (Zhu et al., 2015). Our study further demonstrated that pharmacological inhibition of the PI3K-Akt pathway did not alter the neuroprotective ability of αA-crystallin in the stressed retinal neurons. Supportive of the key role of Akt activation, studies have reported that inhibition of Akt using the inhibitor Akt VIII causes a significant increase in retinal-derived cell death induced by H_2O_2 (Wang et al., 2015).

Several groups, including ours, have reported that α-crystallins reduce stress-induced apoptosis in part by interfering with the mitochondrial translocation of the pro-apoptotic protein Bax (Mao et al., 2004; Dou et al., 2012; Hamann et al., 2013). Furthermore, decreased α-crystallin expression during metabolic disease progression is also correlated with enhanced Bax pro-death activity (Hamann et al., 2013). Our group has also reported the strong association of diabetes-associated reduced chaperone function of α-crystallins with the increased disruption of its interactions with Bax, a function also shown to be critical for the neuroprotective effect of α-crystallins in retinal neurons in culture (Losiewicz and Fort, 2011). While αB-crystallin protects

retinal pigment epithelial cells from ER stress-induced apoptosis by attenuating the increase in Bax (Dou et al., 2012), the C-terminal extension domain of αA-crystallin was sufficient to protect against Bax-induced apoptosis in cone-derived 661W cells (Hamann et al., 2013). Our current study showed that alteration of the Akt survival pathway by overexpression of the KD mutant did not affect the inhibition of the translocation of Bax to the mitochondria by αA-crystallin and that this function was strongly regulated by the phosphorylation of αA-crystallin on residue 148. It is well documented that crystallins undergo numerous post-translation modifications (PTMs), affecting their chaperone activity (Blakytny et al., 1997; Kamei et al., 1997; Ciano et al., 2016). Our group had previously reported that phosphorylation on the serine/threonine 148 residue is essential to retaining the protective role of αA-crystallin under metabolic stress and diabetic conditions (Ruebsam et al., 2018). The current study demonstrated that αA-crystallin protects retinal neurons during metabolic stress by inhibiting the translocation of Bax to the mitochondria and does so completely independently of the Akt signaling pro-survival pathway and that this function is regulated by the phosphorylation of αA-crystallin on residue 148. This observation further confirms the key regulatory role of phosphorylation on the residue 148 of αA-crystallin for its protective function.

In conclusion, this study underlines the neuroprotective role of αA-crystallin and its modulation by phosphorylation on T148 in suppressing pro-apoptotic Bax independent of the PI3K-Akt pathway. Additionally, these findings indicate a potential implication of αA-crystallin modulation for the plausible treatment of neurodegeneration induced by diabetes.

DATA AVAILABILITY STATEMENT

The original contributions presented in the study are included in the article/supplementary material, further inquiries can be directed to the corresponding author/s.

AUTHOR CONTRIBUTIONS

MN performed the experiments and prepared the figures. MN and PF analyzed the data, conceptualized and designed the research, interpreted the results of the experiments, and drafted, finalized, and approved the manuscript. Both authors contributed to the article and approved the submitted version.

FUNDING

This work was supported by the National Eye Institute Grant EY020895, National Institutes of Health (NIH) Grant P30EY007003 (Core Grant for Vision Research at the University of Michigan), NIH Grant P30DK020572 (Michigan Diabetes Research Center), Research to Prevent Blindness, and Lichter Award.

REFERENCES

Abcouwer, S. F., Lin, C. M., Wolpert, E. B., Shanmugam, S., Schaefer, E. W., Freeman, W. M., et al. (2010). Effects of ischemic preconditioning and bevacizumab on apoptosis and vascular permeability following retinal ischemia-reperfusion injury. *Invest Ophthalmol. Vis. Sci.* 51, 5920–5933. doi: 10.1167/iovs.10-5264

Blakytny, R., Carver, J. A., Harding, J. J., Kilby, G. W., and Sheil, M. M. (1997). A spectroscopic study of glycated bovine alpha-crystallin: investigation of flexibility of the C-terminal extension, chaperone activity and evidence for diglycation. *Biochim. Biophys. Acta* 1343, 299–315. doi: 10.1016/s0167-4838(97)00145-3

Brazil, D. P., Yang, Z. Z., and Hemmings, B. A. (2004). Advances in protein kinase B signalling: AKTion on multiple fronts. *Trends Biochem. Sci.* 29, 233–242. doi: 10.1016/j.tibs.2004.03.006

Ciano, M., Allocca, S., Ciardulli, M. C., Della Volpe, L., Bonatti, S., and D'Agostino, M. (2016). Differential phosphorylation-based regulation of alphaB-crystallin chaperone activity for multipass transmembrane proteins. *Biochem. Biophys. Res. Commun.* 479, 325–330. doi: 10.1016/j.bbrc.2016.09.071

Dou, G., Sreekumar, P. G., Spee, C., He, S., Ryan, S. J., Kannan, R., et al. (2012). Deficiency of alphaB crystallin augments ER stress-induced apoptosis by enhancing mitochondrial dysfunction. *Free Radic Biol. Med.* 53, 1111–1122. doi: 10.1016/j.freeradbiomed.2012.06.042

Faghiri, Z., and Bazan, N. G. (2010). PI3K/Akt and mTOR/p70S6K pathways mediate neuroprotectin D1-induced retinal pigment epithelial cell survival during oxidative stress-induced apoptosis. *Exp. Eye Res.* 90, 718–725. doi: 10.1016/j.exer.2010.03.002

Fayard, E., Tintignac, L. A., Baudry, A., and Hemmings, B. A. (2005). Protein kinase B/Akt at a glance. *J. Cell Sci.* 118, 5675–5678. doi: 10.1242/jcs.02724

Fort, P. E., Losiewicz, M. K., Pennathur, S., Jefferson, L. S., Kimball, S. R., Abcouwer, S. F., et al. (2014). mTORC1-independent reduction of retinal protein synthesis in type 1 diabetes. *Diabetes* 63, 3077–3090. doi: 10.2337/db14-0235

Gardner, T. W., Abcouwer, S. F., Losiewicz, M. K., and Fort, P. E. (2015). Phosphatase control of 4E-BP1 phosphorylation state is central for glycolytic regulation of retinal protein synthesis. *Am. J. Physiol. Endocrinol. Metab.* 309, E546–56. doi: 10.1152/ajpendo.00180.2015

Hamann, S., Metrailler, S., Schorderet, D. F., and Cottet, S. (2013). Analysis of the cytoprotective role of alpha-crystallins in cell survival and implication of the alphaA-crystallin C-terminal extension domain in preventing Bax-induced apoptosis. *PLoS One* 8:e55372. doi: 10.1371/journal.pone.0055372

Hua Wang, Y., Wu Wang, D., and Qin Yin, Z. (2020). Synergistic protection of RGCs by olfactory ensheathing cells and alpha-crystallin through regulation of the Akt/BAD Pathway. *J Fr. Ophtalmol.* 43, 718–726. doi: 10.1016/j.jfo.2020.02.003

Ihekwaba, A. E., Broomhead, D. S., Grimley, R. L., Benson, N., and Kell, D. B. (2004). Sensitivity analysis of parameters controlling oscillatory signalling in the NF-kappaB pathway: the roles of IKK and IkappaBalpha. *Syst. Biol.* 1, 93–103. doi: 10.1049/sb:20045009

Kamei, A., Iwase, H., and Masuda, K. (1997). Cleavage of amino acid residue(s) from the N-terminal region of alpha A- and alpha B-crystallins in human crystalline lens during aging. *Biochem. Biophys. Res. Commun.* 231, 373–378. doi: 10.1006/bbrc.1997.6105

Kim, J. H., Kim, J. H., Jun, H. O., Yu, Y. S., Min, B. H., Park, K. H., et al. (2010). Protective effect of clusterin from oxidative stress-induced apoptosis in human retinal pigment epithelial cells. *Invest Ophthalmol. Vis. Sci.* 51, 561–566. doi: 10.1167/iovs.09-3774

Liu, J. P., Schlosser, R., Ma, W. Y., Dong, Z., Feng, H., Lui, L., et al. (2004). Human alphaA- and alphaB-crystallins prevent UVA-induced apoptosis through regulation of PKCalpha, RAF/MEK/ERK and AKT signaling pathways. *Exp. Eye Res.* 79, 393–403. doi: 10.1016/j.exer.2004.06.015

Losiewicz, M. K., and Fort, P. E. (2011). Diabetes impairs the neuroprotective properties of retinal alpha-crystallins. *Invest Ophthalmol. Vis. Sci.* 52, 5034–5042. doi: 10.1167/iovs.10-6931

Mannella, P., and Brinton, R. D. (2006). Estrogen Receptor Protein Interaction with Phosphatidylinositol 3-Kinase Leads to Activation of Phosphorylated Akt and Extracellular Signal-Regulated Kinase 1/2 in the Same Population of Cortical Neurons: A Unified Mechanism of Estrogen Action. *J. Neurosci.* 26, 9439–9447. doi: 10.1523/JNEUROSCI.1443-06.2006

Mao, Y. W., Liu, J. P., Xiang, H., and Li, D. W. (2004). Human alphaA- and alphaB-crystallins bind to Bax and Bcl-X(S) to sequester their translocation during staurosporine-induced apoptosis. *Cell Death Differ.* 11, 512–526. doi: 10.1038/sj.cdd.4401384

Ohba, N., Kiryu-Seo, S., Maeda, M., Muraoka, M., Ishii, M., and Kiyama, H. (2004). Transgenic mouse overexpressing the Akt reduced the volume of infarct area after middle cerebral artery occlusion. *Neurosci. Lett.* 359, 159–162. doi: 10.1016/j.neulet.2004.02.029

Ran, Z., Zhang, Y., Wen, X., and Ma, J. (2019). Curcumin inhibits high glucoseinduced inflammatory injury in human retinal pigment epithelial cells through the ROSPI3K/AKT/mTOR signaling pathway. *Mol. Med. Rep.* 19, 1024–1031.

Reiter, C. E., Wu, X., Sandirasegarane, L., Nakamura, M., Gilbert, K. A., Singh, R. S., et al. (2006). Diabetes reduces basal retinal insulin receptor signaling: reversal with systemic and local insulin. *Diabetes* 55, 1148–1156. doi: 10.2337/diabetes.55.04.06.db05-0744

Ruebsam, A., Dulle, J. E., Myers, A. M., Sakrikar, D., Green, K. M., Khan, N. W., et al. (2018). A specific phosphorylation regulates the protective role of alphaA-crystallin in diabetes. *JCI Insight* 3:e97919. doi: 10.1172/jci.insight.97919

Sale, E. M., and Sale, G. J. (2008). Protein kinase B: signalling roles and therapeutic targeting. *Cell Mol. Life Sci.* 65, 113–127. doi: 10.1007/s00018-007-7274-9

Skeie, J. M., and Mahajan, V. B. (2013). Proteomic interactions in the mouse vitreous-retina complex. *PLoS One* 8:e82140. doi: 10.1371/journal.pone.0082140

Thanos, S., Bohm, M. R., Meyer zu Horste, M., Prokosch-Willing, V., Hennig, M., Bauer, D., et al. (2014). Role of crystallins in ocular neuroprotection and axonal regeneration. *Prog. Retin Eye Res.* 42, 145–161. doi: 10.1016/j.preteyeres.2014.06.004

Vazquez-Chona, F., Song, B. K., and Geisert, E. E. Jr. (2004). Temporal changes in gene expression after injury in the rat retina. *Invest Ophthalmol. Vis. Sci.* 45, 2737–2746. doi: 10.1167/iovs.03-1047

Wang, R., Peng, L., Zhao, J., Zhang, L., Guo, C., Zheng, W., et al. (2015). Gardenamide A Protects RGC-5 Cells from H(2)O(2)-Induced Oxidative Stress Insults by Activating PI3K/Akt/eNOS Signaling Pathway. *Int. J. Mol. Sci.* 16, 22350–22367. doi: 10.3390/ijms160922350

Ying, X., Zhang, J., Wang, Y., Wu, N., Wang, Y., and Yew, D. T. (2008). Alpha-crystallin protected axons from optic nerve degeneration after crushing in rats. *J. Mol. Neurosci.* 35, 253–258. doi: 10.1007/s12031-007-9010-1

Yu, X. R., Jia, G. R., Gao, G. D., Wang, S. H., Han, Y., and Cao, W. (2006). Neuroprotection of insulin against oxidative stress-induced apoptosis in cultured retinal neurons: involvement of phosphoinositide 3-kinase/Akt signal pathway. *Acta Biochim. Biophys. Sin.* 38, 241–248. doi: 10.1111/j.1745-7270.2006.00152.x

Zhang, J., Liu, J., Wu, J., Li, W., Chen, Z., and Yang, L. (2019). Progression of the role of CRYAB in signaling pathways and cancers. *Onco. Targets Ther.* 12, 4129–4139. doi: 10.2147/OTT.S201799

Zhu, Z., Li, R., Stricker, R., and Reiser, G. (2015). Extracellular alpha-crystallin protects astrocytes from cell death through activation of MAPK, PI3K/Akt signaling pathway and blockade of ROS release from mitochondria. *Brain Res.* 1620, 17–28. doi: 10.1016/j.brainres.2015.05.011

Zhu, Z., and Reiser, G. (2018). The small heat shock proteins, especially HspB4 and HspB5 are promising protectants in neurodegenerative diseases. *Neurochem. Int.* 115, 69–79. doi: 10.1016/j.neuint.2018.02.006

Zolov, S. N., Imai, H., Losiewicz, M. K., Singh, R. S. J., Fort, P. E., and Gardner, T. W. (2021). Insulin-like growth factor-2 regulates basal retinal insulin receptor activity. *J. Biol. Chem.* 296:100712. doi: 10.1016/j.jbc.2021.100712

Conflict of Interest: The authors declare that the research was conducted in the absence of any commercial or financial relationships that could be construed as a potential conflict of interest.

Publisher's Note: All claims expressed in this article are solely those of the authors and do not necessarily represent those of their affiliated organizations, or those of the publisher, the editors and the reviewers. Any product that may be evaluated in this article, or claim that may be made by its manufacturer, is not guaranteed or endorsed by the publisher.

frontiers | Frontiers in Neuroscience

ORIGINAL RESEARCH
published: 30 June 2022
doi: 10.3389/fnins.2022.926629

New Retinal Pigment Epithelial Cell Model to Unravel Neuroprotection Sensors of Neurodegeneration in Retinal Disease

*Aram Asatryan‡, Jorgelina M. Calandria‡, Marie-Audrey I. Kautzmann‡, Bokkyoo Jun, William C. Gordon, Khanh V. Do†, Surjyadipta Bhattacharjee, Thang L. Pham†, Vicente Bermúdez†, Melina Valeria Mateos†, Jessica Heap and Nicolas G. Bazan**

Neuroscience Center of Excellence, School of Medicine, Louisiana State University Health New Orleans, New Orleans, LA, United States

Retinal pigment epithelial (RPE) cells sustain photoreceptor integrity, and when this function is disrupted, retinal degenerations ensue. Herein, we characterize a new cell line from human RPE that we termed *ABC*. These cells remarkably recapitulate human eye native cells. Distinctive from other epithelia, RPE cells originate from the neural crest and follow a neural development but are terminally differentiated into "epithelial" type, thus sharing characteristics with their neuronal lineages counterparts. Additionally, they form microvilli, tight junctions, and honeycomb packing and express distinctive markers. In these cells, outer segment phagocytosis, phagolysosome fate, phospholipid metabolism, and lipid mediator release can be studied. ABC cells display higher resistance to oxidative stress and are protected from senescence through mTOR inhibition, making them more stable in culture. The cells are responsive to Neuroprotectin D1 (NPD1), which downregulates inflammasomes and upregulates antioxidant and anti-inflammatory genes. ABC gene expression profile displays close proximity to native RPE lineage, making them a reliable cell system to unravel signaling in uncompensated oxidative stress (UOS) and retinal degenerative disease to define neuroprotection sites.

Keywords: neuroprotectin D1, RPE cell, single cell, gene expression, lipids, apoptosis, autophagy, age-related macular degeneration (AMD)

OPEN ACCESS

Edited by:
Peter Koulen, University of Missouri–Kansas City, United States

Reviewed by:
Andrew W. Taylor, Boston University, United States
Ivan Fernandez-Bueno, University of Valladolid, Spain

***Correspondence:**
Nicolas G. Bazan
nbazan@lsuhsc.edu

†Present addresses:
Khanh V. Do, Faculty of Medicine, PHENIKAA University, Hanoi, Vietnam; PHENIKAA Research and Technology Institute (PRATI), A&A Green Phoenix Group JSC, Hanoi, Vietnam

Thang L. Pham, Faculty of Medicine, PHENIKAA University, Hanoi, Vietnam; PHENIKAA Research and Technology Institute (PRATI), A&A Green Phoenix Group JSC, Hanoi, Vietnam

Vicente Bermúdez, Instituto de Investigaciones Bioquímicas de Bahía Blanca (INIBIBB), Consejo Nacional de Investigaciones Científicas y Técnicas (CONICET), Blanca, Argentina

Melina Valeria Mateos, Departamento de Biología, Bioquímica y Farmacia (DBByF), Universidad Nacional del Sur (UNS), Blanca, Argentina

‡*These authors have contributed equally to this work*

Specialty section:
This article was submitted to Neurodegeneration, a section of the journal Frontiers in Neuroscience

Received: *22 April 2022*
Accepted: *30 May 2022*
Published: *30 June 2022*

INTRODUCTION

The retinal pigment epithelial (RPE) cells conform to a tightly arranged monolayer that serves as a barrier between the photoreceptor cells (PRC) and the choriocapillaris (Bazan, 2007; Lakkaraju et al., 2020). In addition, these cells are critical in nutrient transport, efflux of catabolic products, and the daily phagocytosis of PRC outer segments. The RPE also recycles all-trans-retinal that is oxidized during photo conversion and docosahexaenoic acid (DHA) through the interphotoreceptor matrix (IPM) to the base of inner segments and secretes cytokines, chemokines that locally modulate innate and adaptive immune systems (Bazan et al., 1985; Gordon et al., 1992; Detrick and Hooks, 2020; Lakkaraju et al., 2020; Storm et al., 2020).

Retinal pigment epithelial cells and PRC are at constant risk for uncompensated oxidative stress (UOS) because of their oxygen-rich environment, high flux of polyunsaturated fatty acids (PUFAs) (Bazan et al., 2010), and high metabolic activity (Bazan, 2006, 2007). RPE cell impairments due to disruption in homeostasis are involved in retinal degenerative diseases, including age-related

macular degeneration (AMD), where perturbed phagocytic activity occurs (Mitter et al., 2014; Golestaneh et al., 2017; Inana et al., 2018).

Three phagocytic processes are at crossroads with autophagy in RPE. Daily phagocytosis of the PRC tips engages the microtubule-associated protein 1 light chain 3 (LC3) in LC3-associated phagocytosis (LAP), and autophagy at the basal level requires LC3 for the formation of the phagophores as part of the normal repair process, which includes mitophagy that eliminates damaged mitochondria by oxidative stress (Intartaglia et al., 2021). Downstream, autophagic lysosome-mediated degradation is often positively regulated by AMP-activated protein kinase (AMPK) signaling and negatively regulated by the mammalian/mechanistic target of rapamycin (mTOR) pathway (He and Klionsky, 2009). AMPK regulates lipid metabolism and cell survival via adiponectin and its receptors, Adipor1 and Adipor2, by stimulating ceramidase activity. Previously, we have demonstrated that Adipor1 mutant mice, independent of their cognate ligand adiponectin, result in retinal degeneration (Rice et al., 2015). A single amino acid mutation of *Adipor1* has been found in different forms of retinitis pigmentosa (Xu et al., 2016; Zhang et al., 2016). Membrane frizzled-related protein (MFRP) and AdipoR1 are critical for DHA uptake and retention in the RPE and retina (Rice et al., 2015; Kautzmann et al., 2020). Moreover, a recent study suggests a role for Adipor1 in the pathogenesis of Late-Onset Retinal Degeneration (L-ORD) (Miyagishima et al., 2021). We characterized human primary RPE cells, dubbed ABC, that display features of the native pigment epithelium. Notably, those features include formation of impermeable monolayers with tight junctions and high resistance to UOS. These cells do not undergo senescence and display functional phagocytosis and active lipid dynamics mechanisms. Here we used ABC cells in a case study to unravel the relationship between these mechanisms in the normal cycle of the cell.

MATERIALS AND METHODS

Cell Lines

The ABC cell line was derived from the ocular globes of a 19-year-old male donor provided by the National Disease Research Interchange (NDRI) within 24 h after death (head trauma), following a modification of a previously described protocol by Ishida et al., 1998 (Calandria et al., 2012). After removing the vitreous humor, flaps of the retina, choroid, and RPE were made, and squares of 5 mm × 5 mm were cut and placed in Petri dishes. The RPE cells grew for 3 weeks in the dishes, then were transferred to flasks with Minimum Essential Medium Eagle (MEM, Millipore Sigma, Burlington, MA, United States, Cat# M2279) containing 10% fetal calf serum, 5% newborn calf serum, 1X non-essential amino acids, 4 mM glutamine, amphotericin B (0.5 g/ml), and gentamicin (10 μg/ml). The cells were then trypsinized (0.05%); dead and loosely attached cells were washed and discarded. The remainder of the attached cells was further trypsinized (0.25% trypsin) and passaged several times until a homogeneous culture was obtained. ARPE-19 cells were obtained from ATCC, Manassas, Virginia, Cat# CRL-2302 and cultured as recommended by the commercial vendor. Additionally, primary human RPE49 cell line was developed by isolation of the RPE from a healthy 49-year-old male Caucasian donor and cultured in the same conditions as the ABC cells.

Basal Flux Measurement

ABC cells were grown in Thincert cell culture inserts (Greiner Bio-One, Monroe, NC, United States) with permeable polystyrene membranes of 12 mm diameter and 0.4 mm pore size previously treated with Vitronectin. Basal (lower) and apical (upper) compartments were loaded with 1.5 and 0.5 ml of medium, respectively, for equilibrium. After 7 days of culture, the impermeability of confluent RPE cells was tested by adding a medium containing 0.04% trypan blue (1 ml) to the upper compartment, producing an apical-to-basal hydrostatic pressure. Then cell cultures were incubated under these conditions for up to 12 h. Empty well inserts were used as controls. The basal flux was calculated by photometry measurements after subtracting the background and is expressed in absorbance at 560 nm. After trypan blue treatment, cells were washed with medium and subsequently stained with Alexa Fluor 594 WGA (Invitrogen, Waltham, MA, United States, Cat# W11262) and Hoechst for highly selective staining of the plasma membrane and nucleus, respectively. Control inserts without cells were compared with inserts containing ABC cells.

Cell Culture, Staining, and Morphology

The cells were routinely passaged by dissociation in 0.05% (w/v) trypsin in MEM medium, followed by replating at a split ratio ranging from 1:3 to 1:6 (Sonoda et al., 2009). ABC cells were maintained in T75 flasks in the medium described below. Primary cultures were incubated in the culture medium [MEM medium containing 10% FBS, 5% NCS, MEM-NEAA (Gibco, Carlsbad, CA, United States, Cat# 11140050)] and 1× Penicillin/Streptomycin at 37°C, 5% CO_2, and 99% relative humidity for 2 days. The medium was replaced weekly. Cells of passage numbers 20–25 were used in all of the experiments. Proliferation of cells was determined using anti-Ki67 antibody (rabbit polyclonal, Abcam Cat# ab15580) as described (Al-Hussaini et al., 2008). Briefly, ABC cells were seeded at 250,000 cells/ml in 12-well plates and incubated overnight for 2, 3, 4, 5, 6, 7, and 8 days to reach several degrees of confluency, then they were fixed with 4% paraformaldehyde and immunostained with anti-Ki67 (Millipore Sigma, Burlington, MA, United States, Milli-Mark Anti-Ki67, clone Ki-S5 APC conjugate Cat# FCMAB103AP). Hoechst 33342 counterstain was included to measure apoptosis as previously described (Calandria et al., 2015). To induce UOS, cells were serum-starved for 8 h and exposed to H_2O_2 (1,600 μM)/TNFα (10 ng/ml) for 24 h. After that period, cells were photographed with a DIAPHOT 200 microscope (Nikon, Melville, NY, United States) with fluorescent optics. Images were recorded by a color-chilled 3CCD camera (Hamamatsu, Bridgewater, NJ, United States) and counted with ImageJ[1] using small-size/high-brightness to detect apoptotic cells

[1] http://imagej.nih.gov/ij

with the blue filter, and small red dots in the nuclei on the red filter were counted as positive Ki67 cells. To assess the morphology of ABC cells, they were grown on nitrocellulose membranes for 1 week or pelleted, then fixed and embedded in plastic and thin-sectioned as described (Knott et al., 2011).

Quantitative PCR and Real-Time PCR

RNA was collected at passages from ABC cells (P# 18 and 21), ARPE-19 cells (P# 22), and primary human RPE49 (isolated from a healthy 49-year-old donor). One μg of total RNA was reverse transcribed using an iScript cDNA Synthesis Kit (Bio-Rad, Hercules, CA, United States, Cat# 1708890). Quantitative PCR (qPCR) was performed in a CFX-384 Real-Time PCR system (Bio-Rad) using primers (**Supplementary Table 1**), and then amplification products were loaded on 2% agarose gels (**Supplementary Figure 1A**). Data were normalized using Delta-Delta-Ct ($\Delta\Delta$Ct). All results are expressed as means ± SEM, $n = 4$ (**Supplementary Figure 1B**).

Western Blot

Samples were lysed by RIPA buffer, and protein was determined by Bradford assay (Bio-Rad). After denaturation, 30 μg of total protein for cell samples were separated by SDS-PAGE (4–12% gradient) gel (Thermo Fisher Scientific, Waltham, MA, United States) and transferred to nitrocellulose membranes (Bio-Rad). The membranes were blocked by 5% non-fat dry milk in PBST, probed with anti-Bestrophin (Abcam, Cat# ab2182), anti-Cytokeratin 8 (Santa Cruz Biotechnology, Dallas, TX, United States, Cat# sc-8020), anti-rhodopsin (Abcam, Cambridge, United Kingdom, Cat# ab81702), anti-GAPDH (Millipore Sigma, Burlington, MA, United States, Cat# MAB374) for 1 h, washed three times with PBST, probed with secondary antibodies (GE Healthcare, Chicago, IL, United States) for 1 h, and washed three times with PBST. Protein bands were visualized using the LAS 4000 imaging system (GE Healthcare).

Uncompensated Oxidative Stress Induction and Lipid Treatments

Cells were grown in 6-well plates semi-confluent for 72 h in DMEM/F12 and 10% fetal bovine serum (FBS) media, then serum starved for 8 h before triggering oxidative stress by further incubation with 10 ng/ml of TNF-α plus 600 μM H_2O_2 for 15 h. Bioactivity was assayed by adding 50 nM of neuroprotectin D1 (NPD1) at the outset of oxidative stress.

Phagocytosis Imaging

Eight-well chamber slides (LabTek # 154534) were seeded with 100,000 cells per well for each cell type and incubated overnight at 37°C and 5% CO_2. To evaluate the amount of photoreceptor outer segments (POS, bovine rod photoreceptor outer segments, InVision BioResources, Seattle WA, United States, Cat# 98740) particles to add to each well, we followed the protocol described in Mukherjee et al., 2007 and determined that we needed 10×10^6 POS/well. We used fluorescein isothiocyanate (FITC; Invitrogen # F1906) diluted in DMSO at a 10 mg/ml concentration and labeled the POS at a 3:1 ratio (POS vol:FITC vol). The tube containing FITC + POS was shielded from light and incubated on a rotating well for 1 h at room temperature. The labeled POS were rinsed by adding 1 mL of DMEM + 2.5% sucrose to the sample. The tube was spun at 3,000 *g* for 5 min at room temperature, and then the supernatant was removed, rinsed two additional times, and transferred into a fresh tube. Before distribution into the wells, the labeled POS were added to the culture medium, and this mixture was added to each well at a 10×10^6 density. Yellow-green fluorescent beads (Invitrogen # F13081) at a concentration of 10×10^6 beads/μl were distributed at a density of 10×10^6 beads/well after mixing with culture medium. Cells were incubated at 37°C + 5% CO_2 and collected at 6, 8, and 22 h following the protocol (Mao and Finnemann, 2013) and stained with Hoechst. Cells were imaged using an LSM 710 Zeiss confocal microscope with a 63X oil-immersed objective. Z-stacks with 0.5 μm step-size were acquired in four different areas of the well for each experimental time point. Maximal projections of the z-stacks were captured and exported in ImageJ (see footnote 1) for fluorescence intensity measurements.

Evaluation of POS Phagocytosis by Flow Cytometry

To assess phagocytosis, ABC cells were either plated on Thincerts™ cell culture inserts coated with Vitronectin or plated in an 8-well chamber slide and grown for 3 days to 1 week. Cells were serum starved and then fed with POS for 8 h at a 1:10 ratio (cell:POS). Blue-fluorescent Hoechst 33342 dye (1:500) was from Invitrogen (Carlsbad, CA, United States). Cell samples were treated and then analyzed immediately on a Gallios Flow Cytometer (Beckman Coulter). Cells were gated based on the specific set of cell labeling used in each experiment (**Figure 4** and **Supplementary Figure 4**). After excluding proper gating cell debris and doublets for Apoptosis/Necrosis assay (Enzo Life Sciences, Farmingdale, NY, ENZ-51002-25), a plot of Annexin V versus 7AAD signals was generated (**Supplementary Figure 4**). Twenty thousand or more events were collected per treated sample. Data were analyzed using Kaluza Analysis Software (Beckman Coulter). For each condition for ABC control cells vs. ABC cells exposed to FITC-POS (**Figure 4F**, top and bottom, respectively), 7AAD versus FITC signals and unbound/internalized POS were obtained (100,000 events analyzed in each condition). Then, after gating out unbound POS, viable (7AAD negative) and apoptotic cells (7AAD positive, gated, right) are revealed. Confluent ABC cell cultures were incubated with previously labeled (pHrodo or FITC) or unlabeled bovine POS (1:10 cell:POS ratio) for 16 h. Then cells were trypsinized and labeled for flow cytometry processing (**Supplementary Figure 4**).

Assessment of Phagocytosis by Western Blot

ABC and ARPE-19 cells were incubated with unlabeled POS suspension for 0, 2, 6, 8, and 16 h. To stop the reaction, the cells were washed 3 times with PBS-CM buffer (PBS supplemented with 1 mM $MgCl_2$, 0.2 mM $CaCl_2$). To detect internalized POS only, the cells were washed 1 time with PBS, then incubated

with PBS-EDTA for 5–10 min. Samples designated for total POS detection remained in PBS-CM. The PBS-EDTA was then removed, and the cells were washed three times with PBS-CM. The PBS-CM was removed from all wells, and the cells were lysed with RIPA buffer freshly supplemented with a protease inhibitor cocktail. Analysis of phagocytosed POS content in samples was determined by SDS-PAGE electrophoresis and opsin immunoblotting.

Lipid Extraction and LC-MS/MS-Based Lipidomic Analysis

Cells were grown for 7–10 days before being collected to maximize phagocytosis and utilization and incorporation of lipids from outer segments into the RPE cells. The cells were then washed with ice-cold PBS with calcium to remove any unbound outer segments, and the lipids were extracted. Lipid extraction was performed similarly to our previous work (Do et al., 2019). Briefly, each sample was homogenized in MeOH (3 ml), followed by the addition of CHCl3 (6 ml) and the internal lipid standards (Cayman, Ann Arbor, MI, United States). After sonication in a water bath, samples were centrifuged, and the supernatant was added with pH 3.5 H_2O for phase separation. The bottom phase (organic phase) was dried down under N2 and reconstituted in an AcN:MeOH:CHCl3 (90:5:5) solution. A Xevo TQ-S equipped with Acquity UPLC BEH HILIC 1.7 μm 2.1 × 100 mm column was used with solvent A (acetonitrile:water, 1:1; 10 mM ammonium acetate pH 8.3) and solvent B (acetonitrile:water, 95:5; 10 mM ammonium acetate pH 8.3) as the mobile phase. Solvent B (100%) ran for the first 5 min isocratically was graduated to 20% solvent A for 8 minutes, and then ran at 65% of A for 0.5 min. It ran isocratically at 65% of A for 3 min and then returned to 100% of B for 3.5 min for equilibration. The capillary voltage was 2.5 kV, the desolvation temperature was set at 550°C, the desolvation gas flow rate was 800 l/h, cone gas was 150 l/h, and nebulizer pressure was 7.0 Bars with the source temperature at 120°C.

Matrix–Assisted Laser Desorption/ionization Imaging Mass Spectrometry

Matrix–assisted laser desorption (MALDI) was carried out as described previously (Kautzmann et al., 2020). Briefly, coverslips with cells were attached to MALDI plates and then placed within the sublimation chamber, where matrix (2,5-dihydroxybenzoic acid, DHB) was applied for positive ion mode analysis. Sections were then rasterized by laser, 355 nm, 2000 Hz Scanning control (15 μm, horizontal and vertical movement) and analyzed. Differential spectra represent relative abundance of lipid molecular species detected by matrix–assisted laser desorption/ionization imaging mass spectrometry (MALDI IMS) based on cell type were created.

Isolation of Single Cells and cDNA Synthesis

Control stressed and treated single ABC cells were captured with the C1^{TM} platform (Fluidigm Inc., South San Francisco, CA, United States) using Fluidigm's Integrated Fluidic Circuits^{TM} (IFC) according to the manufacturer's instructions (**Supplementary Figure 7A**). Captured cells were imaged on IFC to confirm the number of cells per site, and the viability of the cell was confirmed using a LIVE/DEAD cell assay (Life Technologies, Waltham, MA, United States, Cat# L3224). Only single, viable cells were used for subsequent analysis. In the IFC, individual cells were lysed, and mRNAs were reverse transcribed and amplified to complementary DNAs. The resulting cDNAs from individual cells were collected from the IFC and diluted three times in TE buffer before utilization in the qPCR reaction with Biomark^{TM}.

High Throughput qPCR by Biomark^{TM}

The qPCR reaction mixture had a volume of 5 μl and contained 2.25 μl of diluted preamplified cDNA, 0.25 μl of DNA Binding Dye (Fluidigm), and 2.5 μl SsoFast EvaGreen Supermix with low ROX (Bio-Rad, Hercules, CA, United States). The primer reaction mixture had a final volume of 5 μl and contained 2.5 μl Assay Loading Reagent (Fluidigm, San Francisco, CA, United States) and 0.25 μl of a mix of all reverse and forward primers (**Supplementary Table 1**), corresponding to a final concentration of 500 nM in the reaction. The Biomark 96.96 IFC was first primed with an oil solution in the Juno Controller (Fluidigm) to fill the fluidic circuit. Ninety-six sample reactions (5 μl each) were loaded into individual sample wells, and 96 forward and reverse primer mixtures were loaded into each assay well (5 μl each). The IFC was then placed in the Juno Controller for automatic loading and mixing. After an hour and a half, the IFC was then transferred to the Biomark^{TM} HD qPCR platform (Fluidigm). The cycling program consisted of Thermal Mix at 70°C for 40 min followed by 60°C for 30 s. Hot Start was 1 min at 95°C, followed by 30 cycles of denaturation at 96°C for 5 s, annealing at 60°C for 20 s. Melting curves were collected between 60°C and 95°C with 1°C increments/3 s. We designed a set of 96 primer pairs (**Supplementary Table 1**) that comprise inflammatory and autophagy pathways in addition to housekeeping genes. The induction of UOS was optimized for the ABC cells by testing a range of H_2O_2 concentrations (**Supplementary Figure 3**). Naïve ABC cells or cells treated with H_2O_2 were isolated using the Fluidigm C1 microfluidics platform. Cells were captured into individual chambers, lysed, and their RNA reverse transcribed and amplified into cDNA. cDNA from single cells was collected, and qPCR was performed using the Fluidigm Biomark^{TM} platform (**Supplementary Figure 7A**). Specific amplification of each targeted cDNA was confirmed by melt curve analysis. Measured Ct values were exported from the BioMark^{TM} software to Excel for data analysis. Ct values of target genes were extracted through the Fluidigm Real-Time PCR Analysis program. The Ct value of target genes was normalized to the housekeeping genes.

RNAseq Analysis

For RNAseq ABC cells, ARPE-19 cells, and hRPE49 cells were used. Cells seeded in 6-well plates (500,000 cells/well) were

grown for at least 72 h. The total RNA was extracted using Trizol, and RNA quality and integrity were verified using NanodropOne (Thermo Fisher Scientific) and Agilent 2100 Bioanalyzer RNA nanochips. Library preparation was done using TrueSeq RNA library prep kit v2 – Set A (catalog #RS-122-2001) (Illumina); libraries were denatured, pooled, and normalized according to Illumina's sample preparation guide. RNASeq was done on Illumina NextSeq 500 sequencing system using NextSeq 500 High Output v2 kit (150 cycles) (catalog# FC-404-2002).

Bioinformatic Analyses of RNAseq and Single-Cell RT-PCR

The RNA reads were mapped to the human genome and processed through bioinformatics pipeline in QIAGEN CLC Genomics Workbench (Qiagen, Redwood City, CA, United States). Then the results were analyzed using R and heat map of gene expression was generated with Heatmap generator. Then the results are analyzed using Ingenuity Pathway Analysis tool (Qiagen, Redwood City, CA, United States). Principal component analysis (PCA), hierarchical clustering, violin plots, and box plots were carried out using the Bio Vinci program (Bioturing Inc., San Diego, CA, United States), GraphPad Software (La Jolla, CA, United States, United States)[2] and Partek Genomics Suite software (Partek Inc., St. Louis, MO, United States).[3] Gene Interaction Prediction was performed using STRING database[4] (Szklarczyk et al., 2017).

Statistics

Data were plotted using GraphPad Software, San Diego, CA, United States.[5] Data are presented as means ± SEM. Comparisons were performed using ANOVA two-way. *P*-values were indicated as follows: ns $P > 0.05$, $^{*}P \leq 0.05$, $^{**}P < 0.01$, $^{***}P \leq 0.001$, $^{****}P \leq 0.0001$. Data were filtered by $P \leq 0.05$ and absolute value fold change ≥ 1.5.

Illustration

The autophagy pathways illustration (**Figure 6E**) was adapted from Intartaglia et al. (2021) and created with BioRender.com.

RESULTS

Human Primary Cells That Phenotypically Resemble RPE in the Human Eye

ABC cells were obtained from retina xenografts of a 19-year-old Caucasian male (**Figure 1A**). At passage 8 and over, they conserved the pigmentation (**Figure 1A**, right panel) and extensive areas of polygonal-shaped cells at higher densities (**Figures 1E,F**). We compared the transcription profile of ABC cells, ARPE-19, and a primary culture originating from a 49-year-old Caucasian male using the same technique utilized for ABC by means of RNAseq. The latter, cultured hRPE49, disclosed a limited life span, reaching passage 9 at most. ABC and ARPE-19 both originated from 19-year-old Caucasian males; the second underwent spontaneous immortalization (Dunn et al., 1996). Of the three cell lines compared, ABC depicted the most abundance of RPE markers. Retinal dehydrogenase 5 (RDH5); Bestrophin 1 (BEST1); MER proto-oncogene, tyrosine kinase (MERTK); retinaldehyde binding protein 1 (RLBP1); Paired box gene 6 (PAX6); Orthodenticle homeobox 2 (OTX2); Microphthalmia-Associated Transcription Factor (MITF); retinoid isomerohydrolase RPE65 (RPE65); cellular retinaldehyde-binding protein (CRALBP); and pigment epithelium-derived factor/serpin family F member 1 (PEDF/SERPINF1) are essential for the function and maintenance of RPE cells and photoreceptors, and their mutation causes retinal degenerating pathologies (Housset et al., 2013; Raviv et al., 2014; Xue et al., 2015; Liu et al., 2017; Audo et al., 2018; Guziewicz et al., 2018; Chen et al., 2019; Ma et al., 2019; Wang et al., 2020; Zhang et al., 2020). These genes are expressed in ABC, and some are underrepresented in the other two cell lines (**Figure 1B**, right panel). Thus, ABC represent a good *in vitro* model to study the role of these genes and their associated retinal diseases. Single-cell Real-Time PCR showed uniform expression of cellular retinaldehyde binding protein (*CRALBP*), *RPE65*, and *OCCLUDIN,* a tight junction protein. *RDH5*, which was represented more in hRPE49 by RNAseq (**Figure 1B**, right panel), evidenced more variability within the ABC cell population, with up to 50% of them exhibiting low expression (**Figure 1C**). RPE65, BEST1, RDH5, RLBP1, and SERPINF1 were confirmed using reverse transcription polymerase chain reaction (RT-PCR) and Real-Time polymerase chain reaction (qPCR) (**Supplementary Figures 1A,B**).

Retinal pigment epithelial cells derived from human embryonic stem cells (hESCs) have recently arisen as a model for RPE-related diseases. Nevertheless, hESC-derived RPE undergoes mesenchymal-epithelial transition in culture before acquiring an epithelial phenotype (Choudhary et al., 2015). ABC cells show minimal expression of mesenchymal cell markers as well as markers of mesenchymal-epithelial transition, thus displaying more phenotypic stability (**Figure 1B**, middle panels). Western blot analysis comparing ARPE-19, ABC, and fibroblasts illustrates that proteins Bestrophin-1 (BEST1) and Cytokeratin 8 (**Figure 1D** and **Supplementary Figure 2**) were only present in the two RPE cell lines, and BEST1 was the highest expressed in ABC, confirming the phenotype stability observed by the low expression of the mesenchymal and the MET transition (**Figure 1B**).

RPE cells generate three types of pigment melanin and fuscin. Melanosomes are developed during brief periods at embryonic stages, while fuscin accumulates with aging as lipofuscin and melanolipofuscin granules (Boulton, 2014). Two mRNAs coding for enzymes implicated in the synthesis of eumelanin from tyrosin, tyrosinase (TYR) and tyrosinase-related

[2]www.graphpad.com

[3]https://www.partek.com/partek-genomics-suite/

[4]http://string-db.org/

[5]www.graphpad.com

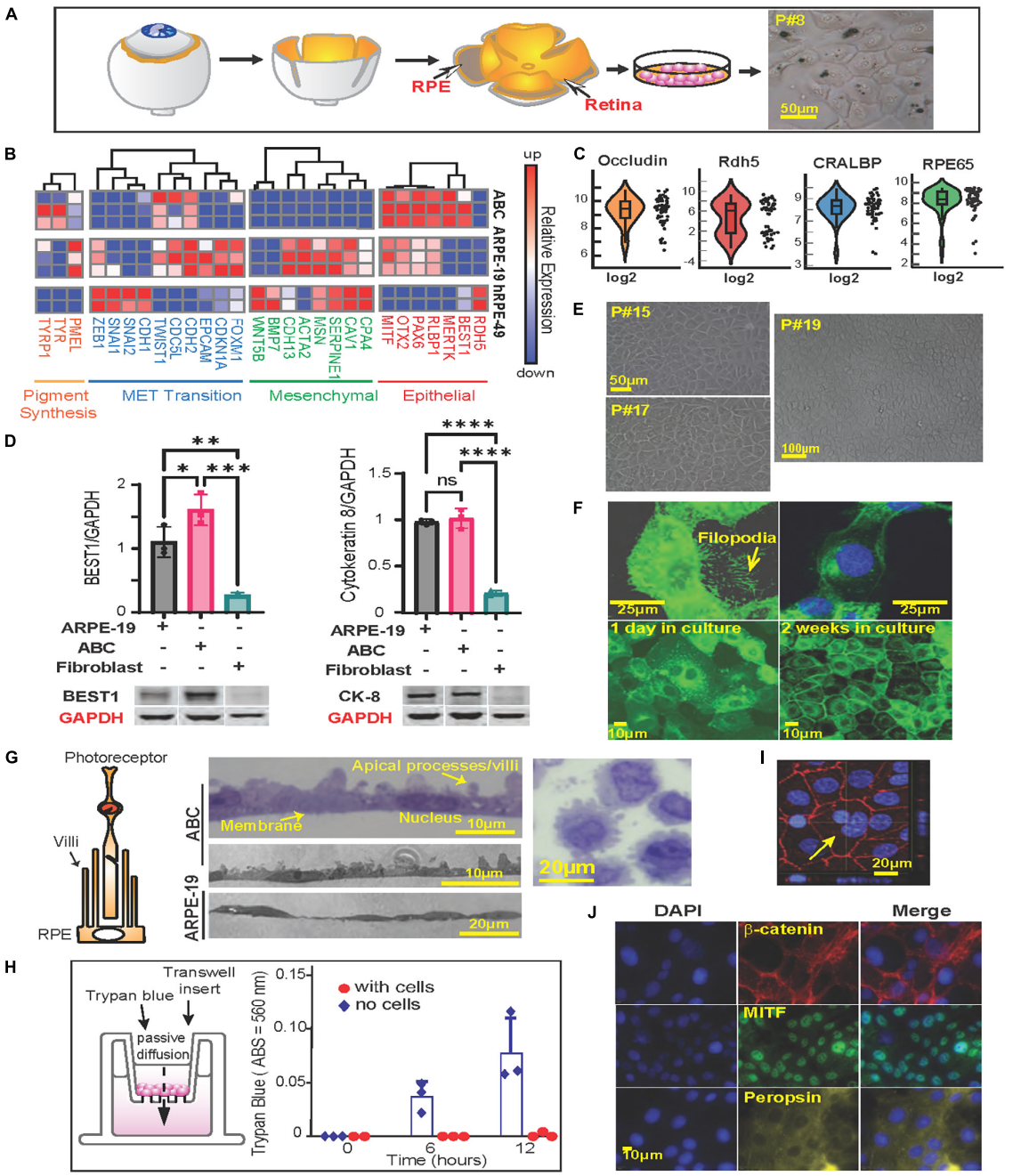

FIGURE 1 | Phenotypycal characteristics of primary human RPE (ABC cells). **(A)** RPE cells were isolated from human donor eyes and grown in tissue culture. Schematic representation of the protocol used for the isolation of RPE cells. Right panel shows light microscopy photograph of passage 8 (P#8) ABC cells with melanosomes. **(B)** Heatmap showing RNA sequencing results comparing ABC, ARPE-19 and human primary RPE cells from a 49-year-old donor (hRPE49) mRNA expression levels for Pigment synthesis, MET Transition signaling, Mesenchymal and Epithelial markers. **(C)** Violin plots of single-cell RT-PCR for ABC cells showing distribution of RPE-specific markers whitin the population. **(D)** Western blot comparison of the levels of Cytokeratin-8, and Bestrophin-1 (BEST1). The bars represent the mean and SEM of 3 independent measurements. GAPDH was used for standardization. One Way ANOVA and *t*-test was applied to determine significance. $*p < 0.05$; $**p < 0.01$; $***p < 0.001$; $****p < 0.0001$. Representative blots are displayed. The whole membranes are depicted in **Supplementary Figure 2**. **(E)** ABC cell passages 15, 17, and 19 forming honeycomb like monolayers. **(F)** Slender cytoplasmic projections (filopodium) in migrating ABC cells are shown in GFP-tagged MFRP overexpressing ABC cells. Monolayer formation. **(G)** Representation of RPE cells microvilli surrounding photoreceptor. Sections of confluent RPE cells growing on a nitrocellulose filter. Sections through an RPE cell pellet show cells to be about 20 μm wide and 15 μm thick with prominent lateral protrusions (apical villar processes) and a single large central nucleus, resembling the *in vivo* retinal RPE cell layer. **(H)** ABC cells seeded on Thincert cell culture inserts treated with vitronectin showing the functional junction formation of ABC cells (**Supplementary Figure 4B**). **(I)** ZO-1 staining of ABC cells in culture, one week after plating. The cells are tightly packed. Yellow arrow shows a double nucleated ABC cell. Basal flux was calculated by photometry measurements after subtracting the background and is expressed in absorbance at 560 nm. **(J)** Immunocytochemistry of ABC cells after 1 week in culture, cells express MITF, beta-catenin, and Peropsin. Blue = DAPI; Red = β-catenin; Green = MITF; Yellow = Peropsin.

protein 1 (TYRP1), were found in high abundance in ABC in comparison to ARPE-19 and hRPE-49. Premlanosome protein mRNA, PMEL, was also present, although in less abundance (**Figure 1B**, left panel). These data confirm the ability of ABC to produce melanin-like granules *in vitro* (**Figure 1A**).

Unlike other human RPE cell lines, ABC were capable of retaining their original characteristics along passages (**Figures 1A,E**). The expression of GFP-tagged-membrane frizzled-related protein (GFP-MFRP), which is localized in cytoplasm and membrane, exhibited filopodial processes (**Figure 1F**). After two weeks in culture, these cells depicted a classical RPE hexagonal shape (**Figure 1F**). Moreover, villar processes appeared on the apical surface when they formed a packed monolayer with well-defined tight junctions (**Figure 1G**, middle panels). ABC cells pelleted, embedded in plastic, and thin-sliced displayed prominent apical villar processes and a single large central nucleus (**Figure 1G**, right panel). The formation of tight junctions was tested using a basal flux assay (**Figure 1H**, left panel) in which trypan blue was placed in the insert chamber, and it was allowed to diffuse freely toward the well through the permeable membrane. ABC cell tight junctions prevented the dye from diffusing across the monolayer, even after 12 h of incubation (**Figure 1H**, right panel and **Supplementary Figure 4B**). Immunostaining with Zona Occludens confirmed the formation of the tight junctions after one week of incubation (**Figure 1I**). Notably, the monolayers depicted incomplete cariocinesis, represented by cells containing more than one nuclei (**Figure 1I**, yellow arrow).

Additionally, microphthalmia-associated transcription factor (MITF), β-Catenin, and Peropsin displayed nuclear, peripheral, and cytoplasmic localization in ABC cultures accordingly with the distribution of the proteins in the monolayer (**Figure 1J**).

These results demonstrate that ABC cells display phenotypic and genetic features closer to the RPE native pigment epithelium than the other two cell lines regarding stability, purity, and structure, indicating that key proteins are correctly localized and that the expression of desirable enzymes for pigmentation and function occurs. From this point forward, we will present evidence to consider ABC a suitable model to use in AMD studies.

Postmitotic ABC Cells Display UOS Resistance

To determine the proliferation rate variation in response to confluency and stress, a time curse was performed, and the dividing cells were detected using Ki67 staining in the presence or absence of UOS (**Figures 2A,B**). In parallel, apoptosis was measured using Hoechst staining. In naïve cells, Ki67 values declined from 100% at day 1 to 30% at day 8, reaching the 50% mark between day 5 and 6 (**Figure 2A**, red curve). When H_2O_2 was applied to induce uncompensated oxidative stress, less than 1% of cells were Ki67 positive at day 1, and the number increased with time as the population recovered, reaching stabilization at around 50% between days 5 and 6 (**Figure 2A**, green curve). Days 1 and 2 depicted the higher values of apoptosis (**Figure 2A**, blue bars), whereas the sensitivity decreased drastically to 25% after 3 days of growth to become almost null by day 8. Accordingly, the appearance of the initial hexagonal-shaped cells occurs one week after plating at this density. Concentration curves confirmed these observations (**Supplementary Figures 3A–D**). Functional tight junctions appeared after 7 days of culturing ABC cells in inserts (**Figure 1H**). When ARPE-19 and ABC cells response was compared under the same conditions, the first cell line reached 60–65% cell death at 600 μM H_2O_2, but the second one did not yield significant differences from their own control (concentration 0 μM). ARPE-19 cell death was raised to 100% with 800 μM, while <75% of ABC cells died at 1200 μM (**Figure 2C**). In addition, the UOS response genes differ between ABC and ARPE19 cells, with 8 out of 14 genes highly expressed in ABC cells (**Figure 2D**), suggesting that in ABC cells, the antioxidant systems are set forth to promote protection against ROS. Notably, mRNAs coding glutathione peroxidases 2, 3, and 8 (GXP2, GXP3, and GXP8) were elevated in ABC. GXP2, GXP3, and GXP8 are three isoenzymes belonging to the glutathione peroxidase family that catalyze the reduction of organic hydroperoxides and hydrogen peroxide (H_2O_2) by glutathione, protecting the cells against oxidative damage (Nirgude and Choudhary, 2021; Ren et al., 2022; Yin et al., 2022). The mRNA encoding Thioredoxin reductase 1 (TXNRD1), a selenocysteine-containing enzyme involved in redox homeostasis (Snider et al., 2013), was over-represented in ABC as well. To determine whether necrosis and apoptosis were occurring, flow cytometry was used to analyze a population of cells stained with Annexin V and 7AAD. Dot charts and histograms indicate the presence of four populations of cells (**Figure 2E** and **Supplementary Figure 4D**). Four cell populations were analyzed: (1) live cells negative for both Annexin V and 7AAD, (2) early apoptotic cells positive for Annexin V, (3) cells positive for both Annexin V and 7AAD, demonstrating late-stage apoptosis, and (4) necrotic cells positive only for 7AAD (red population). A clear concentration-dependent decrease in the ABC viable cell population, with a concomitant increment in the late apoptotic population, is evident (**Figure 2E**). Overall, the majority of dying cells are apoptotic; only a small fraction (10%) are necrotic.

These results suggest ABC cells become postmitotic and increase resistance to uncompensated oxidative stress, probably through the activation of key glutathione-related homeostatic effectors that counteract the oxidized reactive species and stabilize the redox status of the cell.

ABC Cells Undergoing UOS Are Rescued by NPD1

Neuroprotectin D1 synthesis is triggered by stress to promote homeostasis and survival in RPE cells (Calandria et al., 2009). NPD1 modulates the expression of proteins like BIRC3 (Calandria et al., 2009) to rescue RPE cells from apoptosis induced by UOS. To assess the transcriptional response of ABC to NPD1, single-cell RT-PCR was used (**Figure 3A**) to screen

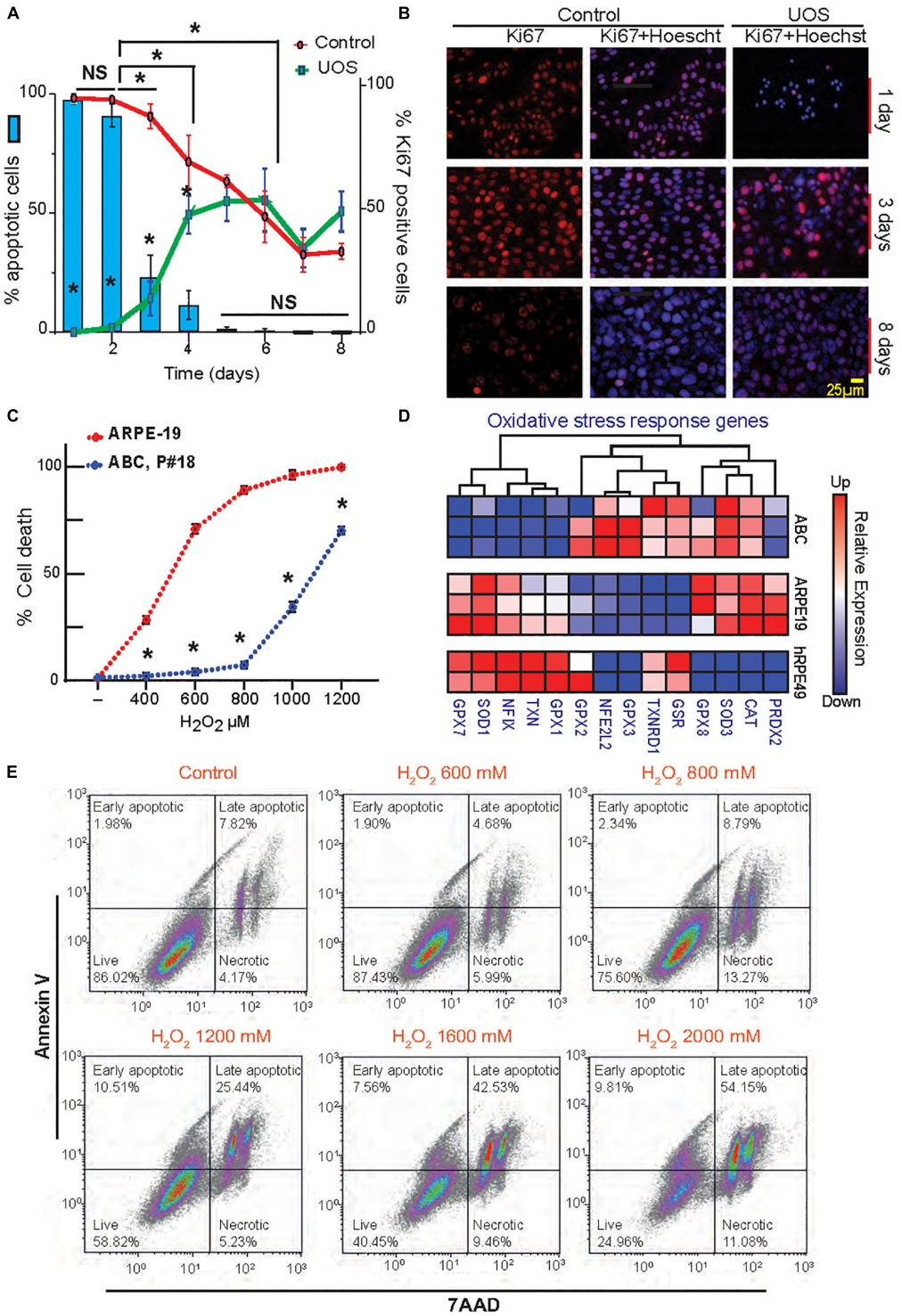

FIGURE 2 | Postmitotic ABC cells become resistant to UOS. **(A)** The expression of Ki67 in ABC cells is represented by green (UOS) and red (control) lines (right y-axis). Histogram shows cell death rate (left y-axis). **(B)** Representative images of Ki67 staining in ABC cells at different times. **(C)** ABC and ARPE-19 cells were exposed to various concentrations of H_2O_2. Apoptotic cell death was detected by Hoechst staining. Nine cells per well/four wells per condition were plotted. **(A,C)** Data were analyzed using two-way ANOVA and Tukey's HSD for pairwise comparisons. *$p < 0.05$. **(D)** RNAseq heatmap for expression levels of genes involved in the oxidative stress response for ABC, ARPE-19, and hRPE49 cells. **(E)** Evaluation of apoptosis and necrosis by flow cytometry relative to the increment in H_2O_2 concentration. Plots showing Annexin V vs. 7AAD signals were made (**Supplementary Figure 4E**) (100k events per condition). Four cell populations were analyzed in each experimental condition: 7-AAD+ cells for necrotic cells, 7AAD and Annexin V + cells for Late Apoptotic cells, Annexin V+ for Early apoptotic cells, and live cells negative for both 7AAD and Annexin V. Quadrants show the types of cell death detected differentiated by shape: Early and late apoptosis and necrosis.

the expression of genes related to inflammasome activation and autophagy, both of which have been widely implicated in the pathogenesis of AMD (Mitter et al., 2014; Celkova et al., 2015). Two different concentrations of H_2O_2 modulate the expression differentially (**Supplementary Figures 5**, **6**). NPD1 uniformly downregulated the expression of NLRP3 (3-fold), IL1B (4.2-fold), and IL23 (1.8-fold) when compared to cells undergoing UOS. Conversely, NPD1 augmented the expression of antioxidant and anti-inflammatory genes, SOD1 (2.1-fold), SOD2 (1.6-fold), and NRF2 (1.5-fold) in comparison to the UOS-only treated cells (**Figure 3B**). Then, RELB, cREL, and BIRC3 expressions were compared to define the mechanism of action of NPD1 in ABC cells (**Supplementary Figure 7B**). The distribution of cells expressing each gene exhibited bimodal expression patterns. NPD1 triggered the expression of RELB in a large population of cells compared to UOS alone or control. NPD1 brought up cREL expression to control levels in cells undergoing UOS and upregulated BIRC3 expression. Not all cells responded to the stress or NPD1, denoting a high heterogeneity in the response. The monophasic distribution of TFRC expression across the three conditions attested to the preservation of the transcriptional machinery in all the cells analyzed (**Supplementary Figure 7B**). To identify functional connections between the relevant genes, a protein-protein interaction network was constructed using the STRING database (**Figure 3C**; Szklarczyk et al., 2017). We used the top differentially expressed genes with P-values < 0.01 as inputs for the STRING database to determine the molecular network of interacting genes and to obtain correlations with a high probability confidence score ($\geq$0.900). The protein-protein interaction analysis performed using STRING indicated that the proteins differentially represented in ABC cells are highly correlated (P-value $<$ 1.04e-10). The results were significantly enriched with BIRC3 and TLR4 as the main nodes in the network.

Autophagy plays an important role in maintaining cellular homeostasis by eliminating damaged organelles and protein aggregates and by removing infectious agents from host cells (Cho and Hwang, 2012; Szatmári-Tóth et al., 2016; Harris et al., 2017). Defects in autophagic machinery generate sensitivity to oxidative stress conditions in RPE cells (Mitter et al., 2014), and it is associated with several disorders, including AMD (Kaarniranta et al., 2017) and neurodegenerative and infectious diseases (Jing and Lim, 2012). Furthermore, the interest in the components of this pathway is enhanced by the fact that RPE cells utilize part of the autophagy complexes to perform phagocytosis of the photoreceptor tip renewal (Mitter et al., 2014). To determine whether NPD1 affects autophagy, ABC cells undergoing UOS were treated with NPD1, and a panel of autophagy-related genes was evaluated using single-cell Real-Time PCR. NPD1 consistently restored the expression of autophagy-related genes to homeostatic levels in single ABC cells (**Figure 3D**). Beclin1 (BECN1), autophagy-related proteins 9A and 2 (ATG9A and ATG2A), which are regulatory parts of the PI3K complex and ATG9A system involved in the nucleation of the Phagophore, were downregulated in a subpopulation of cells by UOS and restored by NPD1 (**Figures 3D,E**, blue dash line). Similarly, ATG7 and ATG3, which are part of the LC3-conjugation system, are downregulated by UOS in a subpopulation and totally recovered by NPD1. Intriguingly, ATG10, ATG5, and ATG16L, which are contained in the ATG12-conjugation system, are downregulated by UOS in the majority of the cells since this complex is the main candidate for disruption by UOS and the levels are brought back to control levels but not in the totality of the cells. These two last complexes work on the conjugation of LC3 to the lipid phosphatidylethanolamine (PE) in the elongation step of the phagophore and the addition of LC3 to the endosome in the LC3 associate phagocytosis.

Therefore, NPD1 contributes to the resistance of ABC cells against UOS by modulating genes involved in inflammasome, apoptosis, antioxidant pathways, and autophagy.

Active Biosynthesis of VLC Fatty Acid Species Indicates an Outer Segment Cycle Renewal Mechanism Preservation Is Expressed in ABC Cells

During daily cycle renewal, the outer segments of the photoreceptors are phagocytized by the mammalian RPE cells, which in turn recycle visual pigment components and DHA in a circadian manner (Bok, 1993; Kolko et al., 2007; Bazan et al., 2010; Asatryan and Bazan, 2017). In fact, RPE cells are among the most phagocytic cells in the whole organism (Mazzoni et al., 2014). To evaluate phagocytosis, ABC and ARPE-19 cells were incubated with Fluorescein isothiocyanate (FITC)-labeled bovine POS or fluorescent polystyrene beads. Both cell types actively ingested these particles with relative fluorescence abundance higher in ABC cells compared to ARPE-19, especially for POS (**Figures 4A,B** and **Supplementary Figure 8**), suggesting that the phagocytic activity was greater in ABC cells. Confocal imaging, along with 3D rendering of human, rat, and bovine POS fed to confluent ABC cells, revealed their intracellular localization (**Figures 4C,D**). Additionally, opsin immunoblotting signal for both internal and total opsin on immunoblots increased with time, reaching its maximum at 16 h (**Figure 4E** and **Supplementary Figure 9**). There was a 4-fold increase in opsin internalization in ABC cells compared to ARPE-19 cells (**Figures 4A,E**). To further confirm the findings, the uptake of labeled bovine POS was analyzed using flow cytometry and 7AAD counterstaining to detect viable cells. The majority of viable cells were POS-positive (**Figure 4F**, bottom right, **Figure 4G**). The gating for Hoechst signal to separate debris from cells and for FITC signal to detect endocytosed labeled POS peak shifted when ABC cells fed with POS were compared to control (**Figure 4G**), implying that the majority of FITC-POS have been phagocytized and internalized.

Phagocytosis triggers the biosynthesis of protective lipid messengers that have an autocrine effect on RPE cells (Mukherjee et al., 2007). In ABC cells exposed to 1200 μM H_2O_2, the phagocytosis of POS attenuated UOS-induced apoptosis (**Figure 4H**). Flow cytometry was used to determine

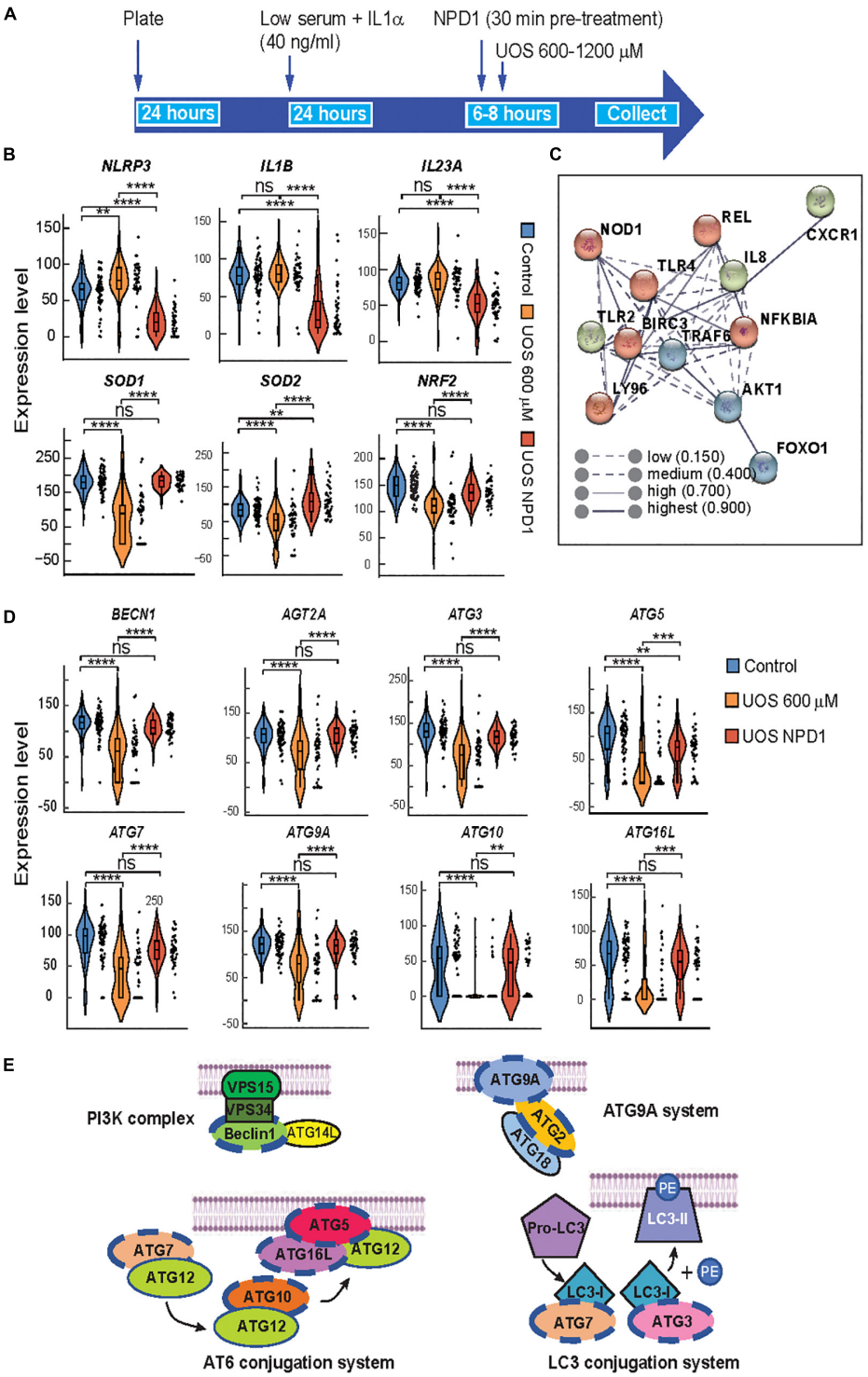

FIGURE 3 | Autophagy and survival signaling are restored by NPD1 in ABC cells undergoing UOS. **(A)** Timeline of experiment for single-cell RT-PCR using Fluidigm Biomark. **(B)** Violin plots showing the expression of inflammasome-related genes. **(C)** STRING interaction network was generated for differentially expressed genes for NPD1-treated cells, showing high correlation and clustering of target genes involved in response to inflammation. **(D)** Violin plots showing autophagy-related genes. Y-axis illustrates the relative expression level for each gene. Each black dot at the right of the violin plots depicts a single-cell gene expression. One-way ANOVA was performed with the *Post Hoc* Tukey HSD test for multiple comparisons. $*p < 0.05$; $**p < 0.01$; $***p < 0.001$; $****p < 0.0001$. **(E)** Regulated genes tested by single-cell RT-PCR are involved in autophagy corresponding to the four depicted complexes that regulate the formation of the phagophore. Genes modulated by NPD1 are marked with a blue dashed line.

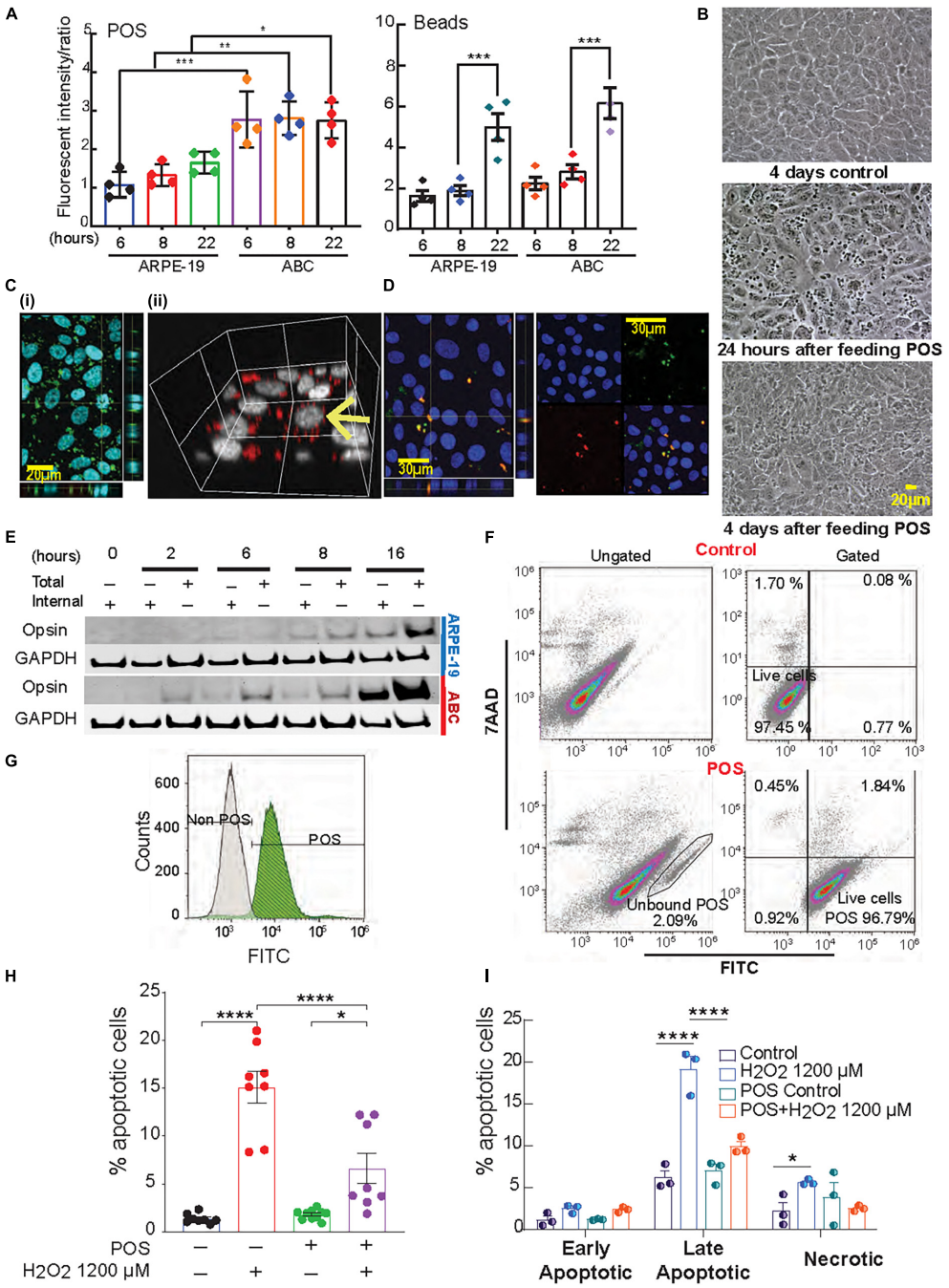

FIGURE 4 | Phagocytosis activity in ABC is higher than ARPE-19 cells. **(A)** Phagocytosis of photoreceptor outer segments (POS) or polystyrene microspheres (beads) by ARPE-19 and ABC cells over time. Confocal microscopy was used to analyze bound and internalized FITC-labeled POS or fluorescent beads (**Supplementary Figure 8**). The ratio of relative fluorescence intensities was determined by measuring total fluorescence intensity of the green signal from the added material (beads or POS) over the total blue signal (Hoechst). **(B)** Live images showing ABC cells fed with and without POS. **(C)** Confocal images (z-stacks) of ABC cells show uptake of **(i,ii)** human POS and **(D)** rat photoreceptor outer segments; orthogonal view displays co-localization of the FITC labeled POS (green) and opsin (red). **(E)** Immunoblots with opsin antibody against the lysates of ABC and ARPE19 cells fed with bovine POS (**Supplementary Figure 9** shows two independent biological whole membrane western blots). **(F,G)** Assessment of POS phagocytosis in ABC cells by flow cytometry. After gating out cell debris and doublets (**Supplementary Figure 4A**), and not bound/internalized POS **(F**, bottom left) in control or cells exposed to FITC-POS, 7AAD versus FITC signals were obtained (**F**, Gated, 100,000 events per condition were assessed). The great majority of viable cells (7AAD negative cell population) are POS + (bottom right). **(G)** Analysis of FITC signal alone showed a shift in the peak of it in ABC cells fed with FITC-labeled POS compared to one of the control ABC cells (white). **(H,I)** Quantitative analysis of Hoechst-stained ABC cells by fluorescence microscopy of POS phagocytosis effects on apoptotic cell population after oxidative stress. **(H)** Analysis of apoptosis by Hoechst staining. **(I)** Quatification of panel **(F)**. **(A,H,I)** One Way ANOVA and Tukey's HSD for pairwise comparisons was applied. Results represent averages ± SEM of repeats of at least three independent experiments. *$p < 0.05$; **$p < 0.01$; ***$p < 0.001$; ****$p < 0.0001$.

the populations of early, late apoptosis, and necrotic cells for the different treatments. Compared to control only, cells incubated with POS under UOS conditions exhibited a negligible amount of necrosis and early apoptosis. Late apoptosis was the predominant form, and the population was significantly smaller than the cells undergoing UOS alone (**Figure 4I**).

ABC and ARPE-19 cells were then fed with bovine POS at a 1:10 ratio (cell:POS), and their membrane lipidome was screened using LC-MS/MS and MALDI. Principal component analysis (PCA) indicate that phosphatidylcholine (PC), phosphatidylethanolamine (PE), and phosphatidylserine (PS) species form distinctive clusters differentiating cell type and presence or absence of POS (**Figures 5A–C**). Random forest PL analysis confirmed differences (**Supplementary Figure 10A**). Moreover, phospholipids with DHA and VLC-PUFAs, lipids that are not considered integral to their membranes, were found in ABC cells after phagocytizing POS (**Figures 5D–F**). ARPE-19 cells fed with POS increased PL species containing DHA and VLC-PUFAs to a lesser extent than the ABC cells (**Figures 5D–F**). The main two phospholipids in the eyes and brain are phosphatidylcholine and phosphatidylethanolamine. Some species in all three types of PL were found to contain docosahexaenoic acid (DHA) of 22 carbons and 6 double bonds (22:6) and arachidonic acid (AA) of 20 carbons and 4 double bonds and other fatty acids omega 6 backbones (**Figures 5D,F**). Species of PE containing AA were more abundant in ARPE-19 despite whether they had undergone phagocytosis of POS or not (**Figure 5E**). PC species contain a fatty acid of 32 carbons and 6 double bonds (32:6), a precursor of Elovanoid 32, in addition to DHA (**Figure 5D**). PE and PS both depict species with two DHA molecules, one in sn1 and the other in sn2 (**Figures 5E,F**). In all the cases except PC(18:0; 22:6) and PE(20:0; 22:6), species containing DHA were increased in ABC cells above the levels observed on ARPE-19 after being fed POS. AdipoR1 and MFRP, contribute to the conservation of DHA in the retina (Rice et al., 2015; Kautzmann et al., 2020). The two genes are expressed in ABC, ARPE-19, and hRPE49 cells, with a higher basal expression of AdipoR1 in ABC cells (**Figure 5G**). ABC cells were then incubated for 32 h in the presence of deuterated DHA to determine the incorporation of the fatty acid into the phospholipids (**Figure 5H**). PE species showed an increase in deuterated DHA content steeper than PCs when species containing 18:1 and 22:6 were measured as representative phospholipids (**Figure 5H**). To compare the two cell types imaged by MALDI IMS, a difference spectrum was constructed, subtracting the ARPE-19 cell profile from the ABC cell profile (**Figure 5I**). The resulting relative plots emphasized lipid abundance, with the prevalent ABC cell lipids (pointing up) and the ARPE-19 lipids as downward peaks. DHA−containing PC [m/z 834, PC (18:0/22:6)] was more prevalent in the ABC cells compared to ARPE-19 cells, whereas PC [m/z 798, PC(16:0/18:1)K^+ and m/z 782 PC(16:0/18:1)Na^+] was enhanced in the other cell types. Image extraction of specific m/z (m/z 603, 739, 754, and 732) from the whole lipid spectrum allowed us to visualize the relative intensity difference between the ABC and ARPE-19 cells (**Figure 5I**, right panel). Overall, this comparison suggests that the ABC cells have a lipid-membrane composition enriched in DHA-containing PLs.

Inhibition of mTOR Explains Why ABC Cells Do Not Become Senescent, a Key Event in AMD

Senescence plays a major role in tumor suppression, aging, tissue repair, and embryonic development (Cho and Hwang, 2012; Leontieva et al., 2014; Sun, 2014). Senescence occurs in two steps of cell arrest, which is common to quiescence, and geroconversion, which makes senescence irreversible (Blagosklonny, 2014). Contact inhibition is a form of quiescence where cell growth is arrested by contact, and it can be reversed when cells are passaged at low density. Pathways associated with geroconversion are p53 and mTOR (Blagosklonny, 2018), while consequences of the decreased senescent program can be noted by the downregulation of IL-8 signaling and PTEN signaling (Jung et al., 2019; **Figure 6A**). Suppression of mTOR is associated with contact inhibition in normal cells, including RPE cells (Cho and Hwang, 2012; Leontieva et al., 2014). mTOR pathway activation favors senescence gene programming and expression of the senescence-associated secretory phenotype (SASP), consisting of inflammatory cytokines (IL-1β, IL-6, or IL-8), growth factors, and proteases (Di Micco et al., 2021). The comparison between the expression signatures of ABC vs. ARPE-19 and hRPE49 vs. ARPE-19 using IPA depicted a reduced neuroinflammatory signaling pathway for the ABC cells (**Figure 6A**). Moreover, decreased glycolysis, gluconeogenesis, and lipolysis suggest that fully confluent ABC cells stop dividing and require less energy to sustain survival than ARPE-19 cells, which do not stop growing and dividing even after becoming confluent, therefore, requiring substantial energy (**Figure 6A**). Except for three of the genes plotted, the remaining mRNAs belonging to the mTOR pathway were downregulated in ABC cells in comparison to the other two cell lines inhibited in our data set, which coincides with the IPA prediction (**Figures 6B,C**; **Supplementary Figure 10B**). Low energy in the cell results in phosphorylation and activation of the TSC2/TSC1 complex formation, yielding inactivation of RHEB and, thus, inactivation of mTOR (**Figures 6C,E**). These results suggest that ABC cells develop a state of contact inhibition but not senescence when they become fully confluent. The senescence SASP network, like IL-1β and IL-6, are downregulated in ABC, and SIRT1 is upregulated (Xu et al., 2020), which marks the note that senescence is reduced in ABC cells (**Figure 6D** and **Supplementary Figure 10B**). In addition, mTOR signaling acts as an initiator of autophagy, and it is involved in the LC3-conjugation for the maturation of the phagosome in the LC3-associated phagocytosis (**Figures 6E,4E**; Intartaglia et al., 2021). Therefore, ABC cells display phenotypical, genetic, and functional characteristics that resemble the native pigment epithelium of the retina, in which the processes and signaling pathways convey the main cellular tasks that define the normal dynamics of the tissue.

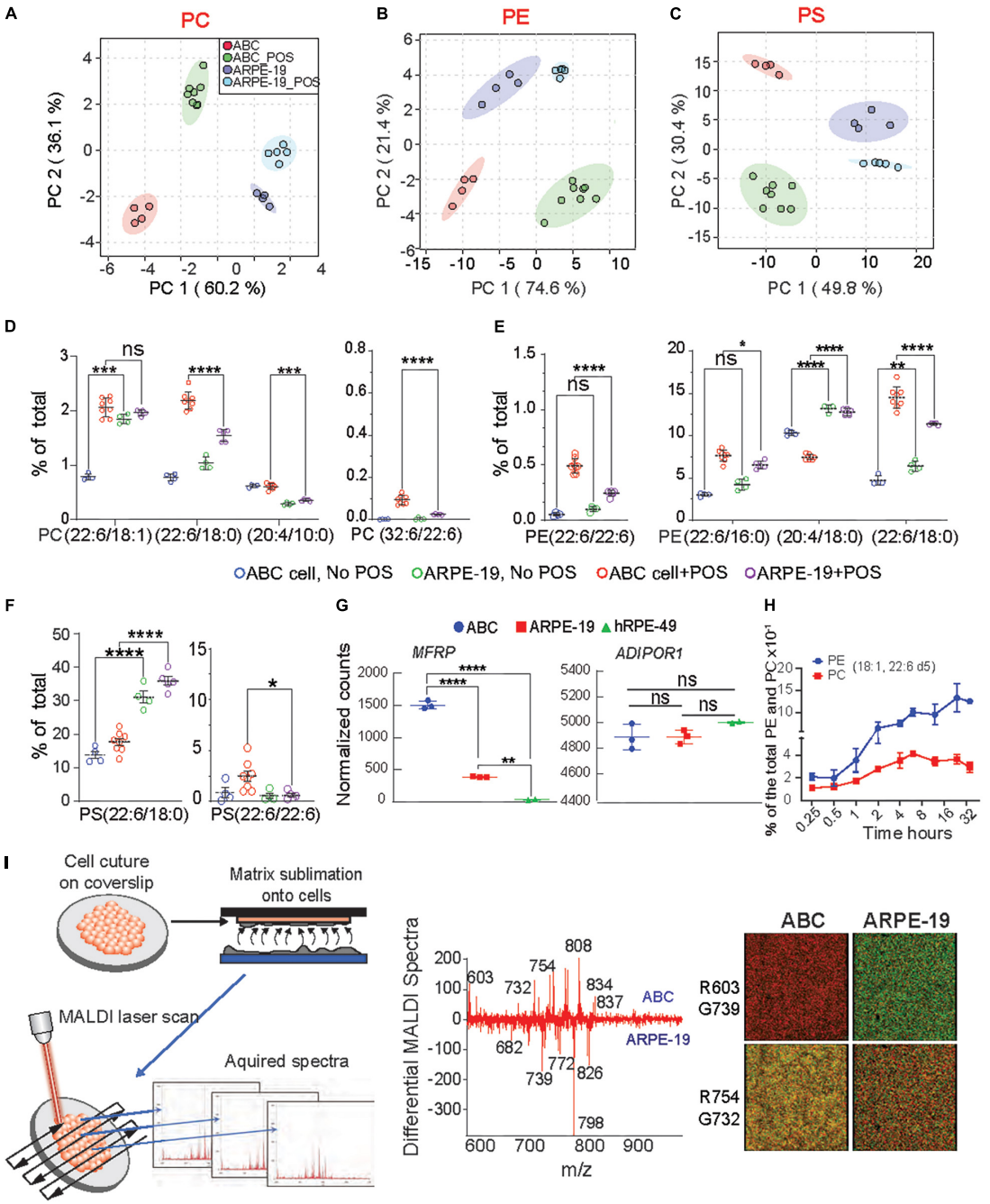

FIGURE 5 | Enhanced incorporation and synthesis of phospholipids containing very-long-chain fatty acids in ABC cells. **(A–C)** Principle component analysis (PCA) were performed for PC, PE, and PS phospholipid species for ABC cells, and ARPE-19 cells after phagocytosis of POS. **(D–F)** LC-MS/MS quantitative distributions in bar graphs for ABC vs. ARPE-19 lipid species with and w/o POS feeding shows the most abundant PLs species found in the cells after feeding, containing either DHA and VLC-PUFAs (iv) or double DHA (iii). Tukey's HSD *post hoc* testing was performed for two-factor ANOVA $^{****}p < 0.0005$, $^{***}p < 0.005$, $^{**}p < 0.05$, $^{*}p < 0.01$. **(G)** RNA sequencing analysis showing normalized counts for *MFRP* and *ADIPOR1* gene expression for each cell type. **(H)** ABC cells fed with deuterated DHA for up to 32 h were analyzed using LC-MS/MS. Line graphs showing two of the most abundant PL species (18:1, 22:6) containing DHA-d5 from ABC cell lysates, demonstrating the ability of the ABC cells to incorporate 22:6. **(I)** MALDI lipidomic comparative analysis. Coverslips with cells were attached to MALDI plates and then placed within the sublimation chamber, where matrix (2,5-dihydroxybenzoic acid, DHB) was applied for positive ion mode analysis. Sections were then rasterized by laser, 355 nm, 2000 Hz Scanning control (15 μm, horizontal and vertical movement) and analyzed. **(Middle panel)** Differential spectra show relative abundance of lipid molecular species detected by MALDI IMS based on the cell type. Molecules more abundant in ABC cells are presented in the upper part of the graph, while molecules more abundant in ARPE-19 are displayed at the bottom; m/z 834 corresponding to PC containing DHA (PC (18:0/22:6) was more abundant in ABC cells than in ARPE-19 cells. PC (16:0/18:1) with K + adduct (m/z 798) was the most dominant molecule in ARPE-19. **(Right panel)** Bicolor (red and green) image composition of lipid signals from MALDI IMS extracted from the cells and generated with positive ion mode. Same m/z shows different abundance from one cell type to another.

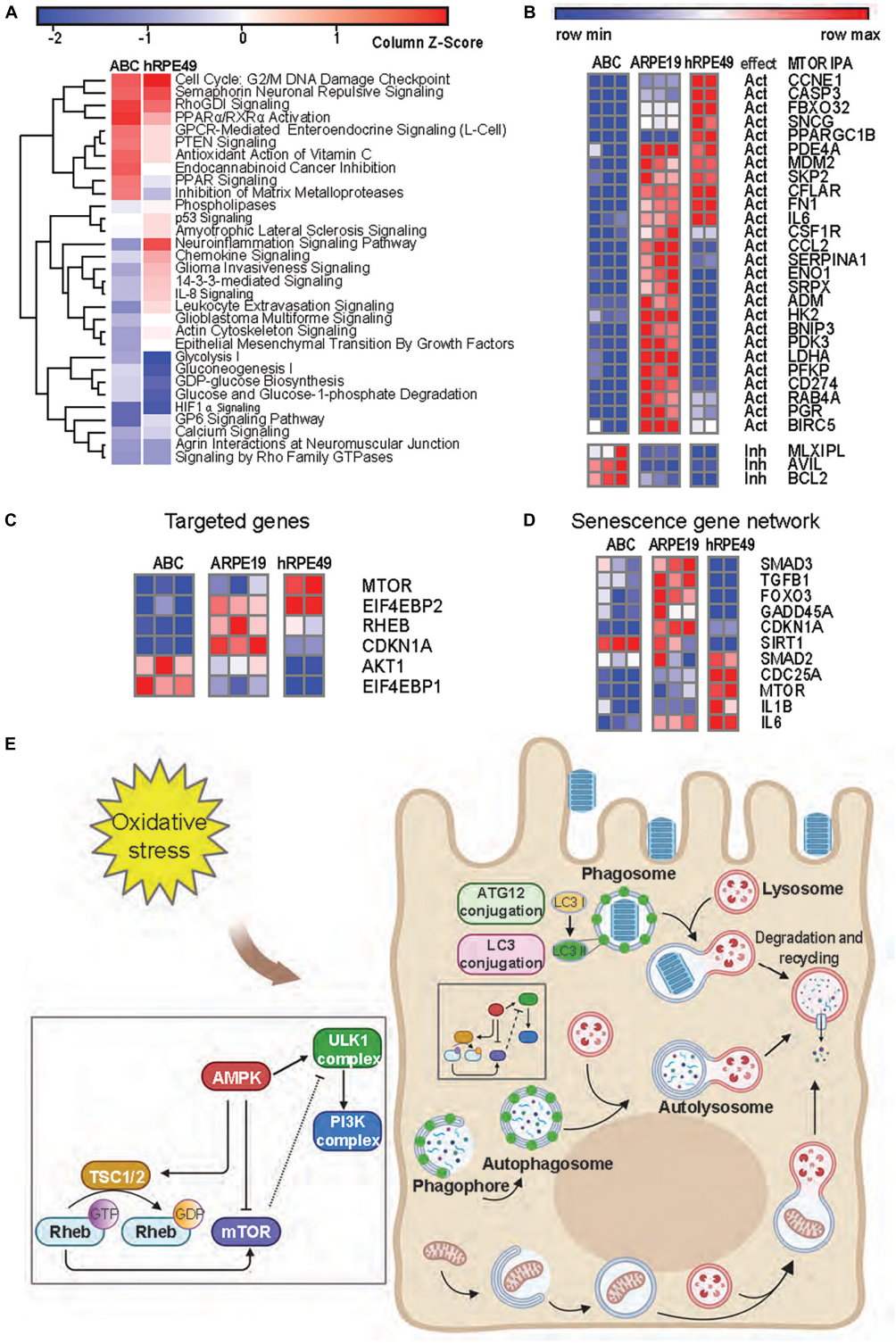

FIGURE 6 | mTOR signaling is reduced in ABC cells as compared to ARPE-19 cells. **(A)** Heatmap from RNA seq analysis of ARPE-19 cells compared to ABC and hRPE49 cells showing canonical pathways with the most significant changes. IPA analysis was performed using ARPE-19 cells as control. Red color means the pathway is upregulated when compared with ARPE19, while blue means it is downregulated. **(B)** Comparative heatmap representation of RNA seq data of mTOR downstream signaling genes (**Supplementary Figure 10** shows IPA network). The expected effect of mTOR on its downstream targets is labeled as "Act" for activation and "Inh" for inhibition. **(C)** Analysis of genes involved in geroconversion and autophagy activation by mTOR signaling and its related genes. **(D)** Heatmap analysis of genes involved in senescence. **(E)** Autophagy pathways in RPE cells.

DISCUSSION

We have developed a human RPE cell that recapitulates native features of those cells in the human eye. RPE cells are essential for photoreceptor functions and integrity, and our cell line provides opportunity to discern the fundamental properties and potential of this cell.

ABC cells become quiescent at 100% confluency due to contact inhibition (**Figure 2A**), and due to a decreased mTOR pathway activity, they resume growing if replating at lower densities. Two opposing events arise in primary RPE (hRPE49) and ARPE-19 cells. The former stop dividing, become senescent, and die when they reach 100% confluency, while ARPE-19 cells sustain viability for many weeks, even at post-confluency. The mechanisms behind this difference can be explained on the basis of mTOR signaling. Cellular senescence is triggered by many stimuli, including telomere attrition and DNA damage, oxidative stress, oncogene activation, and deactivation of tumor suppressor genes. Senescence plays a major role in tumor suppression, aging, tissue repair, and embryonic development (Cho and Hwang, 2012; Leontieva et al., 2014; Sun, 2014). The key feature of senescence is irreversibility, in contrast with quiescence from growth factor deprivation, which can be reversed. Contact inhibition is a form of quiescence where cell growth is arrested due to cells in contact with each other once high density is achieved. Then cells resume division when passaged and cultured at low density. The mTOR pathway is critical for geroconversion, the conversion of reversible cell cycle arrest to senescence (Leontieva et al., 2014). Suppression of mTOR is associated with contact inhibition in normal cells, including RPE cells (Cho and Hwang, 2012; Leontieva et al., 2014). mTOR pathway activation favors senescence gene programming and expression of the senescence-associated secretory phenotype (SASP), consisting of inflammatory cytokines (IL-1β, IL-6, or IL-8), growth factors, and proteases (Di Micco et al., 2021). The canonical pathways for the ARPE-19 transcriptomic dataset obtained by RNAseq were compared to ABC and hRPE49 datasets, and reduced glycolysis, gluconeogenesis, and lipolysis were found, suggesting that the fully confluent ABC cells stop division, requiring less energy to survive than ARPE-19 cells. On the other hand, ARPE-19, which do not stop growing even after becoming confluent, require substantial energy to thrive (**Figure 6A**). Consistent with this observation, the mTOR pathway is downregulated in ABC cells compared to ARPE-19 or hRPE49 cells (**Figures 6B–D**), while the Tuberous Sclerosis Complex 2 (TSC2) pathway is activated (**Figure 6C**). Twenty-six out of 29 genes in the mTOR pathway were inhibited (**Figures 6B,C**). Low energy in the cell results in phosphorylation and activation of the TSC2/TSC1 complex formation, yielding inactivation of RHEB and, thus, inactivation of mTOR (**Figure 6E**). This pathway is central for cellular growth and promotes translation by acting on eukaryotic initiation factor 4E (elF-4E), which needs to form complexes to activate the translation of cap-mRNA. Once 4E is associated with BP1, it is inhibited. Intriguingly, the mTOR activation is intrinsically involved in the initiation of LC3-conjugation leading to autophagy and LC3-associated phagocytosis (**Figures 4E**, **6E**) related to the phagocytosis of the POS, and signaling here comes full circle (Intartaglia et al., 2021). mTOR signaling activation/deactivation equilibrium is of importance in the survival of the retinal pigment epithelium (Zhang et al., 2021) and the reduced gene expression of their component in ABC cells allows them to upregulate the mechanism on demand when the cell needs to, for instance, activate phagocytosis, a process that is not perturbed in this cell line (**Figure 4**).

The ability of ABC cells to form monolayers resembling the native retinal pigment epithelium is demonstrated by their formation of microvilli (**Figures 1F,G**), functional tight junctions that stop the passive diffusion of trypan blue (**Figure 1H**), and honeycomb packing culture (**Figures 1A,E,I**). RNAseq comparing ARPE-19 and ABC, both cell lines derived from 19-years-old Caucasian male donors, evidences significant differences in several important pathways related to senescence, inflammation, oxidative stress response, as well as markers of native RPE, which were more represented in ABC than in the first mention cell line. In regard to the oxidative stress response, ARPE-19 are more susceptible to cell death upon exposure to lower concentrations of H_2O_2 than ABC. The commercially available lowest passage for ARPE-19 is P19. At this passage, ABC undergo contact inhibition without stepping into senescence. ARPE-19, which were spontaneously immortalized (Dunn et al., 1998), displayed a reduced MET transition and Mesenchimal signaling that evidenced a stable RPE phenotype (**Figure 1B**). iRPE cells are a new development to model genetic diseases, such as L-ORD (Miyagishima et al., 2021), as well as expensive, time-consuming, and require expertise. Although this cell line offers several benefits, there are also certain limitations such as gender bias. The male origin of the cells may predispose the culture to enhance sensitivities, especially to steroids like testosterone (Penaloza et al., 2009). Our group is currently working to obtain a mirror culture originating from female donors. During embryonary stages, RPE cells originate from neuroectoderm, following common steps in the differentiation until reaching its final form, an epithelial-type cell. For this reason, RPE cells share many features with astrocytes and neurons (Bharti et al., 2011). This similarity was used to convert RPE cells into photoreceptors, a specialized type of neuron (Liang et al., 2006). Currently, exploration of this alternative from iPS cells is underway (Shrestha et al., 2020), and transdifferentiation of RPE cells, such as our ABC cells, into photoreceptors may offer a simpler option for cellular replacement therapies.

DATA AVAILABILITY STATEMENT

The original contributions presented in this study are included in the article/**Supplementary Material**, further inquiries can be directed to the corresponding author/s.

AUTHOR CONTRIBUTIONS

NB conceived the study. NB, AA, and JC designed the experiments and wrote the manuscript. JC generated the

hRPE49 cell line. JC and AA analyzed the data. AA conducted the IHC experiments. M-AK conducted the beads and POS phagocytosis experiments and MALDI analysis. M-AK, JH, and AA performed the single-cell experiments. AA and BJ conducted the LC−MS/MS experiments. AA, BJ, and TP analyzed the resulting data. WG executed the bright field histology. KD performed the Ki67 analysis, the protein and gene expression phenotyping of the cells, and protein analysis of the phagocytosis experiment. VB and AA conducted the experiments for the POS phagocytosis and challenge with UOS. MVM analyzed the resulting data. SB and TP made the RNAseq gene analysis. JC, WG, M-AK, and NB edited the manuscript with input from all other authors. All authors have read and approved the manuscript.

FUNDING

This work was supported by the National Institutes of Health (NIH)/National Eye Institute (NEI) grant R01 EY005121 and the Eye Ear Nose & Throat (EENT) Foundation of New Orleans, both awarded to NB.

SUPPLEMENTARY MATERIAL

The Supplementary Material for this article can be found online at: https://www.frontiersin.org/articles/10.3389/fnins.2022.926629/full#supplementary-material

REFERENCES

Al-Hussaini, H., Kam, J. H., Vugler, A., Semo, M., and Jeffery, G. (2008). Mature retinal pigment epithelium cells are retained in the cell cycle and proliferate in vivo. *Mol. Vis.* 14, 1784–1791.

Asatryan, A., and Bazan, N. G. (2017). Molecular mechanisms of signaling via the docosanoid neuroprotectin D1 for cellular homeostasis and neuroprotection. *J. Biol. Chem.* 292, 12390–12397. doi: 10.1074/jbc.R117.783076

Audo, I., Mohand-Said, S., Boulanger-Scemama, E., Zanlonghi, X., Condroyer, C., Démontant, V., et al. (2018). MERTK mutation update in inherited retinal diseases. *Hum. Mutat.* 39, 887–913. doi: 10.1002/humu.23431

Bazan, N. G. (2006). Cell survival matters: docosahexaenoic acid signaling, neuroprotection and photoreceptors. *Trends Neurosci.* 29, 263–271. doi: 10.1016/j.tins.2006.03.005

Bazan, N. G. (2007). Homeostatic regulation of photoreceptor cell integrity: significance of the potent mediator neuroprotectin D1 biosynthesized from docosahexaenoic acid: the Proctor Lecture. *Invest. Ophthalmol. Vis. Sci.* 48, 4866–4881. biography 4864-4865. doi: 10.1167/iovs.07-0918

Bazan, N. G., Calandria, J. M., and Serhan, C. N. (2010). Rescue and repair during photoreceptor cell renewal mediated by docosahexaenoic acid-derived neuroprotectin D1. *J. Lipid Res.* 51, 2018–2031. doi: 10.1194/jlr.R001131

Bazan, N. G., Reddy, T. S., Redmond, T. M., Wiggert, B., and Chader, G. J. (1985). Endogenous fatty acids are covalently and noncovalently bound to interphotoreceptor retinoid-binding protein in the monkey retina. *J. Biol. Chem.* 260, 13677–13680.

Bharti, K., Miller, S. S., and Arnheiter, H. (2011). The new paradigm: retinal pigment epithelium cells generated from embryonic or induced pluripotent stem cells. *Pigment. Cell Melanoma. Res.* 24, 21–34. doi: 10.1111/j.1755-148X.2010.00772.x

Blagosklonny, M. V. (2014). Geroconversion: irreversible step to cellular senescence. *Cell Cycle* 13, 3628–3635. doi: 10.4161/15384101.2014.985507

Blagosklonny, M. V. (2018). Rapamycin, proliferation and geroconversion to senescence. *Cell Cycle* 17, 2655–2665. doi: 10.1080/15384101.2018.1554781

Bok, D. (1993). The retinal pigment epithelium: a versatile partner in vision. *J. Cell Sci. Suppl.* 17, 189–195. doi: 10.1242/jcs.1993.supplement_17.27

Boulton, M. E. (2014). Studying melanin and lipofuscin in RPE cell culture models. *Exp. Eye Res.* 126, 61–67. doi: 10.1016/j.exer.2014.01.016

Calandria, J. M., Asatryan, A., Balaszczuk, V., Knott, E. J., Jun, B. K., Mukherjee, P. K., et al. (2015). NPD1-mediated stereoselective regulation of BIRC3 expression through cREL is decisive for neural cell survival. *Cell Death Differ.* 22, 1363–1377. doi: 10.1038/cdd.2014.233

Calandria, J. M., Marcheselli, V. L., Mukherjee, P. K., Uddin, J., Winkler, J. W., Petasis, N. A., et al. (2009). Selective Survival Rescue in 15-Lipoxygenase-1-deficient Retinal Pigment Epithelial Cells by the Novel Docosahexaenoic Acid-derived Mediator. neuroprotectin D1. *J. Biol. Chem.* 284, 17877–17882. doi: 10.1074/jbc.M109.003988

Calandria, J. M., Mukherjee, P. K., de Rivero Vaccari, J. C., Zhu, M., Petasis, N. A., and Bazan, N. G. (2012). Ataxin-1 Poly(Q)-induced Proteotoxic Stress and Apoptosis Are Attenuated in Neural Cells by Docosahexaenoic Acid-derived Neuroprotectin D1. *J. Biol. Chem.* 287, 23726–23739. doi: 10.1074/jbc.M111.287078

Celkova, L., Doyle, S. L., and Campbell, M. (2015). NLRP3 Inflammasome and Pathobiology in AMD. *J. Clin. Med.* 4, 172–192. doi: 10.3390/jcm4010172

Chen, Y., Yang, J., Geng, H., Li, L., Li, J., Cheng, B., et al. (2019). Photoreceptor degeneration in microphthalmia (Mitf) mice: partial rescue by pigment epithelium-derived factor. *Dis. Model Mech.* 12:dmm035642. doi: 10.1242/dmm.035642

Cho, S., and Hwang, E. S. (2012). Status of mTOR activity may phenotypically differentiate senescence and quiescence. *Mol. Cells* 33, 597–604. doi: 10.1007/s10059-012-0042-1

Choudhary, P., Dodsworth, B. T., Sidders, B., Gutteridge, A., Michaelides, C., Duckworth, J. K., et al. (2015). A FOXM1 Dependent Mesenchymal-Epithelial Transition in Retinal Pigment Epithelium Cells. *PLoS One* 10:e0130379. doi: 10.1371/journal.pone.0130379

Detrick, B., and Hooks, J. J. (2020). "The RPE Cell and the Immune System," in *Retinal Pigment Epithelium in Health and Disease*, eds A. K. Klettner and S. Dithmar (Cham: Springer International Publishing), 101–114. doi: 10.1007/978-3-030-28384-1_6

Di Micco, R., Krizhanovsky, V., Baker, D., d'Adda, and di Fagagna, F. (2021). Cellular senescence in ageing: from mechanisms to therapeutic opportunities. *Nat. Rev. Mol. Cell Biol.* 22, 75–95. doi: 10.1038/s41580-020-00314-w

Do, K. V., Kautzmann, M.-A. I., Jun, B., Gordon, W. C., Nshimiyimana, R., Yang, R., et al. (2019). Elovanoids counteract oligomeric β-amyloid-induced gene expression and protect photoreceptors. *PNAS* 116, 24317–24325. doi: 10.1073/pnas.1912959116

Dunn, K. C., Aotaki-Keen, A. E., Putkey, F. R., and Hjelmeland, L. M. (1996). ARPE-19, a human retinal pigment epithelial cell line with differentiated properties. *Exp Eye Res.* 62, 155–169. doi: 10.1006/exer.1996.0020

Dunn, K. C., Marmorstein, A. D., Bonilha, V. L., Rodriguez-Boulan, E., Giordano, F., and Hjelmeland, L. M. (1998). Use of the ARPE-19 cell line as a model of RPE polarity: basolateral secretion of FGF5. *Invest Ophthalmol. Vis. Sci.* 39, 2744–2749.

Golestaneh, N., Chu, Y., Xiao, Y.-Y., Stoleru, G. L., and Theos, A. C. (2017). Dysfunctional autophagy in RPE, a contributing factor in age-related macular degeneration. *Cell Death Dis.* 8, e2537. doi: 10.1038/cddis.2016.453

Gordon, W. C., Rodriguez, de Turco, E. B., and Bazan, N. G. (1992). Retinal pigment epithelial cells play a central role in the conservation of docosahexaenoic acid by photoreceptor cells after shedding and phagocytosis. *Curr. Eye Res.* 11, 73–83. doi: 10.3109/02713689209069169

Guziewicz, K. E., Cideciyan, A. V., Beltran, W. A., Komáromy, A. M., Dufour, V. L., Swider, M., et al. (2018). BEST1 gene therapy corrects a diffuse retina-wide microdetachment modulated by light exposure. *Proc. Natl. Acad. Sci. U.S.A.* 115, E2839–E2848. doi: 10.1073/pnas.1720662115

Harris, J., Lang, T., Thomas, J. P. W., Sukkar, M. B., Nabar, N. R., and Kehrl, J. H. (2017). Autophagy and inflammasomes. *Mol. Immunol.* 86, 10–15. doi: 10.1016/j.molimm.2017.02.013

He, C., and Klionsky, D. J. (2009). Regulation mechanisms and signaling pathways of autophagy. *Annu. Rev. Genet.* 43, 67–93. doi: 10.1146/annurev-genet-102808-114910

Housset, M., Samuel, A., Ettaiche, M., Bemelmans, A., Béby, F., Billon, N., et al. (2013). Loss of Otx2 in the adult retina disrupts retinal pigment epithelium function, causing photoreceptor degeneration. *J. Neurosci.* 33, 9890–9904. doi: 10.1523/JNEUROSCI.1099-13.2013

Inana, G., Murat, C., An, W., Yao, X., Harris, I. R., and Cao, J. (2018). RPE phagocytic function declines in age-related macular degeneration and is rescued by human umbilical tissue derived cells. *J Transl. Med.* 16:63. doi: 10.1186/s12967-018-1434-6

Intartaglia, D., Giamundo, G., and Conte, I. (2021). Autophagy in the retinal pigment epithelium: a new vision and future challenges. *FEBS J.* [Epub ahead of print] doi: 10.1111/febs.16018

Ishida, M., Lui, G. M., Yamani, A., Sugino, I. K., and Zarbin, M. A. (1998). Culture of human retinal pigment epithelial cells from peripheral scleral flap biopsies. *Curr. Eye Res.* 17, 392–402. doi: 10.1080/02713689808951220

Jing, K., and Lim, K. (2012). Why is autophagy important in human diseases? *Exp. Mol. Med.* 44, 69–72. doi: 10.3858/emm.2012.44.2.028

Jung, S. H., Hwang, H. J., Kang, D., Park, H. A., Lee, H. C., Jeong, D., et al. (2019). mTOR kinase leads to PTEN-loss-induced cellular senescence by phosphorylating p53. *Oncogene* 38, 1639–1650. doi: 10.1038/s41388-018-0521-8

Kaarniranta, K., Tokarz, P., Koskela, A., Paterno, J., and Blasiak, J. (2017). Autophagy regulates death of retinal pigment epithelium cells in age-related macular degeneration. *Cell Biol. Toxicol.* 33, 113–128. doi: 10.1007/s10565-016-9371-8

Kautzmann, M.-A. I., Gordon, W. C., Jun, B., Do, K. V., Matherne, B. J., Fang, Z., et al. (2020). Membrane-type frizzled-related protein regulates lipidome and transcription for photoreceptor function. *FASEB J.* 34, 912–929. doi: 10.1096/fj.201902359R

Knott, E. J., Sheets, K. G., Zhou, Y., Gordon, W. C., and Bazan, N. G. (2011). Spatial correlation of mouse photoreceptor-RPE thickness between SD-OCT and histology. *Exp. Eye Res.* 92, 155–160. doi: 10.1016/j.exer.2010.10.009

Kolko, M., Wang, J., Zhan, C., Poulsen, K. A., Prause, J. U., Nissen, M. H., et al. (2007). Identification of intracellular phospholipases A2 in the human eye: involvement in phagocytosis of photoreceptor outer segments. *Invest. Ophthalmol. Vis. Sci.* 48:1401. doi: 10.1167/iovs.06-0865

Lakkaraju, A., Umapathy, A., Tan, L. X., Daniele, L., Philp, N. J., Boesze-Battaglia, K., et al. (2020). The cell biology of the retinal pigment epithelium. *Prog. Retin. Eye Res.* 24:100846. doi: 10.1016/j.preteyeres.2020.100846

Leontieva, O. V., Demidenko, Z. N., and Blagosklonny, M. V. (2014). Contact inhibition and high cell density deactivate the mammalian target of rapamycin pathway, thus suppressing the senescence program. *PNAS* 111, 8832–8837. doi: 10.1073/pnas.1405723111

Liang, L., Yan, R.-T., Ma, W., Zhang, H., and Wang, S.-Z. (2006). Exploring RPE as a source of photoreceptors: differentiation and integration of transdifferentiating cells grafted into embryonic chick eyes. *Invest Ophthalmol. Vis. Sci.* 47, 5066–5074. doi: 10.1167/iovs.06-0515

Liu, Z., Zheng, W. J., Allen, G. I., Liu, Y., Ruan, J., and Zhao, Z. (2017). The International Conference on Intelligent Biology and Medicine (ICIBM) 2016: from big data to big analytical tools. *BMC Bioinform.* 18:405. doi: 10.1186/s12859-017-1797-3

Ma, X., Li, H., Chen, Y., Yang, J., Chen, H., Arnheiter, H., et al. (2019). The transcription factor MITF in RPE function and dysfunction. *Prog. Retin Eye Res.* 73:100766. doi: 10.1016/j.preteyeres.2019.06.002

Mao, Y., and Finnemann, S. C. (2013). Analysis of Photoreceptor Outer Segment Phagocytosis by RPE Cells in Culture. *Methods Mol. Biol.* 935, 285–295. doi: 10.1007/978-1-62703-080-9_20

Mazzoni, F., Safa, H., and Finnemann, S. C. (2014). Understanding photoreceptor outer segment phagocytosis: use and utility of RPE cells in culture. *Exp. Eye Res.* 126, 51–60. doi: 10.1016/j.exer.2014.01.010

Mitter, S. K., Song, C., Qi, X., Mao, H., Rao, H., Akin, D., et al. (2014). Dysregulated autophagy in the RPE is associated with increased susceptibility to oxidative stress and AMD. *Autophagy* 10, 1989–2005. doi: 10.4161/auto.36184

Miyagishima, K. J., Sharma, R., Nimmagadda, M., Clore-Gronenborn, K., Qureshy, Z., Ortolan, D., et al. (2021). AMPK modulation ameliorates dominant disease phenotypes of CTRP5 variant in retinal degeneration. *Commun Biol* 4:1360. doi: 10.1038/s42003-021-02872-x

Mukherjee, P. K., Marcheselli, V. L., Barreiro, S., Hu, J., Bok, D., and Bazan, N. G. (2007). Neurotrophins enhance retinal pigment epithelial cell survival through neuroprotectin D1 signaling. *Proc. Natl. Acad. Sci. U.S.A.* 104, 13152–13157. doi: 10.1073/pnas.0705949104

Nirgude, S., and Choudhary, B. (2021). Insights into the role of GPX3, a highly efficient plasma antioxidant, in cancer. *Biochem. Pharmacol.* 184, 114365. doi: 10.1016/j.bcp.2020.114365

Penaloza, C., Estevez, B., Orlanski, S., Sikorska, M., Walker, R., Smith, C., et al. (2009). Sex of the cell dictates its response: differential gene expression and sensitivity to cell death inducing stress in male and female cells. *FASEB J.* 23, 1869–1879. doi: 10.1096/fj.08-119388

Raviv, S., Bharti, K., Rencus-Lazar, S., Cohen-Tayar, Y., Schyr, R., Evantal, N., et al. (2014). PAX6 regulates melanogenesis in the retinal pigmented epithelium through feed-forward regulatory interactions with MITF. *PLoS Genet.* 10:e1004360. doi: 10.1371/journal.pgen.1004360

Ren, Z., Liang, H., Galbo, P. M., Dharmaratne, M., Kulkarni, A. S., Fard, A. T., et al. (2022). Redox signaling by glutathione peroxidase 2 links vascular modulation to metabolic plasticity of breast cancer. *Proc. Natl. Acad. Sci. U.S.A.* 119, e2107266119. doi: 10.1073/pnas.2107266119

Rice, D. S., Calandria, J. M., Gordon, W. C., Jun, B., Zhou, Y., Gelfman, C. M., et al. (2015). Adiponectin receptor 1 conserves docosahexaenoic acid and promotes photoreceptor cell survival. *Nat. Commun.* 6:6228. doi: 10.1038/ncomms7228

Shrestha, R., Wen, Y.-T., and Tsai, R.-K. (2020). Induced pluripotent stem cells and derivative photoreceptor precursors as therapeutic cells for retinal degenerations. *Ci Ji Yi Xue Za Zhi* 32, 101–112. doi: 10.4103/tcmj.tcmj_147_19

Snider, G. W., Ruggles, E., Khan, N., and Hondal, R. J. (2013). Selenocysteine confers resistance to inactivation by oxidation in thioredoxin reductase: comparison of selenium and sulfur enzymes. *Biochemistry* 52, 5472–5481. doi: 10.1021/bi400462j

Sonoda, S., Spee, C., Barron, E., Ryan, S. J., Kannan, R., and Hinton, D. R. (2009). A protocol for the culture and differentiation of highly polarized human retinal pigment epithelial cells. *Nat. Protoc.* 4, 662–673. doi: 10.1038/nprot.2009.33

Storm, T., Burgoyne, T., and Futter, C. E. (2020). Membrane trafficking in the retinal pigment epithelium at a glance. *J. Cell Sci.* 133:jcs238279. doi: 10.1242/jcs.238279

Sun, P. (2014). Contact inhibition against senescence. *Oncotarget* 5, 7212–7213. doi: 10.18632/oncotarget.2446

Szatmári-Tóth, M., Kristóf, E., Veréb, Z., Akhtar, S., Facskó, A., Fésüs, L., et al. (2016). Clearance of autophagy-associated dying retinal pigment epithelial cells - a possible source for inflammation in age-related macular degeneration. *Cell Death Dis.* 7:e2367. doi: 10.1038/cddis.2016.133

Szklarczyk, D., Morris, J. H., Cook, H., Kuhn, M., Wyder, S., Simonovic, M., et al. (2017). The STRING database in 2017: quality-controlled protein-protein association networks, made broadly accessible. *Nucleic Acids Res.* 45, D362–D368. doi: 10.1093/nar/gkw937

Wang, X., Yu, C., Tzekov, R. T., Zhu, Y., and Li, W. (2020). The effect of human gene therapy for RPE65-associated Leber's congenital amaurosis on visual function: a systematic review and meta-analysis. *Orphanet J. Rare Dis.* 15:49. doi: 10.1186/s13023-020-1304-1

Xu, C., Wang, L., Fozouni, P., Evjen, G., Chandra, V., Jiang, J., et al. (2020). SIRT1 is downregulated by autophagy in senescence and ageing. *Nat Cell Biol.* 22, 1170–1179. doi: 10.1038/s41556-020-00579-5

Xu, M., Eblimit, A., Wang, J., Li, J., Wang, F., Zhao, L., et al. (2016). ADIPOR1 Is Mutated in Syndromic Retinitis Pigmentosa. *Hum. Mutat.* 37, 246–249. doi: 10.1002/humu.22940

Xue, Y., Shen, S. Q., Jui, J., Rupp, A. C., Byrne, L. C., Hattar, S., et al. (2015). CRALBP supports the mammalian retinal visual cycle and cone vision. *J. Clin. Invest.* 125, 727–738. doi: 10.1172/JCI79651

Yin, X., Zhang, P., Xia, N., Wu, S., Liu, B., Weng, L., et al. (2022). GPx8 regulates apoptosis and autophagy in esophageal squamous cell carcinoma through

the IRE1/JNK pathway. *Cell Signal* 93:110307. doi: 10.1016/j.cellsig.2022.110307

Zhang, H. Y., Lam, C. S. Y., Tang, W. C., Leung, M., and To, C. H. (2020). Defocus Incorporated Multiple Segments Spectacle Lenses Changed the Relative Peripheral Refraction: A 2-Year Randomized Clinical Trial. *Invest Ophthalmol. Vis. Sci.* 61:53. doi: 10.1167/iovs.61.5.53

Zhang, J., Wang, C., Shen, Y., Chen, N., Wang, L., Liang, L., et al. (2016). A mutation in ADIPOR1 causes nonsyndromic autosomal dominant retinitis pigmentosa. *Hum. Genet.* 135, 1375–1387. doi: 10.1007/s00439-016-1730-2

Zhang, Q., Presswalla, F., Ali, R. R., Zacks, D. N., Thompson, D. A., and Miller, J. M. L. (2021). Pharmacologic activation of autophagy without direct mTOR inhibition as a therapeutic strategy for treating dry macular degeneration. *Aging* 13, 10866–10890. doi: 10.18632/aging.202974

Conflict of Interest: The authors declare that the research was conducted in the absence of any commercial or financial relationships that could be construed as a potential conflict of interest.

Publisher's Note: All claims expressed in this article are solely those of the authors and do not necessarily represent those of their affiliated organizations, or those of the publisher, the editors and the reviewers. Any product that may be evaluated in this article, or claim that may be made by its manufacturer, is not guaranteed or endorsed by the publisher.

Citation: Asatryan A, Calandria JM, Kautzmann M-AI, Jun B, Gordon WC, Do KV, Bhattacharjee S, Pham TL, Bermúdez V, Mateos MV, Heap J and Bazan NG (2022) New Retinal Pigment Epithelial Cell Model to Unravel Neuroprotection Sensors of Neurodegeneration in Retinal Disease. Front. Neurosci. 16:926629. doi: 10.3389/fnins.2022.926629

frontiers | Frontiers in Neuroscience

SYSTEMATIC REVIEW
published: 13 July 2022
doi: 10.3389/fnins.2022.938029

Implications of Diabetes-Induced Altered Metabolites on Retinal Neurodegeneration

*Dalia I. Aldosari, Ajamaluddin Malik, Abdullah S. Alhomida and Mohammad S. Ola**

Department of Biochemistry, College of Science, King Saud University, Riyadh, Saudi Arabia

Diabetic retinopathy (DR) is one of the major complications of diabetic eye diseases, causing vision loss and blindness worldwide. The concept of diabetic retinopathy has evolved from microvascular disease into more complex neurovascular disorders. Early in the disease progression of diabetes, the neuronal and glial cells are compromised before any microvascular abnormalities clinically detected by the ophthalmoscopic examination. This implies understanding the pathophysiological mechanisms at the early stage of disease progression especially due to diabetes-induced metabolic alterations to damage the neural retina so that early intervention and treatments options can be identified to prevent and inhibit the progression of DR. Hyperglycemia has been widely considered the major contributor to the progression of the retinal damage, even though tight control of glucose does not seem to have a bigger effect on the incidence or progression of retinal damage that leads to DR. Emerging evidence suggests that besides diabetes-induced hyperglycemia, dyslipidemia and amino acid defects might be a major contributor to the progression of early neurovascular retinal damage. In this review, we have discussed recent advances in the alterations of key metabolites of carbohydrate, lipid, and amino acids and their implications for neurovascular damage in DR.

Keywords: metabolites, glucose, lipids, amino acids, neurodegeneration, retina, oxidative stress

OPEN ACCESS

Edited by:
Mohammad Badruzzaman Khan, Augusta University, United States

Reviewed by:
Ilaria Piano, University of Pisa, Italy
Filipa I. Baptista, University of Coimbra, Portugal

****Correspondence:***
Mohammad S. Ola
mola@ksu.edu.sa

Specialty section:
This article was submitted to Neurodegeneration, a section of the journal Frontiers in Neuroscience

Received: *06 May 2022*
Accepted: *09 June 2022*
Published: *13 July 2022*

Citation:
Aldosari DI, Malik A, Alhomida AS and Ola MS (2022) Implications of Diabetes-Induced Altered Metabolites on Retinal Neurodegeneration. Front. Neurosci. 16:938029. doi: 10.3389/fnins.2022.938029

INTRODUCTION

Diabetic retinopathy (DR) is one of the most common diabetic eye diseases, which causes preventable vision impairment and blindness worldwide. According to a recent report, approximately 537 million people are diabetic worldwide, over one-third have signs of DR, and nearly 1 in 10 have vision-threatening levels of DR, including severe non-proliferative DR pro-liferative DR (PDR), and diabetic macular edema (DME) (Federation, 2021; Teo et al., 2021). These estimates are expected to rise further due to the increasing prevalence of diabetes, aging global population, lifestyle changes, and growing lifespan of people living with diabetes (Teo et al., 2021). Current treatments such as laser surgery and intraocular injection of anti-VEGF agents only target the advanced stage of DR, including ME and PDR. These treatments are temporarily effective and usually do not promote tissue repair and sometimes can impair vision; in some patients, the retinopathy continues to progress (Narayanan et al., 2013). Therefore, a better understanding of the pathogenesis of DR in the early stages of the disease would permit the development of more efficient strategies against the progression of DR.

Over the last two decades, the concept of diabetic retinopathy has evolved from microvascular disease into more complex neurovascular diseases in which neurodegeneration plays a significant role in the very early stages of the disease. Retinal neurodegeneration has been found to trigger vascular injury which leads to diabetic retinopathy at the later stages of diabetes (Feng et al., 2009; Moran et al., 2016). However, the exact reasons for neuro-vascular cell damage early in the diabetic retina are not well known.

Retina being highly metabolic active sensory tissue demands an increased amount of energy metabolites for maintaining energy homeostasis and neurotransmitter regulation for normal vision (Kern, 2014; Liu and Prokosch, 2021). However, diabetes disrupts several of those energy metabolites in the retinas of diabetic patients and rodents both systemically and locally. Diabetes-induced hyperglycemia, dyslipidemia, and defects in amino acid metabolism are crucial factors in disturbing the energy metabolism. Numerous studies, suggest that the pathogenesis of DR is potentially related to elevated levels of numerous metabolites of glucose, lipids, and amino acids (Ola and Alhomida, 2014; Chou et al., 2020; Yumnamcha et al., 2020) as depicted in **Figure 1**. Those metabolites may include advanced glycation end products, polyols, hexosamines, excitatory amino acids; glutamate, homocysteine, branched-chain amino acids, cholesterol, polyunsaturated fatty acids, and sphingolipids; whose dysregulated levels may cause neurodegeneration in the diabetic retina by increasing oxidative stress and decreasing neurotrophic support, leading to the progression of DR. In this review, we have highlighted the role of potential metabolites which play a significant role in the pathophysiology of retinal damage in diabetes and more specifically in the neuronal cells damage in retinas and that have been correlated with DR progression. This article would provide a better understanding and guidance to researchers in fostering further research and contributing to the understanding of metabolic stress in DR.

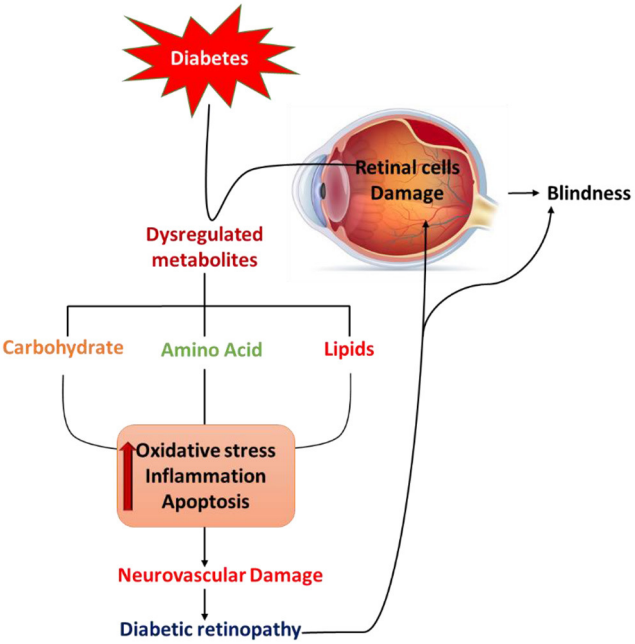

FIGURE 1 | Schematic diagram summarizes diabetes-induced pathological defects in the carbohydrate, lipid, and amino acid metabolism, leading to increases in oxidative stress, activation of apoptosis, and inflammation that may contribute to retinal cell damage and diabetic retinopathy.

Dysregulated Glucose Metabolism

The retina is one of the highest energy-demanding tissues of the human body, and it relies almost exclusively on glucose as its energy source. Therefore, maintenance of euglycemia is critical for normal vision and regulating energy homeostasis in the retina. Glucose homeostasis is tightly controlled by the interplay between glycolysis, Krebs cycle, and oxidative phosphorylation. Many glucose intermediates are produced through the glycolytic pathway, including glucose-6-phosphate, Fructose-6-phosphate, dihydroxyacetone phosphate (D), and glyceraldehyde 3-phosphate, 3-phosphoglycerate, and phosphoenolpyruvate. Under physiological conditions, the retina, similar to the brain depends on the glycolytic pathway to obtain a significant amount of energy and also maintain a steady-state concentration of glycolytic intermediates (Chinchore et al., 2017). However, increased flux through glycolysis, which is commonly seen under diabetic conditions, results in glycolytic overload, which leads to an abnormal increase in the concentrations of glycolytic intermediates that can be shunted into different damaging pathways such as polyol, hexosamine, protein kinase C (PKC) pathways, and advanced glycation end products (AGEs) as shown in **Figure 2** (Yumnamcha et al., 2020). The activation of these damaging pathways leads to an increase in oxidative stress either by the generation of reactive oxygen species (ROS) or by decreasing the level of antioxidants, as summarized below.

Polyol Formation

Under physiological conditions, glucose is phosphorylated by an enzyme called hexokinase; however, when there is excess glucose uptake, this enzyme becomes saturated, and any excess glucose is shunted into the polyol pathway. The polyol pathway involves the conversion of glucose into sorbitol, and the reaction is catalyzed by aldose reductase. Unlike under diabetic conditions, the high activation of the polyol pathway could enhance oxidative stress because aldose reductase requires NADPH as a cofactor, thereby reducing the NADPH level, which is a necessary cofactor for regenerating the intracellular antioxidants. In addition, NADPH is a cofactor for glutathione reductase, which converts oxidized glutathione (GSSG) to the critical cellular reductant, reduced glutathione (GSH). Furthermore, NADPH is required for many anabolic pathways such as nitric oxide and fatty acid synthesis, however, NADPH consumption in the aldose reductase pathway under diabetic conditions causes a harmful effect on the biosynthesis process of these molecules in the retina (Thakur et al., 2021).

Polyol pathway activation has been found in various retinal cells, such as retinal ganglion cells (RGC), and Müller cells under hyperglycemic conditions and in nerve fibers in diabetic patients (Dagher et al., 2004). Many studies have proved that

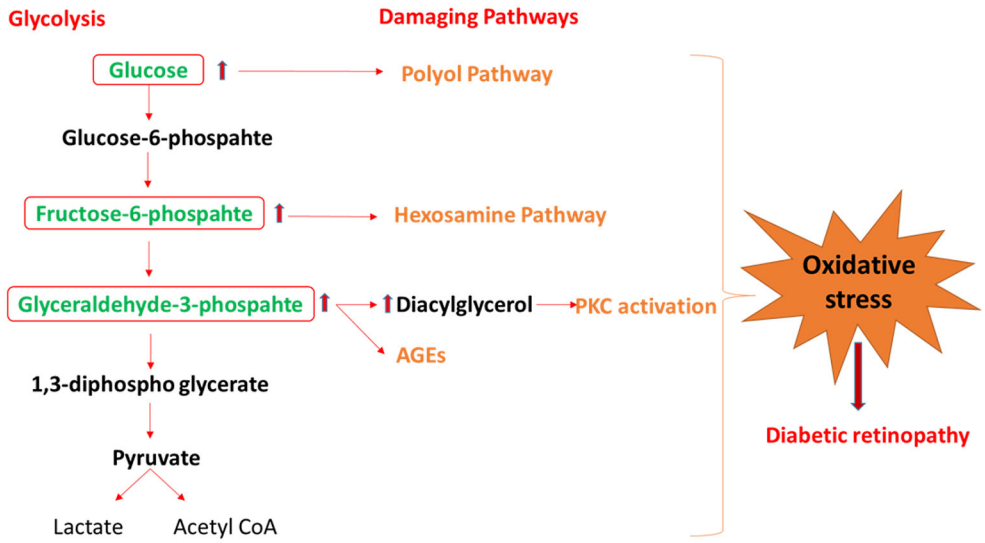

FIGURE 2 | The schematic diagram shows the mechanism by which glycolysis intermediates overload under diabetic condition and activates the damaging pathway of polyol, hexosamine, PKC, and AGEs, that lead to diabetic retinopathy. PKC, protein kinase C; AGEs, advance glycation end-products.

sorbitol is increased in the retina of diabetic animals and diabetic patients (Dagher et al., 2004; Lorenzi, 2007; Ola et al., 2012). The increased levels of sorbitol through the polyol pathway can alter the osmotic pressure of the membrane and cause osmotic stress, which causes electrolyte imbalance, hydration and membrane damage (D'Andrea et al., 2020; Thakur et al., 2021). Additionally, polyol pathway activation in the retina of diabetic rats shows increased lipid peroxidation products and depletion of antioxidant enzymes, suggesting that retinal cells and more specifically neuronal cells might be more prone to oxidative stress induced by the polyol pathway early in diabetes (Ola et al., 2018). Furthermore, recent studies showed that the aldose reductase inhibitors helped to slow DR progression (D'Andrea et al., 2020; Thakur et al., 2021).

ACTIVATION OF HEXOSAMINE PATHWAY

The hexosamine biosynthesis pathway is activated as an alternative to the glycolysis pathway by shunting hyperglycemia-induced overproduction of fructose-6-phosphate to glucosamine-6-phosphate by fructose-6- phosphate amidotransferase (GFAT), and further to uridine-5-diphosphate (UDP)-N-acetylglucosamine (UDP-GlcNAc), which is essential to the formation of O-linked glycoproteins (Du et al., 2000). Alternative O-linked glycoprotein can have diverse effects on cell function and survival by disrupting gene expression of several proteins in the retina, especially in neurovascular cells (Fülöp et al., 2007). Under the diabetic condition, activation of the hexosamine pathway contributes to the pathogenesis of DR by blocking the neuroprotective effect of the insulin/Akt signaling pathway that leads to increases retinal neuronal cell death (Kim et al., 2016). It also promotes retinal ganglion cell death in the retina of diabetic rodents by increasing O-GlcNAcylation of the NF-κB p65 subunit and its activation [reviewed in Yumnamcha et al. (2020)]. In addition, recent research found increased production of UDP-N-acetyl glucosamine under diabetic conditions. This product of the hexosamine pathway competes with phosphorylation at post-translation modification sites on transcription factors and disrupts the regulation of inflammatory responses that generally occurs through transcription growth factor-β (Yumnamcha et al., 2020). Thus, the activation of the hexosamine pathway under diabetic conditions leads to neurodegeneration in the retina, specifically through the activation of pro-inflammatory transcription factors.

ACTIVATION OF PROTEIN KINASE C PATHWAY

Under hyperglycemic conditions, the high intracellular glucose concentration induces a *de novo* pathway of diacylglycerol (DAG) synthesis from glucose to glycerol 3-phosphate, which forms glycerol phosphate (Geraldes and King, 2010; Giacco and Brownlee, 2010). DAG activates different isoforms of protein kinase C (PKC) within the cell, which play an essential role in the pathogenesis of DR by several mechanisms. First, activation of PKC by DAG causes retinal vascular dysfunctions and pericyte losses which is the principal hallmark of the pathogenesis of microvascular damage in DR. Second, the accumulation of DAG under diabetic condition activates PKC-β, which increase the expression of endothelium-derived vasoactive factors such as endothelin-1(ET-1), vascular permeability, and angiogenesis as well as an increase in vascular endothelial growth factor (VEGF) that affect the blood flow in the retina. Third, the increased production of DAG as a result of hyperglycemia under diabetic conditions also activate PKC-δ, which induces pericyte loss

through; increasing oxidative stress by activating nuclear factor-B (NF-κB) and upregulating the expression of a protein tyrosine phosphatase, to weaken the critical survival signaling pathway of platelet-derived growth factor (Yumnamcha et al., 2020). Therefore, PKC activation might be partly responsible for some of the pathologies in DR.

Advanced Glycation End Products

Diabetes-induced high intracellular glucose concentration causes accumulation of the production of advanced glycation end products (AGEs). Increased AGEs formation has been found in retinal blood vessels of diabetic patients and animals and in human serum and vitreous of diabetic patients, which correlate with the severity of retinopathy (Ola et al., 2012). AGEs exert their cellular effects on cells by activating their receptor, RAGE, which contributes to activating the NADPH oxidase system and increasing the production of intracellular ROS (Rains and Jain, 2011). The ROS produced, in turn, increases VEGF, monocyte chemoattractant protein- 1 (MCP-1), and intercellular adhesion molecule-1 (ICAM-1) expression in microvascular endothelial cells, thus leading to leukostasis and breakdown of BRB (Ola et al., 2012). AGEs also induce apoptosis and inflammation by activating NF-κB, with a simultaneous increase in the ratio of Bcl-2/Bax, and activity of caspase-3, a key enzyme in the execution of apoptosis of pericytes (Ola and Nawaz, 2012).

Although hyperglycemia is known to cause a higher risk for the development and progression of DR, however, tight control of glucose does seem to improve the incidence or progression of DR. Even aggressive intervention to improve glycemia may raise the possible increased risk of the retinal damage (Ipp and Kumar, 2021). Our studies including a few others suggest that hyperglycemia per se might not cause oxidative stress in the diabetic retina and cultured retinal cells (Ola, 2021). Therefore, it is imperative that dysregulated metabolites of lipids and amino acids, other than high glucose might be other major metabolic factors that might implicate in the pathophysiology of early retinal damage in DR.

Lipid Metabolism in Diabetic Retinopathy

The retina is a heavily energy-consuming tissue used for several processes, including phototransduction, visual pigment recycling, and synaptic activity. However, Cohen and Noell (1960), reported that almost 65% of the CO_2 produced from the TCA cycle by the retinas is not derived from glucose, which implies that the oxidation of non-carbohydrate carbons is also used to meet the retinal high energy demand (Joyal et al., 2018; Millman et al., 2019). Furthermore, several studies recently found that lipid oxidation acts as another energy source for the retina (Joyal et al., 2016). In addition, for decades numerous research has highlighted the significant role of lipids in retinal function by transferring many signaling through membrane proteins. Retinal lipids also play an essential role in the visual cycle and converting all-trans-retinal to 11-cis retinal (Zemski Berry et al., 2014). Additionally, very long-chain polyunsaturated fatty acids (VLC-PUFA), such as docosahexaenoic acid (DHA), are disproportionately abundant in the retina compared with other tissues (Zemski Berry et al., 2014). The levels of DHA affect the fluidity, flexibility, and thickness of any membrane. Furthermore, the large amount of DHA in the retina permits efficient conformational changes in rhodopsin (Zemski Berry et al., 2014). It is now well known that modifications in fatty acid metabolism can affect various retinal functions and contribute to retinal diseases that lead to visual loss.

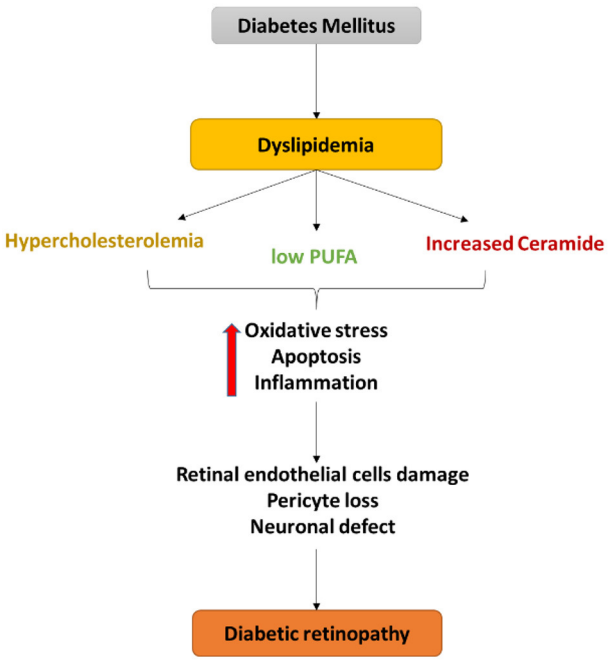

FIGURE 3 | Schematic diagram of the central role of dyslipidemia in endothelial cell damage, pericyte loss as well as a neuronal defect in diabetic retinopathy. Dyslipidemia in diabetes induces oxidative stress, apoptosis, and inflammation that contribute to the retinal neurovascular damage in DR.

Abnormalities in retinal lipid metabolism occur early during diabetes. Diabetic dyslipidemia produces a deleterious effect on the retina. Dyslipidemia is characterized by abnormal circulating of triglycerides, high-density lipoproteins (HDL), low-density lipoproteins (LDL), cholesterol, and polyunsaturated fatty acids. Dyslipidemia in DR is summarized in a series of reviews as depicted in **Figure 3** (Busik et al., 2012; Hammer and Busik, 2017; Fu et al., 2019; Chou et al., 2020; Busik, 2021), and here we have focused on hypercholesterolemia, PUFA, and sphingolipids in DR.

Hypercholesterolemia

Cholesterol levels in the retina are affected by several factors, including systemic delivery, local biosynthesis, and cholesterol elimination (Hammer and Busik, 2017; Busik, 2021). The inner blood-retinal barrier (inner BRB) is created by complex tight junctions of retinal capillary endothelial cells, which, when intact, are impervious to cholesterol. However, the breakdown of inner BRB in DR could lead to the non-specific entry of lipoprotein particles into the retina, increasing retinal cholesterol levels (Busik, 2021). The outer BRB, formed by the retinal

pigmented epithelium (RPE) cells, which contain the Low-Density Lipoprotein Receptor (LDLR), allows for cholesterol transport into the retina obtained from the diet or produced by the liver (Hammer and Busik, 2017). After uptake by the RPE, cholesterol is exported by ABCA1- and ABCG1-transporters either back to the liver in a multi-step process by reverse cholesterol transport or to the neural retina. In addition to exporting cholesterol, both RPE and neural retina metabolize cholesterol to more soluble oxysterols that rapidly diffuse to the systemic circulation by cytochrome P450s (CYPs) enzymes 27A1, and 46A1, key enzymes in cholesterol elimination (Hammer and Busik, 2017; Busik, 2021). Obstructing control of cholesterol metabolism pathways can cause retinal cholesterol accumulation, negatively affecting normal retinal function.

Several studies demonstrated that increased cholesterol levels pass through BRB in the diabetic retina compared to the non-diabetic retina (Fliesler et al., 1993; Hammer and Busik, 2017). In addition, abnormal cholesterol elimination in the diabetic retina leads to hypercholesterolemia increasing non-enzymatic oxidation and glycation (Hammer and Busik, 2017). Oxidized and glycated LDL induced retinal pericyte loss and oxidized LDL immunocomplexes in diabetic retinopathy (Fu et al., 2014). In addition, numerous studies have described the neurotoxic effects of hypercholesterolemia by induced amyloid-beta peptide accumulation (Rao et al., 2021). Elevated levels of Ab peptide in the retina lead to increased production of ROS which has deleterious effects on retinal ganglion cells (Rao et al., 2021). Furthermore, hypercholesterolemia produces several oxidized byproducts such as 7-ketocholesterol (7-kCh) that result in retinal damage. 7-kCh is a potent pro-apoptotic and inflammatory agent shown to activate caspases, p38, MAP/ERK, and AKT-PKCz-NF-kB (Hammer and Busik, 2017; Rao et al., 2021). Activation of the MAP/ERK pathway increases oxidative stress, inflammation, and apoptosis in retinal neurovascular cells (Rao et al., 2021). In addition, activation of the NF-kB pathway by 7kCh facilitates the expression of many cytokines that result in an inflammatory response (Rao et al., 2021). Furthermore, Yang et al. (2019), found that injecting rat retina with 7KCh mainly deposited in the retinal pigment epithelial (RPE) cells and induced marked photoreceptor apoptosis (Yang et al., 2019). Increasing evidence has suggested a positive correlation between hypercholesterolemia and the risk and the severity of hard exudate among diabetic patients (Chou et al., 2020). In addition, the diabetic patients with higher circulating LDL-C were also more inclined to suffer from diabetic retinal hard exudate. Furthermore, lipid-lowering dietary therapy studies demonstrated regression of retinal hard exudates and beneficial effects toward amelioration of the progression of DR (Busik et al., 2012).

Polyunsaturated Fatty Acid (PUFA)

Both systemic and retinal-specific fatty acid profiles are affected by diabetes, especially DHA, the most abundant PUFA in the retina. Several animal and cell culture studies demonstrated that the DHA has anti-inflammatory by inhibiting cytokine-induced NF-κB activation, nuclear translocation, adhesion molecule expression, and anti-apoptotic effects in the retina and retinal cells (Busik et al., 2012). In addition, DHA contributes to cholesterol homeostasis in the retina by incorporation into phospholipids of caveolar membrane microdomains and displacement of cholesterol from these microdomains as essential mechanisms of the anti-inflammatory effects of DHA in the human retinal endothelial cells (HREC) (Busik et al., 2012). However, diabetes has been found to reduce levels of DHA in both the diabetic retina and plasma, with a concomitant increase in pro-inflammatory omega-6 PUFA that was found to contribute to the development of DR (Tikhonenko et al., 2013). *In vivo* experiments revealed that a diet rich with a DHA at the recommended levels is protective against capillary loss in the animal model of diabetic retinopathy. In both type 1 and type 2 diabetic animal models, a DHA-rich diet entirely prevented retinal vascular pathology by inhibiting acid sphingomyelinase (ASM) in the retina and endothelial progenitor cells (EPCs), leading to simultaneous suppression of retinal inflammation and correction of EPC number and function (Tikhonenko et al., 2013). In addition, several studies demonstrated that increased dietary intake of DHA prevents vascular pathology through inhibition of ASM in the retina, leading to an inhibition of retinal endothelial cell activation by inflammatory cytokines and reducing pathological retinal angiogenesis (Busik et al., 2012).

Sphingolipids

Diabetes has also been shown to affect sphingolipid metabolism (Fox et al., 2006; Hammer and Busik, 2017). Sphingolipids are a class of biologically active lipids that have essential roles in regulating tissue development, cell death, inflammation, adhesion, and migration (Hammer and Busik, 2017). One of the primary intermediates involved in sphingolipid metabolism is known as ceramide. This intermediate is a potent messenger in stress signaling and pro-apoptotic sphingolipid that accumulates in endothelial and immune cells (Hammer and Busik, 2017). Ceramide is mainly synthesized through the breakdown of sphingomyelin by sphingomyelinases. There are three types of sphingomyelinases classified depending on the pH optimum, acid, neutral, and alkaline. The alkaline form is only expressed in the gut, while acid and neutral sphingomyelinases are ubiquitously expressed in most tissues (Busik et al., 2012). Both acid and neutral sphingomyelinases are expressed in the retina (Opreanu et al., 2011). Evidence suggests that the ASM is activated by diabetes (Busik et al., 2012; Tikhonenko et al., 2013; Hammer and Busik, 2017). Activation of ASM leads to higher sphingomyelin-ceramide conversion causing retinal endothelial damage in the diabetic retina, macrophage, and microglial activation, and circulating angiogenic cell dysfunction (Hammer and Busik, 2017). In addition, inhibition of ASM in the retina has been shown to prevent diabetes-induced vascular degeneration and cytokine-induced pro-inflammatory changes (Busik et al., 2012).

Amino Acid Metabolism in the DR

Amino acids (AAs) and their metabolites play a critical role in retinal health and function (Pow, 2001). They are not only used

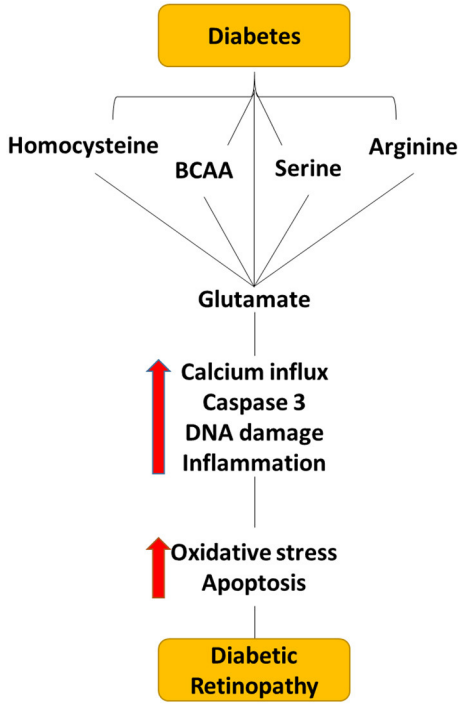

FIGURE 4 | Flow diagram depicting the effect of dysregulated level of amino acid within the diabetic retina. Dysregulated levels of homocysteine, serine, BCAA, arginine, and glutamate cause elevating the glutamate levels in the extracellular space within the retina, which can cause neuro-vascular damage in diabetic retinopathy.

for protein synthesis, but some amino acids act as a significant neurotransmitter in the retina (Pow, 2001; Bui et al., 2009). In addition, the central nervous system, including the retina, requires amino acid and nitrogen balance, however, any changes in the AA metabolism can cause neurological dysfunction and irreversible damage. Many studies have reported altered amino acid levels in serum and retina in DR patients and DR models of rodents (Diederen et al., 2006; Narayanan et al., 2013; Ola et al., 2013). Altered glutamate, glutamine, arginine, tryptophan, BCAA, and homocysteine metabolism have been found to have a greater impact on DR as depicted in **Figure 4** (Ola et al., 2013, 2019). Metabolic abnormalities of these amino acids lead to an increase in oxidative stress, and inflammation and induce apoptosis, thus inducing neuroretina damage in diabetes as discussed below.

EXCITATORY AMINO ACIDS (GLUTAMATE)

Glutamate is a major neurotransmitter in the retina and acts as a precursor for gamma-aminobutyric acid (GABA), an inhibitory neurotransmitter, and glutathione, an endogenously antioxidant; therefore, any changes in glutamate metabolism in the retina have a more significant effect on neuroretinal functioning (Pow, 2001). Photoreceptors, bipolar, and ganglion cells in the retina release glutamate, during light stimulation under the regular state and activate the N-methyl-D-aspartate receptor (NMDA). This Glu receptor is expressed in most cells of neuro-retinal cells (Shen et al., 2006). The activation of NMDA leads to depolarizing of the neuronal cells and increases the influx of calcium and sodium ions into the cell (Shen et al., 2006). However, prolonged exposure of neurons to glutamate leads to cell death by elevating the intracellular Ca^{2+} that subsequently generates free radicals and induces apoptosis in the neuronal cells (Ola et al., 2013). Glu receptors' activation control is achieved by Glu clearance from the synaptic cleft by glutamate transporter proteins expressed on both neurons and Müller cells (Ishikawa, 2013). Within neurons, glutamate can be recycled, while in Müller cells, glutamate is inactivated by conversion to less toxic metabolites such as glutamine and alpha-ketoglutarate through the glial L-glutamate/L-aspartate transporter (GLAST), which is expressed in the Müller cells, and glutamine synthetase (GS), which is described in the cytoplasm of Müller cells (Bringmann et al., 2013). All of this maintain the requisite glutamate homeostasis in the retina after excitation. However, many lines of evidence demonstrate a defect controlling systems of Glu levels in the diabetic retina (Gowda et al., 2011; Ishikawa, 2013). Considerable evidence indicates an increase in Glu levels in the vitreous and retina of diabetic patients with PDR and experimental animal models of diabetes (Diederen et al., 2006; Ishikawa, 2013; Ola et al., 2019). The elevated levels of Glu in the diabetic vitreoretinal are thought to be mediated by the dysfunction of glutamate transporters on retinal Müller cells and possibly, due to the decreased expression of glutamine synthase (Li and Puro, 2002; Ishikawa, 2013). Lau et al. (2013), reported a significant decrease in the expression of glutamate transporter SLC1A3 gene encoding GLAST protein, leading to the decreased removal of glutamate from the synaptic space due to impairment of the glutamate transporter function of Muller cells. Besides the elevated level of Glu in the DR, it also has been observed the high expression of NMDA in experimental diabetes (Smith, 2002). Furthermore, it has been reported that excessive retinal glutamate excitotoxicity contributes to the upregulation of (VEGF) production in diabetic retinas, which is known to induce microcirculatory abnormalities such as disruption of the (BRB) or an increase in the vascular permeability in the advanced stage of DR (Cervantes-Villagrana et al., 2010; Kusari et al., 2010; Ishikawa, 2013). In addition, Kusari et al. (2010), demonstrated that the elevation of VEGF expression and BRB breakdown in STZ-induced diabetic rats is blocked by the NMDA receptor channel blocker and uncompetitive antagonist memantine (Kusari et al., 2010). This explains the relationship between the excitotoxicity and the induction of VEGF in the linking neurodegeneration with vascular impairment in DR. Furthermore, high levels of oxidative stress in diabetics have been proven to be associated with increased glutamate levels, which in turn directly contributes to DR (Narayanan and Shosha, 2019). Glutamate toxicity has been related to the inhibition of glutamate/cystine antiporter activity, which imports cystine to export glutamate outside the cell (Lewerenz et al., 2013). Cystine is required to synthesize the potent intracellular antioxidant glutathione (GSH). When Glu concentration is high outside the cell leads, it inhibits cystine uptake, depleting GSH synthesis

in neuronal cells and inducing oxidative stress and apoptosis (Lewerenz et al., 2013). Several studies have also reported decreased GSH levels in diabetic retinal cells and increased oxidative stress (Al-Dosari et al., 2017; Ola et al., 2019).

Arginine

L-Arginine is metabolized to nitric oxide (NO) and L-citrulline by NO synthases, and to urea and L-ornithine by arginase where the latter is further metabolized to form proline, polyamines, and glutamate. There is some evidence supporting the role of arginase in retinal inflammation, neurotoxicity, pathological angiogenesis, and retinal vascular dysfunction (Narayanan et al., 2013; Hou et al., 2021). Increased arginase activity, elevated expression of arginase, and decreased levels of L-arginine have been reported in plasma of diabetic animals and patients. Several studies have shown that increases in arginase activity are involved in diabetes and high glucose-induced dysfunction of the aorta, coronary and retinal arteries. Increases in arginase activity and arginase expression in neurovascular cells are associated with increased formation of superoxide, increased expression of inflammatory genes, and attachment of leukocytes to the retinal vessels (Elms et al., 2013; Narayanan et al., 2013; Patel et al., 2013; Fouda et al., 2020) High arginase activity leads to the uncoupling of nitric oxide synthase. Uncoupled NOS reacts with molecular oxygen to form superoxide, which will respond rapidly with any available NO to create peroxynitrite, a highly reactive inflammatory and toxic oxidant. Peroxynitrite causes cellular injury either through direct oxidative reactions with lipids, DNA, and proteins or indirect, radical-mediated mechanisms. In addition, inhibiting nitric oxide synthase (NOS) has been shown to prevent diabetes-induced vascular dysfunction implying that reactive nitrogen species play a crucial role in the DR pathology (Elms et al., 2013; Narayanan et al., 2013). Furthermore, *in vivo* experiments revealed that the long-term oral administration of L-citrulline offered protection against hyperglycemia-induced retinal vasodilator dysfunction by stimulates nitric oxide (NO) biosynthesis via the recycling of L-citrulline to L-arginine (Mori et al., 2015, 2021).

In addition, arginase catabolizes L-arginine to form proline, polyamines, and glutamate. The catabolic products of glutamate and polyamine oxidation have been linked to retinal ganglion cell death due to excessive activation of the excitotoxic NMDA receptors, which can induce more oxidative stress and DNA damage (Narayanan et al., 2013). Furthermore, polyamines have been implicated in neurovascular dysfunction in the retina. Polyamine production is further metabolized to spermine and spermidine (Narayanan et al., 2013; Narayanan and Shosha, 2019). Nicoletti et al. (2003), reported that the level of spermidine and spermine was increased in vitreous samples from patients with proliferative retinopathy, suggesting their involvement in retinopathy (Nicoletti et al., 2003). In addition, in the retinal arterioles, spermine inhibits potassium efflux via inwardly rectifying potassium channels, causing it to limit vasodilator responses and is enhanced in microvessels isolated from the diabetic retina.

Branched Chain Amino Acid

BCAAs (valine, leucine, and isoleucine) are essential amino acids needed for protein synthesis, cells' energy needs, and signaling molecules. They are required for growth and development and act as nutrient signals and nitrogen donors for neurotransmitter synthesis and glutamate/glutamine cycling in the brain and retina (LaNoue et al., 2001; Conway and Hutson, 2016). Many reports have consistently demonstrated increased plasma BCAA levels related to obesity, insulin resistance, and diabetes in human studies and experimental rodents during the last decade (Bloomgarden, 2018). Besides, our lab and a few recent metabolomics investigations have shown significant changes in the levels of BCAA in the retina of diabetic animals and the vitreous of diabetic patients with proliferative diabetic retinopathy (Gowda et al., 2011; Bloomgarden, 2018; Ola et al., 2019). In addition, many neurological disease studies found that the build-up of BCAAs in the brain is neurotoxic to cells by increasing glutamate production, which induces excitotoxicity and neuronal death in the brain through mechanisms of NMDA receptor activation. In addition, the antiepileptic drug gabapentin, which is known to inhibit BCAT, an essential enzyme in the BCAA metabolism, has proved successful in reducing caspase-3 activity, a significant marker of oxidative stress, and reducing the increased levels of ROS in the diabetic retina (Ola et al., 2019). Thus, diabetes-induced altered BCAAs metabolism seems to be the potential in damaging neuroretina.

Serine

Serine is a non-essential amino acid but essential in cellular homeostasis, proliferation, and differentiation (Sinha et al., 2020). Free serine is necessary for generating cysteine, glycine, and sphingolipids, which are critical in synthesizing porphyrins/purine nucleotides, glutathione, sphingomyelin formation, respectively (Sinha et al., 2020). Serine metabolism is central to maintaining redox/oxidative balance, ion flux, glutamate levels, and other support functions. Emerging evidence has demonstrated a correlation between serine deficiency and systemic diabetes (Holm and Buschard, 2019; Sinha et al., 2020). Reduced serine levels and increased D-serine have been implicated in the etiology of DR (Ozaki et al., 2018; Sinha et al., 2020). D-serine, the racemization of L-serine forms an enantiomer of L-serine by serine racemase (SRR) in Müller cells. D-serine has been found to have a high affinity for binding and activation of NMDA receptors in the retina (Sinha et al., 2020). Therefore, the elevated levels of D-serine contribute to the glutamate toxicity effect in the retinal environment and induce cell death in RGCs.

Homocysteine

Homocysteine is a sulfur-containing non-proteinogenic amino acid, and its high levels are associated with various ocular complications, including secondary glaucoma optic atrophy, age-related macular degeneration (AMD), and DR (Ola et al., 2013). Homocysteine is biosynthesized from methionine by S-adenosyl-methionine synthetase in the presence of vitamin B12 and folate as cofactors. Homocysteine formed can either be remethylated back to L-methionine by methylenetetrahydrofolate reductase

(MTHFR) and/or trans-sulfuration by cystathionine β-synthase (CBS) to form cysteine, an essential amino acid for the biosynthesis of glutathione (GSH) (Kowluru et al., 2020). Hyperhomocysteinemia in diabetic complications has been associated with impaired activities of CBS and MTHFR, along with deficiencies in folate and vitamin B12 (Kowluru et al., 2020). Naggar et al. (2002), demonstrate that hyperglycemia reduces the expression and activity of the folate transporter and decreases the folate level in the retina, which could have implications for the pathology of DR (Naggar et al., 2002). In addition, supplementation with folic acids and vitamin B is more effective in reducing homocysteine levels and maintaining homocysteine metabolism.

The elevated level of Hcy has a toxic effect on neuronal cells in both the brain and retina. A recent meta-analysis demonstrated an association between high Hcy levels and increased risk of diabetic retinopathy (Lei et al., 2018). In addition, hyperhomocysteinemia in DR has been associated with vitamin-B12 deficiency. *In vitro* and *in vivo* studies have also demonstrated vital roles for elevated homocysteine levels in apoptotic mechanisms leading to ganglion cell loss (Moore et al., 2001; Ganapathy et al., 2009). Several studies have shown that the neurotoxic effects of homocysteine are also associated with the activation of Glu receptors and cause excitotoxicity of retinal ganglion cells in the diabetic retina (Ola et al., 2013). A case study reported a high level of Hcy caused by methionine synthase deficiency demonstrated decreased rod function and RGC loss as determined by ERG and visual evoked potentials, which reflect homocysteine's cytotoxic impact on neurons of the visual pathway (Poloschek et al., 2005).

Additionally, more recently metabolomics approaches have been used by Sun and coworkers for plasma metabolic profiles in patients with DR to better understand the mechanism of this disease and the disease progression. Out of several differentially expressed metabolites associated with DR, a risk score based analysis identified pseudouridine to be strongly associated with the occurrence of DR. Furthermore, circulating plasma metabolites; glutamate, leucylleucine, and N-acetyltryptophan were found to be differentially expressed between patients with PDR and evaluated to be significantly related to PDR (Sun et al., 2021). The same group also identified arginine and carnitine metabolites which are altered in the plasma of DR patients. These metabolites can also be used as biomarkers in the disease progression (Sumarriva et al., 2019).

CONCLUSION AND FUTURE PERSPECTIVES

Diabetic retinopathy is well recognized as a neurovascular disease. The pathophysiology of neurovascular damage is extremely complex, nevertheless, diabetes-induced metabolic disorders are considered the major initiating factors that damage both neuronal and vascular components of the retina. Besides diabetes-induced hyperglycemia, emerging evidence suggests a potential role of dyslipidemia and metabolic defects of amino acids that induce the early neurovascular retinal damage in the DR. However, the connections between diabetes-induced metabolic profiling changes and the exact pathways leading to the development of retinal pathology are still unknown. New tools are becoming available for metabolic profiling studies including specific metabolic enzyme inhibitors, antibodies, and animal genetic models to elucidate the metabolic defects. These strategies would contribute to creating a better understanding of the mechanism of diabetes-induced metabolic damage to allow the development of therapeutic options for the prevention and treatment of the neurodegenerative disease as in the case of DR.

DATA AVAILABILITY STATEMENT

The original contributions presented in the study are included in the article/supplementary files, further inquiries can be directed to the corresponding author/s.

AUTHOR CONTRIBUTIONS

DA designed the outline, wrote the first draft, and made figures. AM and AA reviewed and revised it. MO offered guidance, advice to design of the outline as well as wrote and revised, and edited the manuscript. All authors contributed to the article and approved the submitted version.

FUNDING

This research was funded by King Abdul Aziz City for Science and Technology (KACST-NPST), grant number: 13-MED 1374.

ACKNOWLEDGMENTS

We would like to thank the Department of Biochemistry, King Saud University for providing all the facilities.

REFERENCES

Al-Dosari, D. I., Ahmed, M. M., Al-Rejaie, S. S., Alhomida, A. S., and Ola, M. S. (2017). Flavonoid naringenin attenuates oxidative stress, apoptosis and improves neurotrophic effects in the diabetic rat retina. *Nutrients*. 9, 1161. doi: 10.3390/nu9101161

Bloomgarden, Z. (2018). Diabetes and branched-chain amino acids: What is the link? *J. Diabetes*. 10, 350–352. doi: 10.1111/1753-0407.12645

Bringmann, A., Grosche, A., Pannicke, T., and Reichenbach, A. (2013). GABA and glutamate uptake and metabolism in retinal glial (Müller) Cells. *Front. Endocrinol.* 4, 48. doi: 10.3389/fendo.2013.00048

Bui, B. V., Hu, R. G., Acosta, M. L., Donaldson, P., Vingrys, A. J., Kalloniatis, M., et al. (2009). Glutamate metabolic pathways and retinal function. *J. Neurochem.* 111, 589–599. doi: 10.1111/j.1471-4159.2009.06354.x

Busik, J. V. (2021). Lipid metabolism dysregulation in diabetic retinopathy. *J. Lipid. Res.* 62, 100017. doi: 10.1194/jlr.TR120000981

Busik, J. V., Esselman, W. J., and Reid, G. E. (2012). Examining the role of lipid mediators in diabetic retinopathy. *Clin. Lipidol.* 7, 661–675. doi: 10.2217/clp.12.68

Cervantes-Villagrana, A. R., Garcia-Román, J., González-Espinosa, C., and Lamas, M. (2010). Pharmacological inhibition of N-methyl d-aspartate receptor promotes secretion of vascular endothelial growth factor in müller

cells: effects of hyperglycemia and hypoxia. *Curr. Eye Res.* 35, 733–741. doi: 10.3109/02713683.2010.483312

Chinchore, Y., Begaj, T., Wu, D., Drokhlyansky, E., and Cepko, C. L. (2017). Glycolytic reliance promotes anabolism in photoreceptors. *Elife*. 6, e25946. doi: 10.7554/eLife.25946

Chou, Y., Ma, J., Su, X., and Zhong, Y. (2020). Emerging insights into the relationship between hyperlipidemia and the risk of diabetic retinopathy. *Lipids Health Dis.* 19, 241. doi: 10.1186/s12944-020-01415-3

Cohen LH, and Noell WK. (1960). Glucose catabolism of rabbit retina before and after development of visual function. *J Neurochem*. 5, 253–76.

Conway, M. E., and Hutson, S. M. (2016). BCAA Metabolism and NH(3) Homeostasis. *Adv. Neurobiol.* 13, 99–132. doi: 10.1007/978-3-319-45096-4_5

Dagher, Z., Park, Y. S., Asnaghi, V., Hoehn, T., Gerhardinger, C., Lorenzi, M., et al. (2004). Studies of rat and human retinas predict a role for the polyol pathway in human diabetic retinopathy. *Diabetes*. 53, 2404–2411. doi: 10.2337/diabetes.53.9.2404

D'Andrea, F., Sartini, S., Piano, I., Franceschi, M., Quattrini, L., Guazzelli, L., et al. (2020). Oxy-imino saccharidic derivatives as a new structural class of aldose reductase inhibitors endowed with anti-oxidant activity. *J. Enzyme Inhibit. Med. Chem*. 35, 1194–1205. doi: 10.1080/14756366.2020.1763331

Diederen, R. M., La Heij, E. C., Deutz, N. E., Kijlstra, A., Kessels, A. G., van Eijk, H. M., et al. (2006). Increased glutamate levels in the vitreous of patients with retinal detachment. *Exp. Eye Res.* 83, 45–50. doi: 10.1016/j.exer.2005.10.031

Du, X. L., Edelstein, D., Rossetti, L., Fantus, I. G., Goldberg, H., Ziyadeh, F., et al. (2000). Hyperglycemia-induced mitochondrial superoxide overproduction activates the hexosamine pathway and induces plasminogen activator inhibitor-1 expression by increasing Sp1 glycosylation. *Proc. Natl. Acad. Sci. U S A.* 97, 12222–12226. doi: 10.1073/pnas.97.22.12222

Elms, S. C., Toque, H. A., Rojas, M., Xu, Z., Caldwell, R. W., Caldwell, R. B., et al. (2013). The role of arginase I in diabetes-induced retinal vascular dysfunction in mouse and rat models of diabetes. *Diabetologia*. 56, 654–662. doi: 10.1007/s00125-012-2789-5

Federation, I. D. (2021). *IDF Diabetes Atlas*. 10th edn. Belgium, Brussels. Available online at: https://www.diabetesatlas.org.

Feng, Y., Wang, Y., Stock, O., Pfister, F., Tanimoto, N., Seeliger, M. W., et al. (2009). Vasoregression linked to neuronal damage in the rat with defect of polycystin-2. *PLoS ONE*. 4, e7328. doi: 10.1371/journal.pone.0007328

Fliesler, S. J., Florman, R., Rapp, L. M., Pittler, S. J., and Keller, R. K. (1993). *In vivo* biosynthesis of cholesterol in the rat retina. *FEBS Lett*. 335, 234–238. doi: 10.1016/0014-5793(93)80736-E

Fouda, A. Y., Eldahshan, W., Narayanan, S. P., Caldwell, R. W., and Caldwell, R. B. (2020). Arginase pathway in acute retina and brain injury: therapeutic opportunities and unexplored avenues. *Front. Pharmacol.* 11, 277. doi: 10.3389/fphar.2020.00277

Fox, T. E., Han, X., Kelly, S., and Merrill, A. H., Martin, R. E., Anderson, R. E., et al. (2006). Diabetes alters sphingolipid metabolism in the retina: a potential mechanism of cell death in diabetic retinopathy. *Diabetes*. 55, 3573–3580. doi: 10.2337/db06-0539

Fu, D., Yu, J. Y., Wu, M., Du, M., Chen, Y., Abdelsamie, S. A., et al. (2014). Immune complex formation in human diabetic retina enhances toxicity of oxidized LDL towards retinal capillary pericytes. *J. Lipid. Res.* 55, 860–869. doi: 10.1194/jlr.M045401

Fu, Z., Chen, C. T., Cagnone, G., Heckel, E., Sun, Y., Cakir, B., et al. (2019). Dyslipidemia in retinal metabolic disorders. *EMBO Mol. Med.* 11, e10473. doi: 10.15252/emmm.201910473

Fülöp, N., Marchase, R. B., and Chatham, J. C. (2007). Role of protein O-linked N-acetyl-glucosamine in mediating cell function and survival in the cardiovascular system. *Cardiovasc. Res.* 73, 288–297. doi: 10.1016/j.cardiores.2006.07.018

Ganapathy, P. S., Moister, B., Roon, P., Mysona, B. A., Duplantier, J., Dun, Y., et al. (2009). Endogenous elevation of homocysteine induces retinal neuron death in the cystathionine-beta-synthase mutant mouse. *Invest. Ophthalmol. Vis. Sci.* 50, 4460–4470. doi: 10.1167/iovs.09-3402

Geraldes, P., and King, G. L. (2010). Activation of protein kinase C isoforms and its impact on diabetic complications. *Circ. Res.* 106, 1319–1331. doi: 10.1161/CIRCRESAHA.110.217117

Giacco, F., and Brownlee, M. (2010). Oxidative stress and diabetic complications. *Circ. Res.* 107, 1058–1070. doi: 10.1161/CIRCRESAHA.110.223545

Gowda, K., and Zinnanti, W. J., LaNoue, K. F. (2011). The influence of diabetes on glutamate metabolism in retinas. *J. Neurochem.* 117, 309–320. doi: 10.1111/j.1471-4159.2011.07206.x

Hammer, S. S., and Busik, J. V. (2017). The role of dyslipidemia in diabetic retinopathy. *Vision Res.* 139, 228–236. doi: 10.1016/j.visres.2017.04.010

Holm, L. J., and Buschard, K. (2019). L-serine: a neglected amino acid with a potential therapeutic role in diabetes. *Apmis*. 127, 655–659. doi: 10.1111/apm.12987

Hou, X.-., W., Wang, Y., and Pan, C-, W. (2021). Metabolomics in diabetic retinopathy: a systematic review. *Invest. Ophthalmol. Visual Sci.* 62, 4. doi: 10.1167/iovs.62.10.4

Ipp, E., and Kumar, M. A. (2021). Clinical conundrum: intensifying glycemic control in the presence of advanced diabetic retinopathy. *Diabetes Care*. 44, 2192–2193. doi: 10.2337/dci21-0029

Ishikawa, M. (2013). Abnormalities in glutamate metabolism and excitotoxicity in the retinal diseases. *Scientifica (Cairo)*. 2013, 528940. doi: 10.1155/2013/528940

Joyal, J. S., Gantner, M. L., and Smith, L. E. H. (2018). Retinal energy demands control vascular supply of the retina in development and disease: The role of neuronal lipid and glucose metabolism. *Prog. Retin. Eye Res.* 64, 131–156. doi: 10.1016/j.preteyeres.2017.11.002

Joyal, J. S., Sun, Y., Gantner, M. L., Shao, Z., Evans, L. P., Saba, N., et al. (2016). Retinal lipid and glucose metabolism dictates angiogenesis through the lipid sensor Ffar1. *Nat. Med.* 22, 439–445. doi: 10.1038/nm.4059

Kern, T. S. (2014). Interrelationships between the retinal neuroglia and vasculature in diabetes. *Diabetes Metab. J.* 38, 163–170. doi: 10.4093/dmj.2014.38.3.163

Kim, B. J., Silverman, S. M., Liu, Y., Wordinger, R. J., Pang, I. H., Clark, A. F., et al. (2016). *In vitro* and *in vivo* neuroprotective effects of cJun N-terminal kinase inhibitors on retinal ganglion cells. *Mol. Neurodegener.* 11, 30. doi: 10.1186/s13024-016-0093-4

Kowluru, R. A., Mohammad, G., and Sahajpal, N. (2020). Faulty homocysteine recycling in diabetic retinopathy. *Eye Vision*. 7, 4. doi: 10.1186/s40662-019-0167-9

Kusari, J., Zhou, S. X., Padillo, E., Clarke, K. G., and Gil, D. W. (2010). Inhibition of vitreoretinal VEGF elevation and blood-retinal barrier breakdown in streptozotocin-induced diabetic rats by brimonidine. *Invest. Ophthalmol. Vis. Sci.* 51, 1044–1051. doi: 10.1167/iovs.08-3293

LaNoue, K. F., Berkich, D. A., Conway, M., Barber, A. J., Hu, L. Y., Taylor, C., and Hutson, S. (2001). Role of specific aminotransferases in *de novo* glutamate synthesis and redox shuttling in the retina. *J. Neurosci. Res.* 66, 914–922. doi: 10.1002/jnr.10064

Lau, J. C., Kroes, R. A., Moskal, J. R., and Linsenmeier, R. A. (2013). Diabetes changes expression of genes related to glutamate neurotransmission and transport in the Long-Evans rat retina. *Mol. Vis.* 19, 1538–1553.

Lei, X., Zeng, G., Zhang, Y., Li, Q., Zhang, J., Bai, Z., et al. (2018). Association between homocysteine level and the risk of diabetic retinopathy: a systematic review and meta-analysis. *Diabetol. Metab. Syndr.* 10, 61. doi: 10.1186/s13098-018-0362-1

Lewerenz, J., Hewett, S. J., Huang, Y., Lambros, M., Gout, P. W., Kalivas, P. W., et al. (2013). The cystine/glutamate antiporter system x(c)(-) in health and disease: from molecular mechanisms to novel therapeutic opportunities. *Antioxid. Redox. Signal.* 18, 522–555. doi: 10.1089/ars.2011.4391

Li, Q., and Puro, D. G. (2002). Diabetes-induced dysfunction of the glutamate transporter in retinal Müller cells. *Invest. Ophthalmol. Vis. Sci.* 43, 3109–3116.

Liu, H., and Prokosch, V. (2021). Energy metabolism in the inner retina in health and glaucoma. *Int J Mol Sci*. 22. doi: 10.3390/ijms22073689

Lorenzi, M. (2007). The polyol pathway as a mechanism for diabetic retinopathy: attractive, elusive, and resilient. *Exp. Diab. Res.* 2007, 61038. doi: 10.1155/2007/61038

Millman, J. R., Doggett, T., Thebeau, C., Zhang, S., Semenkovich, C. F., Rajagopal, R., et al. (2019). Measurement of energy metabolism in explanted retinal tissue using extracellular flux analysis. *J. Vis. Exp.* 143, e58626. doi: 10.3791/58626

Moore, P., El-sherbeny, A., Roon, P., Schoenlein, P. V., Ganapathy, V., and Smith, S. B. (2001). Apoptotic cell death in the mouse retinal ganglion cell layer is induced *in vivo* by the excitatory amino acid homocysteine. *Exp. Eye Res.* 73, 45–57. doi: 10.1006/exer.2001.1009

Moran, E. P., Wang, Z., Chen, J., Sapieha, P., Smith, L. E., Ma, J. X., et al. (2016). Neurovascular cross talk in diabetic retinopathy: Pathophysiological roles and therapeutic implications. *Am. J. Physiol. Heart Circ. Physiol*. 311, H738–H749. doi: 10.1152/ajpheart.00005.2016

Mori, A., Morita, M., Morishita, K., Sakamoto, K., Nakahara, T., Ishii, K., et al. (2015). l-Citrulline dilates rat retinal arterioles via nitric oxide- and prostaglandin-dependent pathways *in vivo*. *J. Pharmacol. Sci*. 127, 419–423. doi: 10.1016/j.jphs.2015.02.012

Mori, A., Takei, T., Suzuki, N., Sakamoto, K., Morita, M., Nakagawa, S., et al. (2021). L-Citrulline ameliorates the attenuation of acetylcholine-induced vasodilation of retinal arterioles in diabetic rats. *Heliyon*. 7, e06532. doi: 10.1016/j.heliyon.2021.e06532

Naggar, H., Ola, M. S., Moore, P., Huang, W., Bridges, C. C., Ganapathy, V., et al. (2002). Downregulation of reduced-folate transporter by glucose in cultured RPE cells and in RPE of diabetic mice. *Invest. Ophthalmol. Vis. Sci*. 43, 556–563.

Narayanan, S. P., Rojas, M., Suwanpradid, J., Toque, H. A., Caldwell, R. W., Caldwell, R. B., et al. (2013). Arginase in retinopathy. *Prog. Retin. Eye Res*. 36, 260–280. doi: 10.1016/j.preteyeres.2013.06.002

Narayanan, S. P., and Shosha, E., C. D. P. (2019). Spermine oxidase: a promising therapeutic target for neurodegeneration in diabetic retinopathy. *Pharmacol. Res*. 147, 104299. doi: 10.1016/j.phrs.2019.104299

Nicoletti, R., Venza, I., Ceci, G., Visalli, M., Teti, D., Reibaldi, A., et al. (2003). Vitreous polyamines spermidine, putrescine, and spermine in human proliferative disorders of the retina. *Br. J. Ophthalmol*. 87, 1038–1042. doi: 10.1136/bjo.87.8.1038

Ola, M., and Nawaz, M. (2012). Cellular and molecular mechanism of diabetic retinopathy. In: Ola MS, editor. *Diabetic Retinopathy*. InTech Open. doi: 10.5772/33590

Ola, M. S. (2021). Does Hyperglycemia Cause Oxidative Stress in the Diabetic Rat Retina? *Cells*. 10, 794. doi: 10.3390/cells10040794

Ola, M. S., Al-Dosari, D., and Alhomida, A. S. (2018). Role of oxidative stress in diabetic retinopathy and the beneficial effects of flavonoids. *Curr. Pharm. Des*. 24, 2180–2187. doi: 10.2174/1381612824666180515151043

Ola, M. S., and Alhomida, A. S. (2014). Neurodegeneration in diabetic retina and its potential drug targets. *Curr. Neuropharmacol*. 12, 380–386. doi: 10.2174/1570159X12666140619205024

Ola, M. S., and Alhomida, A. S., LaNoue, K. F. (2019). Gabapentin attenuates oxidative stress and apoptosis in the diabetic rat retina. *Neurotox. Res*. 36, 81–90. doi: 10.1007/s12640-019-00018-w

Ola, M. S., Nawaz, M. I., Khan, H. A., and Alhomida, A. S. (2013). Neurodegeneration and neuroprotection in diabetic retinopathy. *Int. J. Mol. Sci*. 14, 2559–2572. doi: 10.3390/ijms14022559

Ola, M. S., Nawaz, M. I., Siddiquei, M. M., Al-Amro, S., and Abu El-Asrar, A. M. (2012). Recent advances in understanding the biochemical and molecular mechanism of diabetic retinopathy. *J. Diab. Complic*. 26, 56–64. doi: 10.1016/j.jdiacomp.2011.11.004

Opreanu, M., Tikhonenko, M., Bozack, S., Lydic, T. A., Reid, G. E., McSorley, K. M., et al. (2011). The unconventional role of acid sphingomyelinase in regulation of retinal microangiopathy in diabetic human and animal models. *Diabetes*. 60, 2370–2378. doi: 10.2337/db10-0550

Ozaki, H., Inoue, R., Matsushima, T., Sasahara, M., Hayashi, A., Mori, H., et al. (2018). Serine racemase deletion attenuates neurodegeneration and microvascular damage in diabetic retinopathy. *PLoS ONE*. 13, e0190864. doi: 10.1371/journal.pone.0190864

Patel, C., Rojas, M., Narayanan, S. P., Zhang, W., and Xu, Z., lemtalsi T, et al. (2013). Arginase as a mediator of diabetic retinopathy. *Front. Immunol*. 4, 173. doi: 10.3389/fimmu.2013.00173

Poloschek, C. M., Fowler, B., Unsold, R., and Lorenz, B. (2005). Disturbed visual system function in methionine synthase deficiency. *Graefes Arch. Clin. Exp. Ophthalmol*. 243, 497–500. doi: 10.1007/s00417-004-1044-2

Pow, D. V. (2001). Amino acids and their transporters in the retina. *Neurochem. Int*. 38, 463–484. doi: 10.1016/S0197-0186(00)00114-5

Rains, J. L., and Jain, S. K. (2011). Oxidative stress, insulin signaling, and diabetes. *Free Radic. Biol. Med*. 50, 567–575. doi: 10.1016/j.freeradbiomed.2010.12.006

Rao, H., Jalali, J. A., Johnston, T. P., and Koulen, P. (2021). Emerging roles of dyslipidemia and hyperglycemia in diabetic retinopathy: molecular mechanisms and clinical perspectives. *Front. Endocrinol*. 12, 620045. doi: 10.3389/fendo.2021.620045

Shen, Y., Liu, X. L., and Yang, X. L. (2006). N-methyl-D-aspartate receptors in the retina. *Mol. Neurobiol*. 34, 163–179. doi: 10.1385/MN:34:3:163

Sinha, T., Ikelle, L., Naash, M. I., and Al-Ubaidi, M. R. (2020). The intersection of serine metabolism and cellular dysfunction in retinal degeneration. *Cells*. 9, 674. doi: 10.3390/cells9030674

Smith, S. B. (2002). Diabetic retinopathy and the NMDA receptor. *Drug. News Perspect*. 15, 226–232. doi: 10.1358/dnp.2002.15.4.840055

Sumarriva, K., Uppal, K., Ma, C., Herren, D. J., Wang, Y., Chocron, I. M., et al. (2019). Arginine and carnitine metabolites are altered in diabetic retinopathy. *Invest. Ophthalmol. Vis. Sci*. 60, 3119–3126. doi: 10.1167/iovs.19-27321

Sun, Y., Zou, H., Li, X., Xu, S., and Liu, C. (2021). Plasma metabolomics reveals metabolic profiling for diabetic retinopathy and disease progression. *Front. Endocrinol*. 12, 757088. doi: 10.3389/fendo.2021.757088

Teo, Z. L., Tham, Y-C., Yu, M., Chee, M. L., Rim, T. H., and Cheung, N., et al. (2021). Global prevalence of diabetic retinopathy and projection of burden through 2045: systematic review and meta-analysis. *Ophthalmology*. 128, 1580–1591. doi: 10.1016/j.ophtha.2021.04.027

Thakur, S., Gupta, S. K., Ali, V., Singh, P., and Verma, M. (2021). Aldose Reductase: a cause and a potential target for the treatment of diabetic complications. *Arch. Pharm. Res*. 44, 655–667. doi: 10.1007/s12272-021-01343-5

Tikhonenko, M., Lydic, T. A., Opreanu, M., Li Calzi, S., Bozack, S., McSorley, K. M., et al. (2013). N-3 polyunsaturated Fatty acids prevent diabetic retinopathy by inhibition of retinal vascular damage and enhanced endothelial progenitor cell reparative function. *PLoS ONE*. 8, e55177. doi: 10.1371/journal.pone.0055177

Yang, C., Xie, L., Gu, Q., Qiu, Q., Wu, X., Yin, L., et al. (2019). 7-Ketocholesterol disturbs RPE cells phagocytosis of the outer segment of photoreceptor and induces inflammation through ERK signaling pathway. *Exp. Eye Res*. 189, 107849. doi: 10.1016/j.exer.2019.107849

Yumnamcha, T., Guerra, M., Singh, L. P., and Ibrahim, A. S. (2020). Metabolic dysregulation and neurovascular dysfunction in diabetic retinopathy. *Antioxidants*. 9, 1244. doi: 10.3390/antiox9121244

Zemski Berry, K. A., Gordon, W. C., Murphy, R. C., and Bazan, N. G. (2014). Spatial organization of lipids in the human retina and optic nerve by MALDI imaging mass spectrometry. *J. Lipid. Res*. 55, 504–515. doi: 10.1194/jlr.M044990

Conflict of Interest: The authors declare that the research was conducted in the absence of any commercial or financial relationships that could be construed as a potential conflict of interest.

Publisher's Note: All claims expressed in this article are solely those of the authors and do not necessarily represent those of their affiliated organizations, or those of the publisher, the editors and the reviewers. Any product that may be evaluated in this article, or claim that may be made by its manufacturer, is not guaranteed or endorsed by the publisher.

Advantages of publishing in Frontiers

OPEN ACCESS
Articles are free to read for greatest visibility and readership

FAST PUBLICATION
Around 90 days from submission to decision

HIGH QUALITY PEER-REVIEW
Rigorous, collaborative, and constructive peer-review

TRANSPARENT PEER-REVIEW
Editors and reviewers acknowledged by name on published articles

Frontiers
Avenue du Tribunal-Fédéral 34
1005 Lausanne | Switzerland

Visit us: www.frontiersin.org
Contact us: frontiersin.org/about/contact

REPRODUCIBILITY OF RESEARCH
Support open data and methods to enhance research reproducibility

DIGITAL PUBLISHING
Articles designed for optimal readership across devices

FOLLOW US
@frontiersin

IMPACT METRICS
Advanced article metrics track visibility across digital media

EXTENSIVE PROMOTION
Marketing and promotion of impactful research

LOOP RESEARCH NETWORK
Our network increases your article's readership